



Theses and Dissertations

2008-10-08

Pile Downdrag During Construction of Two Bridge Abutments

Brian Keith Sears

Brigham Young University - Provo

Follow this and additional works at: <https://scholarsarchive.byu.edu/etd>



Part of the [Civil and Environmental Engineering Commons](#)

BYU ScholarsArchive Citation

Sears, Brian Keith, "Pile Downdrag During Construction of Two Bridge Abutments" (2008). *Theses and Dissertations*. 1918.

<https://scholarsarchive.byu.edu/etd/1918>

This Thesis is brought to you for free and open access by BYU ScholarsArchive. It has been accepted for inclusion in Theses and Dissertations by an authorized administrator of BYU ScholarsArchive. For more information, please contact scholarsarchive@byu.edu, ellen_amatangelo@byu.edu.

PILE DOWNDRAW DURING CONSTRUCTION OF
TWO BRIDGE ABUTMENTS

by

Brian K. Sears

A thesis submitted to the faculty of

Brigham Young University

in partial fulfillment of the requirements for the degree of

Master of Science

Department of Civil and Environmental Engineering

Brigham Young University

December 2008

BRIGHAM YOUNG UNIVERSITY

GRADUATE COMMITTEE APPROVAL

of a thesis submitted by

Brian K. Sears

This thesis has been read by each member of the following graduate committee and by majority vote has been found to be satisfactory.

Date

Kyle M. Rollins, Chair

Date

Travis M. Gerber

Date

Norman L. Jones

BRIGHAM YOUNG UNIVERSITY

As chair of the candidate's graduate committee, I have read the thesis of Brian K. Sears in its final form and have found that (1) its format, citations, and bibliographical style are consistent and acceptable and fulfill university and department style requirements; (2) its illustrative materials including figures, tables, and charts are in place; and (3) the final manuscript is satisfactory to the graduate committee and is ready for submission to the university library.

Date

Kyle M. Rollins
Chair, Graduate Committee

Accepted for the Department

E. James Nelson
Graduate Coordinator

Accepted for the College

Alan R. Parkinson
Dean, Ira A. Fulton College of Engineering
and Technology

ABSTRACT

PILE DOWNDRAG DURING CONSTRUCTION OF TWO BRIDGE ABUTMENTS

Brian K. Sears

Department of Civil and Environmental Engineering

Master of Science

Two steel pipe piles in place in abutments for two different bridge constructions sites were instrumented with strain gauges to measure the magnitude of negative skin friction. The piles were monitored before, during and up to 19 months after construction was completed. The load versus depth and time in each pile is discussed. Maximum observed dragloads ranged from 98 to 127 kips. A comparison with two methods for calculating dragloads is presented. Both comparison methods were found to be conservative, with the Briaud and Tucker (1997) approach more closely estimating the observed load versus depth behavior.

ACKNOWLEDGMENTS

Completing any large project requires the effort and help of numerous people. I have been assisted in this project by many people who have provided insight, funding and encouragement. I would like to sincerely thank the Utah Department of Transportation (UDOT) for the funding of this research through Contract #05-9122. However, the conclusions and opinions expressed in this thesis do not necessarily reflect the view of UDOT. I would also like to thank the contractors and managers that have been patient and willing to work around our equipment. These include Wadsworth Brothers Construction, Harper Construction and the Salt Lake City Airport Department (SLCAD). Special thanks to Bob Bailey at SLCAD for helping to coordinate the work done on that site.

Dr. Kyle Rollins has been an outstanding mentor and a patient advisor. I thank him for imparting of his time to teach and direct me throughout the project. Likewise, I would like to thank Dr. Travis Gerber and Dr. Norman Jones for serving on my committee and for the helpful advice and encouragement they have also offered.

David Anderson and his assistants have provided valuable and timely help with gauge installation, monitoring, troubleshooting and help to fix various problems that occurred during the data collection process.

Lastly, I wish to thank my wife who has pushed me to finish, showed great patience and given me proper encouragement when needed.

TABLE OF CONTENTS

LIST OF TABLES	xv
LIST OF FIGURES	xvii
1.0 Introduction.....	1
1.1 Skin Friction	2
1.1.1 Process of Developing Skin Friction	2
1.1.2 Evaluation of Ultimate Pile Capacity with Downdrag	5
1.1.3 Research of Negative Skin Friction.....	8
1.2 Objectives	9
1.3 Scope of Work	9
2.0 Literature Review	11
2.1 Theoretical Approaches	12
2.2 Full Scale and Model Testing	14
2.3 Laboratory, Computer Models and Centrifuge Tests	26
2.4 Previous and Current Design Methods	34
2.5 Need for Additional Research.....	42
3.0 Geotechnical Site Characterization.....	45
3.1 Site Characterization of Redwood Road and SR-201 Site	45

- 3.1.1 Laboratory Testing.....49
 - 3.1.1.1 Soil Profile49
 - 3.1.1.2 Gradation of Samples.....55
 - 3.1.1.3 Atterberg Limit Tests.....55
 - 3.1.1.4 Vane Shear Strength.....57
 - 3.1.1.5 Consolidation Testing58
- 3.1.2 In-situ Testing.....59
 - 3.1.2.1 Standard Penetration Testing (SPT).....59
 - 3.1.2.2 Cone Penetrometer Testing (CPT).....61
 - 3.1.2.3 Torvane Tests.....61
- 3.2 Site Characterization of Salt Lake City International Airport Site.....65
 - 3.2.1 Soil Profile.....68
 - 3.2.2 Laboratory Tests68
 - 3.2.2.1 Gradation Tests68
 - 3.2.2.2 Atterberg Limits.....72
 - 3.2.2.3 Consolidation Tests.....72
 - 3.2.2.4 Unconfined Compression Tests76
 - 3.2.3 In-Situ Testing77
 - 3.2.3.1 Standard Penetration Testing (SPT).....78
 - 3.2.3.2 Torvane Tests.....78

3.3	Summary of Geotechnical Investigation.....	78
3.3.1	Summary of Redwood Road Site Geotechnical Investigation	81
3.3.1.1	Laboratory and In-Situ Testing	81
3.3.2	Summary of SLCIA Site Geotechnical Investigation.....	82
3.3.2.1	Laboratory and In-Situ Testing	82
4.0	Pile Instrumentation and Method of Analysis	87
4.1	Instrumentation Procedure for Test Pile in Springville, UT	87
4.1.1	Gauge Type and Characteristics used at Springville, UT	88
4.1.2	Gauge Installation at Springville, UT	89
4.1.3	Lessons Learned from Springville Installation.....	93
4.2	Instrumentation Procedure for Test Sites in Salt Lake City, UT	93
4.2.1	Gauge Type and Characteristics	94
4.2.2	Installation Method.....	94
4.3	Data Logging Equipment Used on Sites.....	99
4.4	Analysis Methods of Collected Data	100
4.4.1	The Double Segment Method for Calculating Unit Side Resistance	102
4.4.2	The Single Segment Method for Calculating Unit Side Resistance	104
4.5	Calculating Pile Settlement.....	106
4.5.1	Method for Calculating Pile Settlement at Gauge Elevations	106
4.5.2	Method for Calculating Pile Settlement at Midpoints between Two Gauges	107

5.0 Results from Redwood Road and SR-201 Site	111
5.1 Construction Site Details, Pile Layout and Construction Timeline.....	111
5.1.1 Abutment Layout.....	111
5.2 Construction Timeline	113
5.3 Gauge Information.....	117
5.3.1 Depth Placement.....	117
5.3.2 Site Installation and Equipment History.....	117
5.3.3 Gauge Performance	122
5.4 Presentation and Discussion of Data and Analyses.....	123
5.4.1 Axial Stress and Axial Load.....	123
5.4.1.1 Derivation of Axial Stress and Axial Load.....	123
5.4.1.2 Presentation and Discussion of Results for Stress and Load Analyses.....	125
5.4.1.2.1 Gauge Inconsistencies.....	125
5.4.1.2.2 Recommendations for Gauge Usage.....	128
5.4.1.3 The Neutral Plane and History of Dragloads.....	135
5.4.1.4 Immediate Effect of Structural Loading	140
5.4.2 Shear Stress.....	141
5.4.2.1 Derivation of Shear Stress Calculations.....	141
5.4.2.2 Shear Stress Data and Analyses.....	144
5.4.2.2.1 Shear Stress between El. 4252 and El. 4238 (Within Approach Fill).....	144

5.4.2.2.2	Shear Stress between El. 4238 and El. 4233.5	145
5.4.2.2.3	Shear Stress between El. 4233.5 and El. 4227	147
5.4.2.2.4	Shear Stress for Section between El. 4227 and El. 4221	148
5.4.2.2.5	Shear Stress for Section between El. 4221 and El. 4213	149
5.4.2.2.6	Shear Stress for Section between El. 4213 and El. 4205	150
5.4.2.2.7	Shear Stress between El. 4205 and El. 4184 (Two Sections)	152
5.4.2.3	Summary of Shear Stress Values for Sections of Piles.....	153
5.4.3	Comparison of Estimated to Measured Results.....	155
5.4.3.1	Estimating the Location of the Neutral Plane	155
5.4.3.2	Estimation of Side Resistance.....	155
5.4.3.3	Derivation of Pile Compression and Pile Settlement.....	158
5.4.3.4	Presentation of Measured Pile Compression vs. Depth Curves.....	162
5.4.3.5	Presentation of Soil Settlement vs. Depth Curves	163
5.4.3.6	Estimating the Location of the Neutral Plane and Magnitude of Loads using Fellenius (1989) and Briaud and Tucker (1997) and Comparison to Actual Results.....	165
5.4.3.7	Comparison of Undrained Shear Strength and Side Friction.....	169
6.0	Results from Salt Lake City International Airport Site.....	173
6.1	Abutment Layout.....	173
6.2	Construction Timeline	175
6.3	Gauge Information.....	177
6.3.1	Depth Placement.....	177

6.3.2	Site Instrumentation and Equipment History	177
6.3.3	Gauge Performance	180
6.4	Presentation and Discussion of Data and Analyses	181
6.4.1	Axial Stress and Axial Load	181
6.4.1.1	Derivation of Axial Stress and Axial Load	181
6.4.1.2	Presentation and Discussion of Results for Load vs. Depth Curve	182
6.4.1.2.1	Gauge Inconsistencies	184
6.4.1.2.2	Recommendations for Gauge Usage	186
6.4.1.3	The Neutral Plane and History of Dragloads	187
6.4.1.4	Immediate Effect of Structural Loading	192
6.4.2	Shear Stress	193
6.4.2.1	Derivation of Shear Stress Calculations	193
6.4.2.2	Presentation of Shear Stress Data and Analyses	194
6.4.2.2.1	Shear Stress between El. 4233 and El. 4225	195
6.4.2.2.2	Shear Stress between El. 4225 and El. 4215.5	195
6.4.2.2.3	Shear Stress between El. 4215.5 and El. 4205	197
6.4.2.2.4	Shear Stress between El. 4205 and El. 4200	198
6.4.2.2.5	Shear Stress between El. 4200 and El. 4195	199
6.4.2.2.6	Shear Stress between El. 4195 and El. 4185	201
6.4.2.2.7	Shear Stress between El. 4185 and El. 4175.5	202

6.4.2.2.8	Shear Stress between El. 4175.5 and El. 4165.5	203
6.4.2.2.9	Shear Stress between El. 4165.5 and El. 4155	204
6.4.2.2.10	Summary of Shear Stress Values for Sections of Pile	205
6.4.3	Comparison of Estimated to Actual Results	206
6.4.3.1	Estimating the Location of the Neutral Plane	206
6.4.3.2	Estimation of Side Resistance	206
6.4.3.3	Derivation of Pile Compression and Pile Settlement	207
6.4.3.4	Presentation of Measured Pile Compression Results	208
6.4.3.5	Presentation of Soil Settlement	209
6.4.3.6	Estimating the Location of the Neutral Plane and Magnitude of Loads using Fellenius (1989) and Briaud and Tucker (1997) and Comparison to Actual Results	210
6.4.3.7	Comparison of Undrained Shear Strength and Side Friction	212
7.0	Summary, Conclusions and Recommendations	217
7.1	Summary	217
7.2	Conclusions and Recommendations	218
References	221
Appendix	227

LIST OF TABLES

Table 2-1 Pile Properties for Study Conducted by Endo et al. (1969)	16
Table 2-2 Pile Dimensions and Coatings for Study by Bush and Briaud (1994)	22
Table 3-1 Atterberg Limit Test Results for Redwood Road & SR-201 Site	56
Table 3-2 Soil Characteristic Data for Samples from Boreholes B-1 & B-4 by AMEC for Redwood Road & SR-201 Site	59
Table 3-3 Consolidation Test Data from Samples from Boreholes B-1 & B-4 by AMEC for Redwood Road & SR-201 Site	59
Table 3-4 Summary of Gradation from Boreholes 03-NB-3, 4 and 5 for SLCIA Site	72
Table 3-5 Summary of Atterberg Limit Data for Boreholes 03-NB-3, 4 and 5 from SLCIA Site	73
Table 3-6 Summary of Consolidation Test Values for Boreholes 03-NB-3 and 5 from SLCIA Site	74
Table 3-7 Unconfined Compressive Strengths from Tests for Boreholes 03-NB-3, 4, & 5 at SLCIA Site	76
Table 5-1 Construction Timeline at Redwood Road and SR-201 Site	116
Table 5-2 Modulus of Elasticity and Cross-Sectional Area for Piles at Redwood Road & SR-201 Site	123
Table 5-3 Combination of Gauges used to Create Consistent Load Plot	131
Table 5-4 History of Dragload for Pile at Redwood Road Site	138

Table 5-5 Summary of Soil Parameters Used to Estimate Side Resistance	157
Table 5-6 Estimated Properties for Settlement Analysis of Cohesive Layers for Redwood Road Site.....	164
Table 5-7 Summary of Contributing Settlement for Soil Profile at Redwood Road and SR-201.....	164
Table 5-8 Summary of Back-Calculated Alpha and Beta Values for Soil Profile at Redwood Road and SR 201	172
Table 6-1 Construction Timeline for SLCIA West Abutment.....	176
Table 6-2 Values for Modulus of Elasticity for Test Pile at the SLCIA Site	182
Table 6-3 Combination of Gauges used to Create Consistent Load Plot	187
Table 6-4 History of Dragload for Pile at SLCIA Site	191
Table 6-5 Summary of Alpha and Beta Values and Estimated Side Resistance for SLCIA Site.....	207
Table 6-6 Summary of Calculated Pile Compression or Settlement Values	208
Table 6-7 Summary of Contributing Settlement for Soil Profile at SLCIA Site	210
Table 6-8 Summary of Alpha and Beta Values for Soils Profile at SLCIA Site	215

LIST OF FIGURES

Figure 1-1 Illustration of (a) Forces Acting on a Pile and (b) Load in the Pile for Typical Case Involving Positive Skin Friction along with (c) Forces Acting on a Pile and (d) Load in the Pile for Case Involving Negative Skin Friction	4
Figure 1-2 Illustration of Potential Reserve Capacity at the Ultimate State due to Reversal of Skin Friction from Positive to Negative after Initial Development of Dragload due to Negative Skin Friction (Briaud and Tucker, 1997)	7
Figure 2-1 Loads in Pile cE43 Over Time and Loads in Each Pile After Two Years as Reported by Endo et al. (1969)	16
Figure 2-2 Comparison of Actual Loads and Calculated Loads from Test by Walker and Darvall (1973)	19
Figure 2-3 Downdrag Loads on Pile Studied by Bozozuk (1981).....	20
Figure 2-4 Loading Schedule for Pile Studied by Bozozuk (1981).....	20
Figure 2-5 Loads in Uncoated Pile from Study Conducted by Bush and Briaud (1994).....	23
Figure 2-6 Loads in Bitumen Coated Pile from Study Conducted by Bush and Briaud (1994)	24
Figure 2-7 Plot Showing Relationship between Pile Batter and Downdrag Force (Koerner and Mukhopadhyay, 1972).....	27
Figure 2-8 Plot Showing Relationship between Pile Spacing and Downdrag Force (Koerner and Mukhopadhyay, 1972).....	27
Figure 2-9 Plot to Show Relationship between Water Content, Pile Material and Downdrag Force (Koerner and Mukhopadhyay, 1972).....	28
Figure 2-10 Depiction to Show Process of Obtaining E_i as Used in Method by Leifer (1994).....	30

Figure 2-11 Plot from Leifer (1994) Showing Relationship between Pile/Soil Flexibility Factor, f , and Pile Loads.....	30
Figure 2-12 Centrifuge Test Setup for Testing Done by Leung et al. (2004).....	31
Figure 2-13 Comparison of Downdrag Loads Due to End-Bearing (from Leung et al. 2004)	32
Figure 2-14 Effects of Applied Load on Location of Neutral Plane (from Leung et al. 2004)	33
Figure 2-15 Comparison of Applied Loading Tests during Testing by Leung et al. (2004).....	34
Figure 2-16 Depiction of Procedure for Locating the Neutral Plane According to the Unified Design Approach (Fellenius, 1989).....	37
Figure 2-17 Comparisons of Method by Wong et al. (1995) to Actual Results by Indraratna et al. (1992).....	39
Figure 2-18 Comparison of Method by Wong et al. (1995) to Actual Results by Walker and Darvall (1973)	40
Figure 3-1 Map of Salt Lake City, UT, with Locations of Test Piles (Mapquest, 2008).....	46
Figure 3-2 Aerial Photo of Redwood Road and SR-201 Site before Construction with Location of Test Pile (USGS, 2003).....	47
Figure 3-3 Redwood Road Site Geotechnical Boring Site Map.....	48
Figure 3-4 Borelog for Borehole B-4 Completed by AMEC for Redwood Road and SR-201 (continued on next page).....	50
Figure 3-5 Borelog for Borehole DH#04-5 Completed by RB&G for Redwood Road and SR-201	53
Figure 3-6 Borelog for Borehole B-35 Completed by Kleinfelder for Redwood Road and SR-201	54
Figure 3-7 Plasticity Chart Showing Identification of Cohesive Soils for Redwood Road Project (modified from AMEC Memorandum No. 20.1).....	57

Figure 3-8 Undrained Shear Strength Profile vs. Depth Based on Laboratory Vane Shear Tests for Boreholes B-1 and B-4 Completed by AMEC for Redwood Road and SR-201	58
Figure 3-9 Uncorrected SPT Blowcount Comparison for Boreholes Nearest to Test Pile Location	60
Figure 3-10 Log of CPT Sounding for CPT-36 at Redwood Road and SR-201 Site	62
Figure 3-11 Undrained Shear Strength Values from Torvane, Unconfined Compression and Vane Shear Tests for Boreholes Near Test Pile Location.....	65
Figure 3-12 Aerial Photo of SLCIA Site before Construction with Location of Test Pile (USGS, 2003).....	66
Figure 3-13 Borehole Locations for SLCIA Site.....	67
Figure 3-14 Fence Diagram of Borehole Logs Near Test Site	69
Figure 3-15 Borelog of Borehole 03-NB-5 for SLCIA Site (continued on next page).....	70
Figure 3-16 Plasticity Chart Showing Identification of Cohesive Soils for SLCIA Site	74
Figure 3-17 Plot of Preconsolidation Pressure and Vertical Effective Stress vs. Elevation and Depth for Borehole 03-NB-5	75
Figure 3-18 Plot of Unconfined Compressive Strength vs. Elevation and Depth for Boreholes 03-NB-3, 4, & 5 at SLCIA Site	77
Figure 3-19 SPT N_{60} Blowcount Values vs. Elevation for Boreholes 03-NB-3, 4, 5 & 6 for SLCIA Site	79
Figure 3-20 Undrained Shear Strength Values from Torvane and Unconfined Compression Tests for Borehole 03-NB-3, 4, 5 & 6 from SLCIA Site.....	80
Figure 3-21 Summary of Uncorrected SPT Blowcount and Undrained Shear Strength Values for Redwood Road & SR-201 Site.....	84
Figure 3-22 Summary of Consolidation Parameters, Undrained Shear Strength Parameters and SPT N_{60} Blowcount Values for SLCIA Site	85

Figure 4-1 Series 4000 Vibrating Wire Strain Gauge (from company website, www.geokon.com).....	89
Figure 4-2 Spacing Bar and Welding Jig Provided to Assist in Correct Placement of End Blocks for Welding (from company website, www.geokon.com).....	90
Figure 4-3 End Block after being Welded to the Pile.....	90
Figure 4-4 Placement of Gauge and Wires along Pile.....	91
Figure 4-5 Vibrating Wire Strain Gauge Model 4200 used for Installations in Salt Lake City, UT	95
Figure 4-6 Metal Star used in Gauge Installation and Assembly for Salt Lake City, UT	95
Figure 4-7 Completed Assembly of Star and Gauges Attached to Inclinometer Pipe for Installation.....	96
Figure 4-8 Installing Pipe Sections One at a Time at Redwood Road and SR-201 (author photo).....	97
Figure 4-9 Installing Multiple Sections using Forklift in Sacramento, CA (author photo)	98
Figure 4-10 Data Logger with other Components and Wires Attached	100
Figure 4-11 Depiction of Double Segment Method for Calculating Unit Skin Friction.....	103
Figure 4-12 Depiction of Single Segment Method for Calculating Unit Skin Friction.....	105
Figure 4-13 Depiction of Calculating Pile Compression at Gauge Elevations.....	108
Figure 4-14 Depiction of Calculating Pile Compression at Midpoint of Gauges.....	109
Figure 5-1 Schematic of East Abutment and Approach Fill at Redwood Road and SR-201 Site	114
Figure 5-2 Reproduction of Pile Load Test Results for Test Pile at Redwood Road Site	115

Figure 5-3 Location of Gauges on Test Pile at Redwood Road & SR-201	119
Figure 5-4 Change in Strain Measurements for West Gauges from Initial Reading on 15 June 2005	120
Figure 5-5 Change in Strain Measurements for East Gauges from Initial Reading on 15 June 2005	120
Figure 5-6 Comparison of Change in West and East Gauges between Readings on 1 July and 14 July 2005	121
Figure 5-7 Comparison of West and East Gauges for Redwood Road and SR-201 Site	126
Figure 5-8 Plot of Axial Load vs. Depth and Time using Best Combination of Gauges for Redwood Road and SR-201	132
Figure 5-9 Simplified Plot of Axial Load vs. Depth and Time for Redwood Road Site	133
Figure 5-10 Expected Development of Downdrag Load for Piles at a Bridge Abutment (Briaud and Tucker, 2007)	134
Figure 5-11 Settlement Time History Near East Abutment for Redwood Road and SR-201 Site	137
Figure 5-12 Plot of Hourly Readings for West Gauge on 28 February 2006	140
Figure 5-13 Comparison of Single Segment and Double Segment Methods for Calculating Shear Stress between El. 4233.5 and El. 4221	142
Figure 5-14 Comparison of Single Segment and Double Segment Methods for Calculating Shear Stress between El. 4227 and El. 4213	142
Figure 5-15 Comparison of Single Segment and Double Segment Methods for Calculating Shear Stress between El. 4205 and El. 4184	143
Figure 5-16 Shear Stress on Pile at Redwood Road & SR-201 from El. 4252 to El. 4238 (Within Approach Fill)	145
Figure 5-17 Shear Stress on Pile from El. 4238 to El. 4233.5	146

Figure 5-18 Shear Stress on Pile from El. 4233.5 to El. 4227	148
Figure 5-19 Shear Stress on Pile from El. 4227 to El. 4221	149
Figure 5-20 Shear Stress on Pile from El. 4221 to El. 4213	151
Figure 5-21 Shear Stress on Pile from El. 4213 to El. 4205	152
Figure 5-22 Shear Stress on Pile from El. 4205 to El. 4196	154
Figure 5-23 Shear Stress on Pile from El. 4196 to El. 4184	154
Figure 5-24 Pile Compression over Time for Redwood Road and SR-201 Site	163
Figure 5-25 Plot of Select Load vs. Depth Curves for Redwood Road and SR-201 Site Showing Comparison of Estimated Load in Pile from Methods by Fellenius (1989) and Briaud and Tucker (1997)	168
Figure 5-26 Settlement of Pile and Soil for Redwood Road and SR-201	169
Figure 5-27 Close up of Pile and Soil Settlement for Redwood Road and SR-201	170
Figure 5-28 Comparison Plot of Measured Undrained Cohesion or Calculated Side Friction and Maximum Measured Shear Stress vs. Depth for Redwood Road and SR 201 Site	171
Figure 6-1 Plan and Profile View of West Abutment at SLCIA Site	174
Figure 6-2 Location of Gauges on Test Pile at SLCIA Site Relative to the Soil Layering	179
Figure 6-3 Comparison of West and East Gauges for SLCIA Site	183
Figure 6-4 Plot of Axial Load vs. Depth and Time using Best Combination of Gauges for SLCIA Site	188
Figure 6-5 Simplified Plot of Axial Load vs. Depth and Time for SLCIA Site	189
Figure 6-6 Settlement vs. Fill Height for SLCIA Site (data provided by RB&G Engineering)	190

Figure 6-7 Comparison of Single Segment and Double Segment Methods for Calculating Shear Stress between El. 4185 and El. 4165.5	194
Figure 6-8 Plot of Shear Stress between El. 4233 and El. 4225	196
Figure 6-9 Plot of Shear Stress between El. 4225 and El. 4215.5	197
Figure 6-10 Plot of Shear Stress between El. 4215.5 and El. 4205	198
Figure 6-11 Plot of Shear Stress between El. 4205 and El. 4200	200
Figure 6-12 Plot of Shear Stress between El. 4200 and El. 4195	201
Figure 6-13 Plot of Shear Stress between El. 4195 and El. 4185	202
Figure 6-14 Plot of Shear Stress between El. 4185 and El. 4175.5	203
Figure 6-15 Plot of Shear Stress between El. 4175.5 and El. 4165.5	205
Figure 6-16 Plot of Shear Stress between El. 4165.5 and El. 4155	206
Figure 6-17 Pile Compression over Time for SLCIA Site	209
Figure 6-18 Plot of Load versus Depth for the SLCIA Site Showing Comparison of Estimated Load in the Pile from the "Unified Design" Approach by Fellenius (1989) and Briaud and Tucker (1997) Method	213
Figure 6-19 Settlement of Soil and Pile for SLCIA Site	214
Figure 6-20 Close-up of Soil and Pile Settlement for SLCIA Site	215
Figure 6-21 Comparison Plot of Measured Undrained Cohesion or Calculated Side Friction and Maximum Measured Shear Stress vs. Depth for SLCIA Site	216
Figure A-1 Borelog of Boring B-1 Performed by AMEC for Redwood Road Site	228
Figure A-2 Borelog of Boring B-04-1 Performed by RB&G for Redwood Road Site	232

Figure A-3 Borelog of Boring B-04-2 Performed by RB&G for Redwood Road Site	233
Figure A-4 Consolidation Test Results for Samples from AMEC for Redwood Road Site.....	234
Figure A-5 Borelog of Boring 03-NB-3 Performed by RB&G for SLCIA Site.....	235
Figure A-6 Borelog of Boring 03-NB-4 Performed by RB&G for SLCIA Site.....	237
Figure A-7 Borelog of Boring 03-NB-6 Performed by RB&G for SLCIA Site.....	240
Figure A-8 Void Ratio vs. Pressure Curve for Consolidation Test from Boring 03-NB-2, 9' - 10.5'	241
Figure A-9 Log of Time Series Curve for Sample from Boring 03-NB-3, 9' - 10.5', 1.15 to 2.3 Tons	241
Figure A-10 Log of Time Series Curve for Sample from Boring 03-NB-3, 9' - 10.5', 2.3 to 4.6 Tons.....	242
Figure A-11 Square Root of Time Series Curve for Sample from Boring 03-NB-3, 9' - 10.5', 1.15 to 2.3 Tons.....	242
Figure A-12 Square Root of Time Series Curve for Sample from Boring 03-NB-3, 9' - 10.5', 2.3 to 4.6 Tons.....	243
Figure A-13 Void Ratio vs. Pressure Curve for Consolidation Test from Boring 03-NB-2, 21' - 22.5'.....	243
Figure A-14 Log of Time Series Curve for Sample from Boring 03-NB-3, 21' - 22.5', 1.15 to 2.3 Tons.....	244
Figure A-15 Log of Time Series Curve for Sample from Boring 03-NB-3, 21' - 22.5', 2.3 to 4.6 Tons.....	244
Figure A-16 Square Root of Time Series Curve for Sample from Boring 03-NB-3, 21' - 22.5', 1.15 to 2.3 Tons.....	245
Figure A-17 Square Root of Time Series Curve for Sample from Boring 03-NB-3, 21' - 22.5', 2.3 to 4.6 Tons.....	245

Figure A-18 Void Ratio vs. Pressure Curve for Consolidation Test from Boring 03-NB-3, 3' - 4'.....	246
Figure A-19 Void Ratio vs. Pressure Curve for Consolidation Test from Boring 03-NB-3, 12' - 13.5'.....	246
Figure A-20 Void Ratio vs. Pressure Curve for Consolidation Test from Boring 03-NB-4, 93.5' - 95'.....	247
Figure A-21 Void Ratio vs. Pressure Curve for Consolidation Test from Boring 03-NB-5, 3' - 4.5'.....	247
Figure A-22 Void Ratio vs. Pressure Curve for Consolidation Test from Boring 03-NB-5, 21' - 22.5'.....	248
Figure A-23 Void Ratio vs. Pressure Curve for Consolidation Test from Boring 03-NB-3, 35' - 36.5'.....	248
Figure A-24 Void Ratio vs. Pressure Curve for Consolidation Test from Boring 03-NB-6, 18' - 19.5'.....	249
Figure A-25 Log of Time Series Curve for Sample from Boring 03-NB-6, 18' - 19.5', 1.15 to 2.3 Tons.....	249
Figure A-26 Log of Time Series Curve for Sample from Boring 03-NB-6, 18' - 19.5', 2.3 to 4.6 Tons.....	250
Figure A-27 Square Root of Time Series Curve for Sample from Boring 03-NB-6, 18' - 19.5', 1.15 to 2.3 Tons.....	250
Figure A-28 Square Root of Time Series Curve for Sample from Boring 03-NB-6, 18' - 19.5', 2.3 to 4.6 Tons.....	251
Figure A-29 Void Ratio vs. Pressure Curve for Consolidation Test from Boring 03-NB-6, 27' - 28.5'.....	251
Figure A-30 Log of Time Series Curve for Sample from Boring 03-NB-6, 27' - 28.5', 1.15 to 2.3 Tons.....	252
Figure A-31 Log of Time Series Curve for Sample from Boring 03-NB-6, 27' - 28.5', 2.3 to 4.6 Tons.....	252

Figure A-32 Square Root of Time Series Curve for Sample from Boring 03-NB-6,
27' - 28.5', 1.15 to 2.3 Tons..... 253

Figure A-33 Square Root of Time Series Curve for Sample from Boring 03-NB-6,
27' - 28.5', 2.3 to 4.6 Tons..... 253

1.0 Introduction

In the age of modern construction, finely-engineered structures soar majestically above the ground. On the outside, the appearance of these buildings excites the awe of people with many different backgrounds. Within the engineering community it is known that each building has been designed to withstand various loading demands to which the superstructure and foundation will be subjected. The future of the building is dependant upon multiple interactions in the engineering world, some of which are well known and others where understanding is still evolving. As time has progressed, significant progress has been made in understanding the interaction of structural elements with natural and man-made forces and also the interaction of foundation elements with subsurface conditions.

The presence of multi-story buildings and large-span bridges coupled with the existence of weak surface soils often necessitates the use of deep foundation systems to prevent bearing capacity failure or excessive settlement. Deep foundations can transfer the structural load through a weak soil to a stronger bearing stratum. If a bearing stratum is too deep, the structural load can also be transferred by skin friction between the pile and surrounding soil. The use of pile foundations is not new in the engineering community, but many of the interactions between the superstructure and the surrounding soil are constantly under scrutiny and extensive research. The use of structural members

manufactured to certain specifications facilitates understanding of how loads will be transmitted between structural members and from the superstructure to the foundation. However, since the soil upon which the structure is built is not engineered, less certain understanding exists regarding how the soil will react when in contact with the foundation elements.

1.1 Skin Friction

The influence of skin friction on pile foundations, both positive and negative, has been known for many years. Although the presence of positive friction has historically been the more researched aspect, the presence of negative skin friction, commonly referred to as downdrag, is being researched at an increased rate due the consequences of its neglect in design. Positive skin friction develops when the pile settles relative to the surrounding ground. In contrast, negative skin friction develops when the surrounding soil settles relative to the pile. Both frictions require some degree of movement between the pile and soil in order to be mobilized. Negative skin friction can develop from a number of causes, such as settlement of a compressible clay layer, settlement of a collapsible soil due to wetting, settlement of a layer due to liquefaction or settlement due to a dewatering.

1.1.1 Process of Developing Skin Friction

A depiction of the development of skin friction, both positive and negative is shown in Figure 1-1. In Figure 1-1(a), dead and live loads imposed on a pile foundation by a bridge or building are typically resisted by positive skin friction acting on the side of the pile and by toe resistance acting at the toe of the pile. As load is applied to the pile, it

settles relative to the surrounding soil, thus inducing positive skin friction. Skin friction, in general, is usually fully developed or “mobilized” with pile movement of 2.5 to 5 millimeters (0.1 to 0.2 inches) while to fully develop toe resistance, movement equal to 5% to 10% of the pile diameter/width may be required. The load in the pile for this situation is shown in Figure 1-1(b). At the head of the pile, the load is equal to the dead and live load, but the load in the pile decreases with depth as the load is transferred to the surrounding soil by positive skin friction. The load in the pile at the toe is equal to the toe resistance provided by the soil below the toe of the pile.

If the pile is driven through a compressible soil layer near the surface to a stronger soil layer at depth and fill is placed around the pile, as could be the case for an approach fill for a bridge, then the settlement of the compressible soil may exceed the settlement of the pile. When the settlement of the compressible soil exceeds the settlement of the pile sufficiently – a few millimeters as mentioned above – negative skin friction develops as shown in Figure 1-1(c). At some depth, the pile will once again settle more than the surrounding soil and positive skin friction will develop as illustrated in Figure 1-1(c).

The boundary between positive and negative skin friction is known as the neutral plane and represents the depth where the settlement of the pile and surrounding ground are equal, and where the load in the pile is the greatest. Negative skin friction acting on the pile creates a “dragload” on the pile in addition to the pile head load. As a result, the load in the pile increases from the pile head to the neutral plane and then decreases from the neutral plane to the pile toe as illustrated in Figure 1-1(d). Therefore, the increased load in the pile must be appropriately considered in designing the pile foundation.

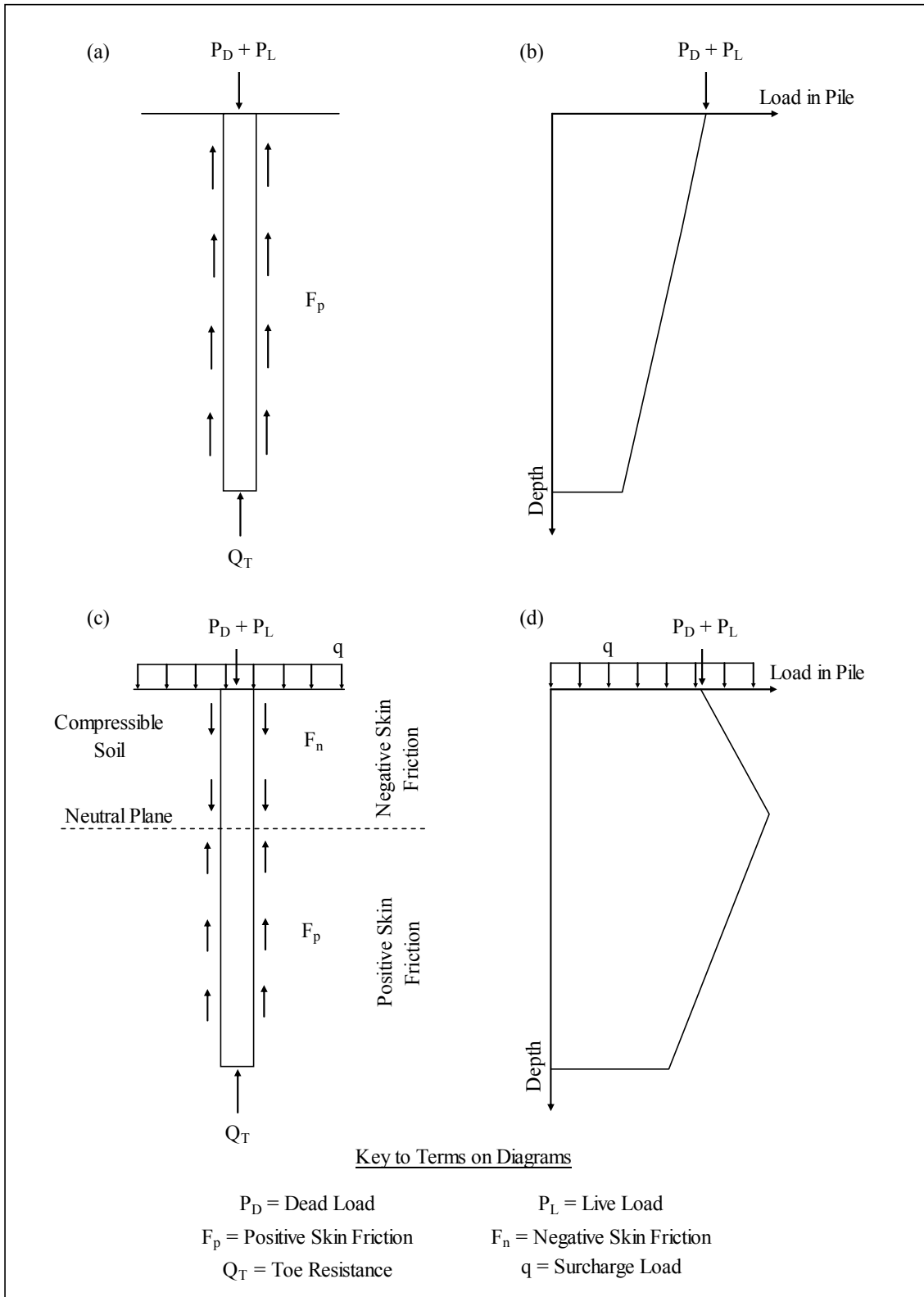


Figure 1-1 Illustration of (a) Forces Acting on a Pile and (b) Load in the Pile for Typical Case Involving Positive Skin Friction along with (c) Forces Acting on a Pile and (d) Load in the Pile for Case Involving Negative Skin Friction

1.1.2 Evaluation of Ultimate Pile Capacity with Downdrag

Although the concepts discussed above are widely recognized, there is significant variation in how designers consider negative skin friction in engineering practice. For example, some designers try to ensure that the dead load (P_D) and live load (P_L) at the pile head, plus the dragload (F_n) is less than the resistance provided by the sum of positive skin friction (F_p) and toe resistance (Q_T) divided by a factor of safety (FS), typically ranging from 2.0 to 2.5, as shown in Equation 1-1.

$$P_D + P_L + F_n \leq \frac{(F_p + Q_T)}{FS} \quad (1-1)$$

Accounting for the negative skin friction has a double effect. First, since some of the pile is experiencing negative skin friction, that same portion of the pile cannot be counted on for positive skin friction, thus reducing the quantity of resistance supplied by positive skin friction. Secondly, the negative skin friction, as accounted for in this equation, becomes another load that must be counteracted by the resisting forces on the pile, thus requiring a significantly greater pile length or diameter to support the structure.

In contrast, Fellenius (1998) recommends that the pile be designed such that the dead and live load do not exceed the ultimate load capacity of the pile using Equation 1-2.

$$P_D + P_L \leq \left(\frac{Q_S + Q_P}{FS} \right) \quad (1-2)$$

In Equation 1-2, Q_s is the ultimate positive side resistance along the entire length of the pile (not just below the neutral point) and Q_p is the ultimate resistance at the base of the pile. P_D , P_L and FS are the same as in Equation 1-1. The rationale for this equation is that if the applied axial load began to reach the ultimate state, the pile would settle relative to the surrounding soil at very small displacements and positive skin friction would redevelop in the soil above the original neutral plane. Therefore, for the ultimate state the influence of dragload force is neglected and the ultimate capacity is identical to what one would use for the conventional loading case illustrated in Figure 1-1(a) and (b).

According to Fellenius (1998), dragload only needs to be considered to evaluate the structural axial capacity of the pile and the potential for excessive pile settlement. The allowable axial capacity of the pile (Q_{Struct}) should be designed as shown in Equation 1-3, so that the dead load combined with the dragload (F_n) above the neutral plane does not exceed the compressive strength of the pile.

$$Q_{Struct} \geq P_D + F_n \quad (1-3)$$

The load distribution along the length of the pile after the development of dragload and at the ultimate state is illustrated in Figure 1-2. This figure highlights the concept that at the ultimate state, an increased amount of reserve capacity (remaining capacity before failure of the pile) could be developed due to negative skin friction changing to positive and toe resistance becoming fully developed. In Figure 1-2, D is the applied dead load, PL is the permanent live load, Q_u is the ultimate soil capacity, F_n is the

dragload, F_{pu} is the positive shear resistance and Q_{pu} is the ultimate toe resistance of the pile.

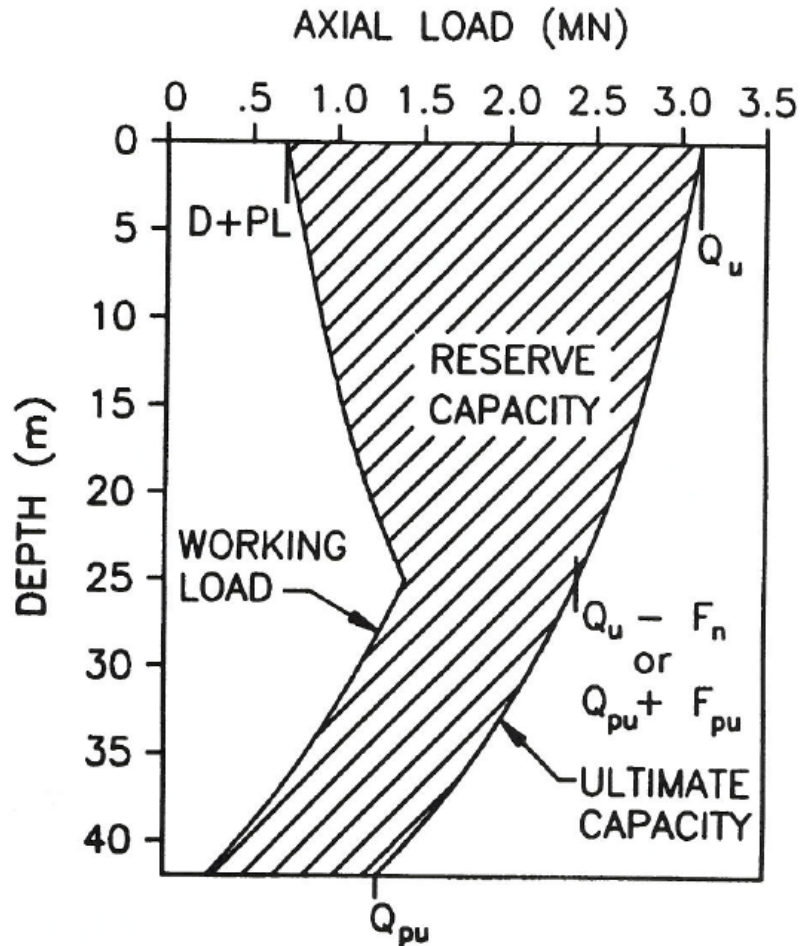


Figure 1-2 Illustration of Potential Reserve Capacity at the Ultimate State due to Reversal of Skin Friction from Positive to Negative after Initial Development of Dragload due to Negative Skin Friction (Briaud and Tucker, 1997)

As illustrated in Figure 1-1(c), the maximum load in the pile for the downdrag loading condition would occur at the neutral plane. In addition, Fellenius recommends that the pile settlement be evaluated when the pile is subjected to the dead load and dragload combined to ensure that settlements are within tolerable limits.

Because the two approaches for addressing downdrag effects are notably different from each other and lead to considerably different pile designs, it becomes of significant practical consequence to know which method best represents the physical conditions which develop in the field. This study was undertaken to improve our understanding of pile behavior when negative skin friction is anticipated. Test piles were monitored to evaluate negative skin friction during embankment construction and then after construction of bridge overpasses. Monitoring continued for about a year after construction to evaluate secondary consolidation effects on behavior.

1.1.3 Research of Negative Skin Friction

As stated previously, the phenomenon of downdrag has been known for many years and has been the topic of research, in the laboratory and in the field, for the past five or six decades. From the results of research on both positive and negative skin friction, the character of downdrag forces has become better known and accessible by design methods and computation methods. Research has also resulted in methods to mitigate or remove the downdrag forces in piles.

Research conducted in the laboratory, with computer models and with full-scale field tests on both positive and negative skin friction, has yielded multiple methods to compute the magnitude and location of the downdrag forces present. These methods range from the use of the alpha or beta coefficients, similar to approaches for positive skin friction, to computer models employing q-z and t-z curves. The complexity available in computer models potentially allows for more accurate solutions, but the other approaches can be sufficient given that enough information is available.

1.2 Objectives

Research for this study was performed to gain a better understanding of the development of dragload on abutment piles for bridges due to construction of approach fills. In addition, the effect of subsequent dead loads produced by the construction of the bridge on the load distribution in the pile was investigated. Specifically, the objectives of this study were:

1. Measure the development of dragload on piles resulting from construction of an embankment followed by bridge construction and long-term settlement.
2. Evaluate methods for predicting axial pile capacity for piles subjected to downdrag and the location of the neutral plane.
3. Develop recommendations for axial pile capacity considering downdrag.

The ultimate objective of this thesis is to provide a better understanding of the effects of structural loading on the dragload force and examine appropriate methods for predicting this force.

1.3 Scope of Work

To achieve the objectives of this study, abutment piles were instrumented at two new overpasses in Salt Lake City, Utah, after installation of the piles but before construction of the approach fills. The first site was an overpass at the Redwood Road and SR-201 intersection, while the second site was an overpass at the entrance to the Salt Lake International Airport. A third test site near Springville, Utah was instrumented and subsequently abandoned due to the malfunction of nearly all the instrumentation. One abutment pile was instrumented with 16 vibrating wire embedment type strain gauges at 8 levels at the Redwood Road site and 18 gauges at 9 levels at the Salt Lake Airport. The

gauges were placed in the piles prior to filling the piles with concrete to monitor the forces within the pile on a continuous basis. After installation of wick drains and construction of the approach fill, settlement was monitored over time. Monitoring of the instrumentation continued on a long-term basis while the bridge was constructed and dead load was applied to the pile. Monitoring then continued for another 12 to 19 months following the completion of bridge construction to evaluate the effect of secondary consolidation. Therefore, the distribution of load within the test piles can be evaluated after fill placement, then after bridge construction, and finally during secondary consolidation.

Using data from this study, skin friction was computed along the length of each pile as a function of depth during fill placement, ground settlement and structural load placement. The measured negative and positive skin friction and the location of the neutral plane were also compared with several available methods for predicting these parameters.

Although it is not within the scope of this work to develop a new method for calculating downdrag forces, the measured force distributions have been compared with available methods for predicting the force distribution in an attempt to recreate the magnitude and location of downdrag forces. Recommendations regarding appropriate methods to account for downdrag are also made.

2.0 Literature Review

The concept of downdrag and its subsequent effects has been known for more than 60 years and full-scale research has been conducted for the past 40 years or more. Various approaches to downdrag have been proposed. These include theoretical approaches (not necessarily based on test results) to determine the location and magnitude of downdrag forces; full-scale tests; model scale laboratory and centrifuge tests; and computation methods stemming from field measurements. Little (1994) gave an excellent summary of many published experiments or theories regarding downdrag. As with most other areas in geotechnical engineering, the ability to assess and compute the various aspects of downdrag loading has improved, but various conflicting arguments continue today regarding the best way to account for downdrag in the design of pile foundations. This review of testing and analysis methods will illustrate the current state of design and recommendations regarding downdrag.

For ease in approaching the subject of downdrag, the various approaches will be divided into two categories. Theoretical approaches will be treated first to give a proper foundation on which the various testing to quantify and monitor downdrag can then be based. Following the theoretical information, the various methods and testing used to measure, monitor and estimate downdrag will be discussed. This portion will be split

into three areas, namely; full scale and model testing; laboratory, computer models and centrifuge tests; and past and present design methods.

2.1 Theoretical Approaches

As a general reference in computing side friction (positive or negative), Little (1994) refers to the total stress approach that proposes that unit side resistance (τ) on piles is a function of adhesion in cohesive soil using Equation 2-1.

$$\tau = \alpha s_u \quad (2-1)$$

In Equation 2-1, α is an empirical adhesion factor and s_u is the undrained shear strength of the clay. Tomlinson (1957) identified various factors which could affect the adhesion during the pile driving relative to undrained shear strength. Gap formation between the pile and soil, ground heave and pile shape were the primary topics identified. Little doubt can exist that a gap forms as the pile is driven, which in soft clays closes up quickly and regains most or all of its previous strength. However in stiff clays, the gap will not usually close near the ground surface, leaving a permanent opening, and thereby lowering the ultimate strength. In regards to ground heave, various experiments have been done showing that soil tends to be pushed up and away from the pile creating a permanently softened zone around the pile in some cases. Effects of pile shape on the adhesion are more inconclusive from the available data. Then current results did not show an increase in adhesion for an increase in diameter or for open ended piles. Tapered piles do seem to show an increase because of the closing of the gaps formed during driving.

Bozozuk (1972) reasserted the claim that the horizontal effective stress was related to the downdrag forces. In this approach the unit side resistance is computed with the effective stress approach utilizing Equation 2-2.

$$\tau = K\sigma'_v \tan \delta \quad (2-2)$$

In Equation 2-2, K is an earth pressure coefficient, σ'_v is the vertical effective stress and δ is the angle of friction at the soil-pile interface. He asserted that the location of the neutral point is a function of the friction angle between the soil and pile, the angle of internal friction in the soil, the submerged unit weight of the soil and the at-rest earth pressure coefficient. Bozozuk was joined in the horizontal effective stress assertion by Bjerrum et al. (1969).

Burland (1973) used the effective stress approach to analyze a large number of piles subjected to downdrag in soft clays. In this study he back-calculated a β factor as shown in Equation 2-3.

$$\beta = K \tan \delta \quad (2-3)$$

From his analysis, he concluded that the shaft friction coefficient β lies in the range of 0.25 to 0.40 regardless of the type of clay. Using this conclusion, he suggested the same approach could be used to find the magnitude of negative skin friction and set an upper limit of 0.25 for β in soft clay.

Little (1994) indicates that Zeevaert (1959) proposed the existence of a “hang-up” effect which occurs in pile groups. This “hang-up” effect is used to explain the cause for

cases where the inner piles in a group may have a lower magnitude of downdrag than piles on the outer edges and corners.

Little (1994) also cites Buisson et al. (1960) as being the first to have explained that the shear stress and shear strain of the pile are related and that a point exists on the pile in which there is no relative movement between the pile and surrounding soil, therefore at this point no loads are being transferred between the soil and pile. Theoretically, negative skin friction develops above this point while positive skin friction develops below this point. This method acknowledges the neutral point concept, but differs from the approach of Terzaghi and Peck (1948) in that the neutral point is not necessarily located on the level of the bearing layer.

2.2 Full Scale and Model Testing

Chellis (1951) reports on a number of case histories where failure occurred due to dragload. These case histories come from pile supported structures such as an oil mill, water-front structures, a concrete stadium, a steel mill and battered piles. In each case, settlement in underlying layers, from a variety of causes, produced a dragload on the piles sufficient to overcome design loads and cause excessive settlement and failure of the structure.

Locher (1965) reported the results of tests using a combination of cast-in-place and precast piles to reduce the amount of downdrag for a project near Berne, Switzerland. Downdrag forces were assumed to be very large for the project. Therefore to minimize cost and time, they developed a foundation where a smaller diameter precast concrete pile was placed on top of a bored, cast-in-place pile that was terminated in the bearing layer. This created larger bearing forces for the cast-in-place pile and less surface area to

generate downdrag in the remaining precast pile. Previous methods suggested by Terzaghi and Peck (1948), Zeevaert (1959) and Elmasry (1963) were compared to each other and the actual capacity of the piles used.

Johannessen and Bjerrum (1965) instrumented two steel pipe piles driven through approximately 44 m of soft clay to bedrock. A fill with a total height of 10 m was placed one year after the piles were driven. Eleven months following the placement of the fill, a total settlement of 1.7 m was observed, at the top of the fill with 0.5 m of the total being caused by a slide that occurred because of nearby dredging. From the settlement occurring at the site, a dragload of approximately 250 tons was measured, with the neutral plane appearing to be located at the top of bedrock. This level of force, overcame the bearing capacity of the bedrock, and resulted in 6 cm of settlement of the pile head. It was determined that the negative skin friction forces could be approximated by the effective stress method, with a β value of 0.20 at the maximum load on the pile.

Endo et al. (1969) conducted studies on four piles with varying characteristics placed in silty sand and sandy silt soil conditions. The soil at the site was settling approximately 15 cm/year due to dewatering. Properties of the four piles used in the study are shown in Table 2-1.

The maximum downdrag load measured on any pile was approximately 610,000 lbs. Results from this study showed an obvious difference in loads experienced for the variety of pile types. Differences between open- and closed-ended piles were the largest noted after the two year study was completed. The results for pile cE43 during the two years is found in the plot to the left in Figure 2-1, and loads for each pile after two years are shown on the plot to the right in Figure 2-1. Beta values for the various piles were

calculated to be between 0.2 for the open point pile and 0.35 in the closed point bearing pile. Endo et al. (1969) showed that results for downdrag loads could be estimated with fair accuracy by half the unconfined compressive strength (i.e. $q_u/2$), but the recommendation was made to use the effective stress approach.

Table 2-1 Pile Properties for Study Conducted by Endo et al. (1969)

Type of Test Piles	Dimension (mm)	Length (m)	Symbols
Point Closed Vertical Point Bearing Pile	Diameter = 609.6 Thickness = 9.5	43	cE43
Point Closed Battered (Angle = 8°) Point Bearing Pile	Same as above	43	cB43
Point Opened Vertical Point Bearing Pile	Same as above	43	oE43
Point Closed Vertical Friction Pile	Same as above	31	cF31

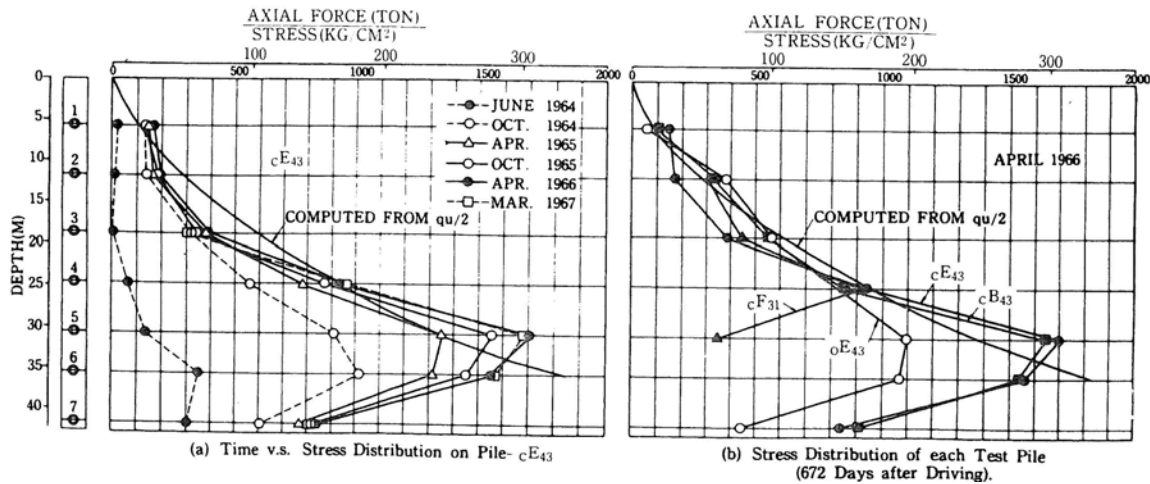


Figure 2-1 Loads in Pile cE43 Over Time and Loads in Each Pile After Two Years as Reported by Endo et al. (1969)

Bjerrum et al. (1969) reports the then-current results of a full-scale test on five steel pipe piles in soft clay. Four of the piles were driven to a bearing rock stratum and about ten meters of fill was placed to induce settlement. Two piles were used as control piles, while one was coated with a one mm layer of bitumen and the other was used to test cathodic protection using a current of four amperes at 0.6 volts. Enlarged points were used on the bitumen coated pile, the cathodic protected pile and one control pile. Results of the test showed that bitumen coating reduced the downdrag load to a mere 10% of that of the control pile. The pile using cathodic protection showed only 33% of the downdrag load of the control pile. Results of this experimentation were used to save a future project approximately 80% of the originally estimated cost.

Bozozuk (1970) conducted a full-scale test on 39-inch diameter pipe piles 270 feet long driven in marine clays. It was estimated that ten feet of settlement would be seen from the construction of an embankment to be used for an overpass. The soil profile consisted primarily of silty clay underlain by sand and then shale. During the period of record, loads up to 840 tons were attributed to downdrag. It was also noticed that the highest values of unit skin friction were seen in the upper part of the soil profile where the pore pressures had declined. This fact strongly indicated that negative skin friction is related to effective stress.

Walker and Darvall (1973) instrumented two steel pipe piles. They were driven in a soil profile consisting of an upper layer of medium fine sand, followed by a 15.5 m layer of silty clay. The silty clay layer was underlain by three meters of sandy silt and then by eight meters of dense sand and gravel. One pile was coated with 60/70 penetration bitumen with an average thickness of 1.5 mm. The coated pile was

embedded into the sandy silt layer, but not to the bearing layer. The uncoated pile was driven two meters into the bearing layer. Loads in the uncoated pile after four months reached 180 tons while the load on the coated pile reached only three tons. The apparent effectiveness of the bitumen coating was obvious. A theoretical approach based on the finite element method was proposed and shown to have sufficient accuracy in calculating the loads at the four month time interval (see Figure 2-2).

Bozozuk (1981) reported on the ultimate bearing capacity of a single, steel pipe pile that had been subjected to previous dragloads. The pile was driven in marine clay and left for ten years while settlement occurred in the soil surrounding the pile. Figure 2-3 provides a plot of the load in the pile as a function of depth at the end of ten years. The dragload had reached nearly 1.5 MN (170 tons) at the neutral plane which was located at a depth of about 20 meters.

After the ten year period had passed, the pile was loaded with loads ranging from one-third to two times the maximum downdrag load. Following these loadings, the pile was subjected to cyclic loadings at various ranges. Figure 2-4 shows the loading schedule of the pile.

As the applied load increased, the magnitude of negative skin friction decreased above the neutral plane so that the net increase in load at the neutral plane was negligible. Eventually, as applied load increased, the friction above the original neutral plane became progressively more positive. Finally, at a load equal to two times the original dragload, the friction above the original neutral plane was almost all positive, yet the load below the neutral plane was not significantly increased. These results suggest that the presence

of downdrag is unlikely to change the ultimate capacity of the pile as applied load is increased.

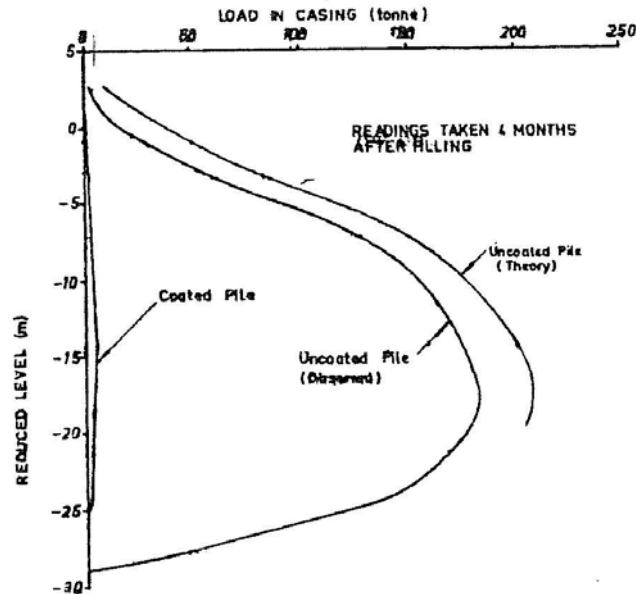


Figure 2-2 Comparison of Actual Loads and Calculated Loads from Test by Walker and Darvall (1973)

The settlement of the pile was also monitored during the loading. The results showed that the pile was able to carry loads equal to the maximum downdrag load without excessive settlement occurring. If loads exceeded the downdrag load, only short-term loading would be permissible without some additional settlement. This study concludes that downdrag loads produce a pre-stressing effect on the pile, similar to that produced by pre-stressing a concrete beam. Results of this experiment concluded that the downdrag load on a pile can prepare the pile to carry transient loads without significant settlement.

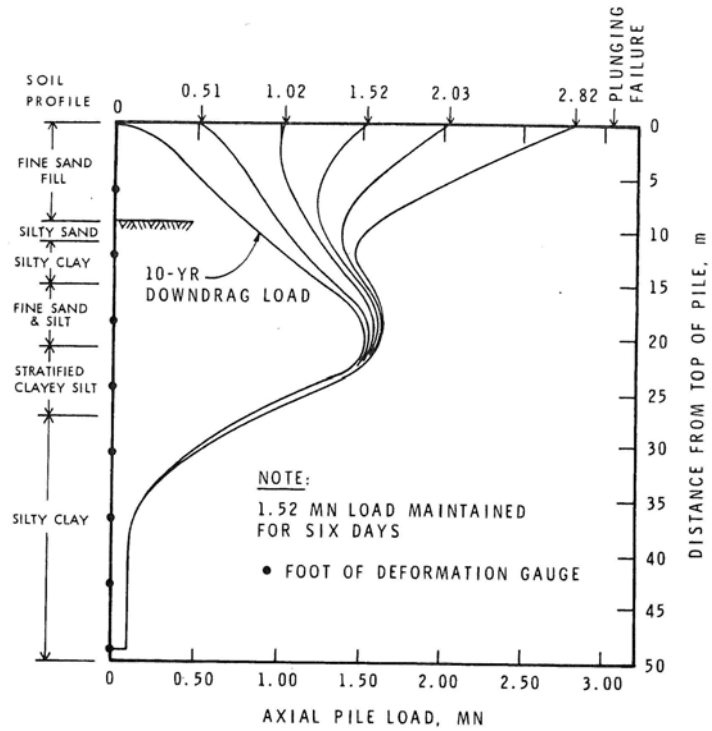


Figure 2-3 Downdrag Loads on Pile Studied by Bozozuk (1981)

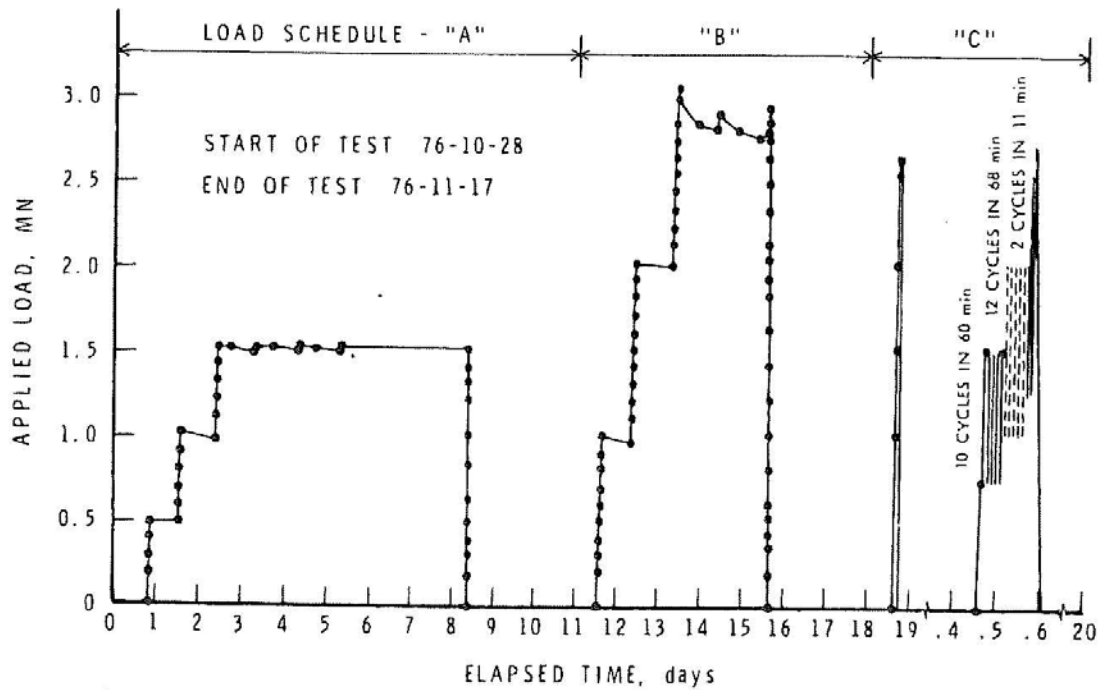


Figure 2-4 Loading Schedule for Pile Studied by Bozozuk (1981)

Mohan et al. (1981) conducted a study on a five meter long pile driven into soft clay. Fill was placed incrementally and the pile top was anchored to a yoke on the surface. Load readings were available from a load gauge placed between the yoke and a girder. After the test was completed the pile was pulled to test the ultimate skin friction. The total drag load measured in 125 days was 4.10 tons. Values for α and β were calculated with the value for α being 0.43 and the value for β equal to 0.145. The β value was acknowledged to be low in comparison to other values computed for similar clay at other sites.

Clemente (1982) instrumented five pre-stressed concrete piles to test the effectiveness of bitumen to reduce downdrag forces in the warm climate of Hawaii. Numerous difficulties were experienced through the coating process, but sufficient coatings were finally achieved. Downdrag reduction efficiencies ranging from 60 to 80 percent were observed for the coated piles versus the uncoated.

Auvinet and Hanell (1982) conducted a study of two precast concrete piles, one 30.5 m long and the other 32 m, in Mexico City where soil subsidence is heavily prevalent. Settlement of 21 cm was observed over a two-year period, being caused by nearby pumping operations. After two years, the pumps were turned off and the settlement almost stopped and in some areas heave was observed. A maximum dragload of 21 tons was measured in the friction pile (30.5 m pile) and a 32 ton load was measured in the point bearing pile (32.0 m pile). However, the point bearing pile penetrated the thin sand layer into which it was driven and ultimately acted as a friction pile. In the attempt to estimate the skin friction from equations, Equation 2-4 proved to be the most accurate to estimate the magnitude, s , at any depth, z , where c_u is the undrained shear

strength and ϕ is the friction angle of the soil. It was suggested that a settlement of two cm was required to fully mobilize the negative skin friction, instead of the few millimeters suggested previously by others.

$$s(z) = 1.5c_u \tan \phi \quad (2-4)$$

Bush and Briaud (1994) conducted measurements of dragloads on eight piles near New Orleans. The set of piles consisted of three types; steel, pre-stressed concrete and wood. One pile of each type was left uncoated with the others being coated with a variety of bitumen or other compounds to compare dragloads for the various cases. See Table 2-2 for pile dimension and coating information.

The site was located on a reclaimed marsh area with normally consolidated soft clay with interbedded layers of sands and silts. The clay became medium-stiff after about 16 meters and stiff after 24 meters. Laboratory and fields tests were done, and additional monitoring was done during the study time of two years.

Table 2-2 Pile Dimensions and Coatings for Study by Bush and Briaud (1994)

Pile Type	Pile Symbol	Diameter or Width, mm	Wall Thickness	Bitumen Coating
Closed-end Steel Pipe	SPU	324 (O.D.)	10 mm	None
	SP3			Trumbull Type 3
Square Precast, Prestressed Concrete	CPU	356	N/A	None
	CPI			Intec Blue Compound
	CPM			Intec Blue Membrane
Timber	TPU	432 (Top) 229 (Tip)	N/A	None
	TPM			Gulfseal Mastic
	TP1			Trumbull Type 1

Downdrag loads on the uncoated pile reached about 340 kN and the other two coated concrete piles had observed downdrag loads of 900 to 1000 kN. Instrumentation on all three timber piles malfunctioned and no results were available. Downdrag loads on the uncoated steel pile reached about 440 kN while the coated pile experienced only about 60 kN of downdrag forces. Loads on the uncoated and coated piles are shown in Figure 2-5 and Figure 2-6, respectively. Ground surface settlement (approximately 220 mm) and pile settlement relative to the soil were observed and recorded.

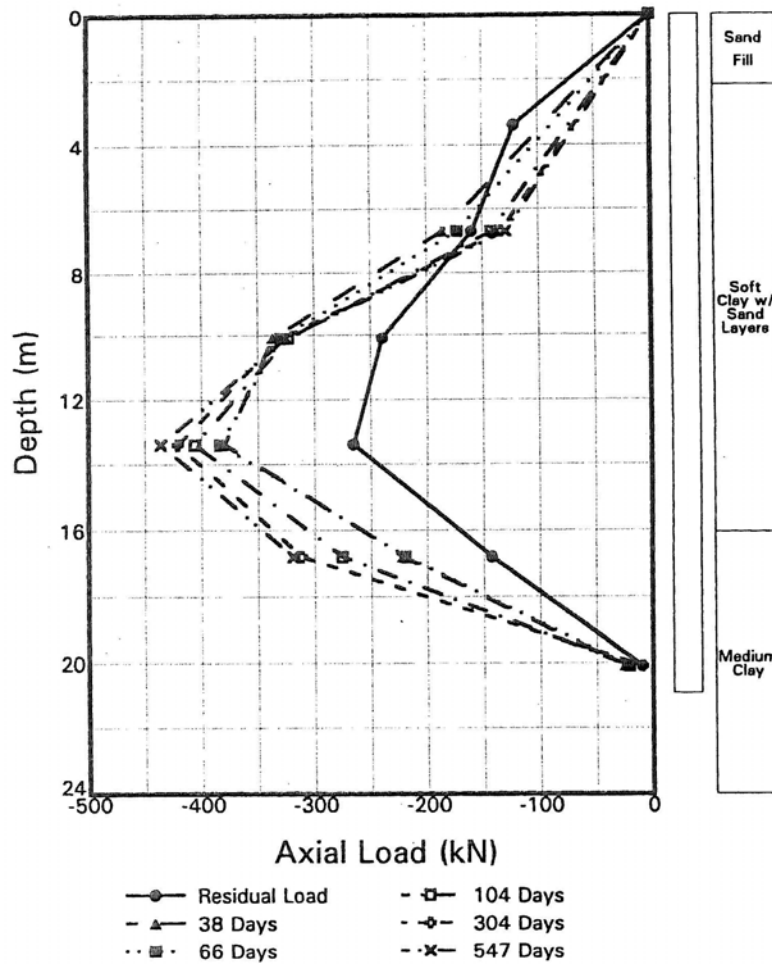


Figure 2-5 Loads in Uncoated Pile from Study Conducted by Bush and Briaud (1994)

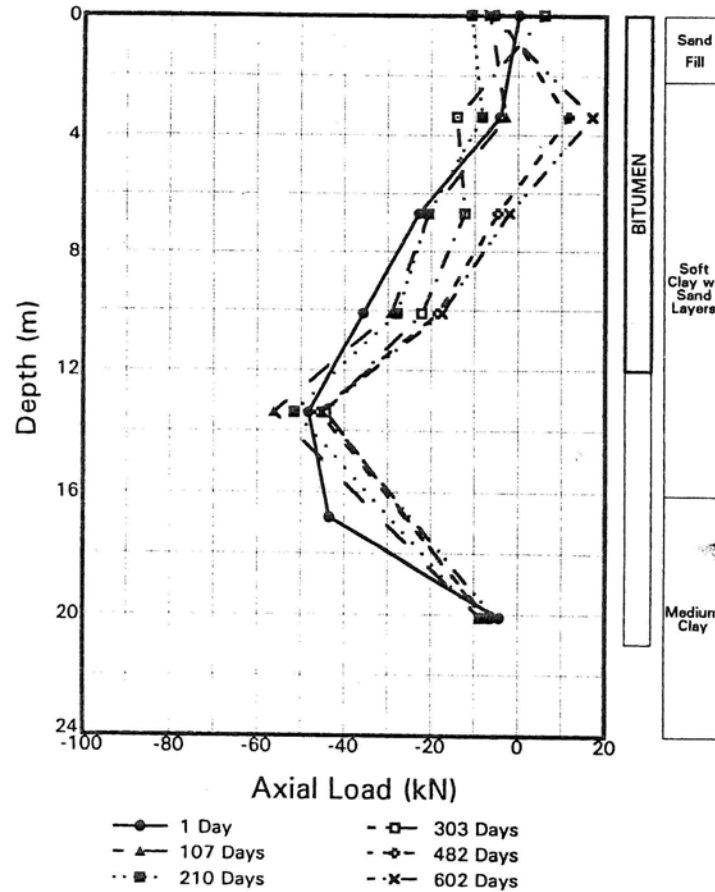


Figure 2-6 Loads in Bitumen Coated Pile from Study Conducted by Bush and Briaud (1994)

Little (1994) conducted a full-scale test in Scotland with 23 piles placed in soft to firm, normally consolidated clay. Laboratory and in-situ tests showed the soil to be highly compressible. The effect of downdrag on pile groups and a comparison of friction piles versus end-bearing piles were the focus of this study. The piles ranged in length from 16 to 20.5 meters in length.

It was found that the corner pile in the groups developed the largest dragloads and that the end bearing piles developed larger dragloads than the friction piles. Dragloads up to 250 kN were recorded for the end bearing corner pile. The depth of the neutral plane did not change much from the friction to end bearing piles. The neutral plane was only two to three meters deeper for the end-bearing piles when compared to the friction

piles. Total settlement, the combination of fill and original soil settlement, of approximately 180 mm was recorded.

Acar et al. (1994) performed a study on the downdrag of the piles supporting a supermarket in New Orleans after the foundation system failed. Foundation piles were found to have failed because of the downdrag forces induced on the piles from a 1.38 meter surcharge fill. This study was completed after the failure had occurred and could therefore not be accompanied by actual measurements of the quantity of downdrag forces.

Fellenius (1998) gave a summary of the knowledge gained to that point in the field of downdrag based on a number of case histories not cited above. It was pointed out that downdrag is a settlement problem and that dragload can produce a prestressing effect in the pile. Other primary points singled out were that live loads added to the structure reduce the dragload by the same amount as the live load, and that dragloads are not to be included in the calculations for ultimate pile capacity.

Gue et al. (1999) instrumented two piles (one center and one edge) in an embankment alongside a reinforced earth wall in Malaysia. They monitored settlement, lateral movement and downdrag forces. Observed settlement at the original ground surface amounted to 65 mm. The soil profile consisted primarily of clayey silt with occasional layers of silty sand. Instrumentation for the research was placed in the piles after driving to minimize damage to the gauges. Downdrag forces from 440 to 820 kN were observed in the middle and edge piles respectively. The lower magnitude of downdrag for the middle pile was explained by the “hang up” effect described by Zeevaert (1959).

2.3 Laboratory, Computer Models and Centrifuge Tests

Koerner and Mukhopadhyay (1972) conducted a series of laboratory tests to assess the effects of different variables not economically feasible to do by full-scale tests such as the effect of batter, group spacing, water content, pile material, asphalt viscosity and asphalt thickness. Most test yielded foreseeable results which confirmed previous ideas and theories of the character of downdrag. Tests were performed using a one-inch outer diameter pile with 10 gauges located at five different depths.

Tests showed that dragloads begins to accumulate at the top of the pile and then works its way down as more surface loading is applied. Pile batter tests showed a dramatic increase in downdrag for piles at a batter flatter than about 1:10 (horizontal:vertical). Figure 2-7 shows the relationship from their published results. The tests of pile group spacing showed an increase in downdrag until a spacing of 2.5 diameters. At spacings greater than 2.5 diameters little to no change in downdrag was observed (see Figure 2-8).

Tests on pile material were inconclusive, although tests showed that steel tends to follow the undrained shear strength curve until the water content becomes greater than the plastic limit. Concrete and wood begin lower, but tend to become parallel to the undrained shear strength curve with wood developing the full shear strength at the liquid limit. As was expected, the downdrag decreased as the water content increased due to the soil becoming less stiff as shown in Figure 2-9. This is expected because the soil loses shear strength as the water content increases.

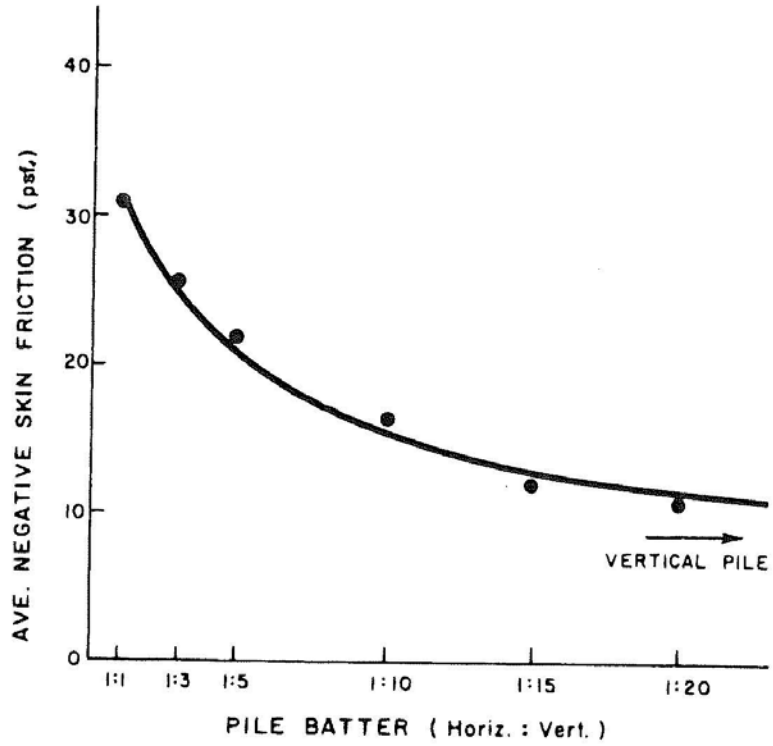


Figure 2-7 Plot Showing Relationship between Pile Batter and Downdrag Force (Koerner and Mukhopadhyay, 1972)

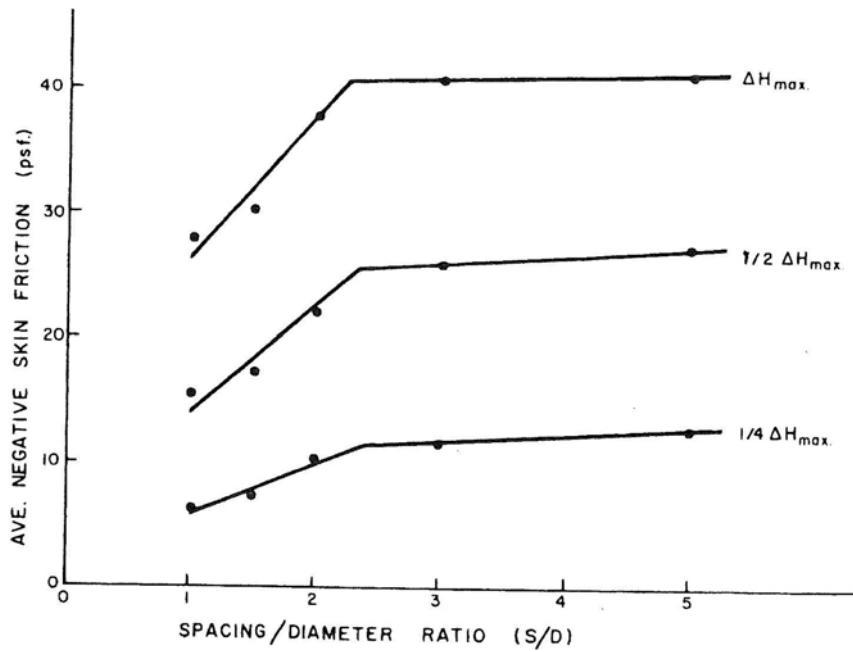


Figure 2-8 Plot Showing Relationship between Pile Spacing and Downdrag Force (Koerner and Mukhopadhyay, 1972)

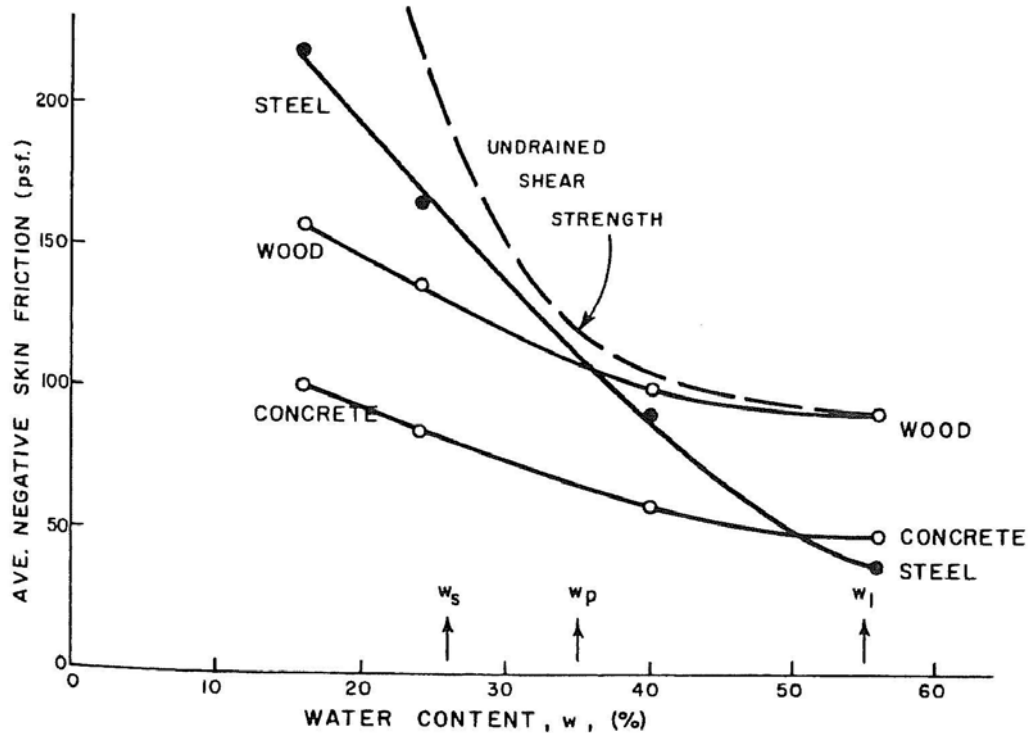


Figure 2-9 Plot to Show Relationship between Water Content, Pile Material and Downdrag Force (Koerner and Mukhopadhyay, 1972)

Tests done on piles with asphalt coating showed that as the penetration (e.g. hardness) increases so does the downdrag. This is understandable because the surface is rougher and more friction is able to build. In respect to the thickness of the asphalt layering, it was found that the thicker the coating the less downdrag was developed. All piles showed marked differences in load from the original piles tested without coating.

Leifer (1994) performed computer analyses of several piles to ascertain the effect of live loads on downdrag. Analyses were conducted using the computer program APILE2. The program determines the load-deflection response and the distribution of load and deflection with depth for a pile. Results of the analysis show that the release of downdrag loads depend heavily upon the characteristics of the pile. Leifer introduced a

pile/soil flexibility factor, f , to use in relating the decrease in dragloads. The value for f can be found using Equation 2-5.

$$f = \left(\frac{E_i}{AE} \right) \left(\frac{\pi D K L^2}{2} \right) \quad (2-5)$$

In this equation, E_i is the deflection modulus (defined in Equation 2-6), A is the cross-sectional area of the pile, E is the modulus of elasticity of the pile, D is the pile diameter, K is the portion of pile subject to downdrag (ranges from 0 to 1.0), and L is the pile length.

$$E_i = \frac{\tau_{\max}}{(Wz)_{DD}} \quad (2-6)$$

As seen in Equation 2-3 above, the deflection modulus (E_i) is found by taking the maximum shear strength (τ_{\max}) divided by the relative pile soil movement required to fully relieve negative skin friction ($(Wz)_{DD}$). Figure 2-10 shows graphically the terms of Equation 2-3.

Figure 2-11 shows the main result from the work performed by Leifer (1994). On the vertical axis the quantity DD/DD_{\max} is the value of the downdrag load remaining on the pile divided by the maximum downdrag load existing before the live load was applied. The quantity LL/DD_{\max} is the live load applied divided by the maximum downdrag load defined previously.

The shaded regions toward the right of Figure 2-11 representing smaller values of f show the sensitivity of these results for flexible piles. Site specific analyses are

recommended by the author if the pile being used falls into this category. Results from these computer models indicate that as much as six times the amount of the downdrag load be placed on the pile to fully release the downdrag load.

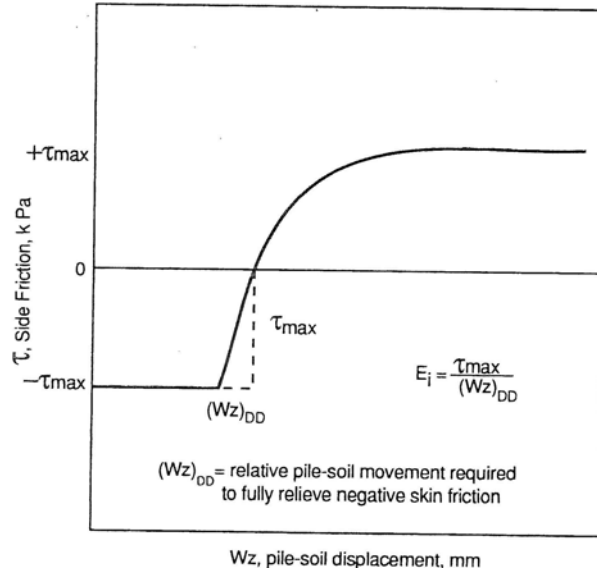


Figure 2-10 Depiction to Show Process of Obtaining E_i as Used in Method by Leifer (1994)

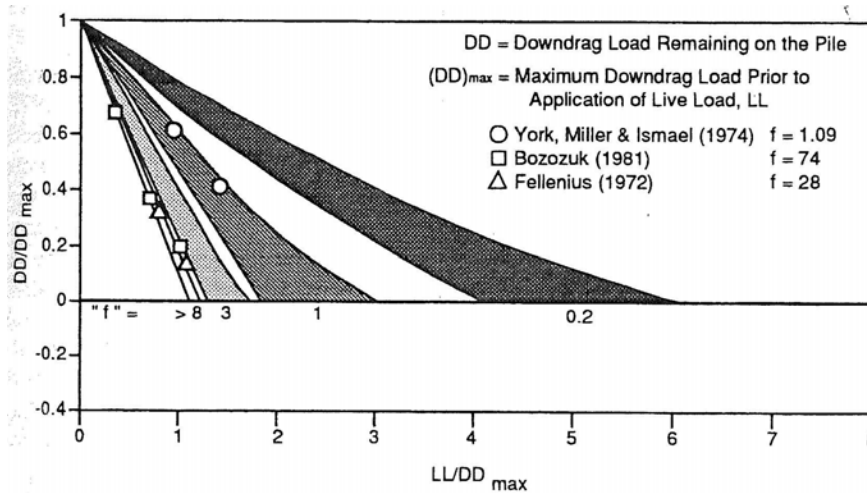


Figure 2-11 Plot from Leifer (1994) Showing Relationship between Pile/Soil Flexibility Factor, f , and Pile Loads

Leung et al. (2004) conducted several centrifuge tests to model the behavior of piles undergoing forces of negative friction and axial loading. Two separate types of tests were completed to give a better understanding of this phenomenon. The first set of tests was to study downdrag without any applied loads. The tests were done to model a prototype pile 27 m long with a diameter of 1.6 m. A diagram of the test setup is shown in Figure 2-12 (units are in mm). Tests were performed using a sand layer spun to high compaction with a layer of soft clay above the sand. The pile was inserted and the centrifuge spun until self-consolidation of the clay was complete. A surcharge layer of sand was then added to induce additional consolidation.

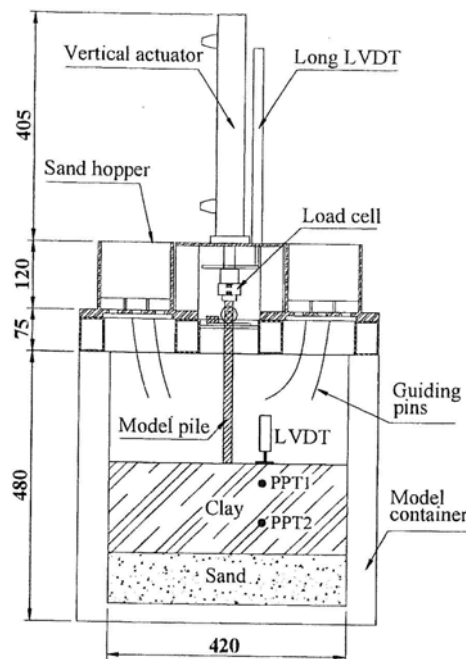


Figure 2-12 Centrifuge Test Setup for Testing Done by Leung et al. (2004)

The first series of tests evaluated the differences of a pile socketed into a bearing layer versus a pile resting on bedrock (end-bearing). Tests showed the elevation of the neutral plane for the socketed pile to be above the bearing layer and the end-bearing pile

to have its neutral plane at bedrock. The load profiles for the two tests showed very similar results until the neutral plane was encountered as shown in Figure 2-13. In Figure 2-13, Test N1 is the test for the pile socketed into the sand layer and Test N2 is for the end-bearing pile.

The next series of tests looked into the effects of applied loads. After self-weight consolidation had been achieved, yielding a dragload very close to that found in the first test, a load was applied gradually to the pile head. The dragload already in place on the pile was slowly overcome and at a load three times the dragload was finally overcome completely. This was seen as the neutral plane shifted from near the bottom of the pile to the surface of the clay layer. After the full load, half of the ultimate pile capacity, was applied, the sand surcharge layer was again placed and the model spun to achieve additional consolidation of the clay. During this process, dragloads gradually overcame the applied load and the neutral plane returned to near the base of the pile (see Figure 2-14).

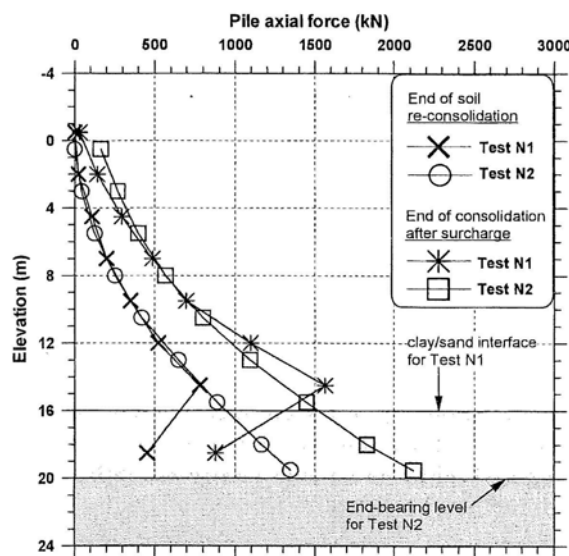


Figure 2-13 Comparison of Downdrag Loads Due to End-Bearing (from Leung et al. 2004)

Other applied loads were attempted, showing similar results. Figure 2-15 shows a comparison of the dragload recorded from the three loading tests.

The last part of the second series of tests looked into the effects of socket length into the bearing layer. Results from the additional test showed that dragload increased slightly, the neutral plane lowered slightly and the settlement of the pile head decreased for the greater socket length.

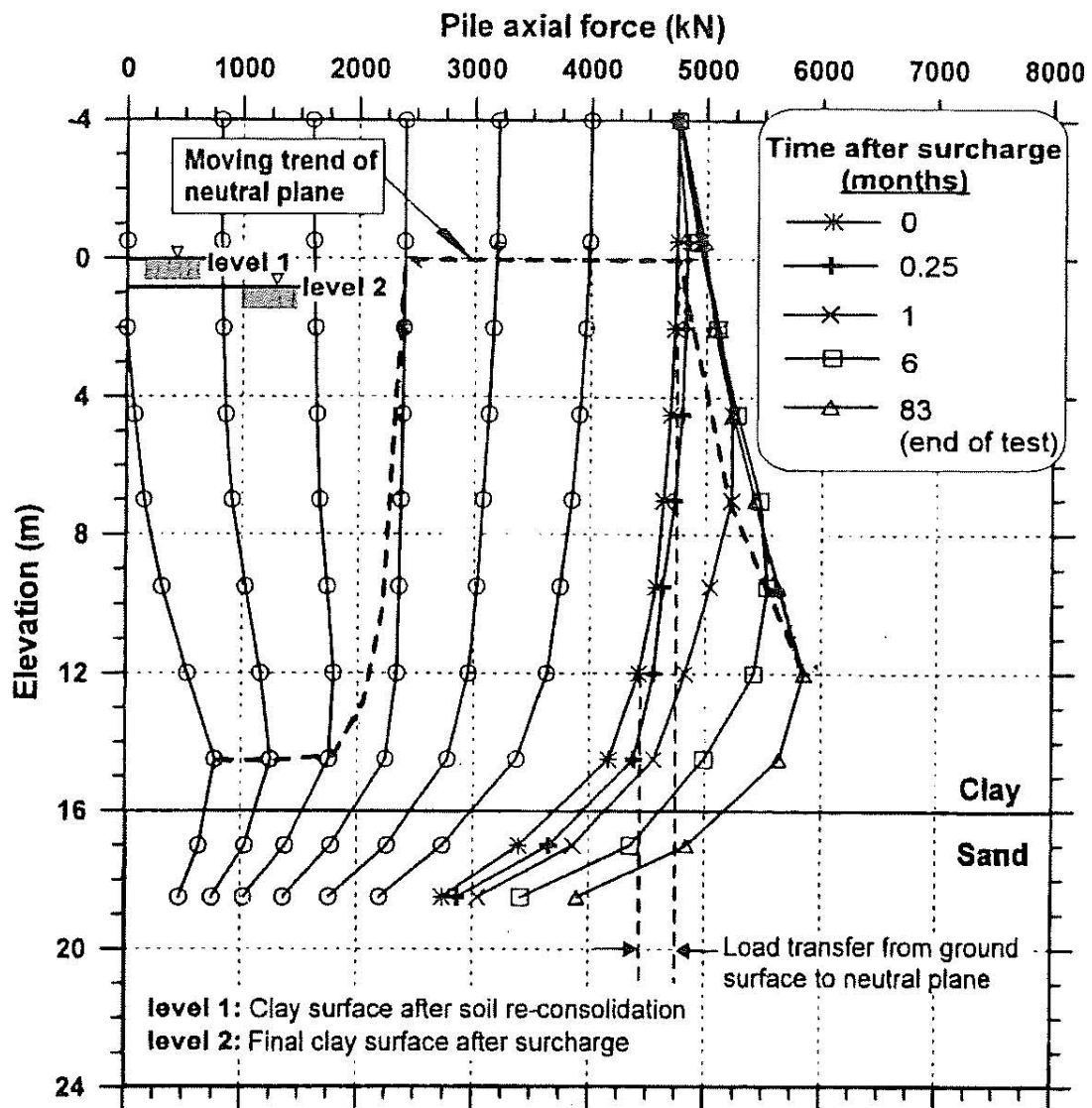


Figure 2-14 Effects of Applied Load on Location of Neutral Plane (from Leung et al. 2004)

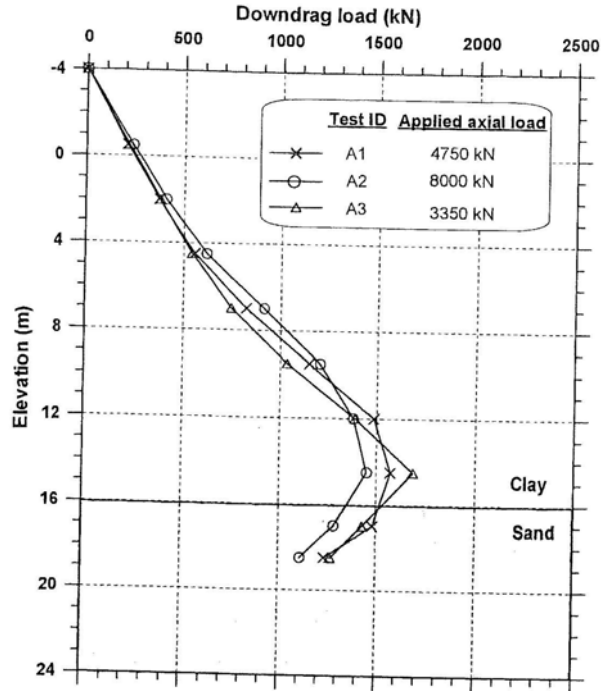


Figure 2-15 Comparison of Applied Loading Tests during Testing by Leung et al. (2004)

2.4 Previous and Current Design Methods

Terzaghi and Peck (1948) introduced one of the earliest methods to approximate the magnitude of the downdrag force. Downdrag forces are said to begin after “an imperceptible downward movement of the fill with respect to the piles.” A quantitative amount of movement was not given.

The area of a horizontal section within the boundaries of a cluster of piles multiplied by the height and unit weight of the fill, then divided by the number of piles in the cluster is the equation given to calculate the downdrag force. The maximum magnitude of the downdrag force was implied to be the product of the thickness of the clay stratum, the circumference of the pile cluster and the average shearing resistance of the clay divided by the number of piles in the cluster.

The actual value for the dragload will be between 0 and the maximum magnitude, but it was acknowledged that at various times an appropriate value could only be estimated by judgment. Terzaghi and Peck recommended that piles be spaced at a maximum of 2.5 pile diameters to minimize the effects of downdrag, assuming that the closer the piles in a cluster are spaced, the less downdrag each pile each pile will experience.

Poulos and Mattes (1969) presented a method to analyze dragload on piles using elastic theory. Approximate solutions for cases involving situations where slip occurs between the pile and soil are also presented. However, no comparisons to actual full-scale tests are given.

Zeevaert (1973) proposed a method to calculate the magnitude of the downdrag force to be expected from the surrounding soil. In this analysis, the remolding of surrounding soil is taken into consideration. The method also points out the importance of consideration of time in the overall analysis.

Poulos and Davis (1980) observed that the analysis of downdrag is affected by various factors including pile characteristics (type, method of installation, length and shape of cross section), soil characteristics (type, strength, compressibility, depth of layer and stiffness of bearing stratum), cause of soil movement and time since installation. A method was presented to calculate the magnitude of the downdrag forces and a comparison was made to previous full-scale tests conducted by Bjerrum et al. (1969) and Walker and Darvall (1973). The computed results compare well with the measured results in most cases.

Tomlinson (1986) indicates that loads imposed by downdrag must be included when considering the factor of safety for the ultimate capacity of the pile. The amount of movement to mobilize the negative skin friction is assumed to be the same as for positive skin friction, and is stated to be on the order of one percent of the pile diameter. Design curves for cases of the pile resting on a firm stratum and compressible stratum are given. For the firm stratum case, the peak downdrag force is located at a depth of 90% of the height of the fill with a magnitude equal to the effective overburden pressure multiplied by a reduction factor supplied by Meyerhof (1976) which ranges from 0.1 to 0.3 and is dependant upon the length of pile embedment. For the compressible stratum case, the peak magnitude is located where the settlement of the pile becomes greater than the settlement of the overlying soil. The magnitude of the downdrag force is calculated the same way for both cases.

Fellenius (1989) proposed a “Unified Design” approach for the design of single piles or pile groups. This design was at least partially based on his own observations of downdrag on piles (Fellenius, 1972). The approach is the same for either single piles or groups. It was noted that very small settlements are required to mobilize the skin friction on piles. The design process is broken into three parts, namely; finding the neutral plane, checking the structural capacity, and calculating settlement. Locating the neutral plane is done by satisfying the equilibrium in the pile between applied and resisting loads. The process is iterative and involves sketching the pile and scaling the loads involved. The loads involved in the pile are the dead load from the structure, the dragload from the top of the pile to the neutral plane, the positive skin friction from the base of the pile up to the neutral plane and the end bearing (see Figure 2-16). The most conservative estimate of

the neutral plane in this manner requires the assumption that the full end-bearing resistance has been mobilized. After the dead load and end bearing have been placed to scale on the top and bottom of the pile respectively, curves are drawn to represent the positive and negative skin friction. It is assumed that the slope of the lines for both friction cases is equal for a given soil layer. The approximate slope of these lines can be obtained by using shear strength properties. The location where the two curves intersect is the location of the neutral plane. As more dead load is placed on the pile, the neutral plane will move up.

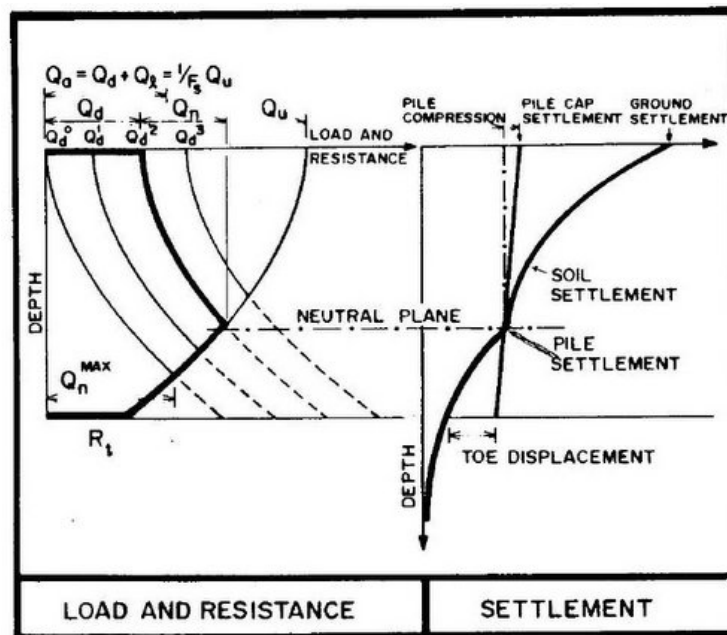


Figure 2-16 Depiction of Procedure for Locating the Neutral Plane According to the Unified Design Approach (Fellenius, 1989)

In considering the structural capacity of the pile, it was emphasized that two different loading situations must be considered. The first is to design for live loads and dead loads, but no dragloads. This case is used for determining the needed structural capacity of the pile at or near the pile cap. The second case is to include dead loads and

dragloads, but no live loads. The second case is used for determining the needed structural capacity of the pile at or near the neutral plane.

Settlement of the pile cap can be obtained by plotting the settlement of the soil as a function of depth, including layers below the bearing layer if any weak layers exist at depth, and then drawing a horizontal line from the previously found neutral plane to the settlement curve. The intersection of the two lines shows the settlement of the pile at the neutral plane. The elastic compression of the pile due to dragloads and dead loads is included from the neutral point and up and the settlement of the pile toe is obtained by continuing the elastic compression line down to the bottom of the pile. This process is also shown on the right side of Figure 2-16.

The last main point stressed in the Unified Design method is related to bearing capacity. The argument is given that dragloads must not be included in the analysis of the bearing capacity of the soil. The reason is given that bearing capacity checks against plunging failure, in which case the entire pile is moving down with respect to the soil and therefore downdrag will be eliminated. The Unified Design method stresses that only a combination of dead and live loads from the structure should be included in assessing bearing capacity.

Matyas and Santamarina (1994) presented a closed-form solution to determine the magnitude of downdrag forces and the location of the neutral plane. Rigid-plastic and elastic-plastic models were developed and presented. It was noted that the rigid-plastic model may overestimate loads by 50% and over-predict the depth for the neutral plane.

Wong and Teh (1995) proposed a method to analyze downdrag in layered soil deposits using finite element techniques. This method uses hyperbolic soil springs to

model the development of side resistance as a function of vertical deflection (t-z) curves and the development of end-bearing resistance as a function of vertical deflection (q-z) curves for each soil layer. Determination of soil parameters required to perform the analysis are described and the mention of a computer program named NSFPile is made. NSFPile was created previously to handle the procedure outlined by Wong and Teh (1995). The method was used to calculate downdrag forces reported for several previous full-scale tests. The calculations show remarkable accuracy for the five cases presented. Three of the cases presented have been presented previously (Bjerrum et al., 1969; Walker and Darvall, 1973; and Endo et al., 1969) and the other two (Fukuya et al., 1982; and Indraratna et al., 1992) are original to this paper. (See Figure 2-17 and Figure 2-18 for examples of the accuracy of the model to the actual results.) The plot in Figure 2-17 is a match to the results reported by Indraratna et al. (1992). The plot in Figure 2-18 is a match to results from Walker and Darvall (1973).

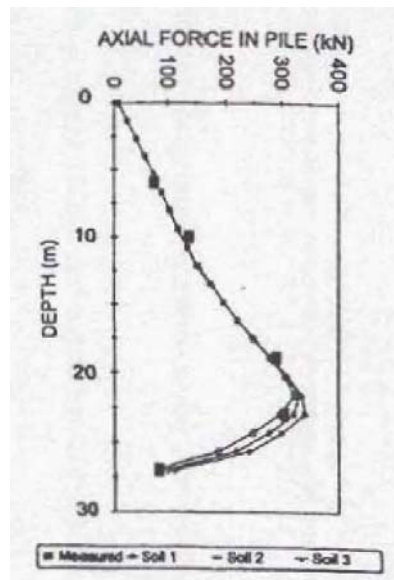


Figure 2-17 Comparisons of Method by Wong et al. (1995) to Actual Results by Indraratna et al. (1992)

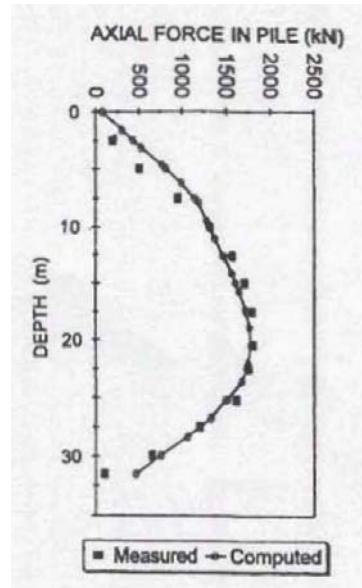


Figure 2-18 Comparison of Method by Wong et al. (1995) to Actual Results by Walker and Darvall (1973)

Das (1999) proposes “tentative” methods for piles in clay fill over granular soils and granular fill over clay. In the clay fill over granular soil method, the beta method is used. The equation given for the total downdrag load is

$$Q_n = \frac{pK' \gamma_f' H_f^2 \tan \delta}{2} \quad (2-7)$$

where, p is the perimeter of the pile, K' is the earth pressure coefficient (K_o), γ_f' is the effective unit weight of the fill, H_f is the height of the fill and δ is the soil-pile friction angle (suggested as $0.5 - 0.7\phi$). The location of the maximum force is not indicated, but the method seems to imply that the neutral plane would be at the bottom of the fill. For the second case of granular fill over clay, equations are supplied for both the location and magnitude of the downdrag force. The location of the maximum magnitude is found by using the equation

$$L_1 = \frac{(L - H_f)}{L_1} \left[\frac{L - H_f}{2} + \frac{\gamma'_f H_f}{\gamma'} \right] - \frac{2\gamma'_f H_f}{\gamma'} \quad (2-8)$$

where additional terms are defined as follows: L_1 is the depth to the neutral plane below the bottom of the granular fill, L is the total length of the pile, and γ' is the effective unit weight of the clay. The magnitude of the downdrag force is found by using the equation

$$Q_n = (pK' \gamma'_f H_f \tan \delta) L_1 + \frac{L_1^2 pK' \gamma' \tan \delta}{2} \quad (2-9)$$

Briaud and Tucker (1997) proposed a method for calculating the location of the neutral plane and the magnitude of the dragload in the pile. This method is performed by calculating a pile movement envelope. This envelope is calculated by assuming a variety of locations for the neutral plane along the length of the pile and then calculating the dragload and positive skin friction accordingly. The pile movement envelope is then compared to the settlement profile of the surrounding soil. The location where the two profiles intersect is the neutral plane.

The method requires the balancing of forces acting on the pile, as shown in Equation 2-10, where Q_t is the structural load applied to the pile, F_n is the dragload, F_p is the mobilized positive skin friction and Q_p is the point resistance.

$$Q_t + F_n = F_p + Q_p \quad (2-10)$$

In Equation 2-10, the structural load is the only value known a priori and the remaining three must be determined for each elevation along the pile.

The settlement of the pile at any depth Z is the sum of the elastic settlement in the pile below that point plus the settlement of the pile tip under the load Q_p . The elastic settlement of the pile ($\omega_{elastic}$) below the neutral point is computed using the equation

$$\omega_{elastic} = \left(Q_p + \frac{1}{2} F_p \right) \frac{L - Z}{AE} \quad (2-11)$$

where L is the total length of the pile, Z is the depth from the top of the pile to the elevation in question and AE is the axial stiffness of the pile.

The settlement of the pile tip into the bearing stratum (ω_{punch}) is computed with the equation

$$\omega_{punch} = \frac{\pi}{4} (1 - \nu^2) \frac{Q_p D}{AE_s} \quad (2-12)$$

where ν is the Poisson's ratio of the bearing soil, D is the diameter of the pile at the base, A is the area of the pile point and E_s is the Young's modulus of the bearing soil. The calculation of the dragload and the positive skin friction is performed layer by layer using the traditional method of multiplying the maximum side friction by the area of the pile in that layer. Using this method, Briaud and Tucker created a computer program by the name of PILENEG.

2.5 Need for Additional Research

The research discussed in this chapter suggests that large amounts of laboratory, field and computer tests have been completed to better understand the process of downdrag. Although additional case studies of measured downdrag will always be

needed, each study should have a more specific purpose in contributing to the overall ability to analyze the potential causes and effects of downdrag before construction begins. Plentiful research exists of downdrag magnitudes and the location of the neutral plane, while less research seems to have been completed regarding the effect of structural loading on the magnitude and location of the downdrag forces. Few full-scale tests discuss the effect of structural loading beyond the theoretical expectations of what will occur. Laboratory research done by Leung et al. (2004) has found trends for the downdrag forces and Fellenius (1989, 1998) has spoken on the overall picture of the effects of structural loading. In addition to these, Bozozuk (1981) discussed the pre-stressing mechanism of downdrag. With these exceptions, very little has been said of the effects of structural loading on the presence, location and magnitude of downdrag.

This study will add to the state of knowledge regarding dragload magnitude and load distribution, but will endeavor to more specifically study the effects that structural loading has on the location and magnitude of the maximum dragload. The measurements obtained from the work presented in this thesis will add a better understanding of dragload during the complete construction process, rather than just before and after.

3.0 Geotechnical Site Characterization

Two test sites were used to gather data regarding dragload for this thesis. Both sites are located in Salt Lake City, Utah. One site is located at the intersection of Redwood Road and SR-201 (21st South Freeway) and the other is located at the entrance to the Salt Lake City International Airport. Figure 3-1 shows a general map of Salt Lake City (Mapquest, 2008), identifying the test pile locations. Each pile is located in an abutment of an overpass. Since each site has its own geotechnical characteristics, the geotechnical investigation conducted for each site will be detailed separately.

3.1 Site Characterization of Redwood Road and SR-201 Site

The first site is located at the intersection of Redwood Road and SR-201. The existing overpass located at this intersection required replacement. The reconstruction consists of a main overpass containing three lanes in each direction. This overpass will be constructed in the same location as the current overpass. Another overpass called a “CD-Line” was constructed to the north of the main overpass, which holds two lanes. The test pile is located in the east abutment on the CD-Line. Figure 3-2 provides an aerial photo of the intersection as it appeared before construction and shows the location of the test pile.



Figure 3-1 Map of Salt Lake City, UT, with Locations of Test Piles (Mapquest, 2008)

The Utah Department of Transportation oversaw the construction process with Ralph L. Wadsworth Construction Company, Inc serving as the general contractor.

The east abutment is approximately 42 feet wide with fill being placed to a height of approximately 25-26 feet. The approach fill continues for approximately 100 feet to the east of the abutment. A surcharge fill of eight feet was placed to accelerate settlement

which was later removed. More details regarding of the approach abutment construction will be discussed later in the thesis.



Figure 3-2 Aerial Photo of Redwood Road and SR-201 Site before Construction with Location of Test Pile (USGS, 2003)

Geotechnical borings were performed by three separate firms, namely; Kleinfelder Consultants Inc. (hereafter referred to as Kleinfelder), RB&G Engineering (hereafter referred to as RB&G) and AMEC Earth and Environmental (hereafter referred to as AMEC).

In total, 11 borings were performed and three cone penetrometer tests (CPT) were completed. A location map of the area with the locations of the borings and CPT

soundings is shown in Figure 3-3. Following construction, an additional boring was performed by RBG to obtain samples for unconfined compression tests.

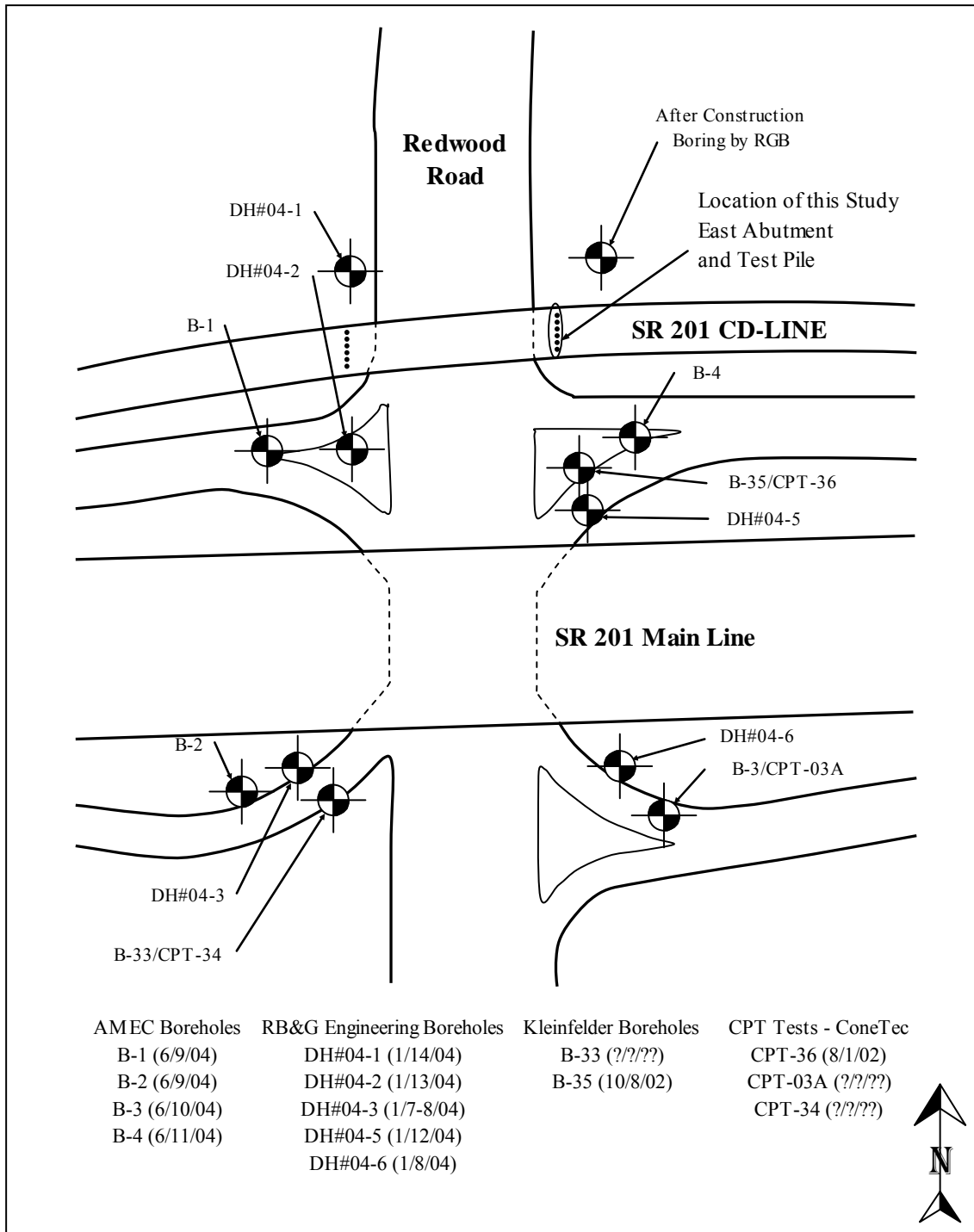


Figure 3-3 Redwood Road Site Geotechnical Boring Site Map

3.1.1 Laboratory Testing

Laboratory testing for this site consisted of determinations of gradation, Atterberg limits, undrained shear strength and consolidation parameters.

3.1.1.1 Soil Profile

Borehole data show a fairly consistent pattern of soil layering throughout the area. From the surface to a depth of about 50 feet, the soil profile consists of alternating layers of lean clay (CL) and silty sand (SM). There are occasional relatively thin layers (1 – 2 feet thick) of lean to fat clays (CL/CH). These alternating layers are underlain by a silty sand layer at approximately 50 feet below the original ground surface. A total of six boreholes were completed on the north side of the project, relatively close to the test pile, with the three boreholes in the northeast section being situated closest to the test pile as shown in Figure 3-3. The three northeast boreholes consist of boreholes B-4, DH#04-5 and B-35. Borehole B-4, completed by AMEC and shown in Figure 3-4, was completed to a depth of 76 feet. Borehole DH#04-5, completed by RB&G and shown in Figure 3-5 was drilled to a depth of nearly 50 feet. Borehole B-35, completed by Kleinfelder and shown in Figure 3-6, was bored to a depth of 81 feet. The piles extend to a depth of 54 to 55 feet below the original ground surface (ground surface varied slightly between borings), thereby resting on the silty sand layer, reaching an elevation (El.) of 4183 feet (since all elevations are given in feet, the unit will no longer be indicated).

Depth in Feet	Continuous Penetration Resistance	Graphical Log	Sample Type	Sample	Blows/foot 140 lb free-fall drop hammer	Dry Density lbs per cubic foot	Moisture Content Percent Dry Weight	Unified Soil Classifi- cation	REMARKS	VISUAL CLASSIFICATION
0								GM FILL CL	dry to slightly moist loose	SILTY FINE AND COARSE GRAVEL with some fine to coarse sand; major roots (topsoil) to 3"; brown; FILL
			D	20 4-1b-1b					slightly moist stiff	SILTY CLAY with trace fine sand; blocky; light brown to brown
5			D	14 4-6-8	91	14.3	MI/ SM		moist loose	ALTERNATING LAYERS TO 3" THICK OF CLAYEY AND FINE SANDY SILT AND SILTY FINE SAND; brown
							CL/ ML		moist to saturated stiff	ALTERNATING LAYERS UP TO 3" THICK OF SILTY CLAY AND CLAYEY SILT with some fine sand; numerous silty fine sand layers to 1/4" thick; brown to gray-brown
15			D	pushed	87	36.6	CL		saturated medium stiff	SILTY CLAY with some fine sand and numerous silty clay and silty fine sand layers to 1/2" thick; brown-gray
20			D	13 7-6-7			ML		saturated loose	ALTERNATING LAYERS TO 6" OF SILTY FINE SAND AND FINE SANDY SILT; gray grades with occasional silty clay layers to 1/2" thick
25			D	16 11-7-9						

GROUNDWATER			SAMPLE TYPE	
DEPTH	HOUR	DATE	A	S
9.2		06-11-04		
7.1	16:00	07-13-04		

A - Auger cuttings
 S - 2" O.D. 1.38" I.D. tube sample.
 U - 3" O.D. 2.42" I.D. tube sample.
 T - 3" O.D. thin-walled Shelby tube.
 D - 3 1/4" O.D. 2.42" I.D. tube sample.
 C - California Split Spoon Sample



Figure 3-4 Borelog for Borehole B-4 Completed by AMEC for Redwood Road and SR-201 (continued on next page)

LOG OF TEST BORING NO. B-4

JOB NO. 4-817-004821 DATE 06-11-04

Depth in Feet	Continuous Penetration Resistance	Graphical Log	Sample Type	Blows/ft 140 lb. 30" free-fall drop hammer	Dry Density lbs. per cubic foot	Moisture Content Percent of Dry Weight	Unified Soil Classifi- cation	REMARKS	VISUAL CLASSIFICATION
25									
30			D pushed		83	35.0	CL/ CH	saturated medium stiff	SILTY CLAY with trace fine sand and numerous clayey silt layers to 1/4" thick; gray
35			D pushed				CL	saturated medium stiff	SILTY CLAY with trace fine sand and numerous clayey silt and fine sandy silt layers to 1/4" thick; gray
40			D 38 10-18-20				ML/ SM	saturated medium stiff	ALTERNATING LAYERS TO 6" THICK OF FINE SANDY SILT AND SILTY FINE SAND; occasional clayey silt layers to 1/4" thick; gray
45			D 17 5-6-11				CL	saturated stiff	SILTY CLAY with trace fine sand and numerous clayey silt and silty fine sand layers to 1" thick; dark gray
50			D 117 18-40-77				SP/ SM	saturated very dense	FINE TO COARSE SAND with some silt; gray

GROUNDWATER		
DEPTH	HOUR	DATE
9.2		06-11-04
7.1	16:00	07-13-04

- SAMPLE TYPE
- A - Auger cuttings
 - S - 2" O.D. 1.38" I.D. tube sample.
 - U - 3" O.D. 2.42" I.D. tube sample.
 - T - 3" O.D. thin-walled Shelby tube.
 - D - 3 1/4" O.D. 2.42" I.D. tube sample.
 - C - California Split Spoon Sample



Figure 3-4 Borelog for Borehole B-4 Completed by AMEC for Redwood Road and SR-201 (continued from previous page)

LOG OF TEST BORING NO. B-4

JOB NO. 4-817-004821 DATE 06-11-04

Depth In Feet	Continuous Penetration Resistance	Graphical Log	Sample Type	Blows/foot 140 lb. 30" free-fall drop hammer	Dry Density lbs. per cubic foot	Moisture Content Percent of Dry Weight	Unified Soil Classifi- cation	REMARKS	VISUAL CLASSIFICATION
50									
55			D 80/5"						grades to layered fine to medium sand with some silt and silty fine sand; gray and brown-gray
60			D 80/5"						grades to fine to coarse sand with some silt; gray
65			D 13 4-6-7				CL	saturated medium stiff	SILTY CLAY with trace fine sand; gray
70			D 30 5-14-16				ML/ SM	saturated medium dense to dense	FINE SANDY SILT/SILTY FINE SAND; gray
75			D 92 11-26-66				SM	saturated dense	SILTY FINE SAND; gray

GROUNDWATER			SAMPLE TYPE
DEPTH	HOUR	DATE	
9.2		06-11-04	A - Auger cuttings S - 2" O.D. 1.38" I.D. tube sample. U - 3" O.D. 2.42" I.D. tube sample. T - 3" O.D. thin-walled Shelby tube. D - 3 1/4" O.D. 2.42" I.D. tube sample. C - California Split Spoon Sample
7.1	16:00	07-13-04	



Figure 3-4 Borelog for Borehole B-4 Completed by AMEC for Redwood Road and SR-201 (continued from previous page)

DRILL HOLE LOG		PROJECT: SR-201 / REDWOOD ROAD		PROJECT NO.: 200301058											
BORING NO. 04-5		CLIENT: UTAH DEPT. OF TRANSPORTATION		DATE: 1/12/04											
Sheet 1 of 2		LOCATION: SEE SITE PLAN: N 8027 E 4324 S		ELEVATION: 4238.2'											
		DRILLER: D. SAMPSON, N. BAILEY		LOGGED BY: M.H. V.N.B.											
		EQUIP./DRILL METHOD: CME-55 / N.W. CASING													
		DEPTH TO WATER - INITIAL: 9.7'		AFTER 24 HOURS: 9.4'											
Elev. (feet)	Depth (feet)	Lithology	SAMPLE		USCS (ASTM)	Material Description	Lab. No.	Water Content (%)	Liquid Limit (%)	Plasticity Index (%)	Coneq. 1	Coneq. 2	Coneq. 3	Pen. (lb/in)	SPT
			No.	Size (in)											
4235	5		88	7.0, 8	CL	Brown, dry LEAN CLAY									
4230	10		90	3.3, 2	CL	R. green-brown, moist to wet w/silty lenses									
	10		92	3.3, 4	CL	R. green-brown									
	10		93	3.3, 4	M	R. green-brown, wet SILT									
	10		94	3.3, 4	SM	R. brown, wet									
	10		95	4.7, 9	SM	Brown, wet, 2" brown silty layer					26.7	NP	0	65	24
	10		96	4.7, 9	SM										
4225	15		97	6.7, 7	SP-SM	POORLY GRADED SAND W/SILT					3.0	NP	2	91	7
	15		98	6.7, 7	SM										
	15		99	2.1, 2	CL	R. brown, wet, w/silty silty sand lenses									
	15		100	2.1, 2	CL	R. green, wet, w/silty silty sand layers									
	15		101	2.1, 2	CL	LEAN CLAY									
	15		102	2.1, 2	CL	R. brown, wet, 1" silty sand layer									
4220	20		103	2.1, 2	CL										
	20		104	0.0	CL/CH	dk. gray, wet, very soft									
	20		105	0.0	CL/CH	LEAN TO FAT CLAY									
	20		106	2.1, 2	CL/CH	dk. to R. gray, wet, w/silty sand lenses									
	20		107	0.0	CL/CH	LEAN TO FAT CLAY W/SILTY SAND LENSES									
	20		108	0.0	M	dk. gray									
	20		109	0.0	SM/SP-SM	SANDY SILT									
	20		110	0.0	SM/SP-SM	dk. gray, wet									
4215	25		111	7.4, 4	M	dk. gray, wet									
	25		112	8.3, 3	M	2" silty layer									
	25		113	8.3, 3	M	FINE SANDY SILT									
	25		114	0.2, 8	SM	gray/black					26.5	NP	0	45	24
	25		115	0.2, 8	SM	LEAN CLAY					45.4	44	21	0	15
	25		116	0.2, 8	SM	gray/black, wet									
	25		117	7.4, 4	SM	SILTY SAND					6.2	NP	0	64	16
	25		118	7.4, 4	SM	gray, wet					6.4	NP	0	62	18
4210	30		119	3.4, 3	SM	SILTY SAND W/CLAY LAYERS									
	30		120	3.4, 3	SM	0.25" THICK & 2" APART					24.2	NP	0	68	21
	30		121	0.0	CL/CH	mottled gray, dk. gray & black									
	30		122	0.0	CL/CH										
4205	35		123	1.3, 3	CL/CH	dk. gray & R. gray									
	35		124	0.0	CL/CH	LEAN TO FAT CLAY									
	35		125	0.2, 3	CL/CH	gray/black, wet, trace organics, slight odor									
	35		126	0.2, 3	CL/CH										
4200	40		127	1.4, 2	M	brownish-gray, wet									
	40		128	1.4, 2	M	VERY FINE SANDY SILT									
	40		129	1.4, 2	M	brownish-gray, wet									
	40		130	1.4, 2	M	1" silty layer									
	40		131	3.3, 7	SM	SILTY SAND W/SILT LAYERS									
	40		132	3.3, 7	SM	2" SILTY W/SAND									
	40		133	3.3, 7	SM	1" SILTY SAND									
	40		134	4.8, 8	SM	gray brown, wet, 1" silty layer									
4195	45		135	4.8, 8	SM	SILTY SAND W/SILT LAYERS									
	45		136	3.3, 21	SM	4" SANDY SILT									
	45		137	3.3, 21	SM	gray-brown, wet									
	45		138	3.3, 21	SM										
	45		139	3.4, 2	SM	gray-brown, wet					22.0	NP	0	62	16
	45		140	3.4, 2	SM	SILTY SAND									
	45		141	3.4, 2	SM	gray-brown, wet									
	45		142	3.4, 2	SM										
4190	50		143	4.8, 2	SM	gray-brown, wet, 4" silty layer					27.5	NP	0	61	15
	50		144	4.8, 2	SM										
	50		145	11.6, 28	SM/SP-SM	gray-brown									
	50		146	11.6, 28	SM/SP-SM	SILTY SAND TO SAND W/SILT LAYERS									

Figure 3-5 Borelog for Borehole DH#04-5 Completed by RB&G for Redwood Road and SR-201

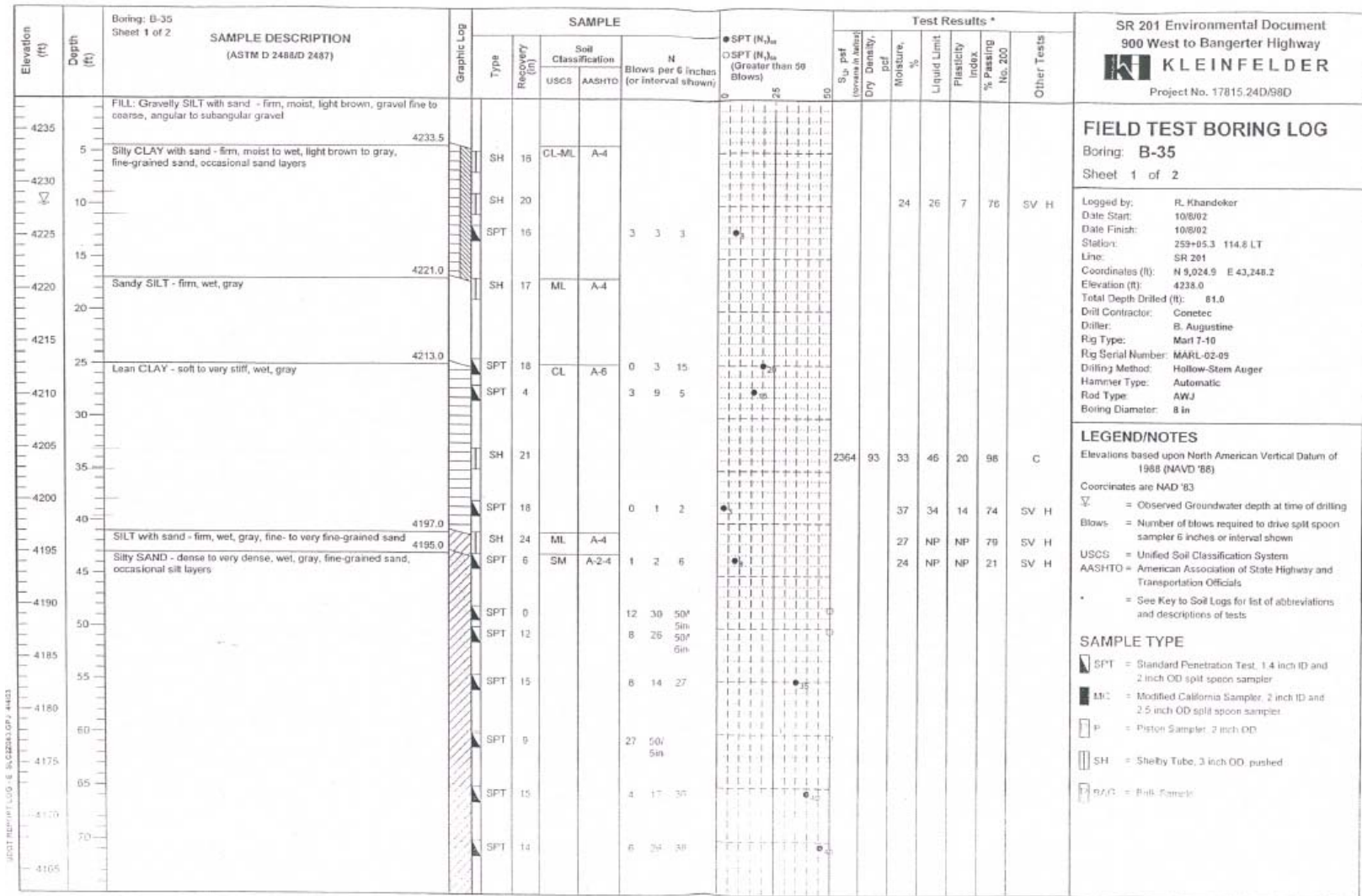


Figure 3-6 Borelog for Borehole B-35 Completed by Kleinfelder for Redwood Road and SR-201

In boring B-4 another lean clay layer was found below the silty sand layer from 63 – 69 feet below the ground surface, but this is the only borehole reporting such a layer. The water table ranged in depth from 8 to 11 feet below the original ground surface.

Boreholes located on the northwest corner, B-1, DH#04-1 and DH#04-2, were completed to depths of 76.5, 52.5 and 54 feet respectively. Data from these boreholes are consistent with soil profile seen in the northeast corner boreholes. Borelogs for these boreholes are found as Figure A-1, Figure A-2 and Figure A-3 in the Appendix.

3.1.1.2 Gradation of Samples

Gradation tests for the various samples were performed by RB&G Engineering. Only boreholes DH#04-1, 2 and 5 will be discussed from this point on because of their proximity to the test pile. The tests show that those soils classified as silty sands (SM) having an average of 73% sand and 27% fines. Those soils classified as sandy silts (ML) average 36% sand and 64% fines. The remaining gradation tests were completed on lean clays (CL) and poorly graded silty sand (SP-SM). Gradation values for the lean clays averaged 11% sand and 89% fines. The gradation for the poorly graded silty sands shows 87% sand; 5% gravel and 8% fines.

3.1.1.3 Atterberg Limit Tests

A total of ten Atterberg limit tests were completed by the three companies for this site for boreholes positioned relatively close to the test pile. A summary of these results is shown in Table 3-1.

Table 3-1 Atterberg Limit Test Results for Redwood Road & SR-201 Site

Company	Borehole	Depth Interval (ft)	USCS Soil Type	Liquid Limit (%)	Plastic Limit (%)	Plasticity Index (%)
RB&G	DH#04-1	22.5 – 24	CL-ML	25	20	5
RB&G	DH#04-1	32.5 – 33.25	CL	32	23	9
RB&G	DH#04-2	15 – 16.5	ML	27	23	4
RB&G	DH#04-2	24 – 25.5	CL	30	22	8
RB&G	DH#04-5	25.5 – 26.25	CL	44	23	21
AMEC	B-1	10 – 11.5	CL	34	20	14
AMEC	B-4	14 – 15.5	CL	29	20	9
Kleinfelder	B-35	9 -11	CL-ML	26	19	7
Kleinfelder	B-35	33 – 35	CL	46	26	20
Kleinfelder	B-35	38 – 39.5	CL	34	20	14
Average for All Tests		-----	-----	32.7	21.6	11.1

The plastic limit remains fairly constant for all of the samples with an average value of about 22. The plasticity index ranged from 5 to 21 with an average of 11, while the liquid limit ranged from 25 to 44 with an average of about 33. Figure 3-7 shows a comparison of the test results for all the Atterberg limit tests done for this site plotted on a plasticity index chart. The tests shown as being done by UDOT were completed for an earlier construction project at this site in the 1960's. As can be seen in Figure 3-7, most of the test results plot just above the "A" line in the lean clay region, with occasional tests plotting in the silt-clay or silt regions. In the general USCS plasticity index chart, the sub-regions for CL-1 and CL-2 do not exist. These have been created to enable a comparison with the plasticity index chart supplied for the Airport site that will be discussed subsequently.

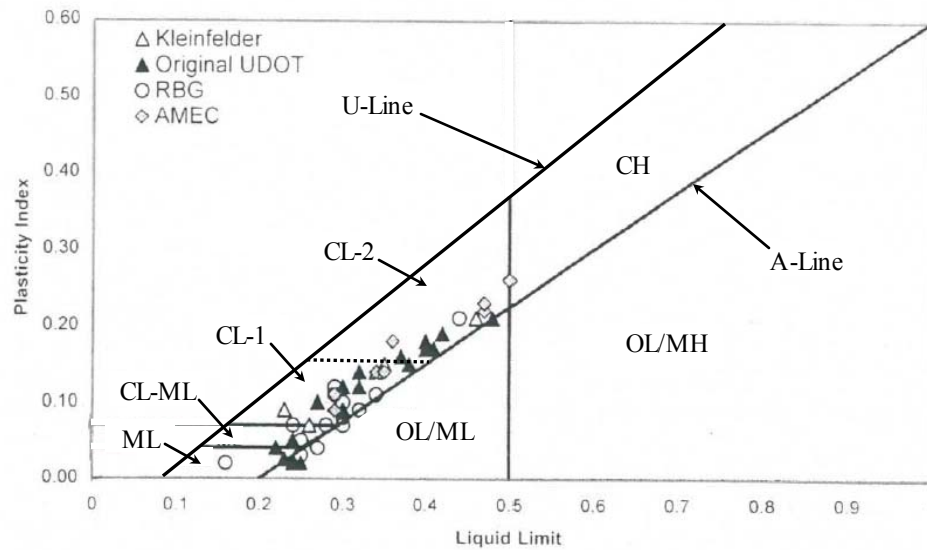


Figure 3-7 Plasticity Chart Showing Identification of Cohesive Soils for Redwood Road Project (modified from AMEC Memorandum No. 20.1)

3.1.1.4 Vane Shear Strength

A total of five vane shear tests were completed in the laboratory by AMEC for boreholes B-1 and B-4. Two were taken from borehole B-1 and the other three from borehole B-4. Measured undrained shear strength ranges from a maximum of 4225 psf to a minimum 1438 psf. However the maximum value is located above the water table only four feet from the surface and consists of sandy silt and silty sand. Therefore, this test has been ignored. The undrained strength of the lean clays tends to range from 1500 to 1800 psf. Plots of the vane shear strength results versus depth are provided for both boreholes in Figure 3-8. This figure also shows the stratigraphy for each borehole with the original ground surface at a depth of zero feet. For more details, refer to Error! Reference source not found. for the information on borehole B-4 and the appendix for information on borehole B-1.

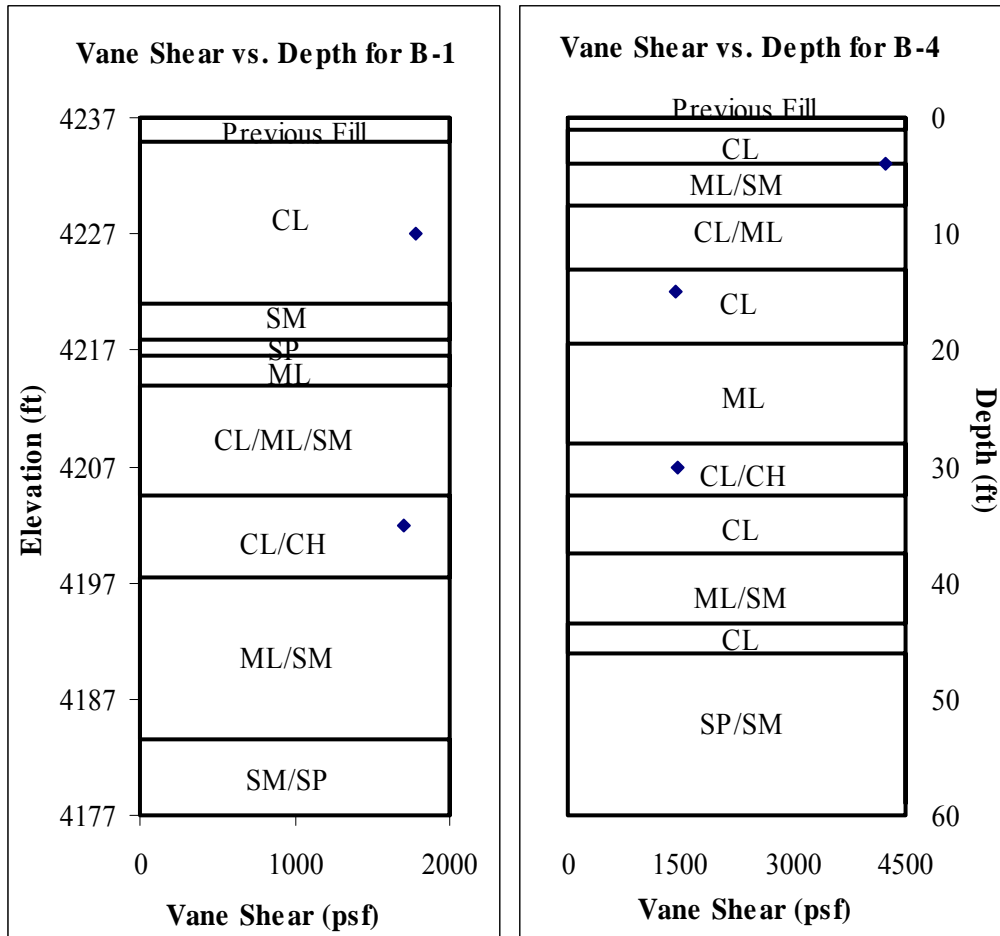


Figure 3-8 Undrained Shear Strength Profile vs. Depth Based on Laboratory Vane Shear Tests for Boreholes B-1 and B-4 Completed by AMEC for Redwood Road and SR-201

3.1.1.5 Consolidation Testing

Consolidation tests were performed on samples retrieved by AMEC from boreholes B-1 and B-4. Test results are shown in Table 3-2 and the consolidation curves are included in Figure A-4 of the Appendix. Tests completed in other boreholes tend to be closer to the results from borehole B-4. From engineering analyses for this site, it was predicted that nine inches of consolidation settlement would take place near the piles because of the embankment placement. These analyses were based on induced stresses computed using elastic theory.

Table 3-2 Soil Characteristic Data for Samples from Boreholes B-1 & B-4 by AMEC for Redwood Road & SR-201 Site

Borehole	Depth ft	USCS Classification	Water Content %	Measured Dry Unit Weight pcf	Atterberg Limits		
					LL	PL	PI
B-1	10	CL	25.9	91.1	34	50	14
B-4	15	CL	31.6	86.7	29	20	9

Table 3-3 Consolidation Test Data from Samples from Boreholes B-1 & B-4 by AMEC for Redwood Road & SR-201 Site

Borehole	Depth ft	Initial Void Ratio	σ'_v psf	σ'_o psf	Compression Ratio %	Recompression Ratio %
B-1	10	0.85	886.9	6400	0.16	0.009
B-4	15	0.94	1152.5	4000	0.095	0.008

3.1.2 In-Situ Testing

In-situ tests were completed at this site by all three firms during their field investigations. These tests include standard penetration testing (SPT), cone penetrometer testing (CPT) and torvane tests.

3.1.2.1 Standard Penetration Testing (SPT)

Sufficient SPT testing was completed to obtain a fairly good representation of the soil profile. All values of SPT tests display the uncorrected SPT value. SPT testing performed in the lean clays gave SPT values ranging from 2 to 7, while the upper sandy silt layers often had N values of 20 to 40. The base silty sand layer at the bottom of most of the boreholes yielded very high values, up to 126, showing the compact nature of the

underlying silty sand layer. Figure 3-9 shows a comparison plot of the uncorrected SPT N values versus elevation for the three boreholes nearest to the test pile location.

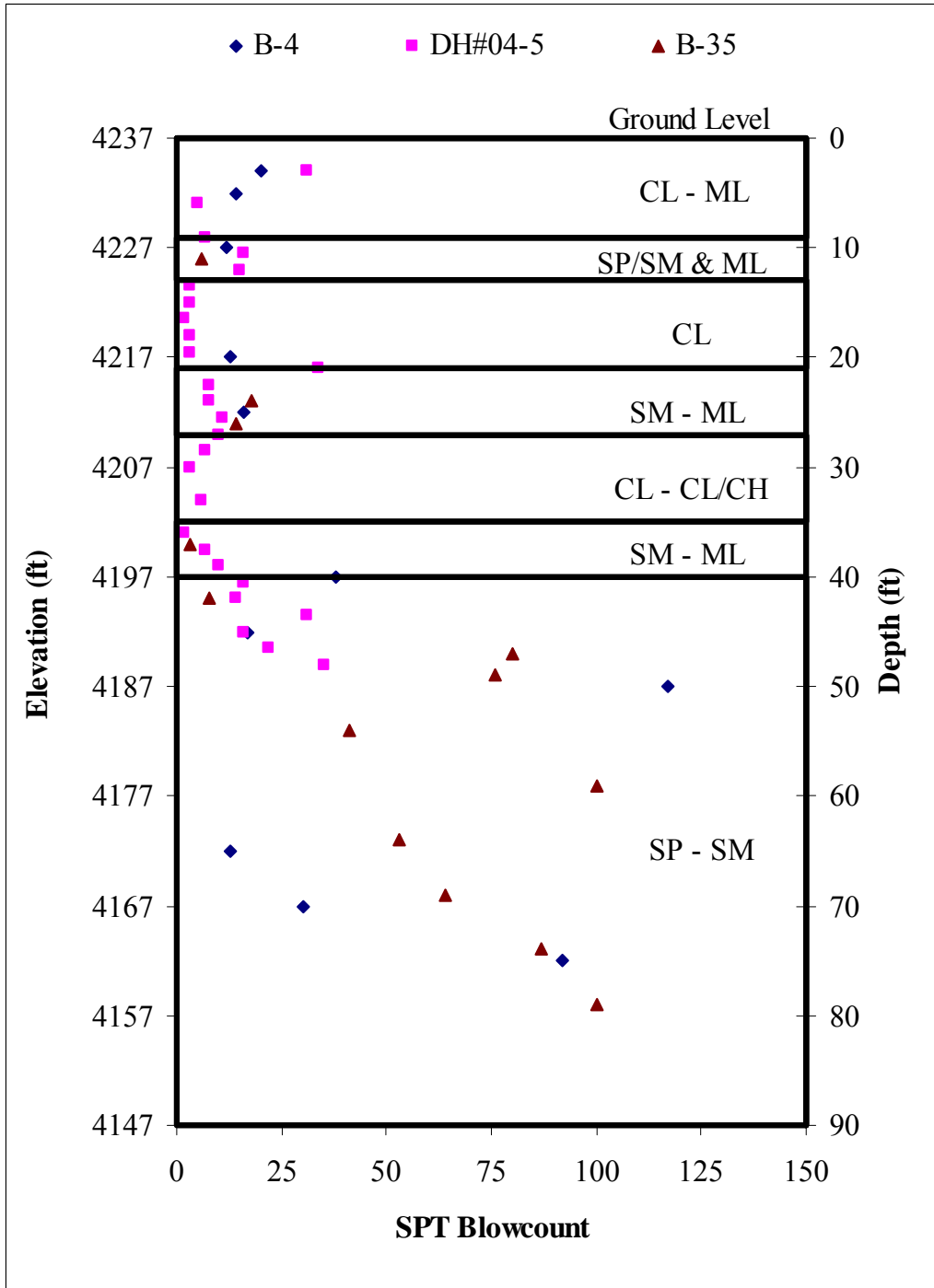


Figure 3-9 Uncorrected SPT Blowcount Comparison for Boreholes Nearest to Test Pile Location

3.1.2.2 Cone Penetrometer Testing (CPT)

Three CPT soundings were performed at the site. Only one CPT sounding (CPT-36) was completed near the test pile location and this sounding will be used primarily in the assessment of soil conditions at the site. In the cohesive zone within the upper 38 feet of the profile, cone tip resistance values were typically 10 to 25 tsf for the upper 38 feet of the profile with the exception of occasional spikes when sand and gravel layers were encountered. One such location is near the surface which exhibited a tip resistance of 320 to 450 tsf. Between El. 4220 and 4210 (approximately 20 to 30 feet below ground surface) the tip resistance occasionally spiked to values ranging from 100 to 300 tsf. Below El. 4200 (approximately 40 feet below ground surface), tip resistance began to increase to approximately 250 tsf by El. 4190 and then, for most depth intervals, remained at approximately 350 to 400 tsf with occasional drops. At approximately El. 4130, tip resistance dropped to approximately 50 tsf for about 10 feet and then began to climb back up. Figure 3-10 shows the values of cone tip resistance, sleeve friction, friction ratio, pore pressure and interpreted soil profile for the CPT sounding.

3.1.2.3 Torvane Tests

Torvane tests were performed on undisturbed samples obtained from boreholes performed by RB&G Engineering. Results from DH#04-1 and DH#04-5, shown in Figure 3-11 indicate undrained strength values greater than 0.50 tsf for the first 15 feet, but then decrease to below 0.25 tsf until 33 feet below the ground surface. Below 33 feet the torvane values tend to increase again to over 0.50 tsf with a few scattered points located at various depths. This data shows the existence of an overconsolidated surface crust due to dessication of the near surface soils.

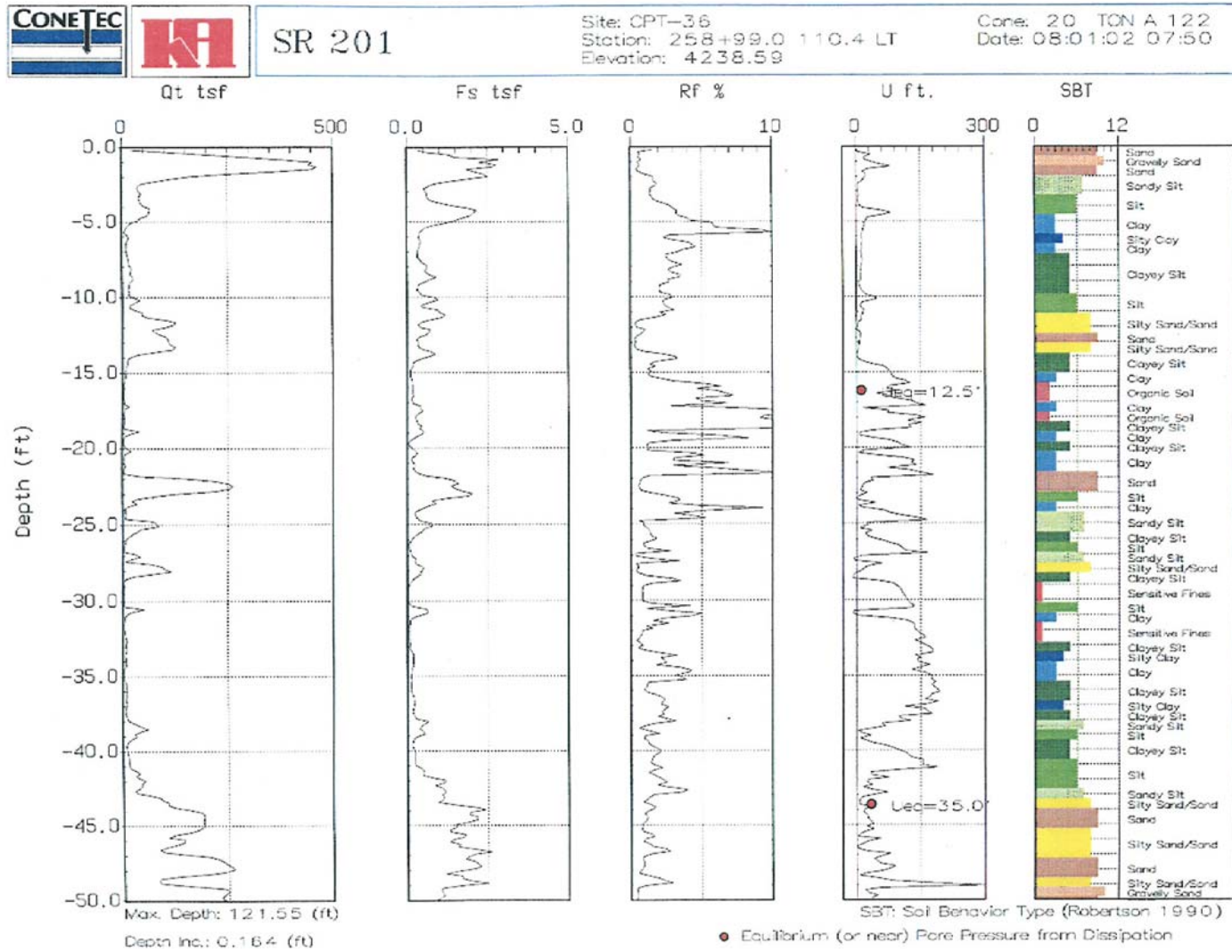


Figure 3-10 Log of CPT Sounding for CPT-36 at Redwood Road and SR-201 Site

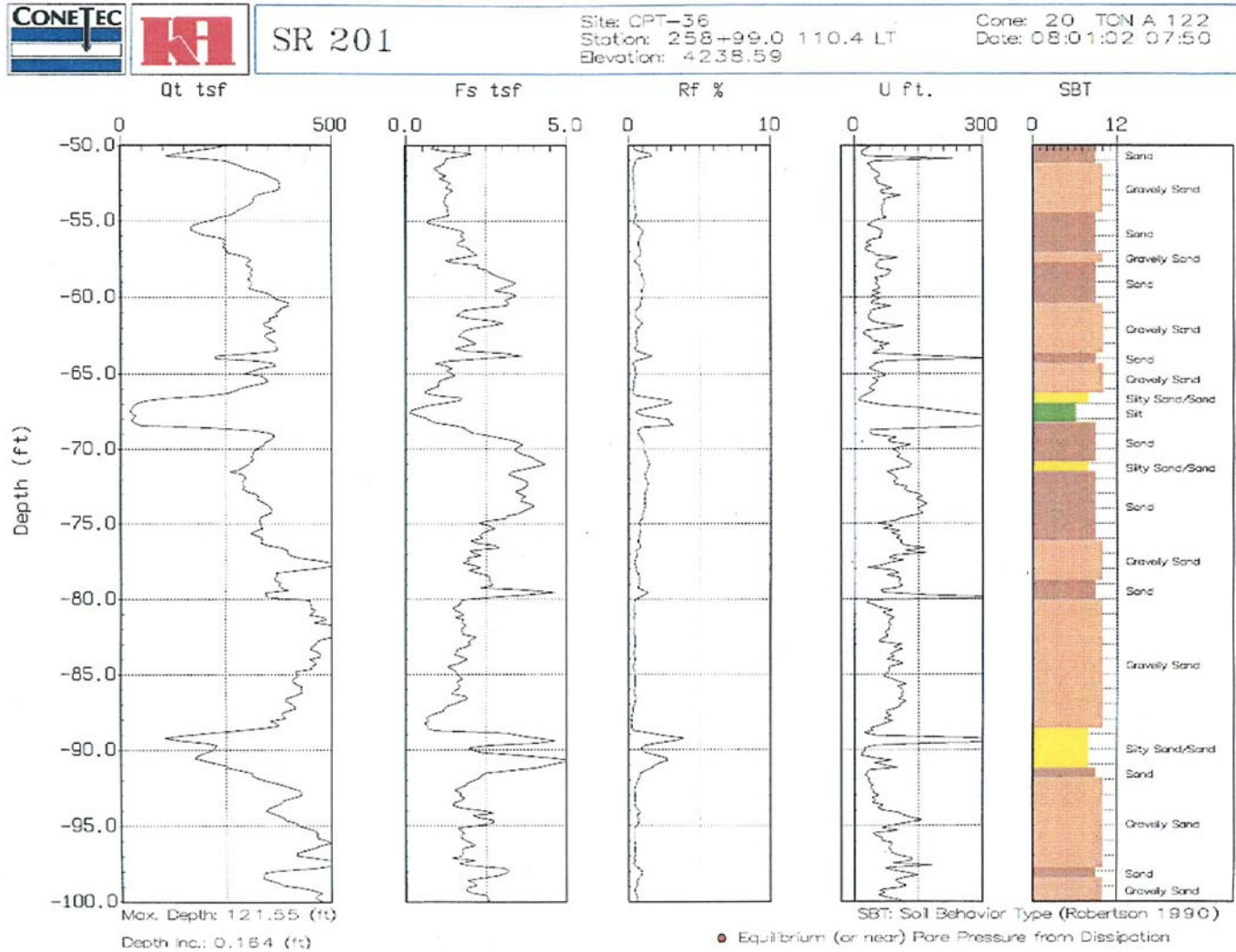


Figure 3-10 Log of CPT Sounding for CPT-36 at Redwood Road and SR-201 Site (continued)

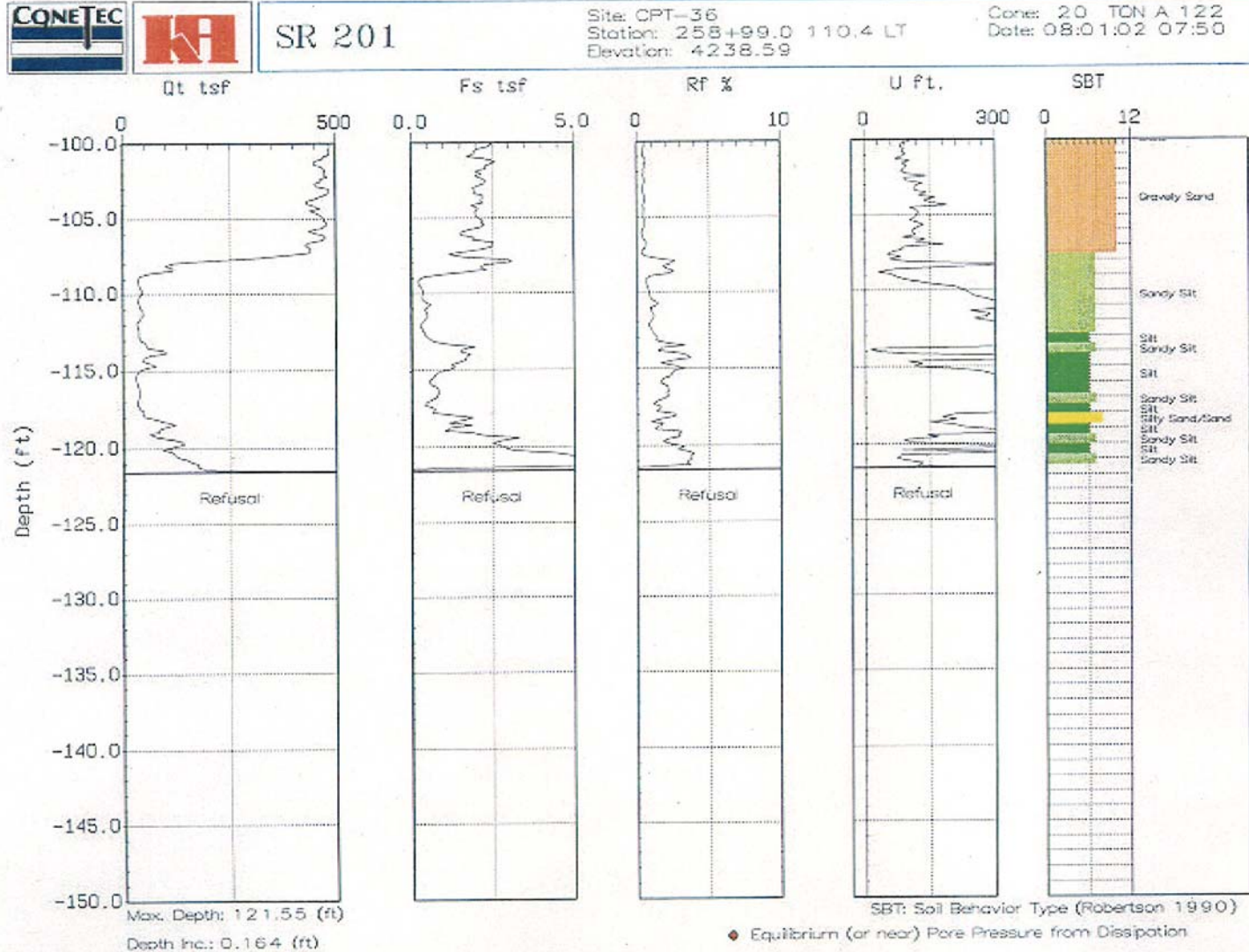


Figure 3-10 Log of CPT Sounding for CPT-36 at Redwood Road and SR-201 Site (continued)

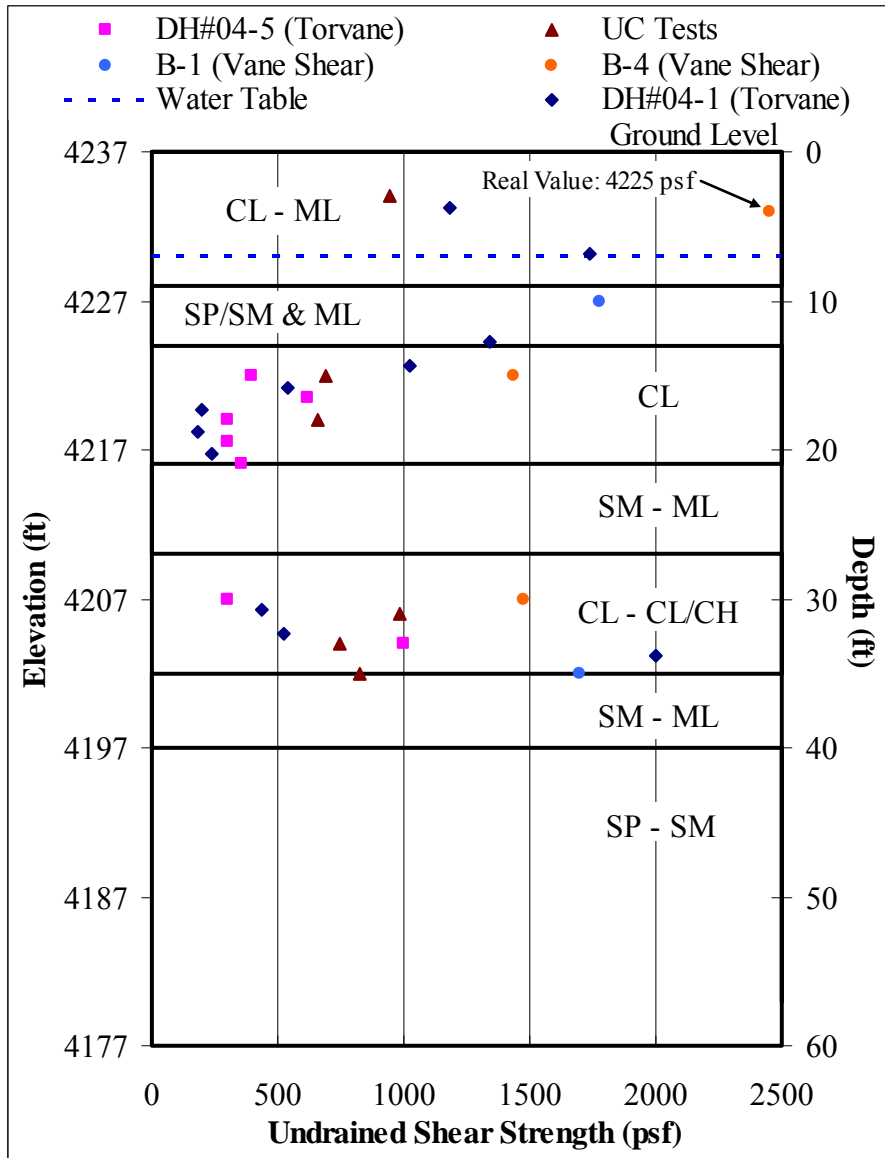


Figure 3-11 Undrained Shear Strength Values from Torvane, Unconfined Compression and Vane Shear Tests for Boreholes Near Test Pile Location

3.2 Site Characterization of Salt Lake City International Airport Site

The second site, located at the Salt Lake City International Airport, which will be referred to as the SLCIA site hereafter in this thesis. The test pile is located south of the main airport complex as shown in Figure 3-12, which is an aerial photo showing the airport and the tests site as it was before this stage of construction began.



Figure 3-12 Aerial Photo of SLCIA Site before Construction with Location of Test Pile (USGS, 2003)

A total of six boreholes were completed by RB&G Engineering for the characterization of the soil profile for this project. Three of the six boreholes were relatively shallow (only 52 feet deep) and the other three reached depths over 100 feet. Two of the three deep boreholes were located at the each of the bridge abutments and the third was located at the center support, to provide soil properties for the pile design. The

layout of the boreholes can be seen in the scanned image from the geotechnical report from RB&G Engineering shown in Figure 3-13. The three deep borings are 03-NB-03, 04 and 05.

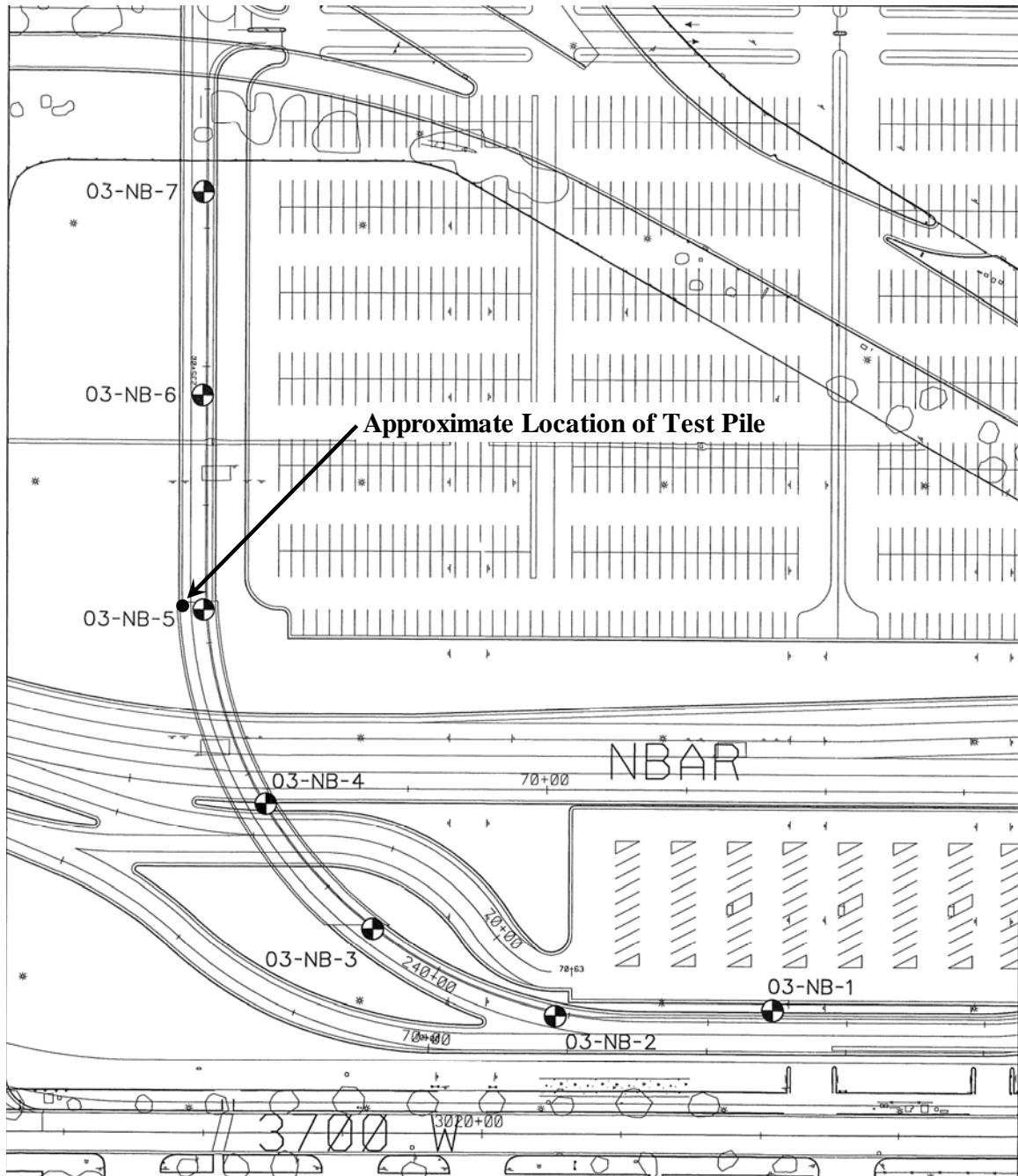


Figure 3-13 Borehole Locations for SLCIA Site

3.2.1 Soil Profile

The soil profile consists primarily of alternating layers, approximately 5 feet thick, of lean clay (CL) and silty sand (SM) to a depth of approximately 31 feet. Below this depth the layers continue to alternate, but become thicker. A fence diagram supplied by RB&G Engineering, shown in Figure 3-14, demonstrates the layering of the soil profile. The fence diagram is only shown here to give an overview of the soil profile. Individual borelogs are included as Figure A-5, Figure A-6 and Figure A-7 in the Appendix which allow for easier access to individual test data. The borelog on the far left is for borehole 03-NB-1, and increases to the right with the rightmost borelog being for borehole 03-NB-6. Borehole 03-NB-5 is located nearest to the site with the instrumented pile, and is thus best to indicate soil conditions surrounding the test pile. The borelog for borehole 03-NB-5 is shown in Figure 3-15. Various laboratory and in-situ tests were completed at these boreholes and will be discussed subsequently.

3.2.2 Laboratory Tests

The laboratory tests performed on samples taken from the boreholes for this site included gradation tests, Atterberg limit tests, consolidation tests and unconfined compression tests.

3.2.2.1 Gradation Tests

For the non-plastic samples, gradation testing shows the absence of gravel and, in most cases, quantities of sand in excess of 50%. It is common to see ratios of about 2/3 sand and 1/3 fines. Table 3-4 contains a breakdown of the grain size distribution found for the samples from boreholes 03-NB-3, 4 and 5.

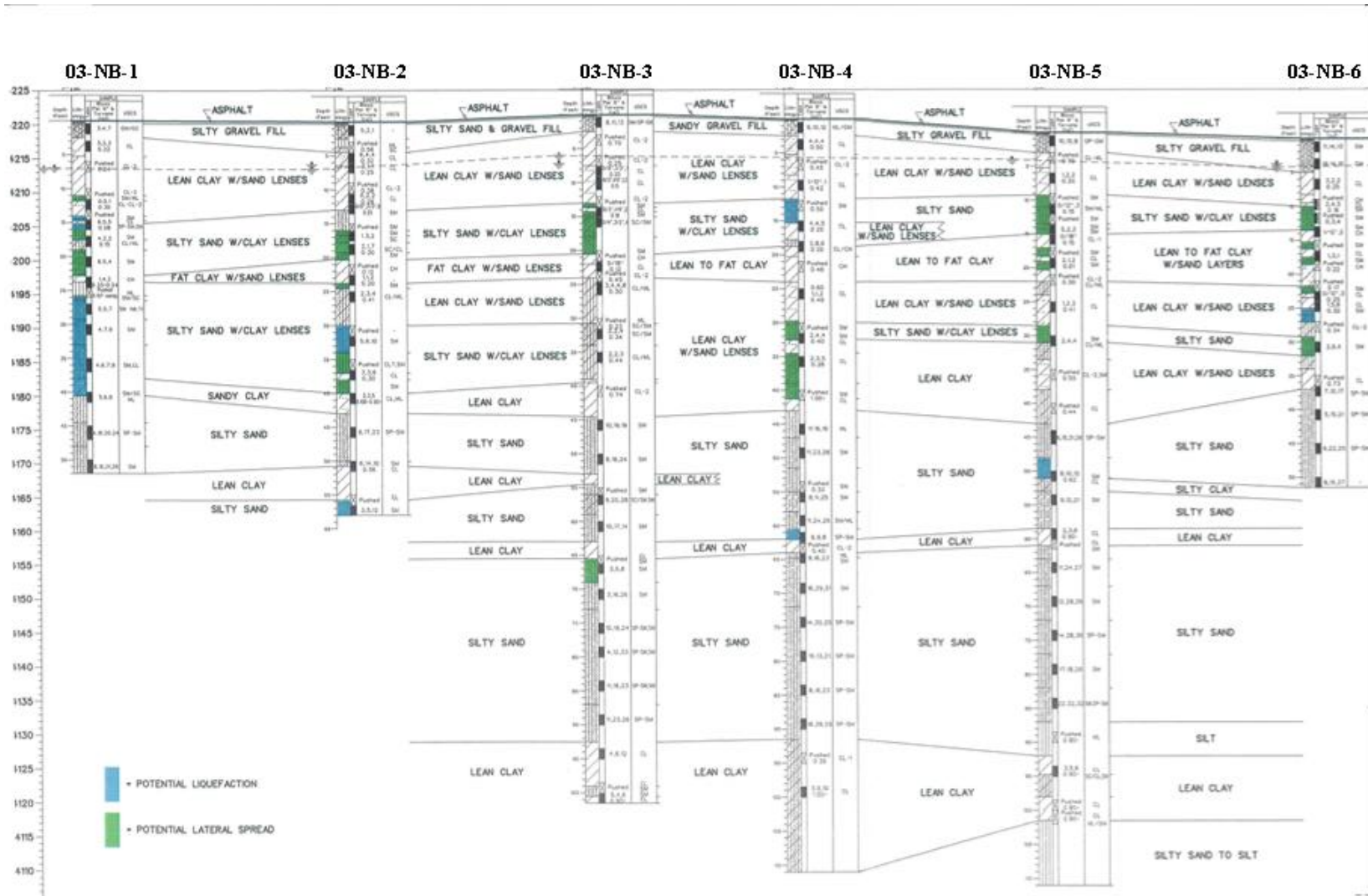


Figure 3-14 Fence Diagram of Borehole Logs Near Test Site

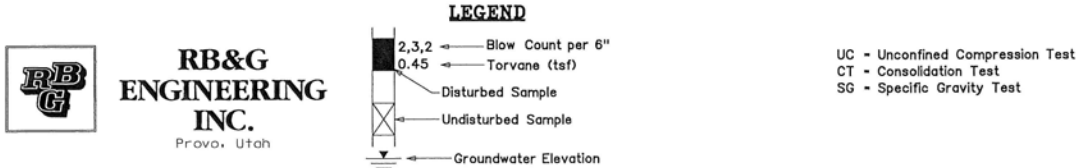
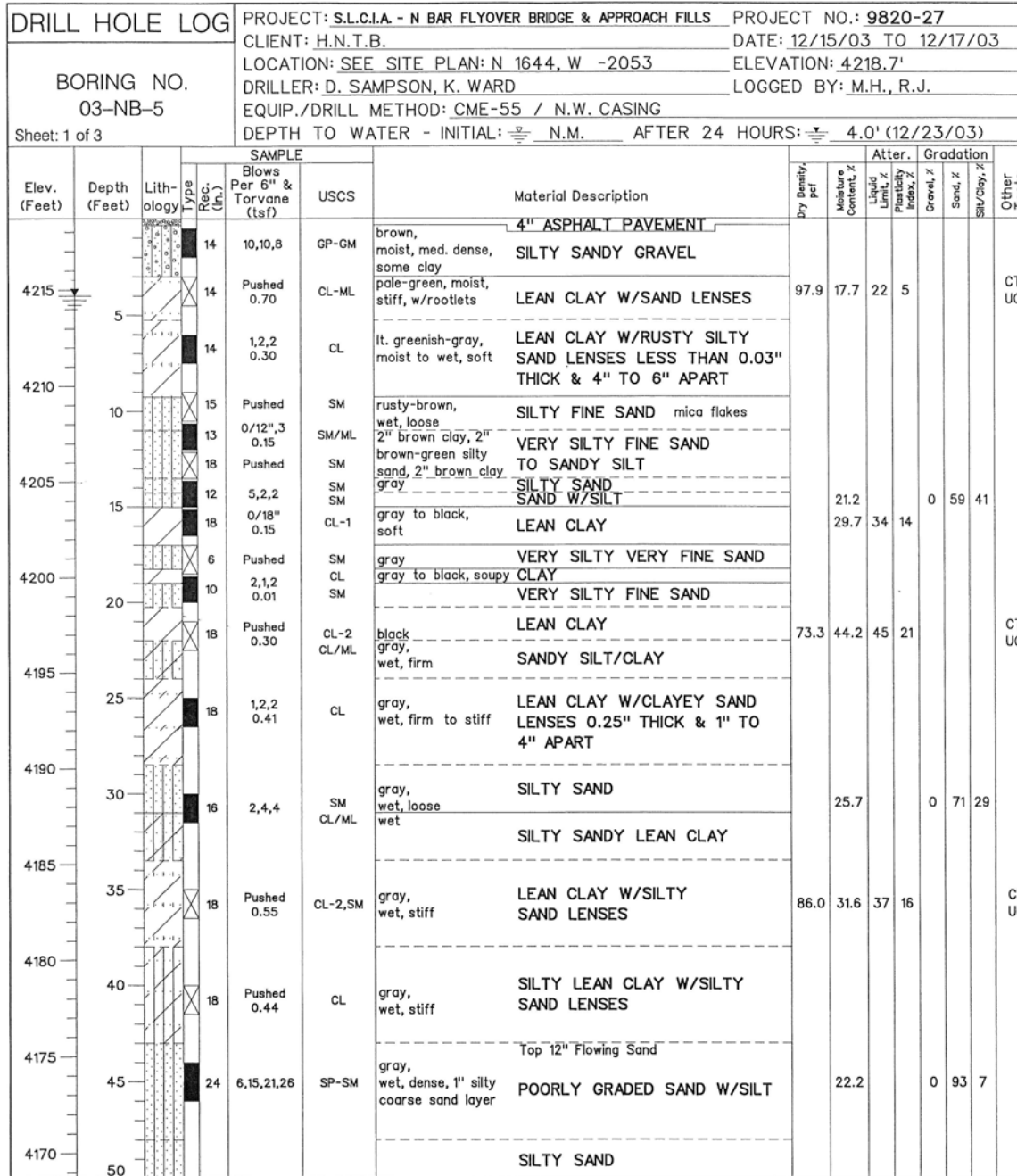
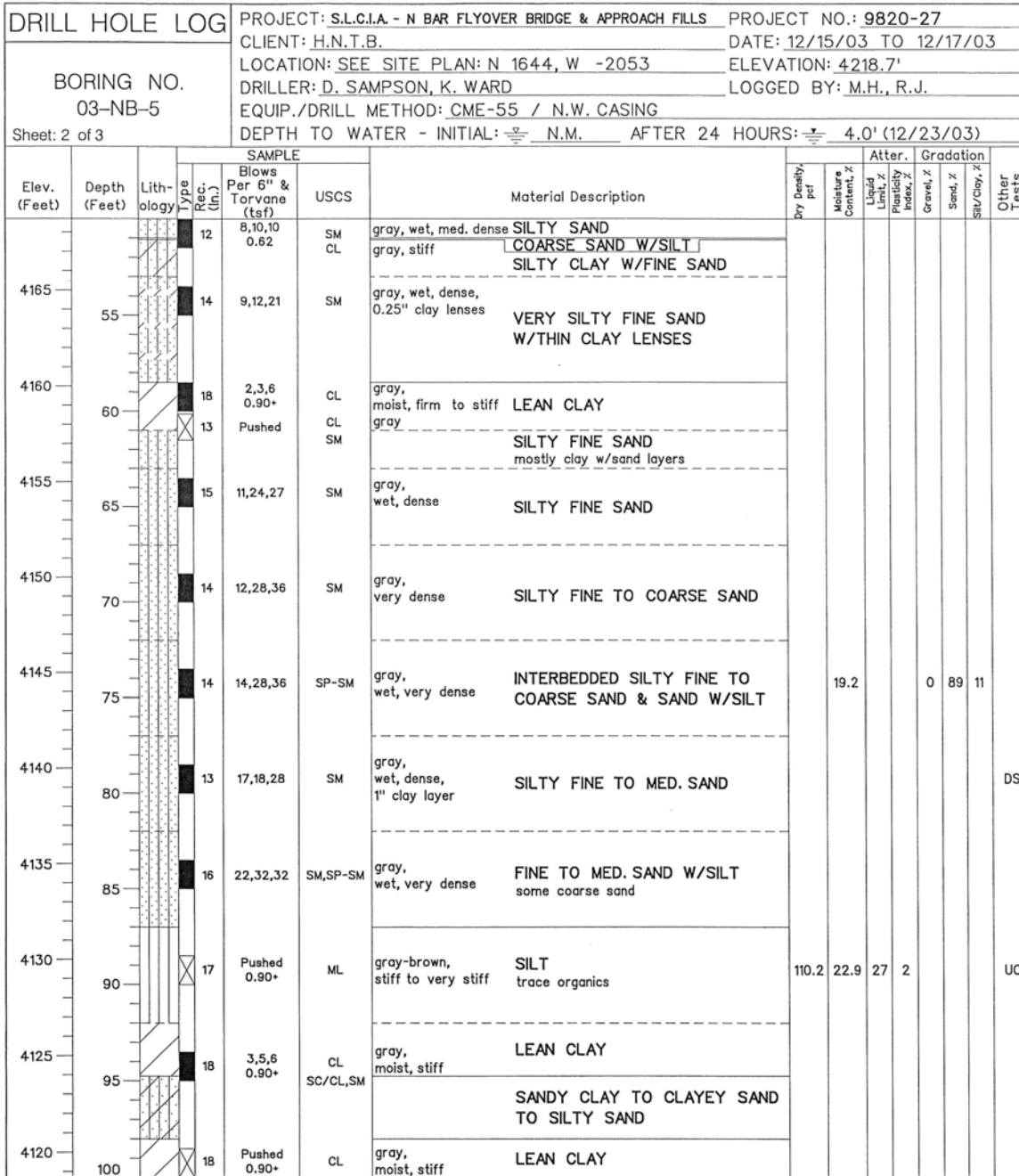



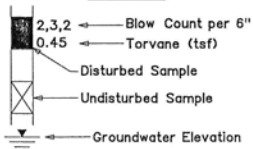
Figure 3-15 Borelog of Borehole 03-NB-5 for SLCIA Site (continued on next page)





**RB&G
ENGINEERING
INC.**
Provo, Utah

LEGEND



2,3,2 ← Blow Count per 6"
0.45 ← Torvane (tsf)
Disturbed Sample
Undisturbed Sample
Groundwater Elevation

UC - Unconfined Compression Test
CT - Consolidation Test
SG - Specific Gravity Test
DS - Direct Shear Test

Figure 3-15 Borelog of Borehole 03-NB-5 for SLCIA Site (continued from previous page)

3.2.2.2 Atterberg Limits

The plasticity index (PI) in the cohesive soils varied from 2 to 39 in the samples taken from boreholes 03-NB-3, 4 and 5. The average PI for the samples is 18 with a median of 19. Liquid limits varied from 25 to 69 and plastic limits varied from 18 to 30. Table 3-5 contains a summary of the Atterberg limits from the samples taken. The majority of the samples fall in the CL-2 (above the “A” line and $PI > 15$) range indicating high liquid limits and plasticity indices. Figure 3-16 shows the test results plotted on a plasticity chart.

Table 3-4 Summary of Gradation from Boreholes 03-NB-3, 4 and 5 for SLCIA Site

Borehole ID	Depth Below Ground Surface (feet)	Percent Gravel	Percent Sand	Percent Silt & Clay
03-NB-3	30 - 31.5	0	39	61
03-NB-3	66 - 67.5	0	78	22
03-NB-3	83.5 - 85	0	88	12
03-NB-4	30 - 31.5	0	71	29
03-NB-4	45 - 46.5	0	46	52
03-NB-4	53.5 - 55	0	81	19
03-NB-5	13.5 - 15	0	59	41
03-NB-5	30 - 31.5	0	71	29
03-NB-5	44 - 45.5	0	93	7
03-NB-5	73.5 - 75	0	89	11

3.2.2.3 Consolidation Tests

In total, five consolidation tests were performed on the samples from the aforementioned boreholes, of which two were completed for samples from borehole 03-NB-3 and the other three from 03-NB-5. The average initial void ratio (e_0) was 0.969 for the two boreholes. The compression index (C_c) averaged out at 0.333 (compression ratio

of 0.165) and the recompression index (C_r) averaged out at 0.037 (recompression ratio of 0.019).

Overconsolidation ratios (OCR) were large near the surface (from 5.2 to 15.5) but decreased to between 1 and 2 at greater depths. A summary of the results for these tests is shown in Table 3-6 and available consolidation test data curves are included in the Appendix in Figure A-8 through Figure A-33. A plot of the preconsolidation pressure and vertical effective stress versus depth (and elevation) is shown in Figure 3-17. Average values for OCR and the preconsolidation pressure are not included because the value from the first depth in borehole 03-NB-3 misrepresents the remaining values.

Table 3-5 Summary of Atterberg Limit Data for Boreholes 03-NB-3, 4 and 5 from SLCIA Site

Borehole ID	Depth Below Ground Surface (feet)	USCS Soil Type	Liquid Limit (%)	Plastic Limit (%)	Plasticity Index (%)
03-NB-3	3 - 4.5	CL-2	45	22	23
03-NB-3	6 - 7.5	CL-2	49	22	27
03-NB-3	12 - 13.5	CL-2	40	22	18
03-NB-3	23 - 24.5	CL-2	47	25	22
03-NB-3	40 - 41.5	CL-2	43	24	19
03-NB-4	6 - 7.5	CL-2	44	23	21
03-NB-4	21 - 22.5	CH	69	30	39
03-NB-4	62.5 - 64	CL-2	39	20	19
03-NB-4	93.5 - 95	CL-1	29	18	11
03-NB-5	3 - 4.5	CL-ML	25	20	5
03-NB-5	15 - 16.5	CL-1	34	20	14
03-NB-5	21 - 22.5	CL-2	45	24	21
03-NB-5	35 - 36.5	CL-2	37	21	16
03-NB-5	87.5 - 90	ML	27	25	2
Averages	-----	-----	40.9	22.6	18.4

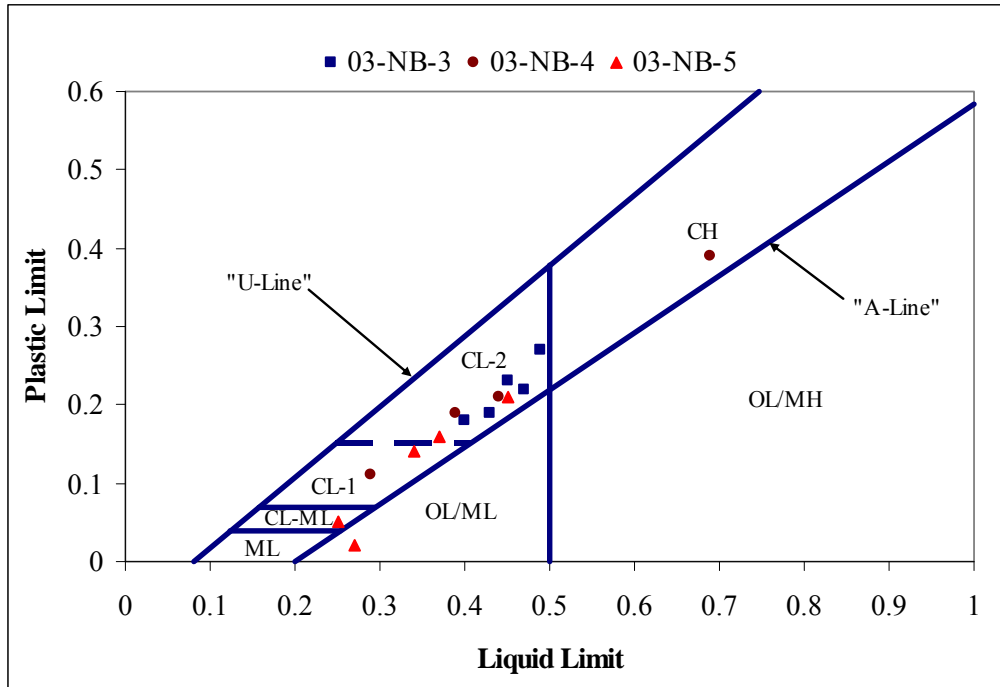


Figure 3-16 Plasticity Chart Showing Identification of Cohesive Soils for SLCIA Site

Table 3-6 Summary of Consolidation Test Values for Boreholes 03-NB-3 and 5 from SLCIA Site

Borehole ID	Depth Below Surface (ft)	Initial Void Ratio (e_0)	Comp. Index (C_c)	Recomp. Index (C_r)	Overconsolidation Ratio (OCR)	Preconsol. Pressure (psf)
03-NB-3	3 – 4	0.590	0.235	0.018	15.5	6,800
03-NB-5	3 – 4.5	0.716	0.174	0.012	5.2	2,100
03-NB-3	12 – 13.5	1.294	0.522	0.085	1.02	1,140
03-NB-5	21 – 22.5	1.290	0.433	0.045	1.7	2,200
03-NB-5	35 – 36.5	0.953	0.302	0.025	1.8	3,600
Average	-----	0.969	0.333	0.037	-----	-----

Engineering analyses based on the consolidation testing indicate that between 8.5 and 9.0 inches of consolidation settlement will occur at the face of the MSE wall along the side of the abutment near the piles. This settlement results from consolidation of the

cohesive soils in the upper 40 feet of the profile due to the construction of the 27 ft high approach fill at this site.

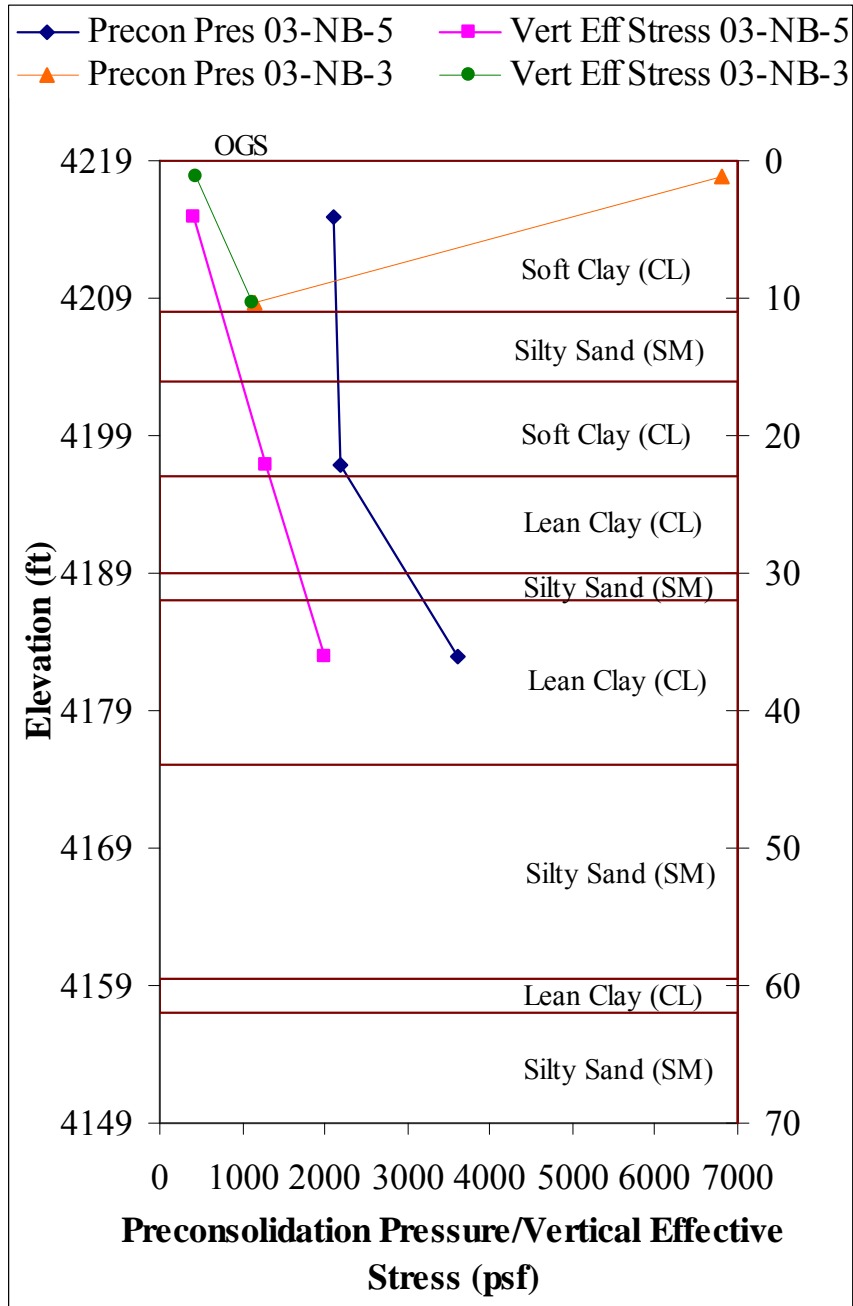


Figure 3-17 Plot of Preconsolidation Pressure and Vertical Effective Stress vs. Elevation and Depth for Borehole 03-NB-5

3.2.2.4 Unconfined Compression Tests

The unconfined compression tests are especially useful for this research. In past full scale tests, the negative skin friction has been approximately equal to the undrained shear strength, which can be gained from the unconfined compression test. The values for the unconfined compression tests on the four boreholes vary widely, from 320 to 3786 psf. Values above 3000 psf only occur below 40 feet. In general, the values tend to increase with depth below about 40 feet. Table 3-7 contains a summary of the unconfined compressive strength values from the tests completed on samples from boreholes 03-NB-3 through 03-NB-6. Figure 3-18 shows a plot of the strength values as a function of elevation and depth.

Table 3-7 Unconfined Compressive Strengths from Tests for Boreholes 03-NB-3, 4, & 5 at SLCIA Site

Borehole ID	Depth Interval (ft)	Representative Elevation (ft)	Unconfined Compressive Strength (psf)
03-NB-3	3 - 4.5	4217.65	1549
03-NB-5	3 - 4.5	4214.95	747
03-NB-3	6 - 7.5	4214.65	674
03-NB-4	6 - 7.5	4213.95	880
03-NB-3	12 - 13.5	4208.65	320
03-NB-6	18 - 19.5	4198.95	975
03-NB-4	21 - 22.5	4198.95	1377
03-NB-3	23 - 24.5	4197.65	959
03-NB-5	21 - 22.5	4196.95	1055
03-NB-6	27 - 28.5	4189.95	1568
03-NB-5	35 - 36.5	4182.95	1794
03-NB-3	40 - 41.5	4180.65	3527
03-NB-4	62.5 - 64	4157.45	3786
03-NB-5	87.5 - 89	4130.45	3672
03-NB-4	93.5 - 95	4126.45	2457

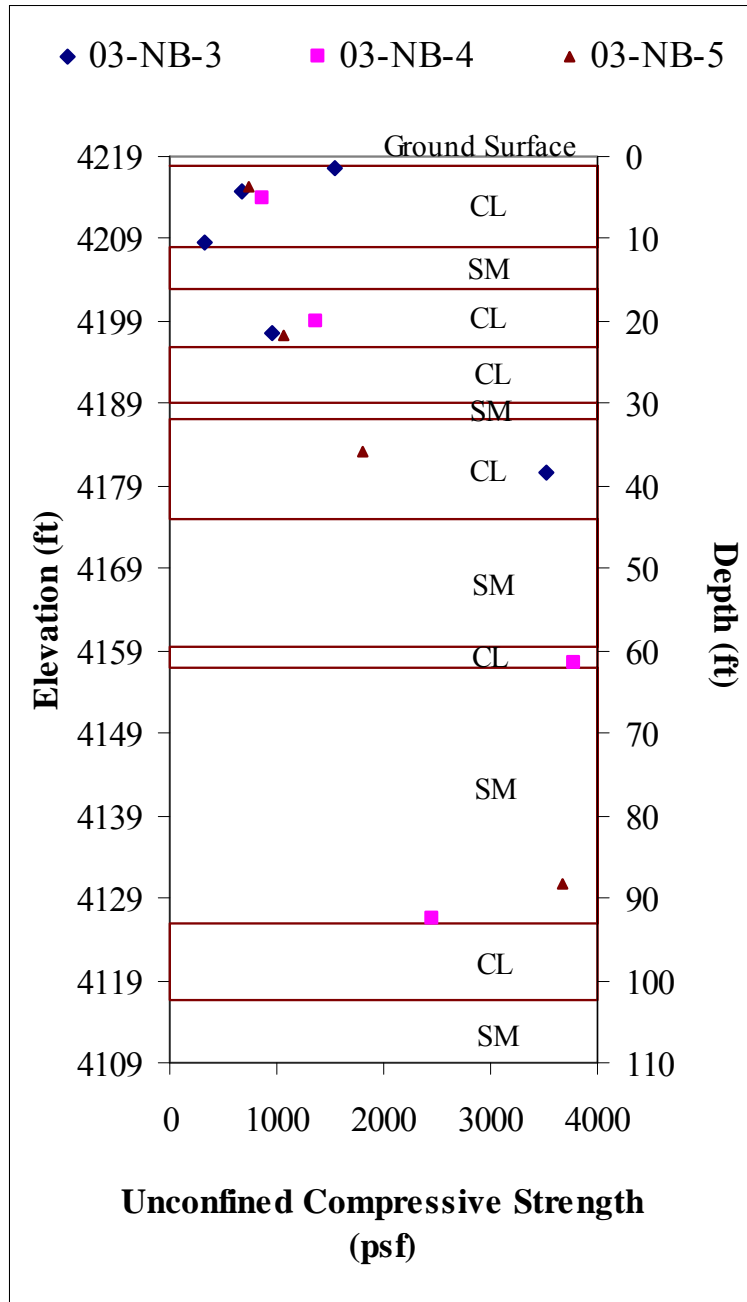


Figure 3-18 Plot of Unconfined Compressive Strength vs. Elevation and Depth for Boreholes 03-NB-3, 4, & 5 at SLCIA Site

3.2.3 In-Situ Testing

Various in-situ tests were performed during the investigation by RB&G Engineering. These tests include SPT and torvane tests.

3.2.3.1 Standard Penetration Testing (SPT)

An automatic hammer with an efficiency of 75% was used for the SPT sampling in these boreholes. The field SPT values have been multiplied by a factor of 1.25 to obtain the N_{60} blowcount. The SPT values demonstrate the existence of a hard bearing layer at an elevation of approximately 4180 feet (close to 42 feet below the ground surface). After passing the fill near the surface, average SPT N_{60} blowcounts range from 6 to 9 with the upper cohesive layer until the bearing surface at 42 feet is reached. Below this depth, the average N_{60} value in the sand layers increases to as much as 80, although the blowcounts in the thin cohesive layer is considerably lower. Maximum N_{60} values of 80 were reached in Borehole 03-NB-5 at depths of 69 and 74 feet. Figure 3-19 shows a comparison of the SPT N_{60} blowcount values for the boreholes 03-NB-3 – 6.

3.2.3.2 Torvane Tests

The torvane tests completed in the boreholes show widely varying results. The results indicate that overconsolidation near the crust decreases soil strength. The soil gains strength with depth as shown by most of the tests done below a depth of 60 feet yielding values above 0.90 tsf. Figure 3-20 shows a plot of the undrained shear strengths of the soil with the torvane and unconfined compression strength values gathered from boreholes 03-NB-3, 4, 5 & 6.

3.3 Summary of Geotechnical Investigation

Geotechnical investigation information for each site has been presented in the previous sections. The conditions at each site can be summarized as follows.

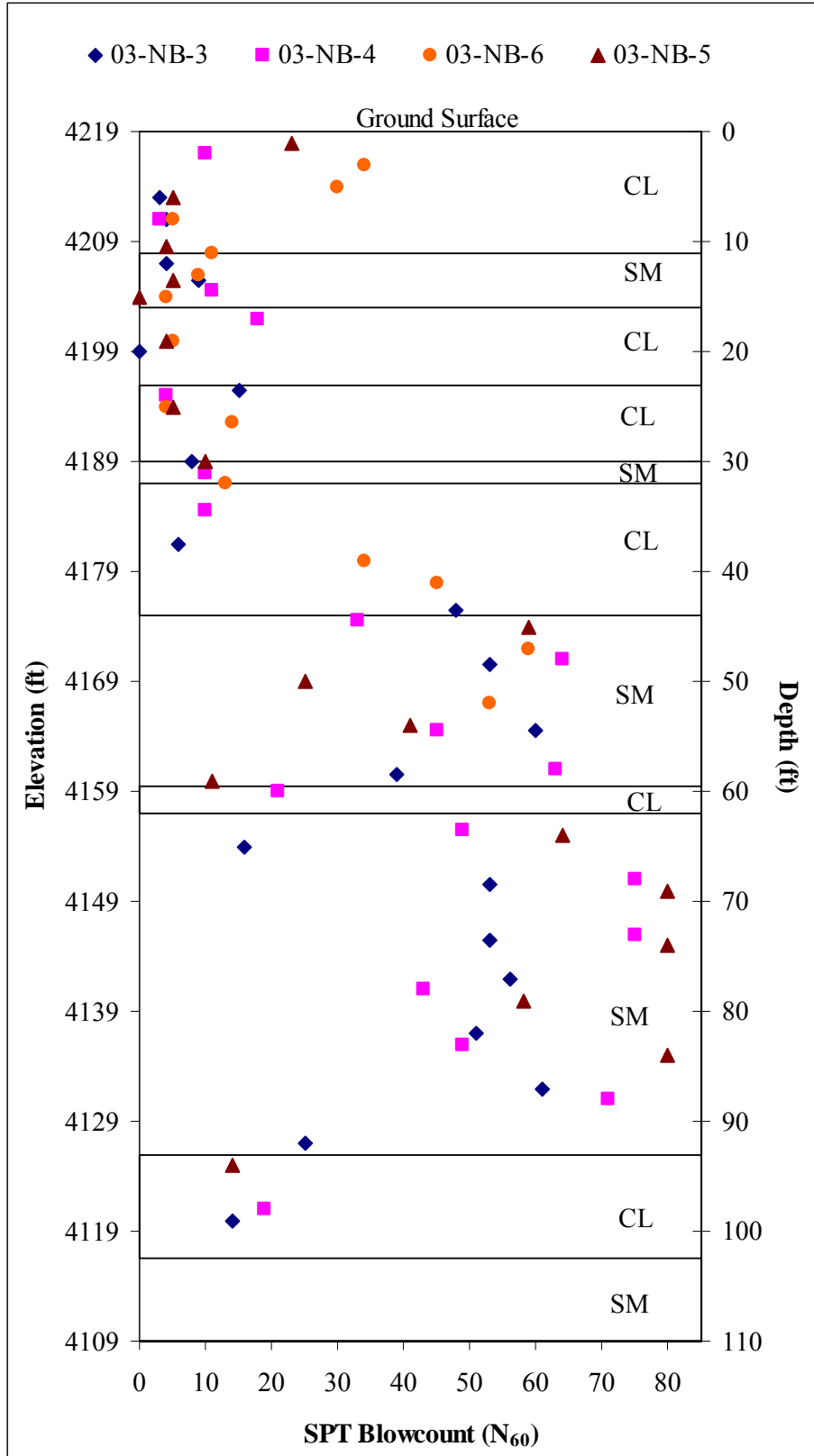


Figure 3-19 SPT N_{60} Blowcount Values vs. Elevation for Boreholes 03-NB-3, 4, 5 & 6 for SLCIA Site

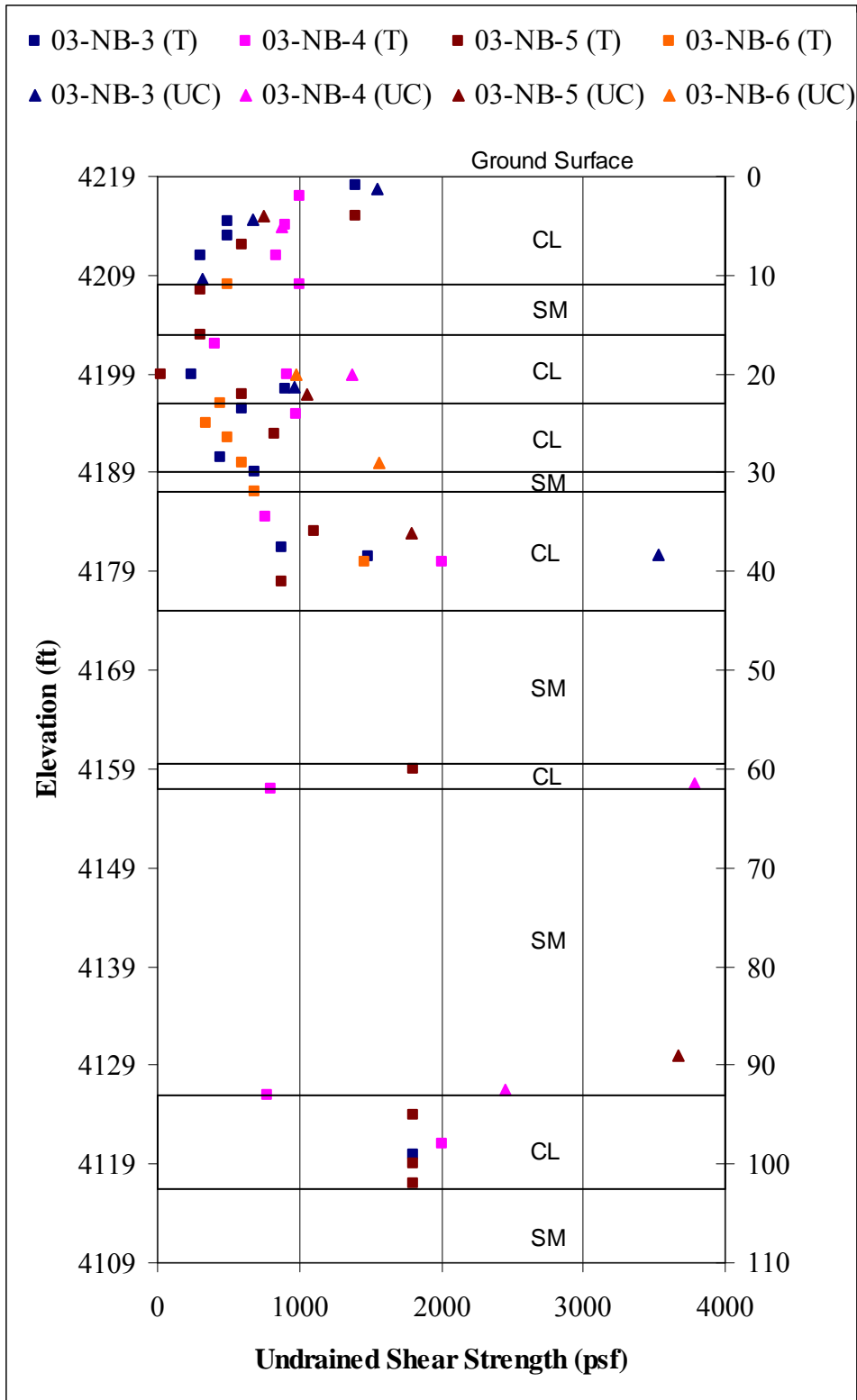


Figure 3-20 Undrained Shear Strength Values from Torvane and Unconfined Compression Tests for Borehole 03-NB-3, 4, 5 & 6 from SLCIA Site

3.3.1 Summary of Redwood Road Site Geotechnical Investigation

Primary information for the geotechnical investigation is taken from boreholes B-4, B-35, and DH#04-1, 2 & 5. Boreholes B-4 and B-35 are closest to the test pile location. The soil profile of the site located at Redwood Road and SR-201 consists primarily of alternating layers of compressible lean clay and silty sand to a depth of about 50 feet. Layer thicknesses vary from a few inches to several feet. A relatively dense sand bearing layer was encountered below a depth of 50 feet. The pile foundations at this site were eventually driven into the dense sand layer to a depth of 54 to 55 feet.

3.3.1.1 Laboratory and In-Situ Testing

The Atterberg limits for the site give average values of 33 for the liquid limit, 22 for plastic limit and 11 for the plasticity index. However, values for the liquid limit and plasticity index are greatly influenced by two tests which yielded high values for each. Median values are 31, 21 and 9 for the liquid limit, plastic limit and plasticity index respectively.

Undrained shear strength tests, including the vane shear tests performed in the laboratory by AMEC and the torvane tests performed in the field by RBG, show in general, that strength begins high (up to 4225 psf) and gradually decreases in the upper 22 feet. Strengths then tend to rebound and gain strength with depth. Values ranged from 180 to 4225 psf for the boreholes close to the test pile. Consolidation tests showed varying results for the compression ratio, but similar results for the recompression ratio. Engineering analyses indicated that consolidation settlement in the silt and clay layers above 50 feet would result in approximately nine inches of settlement due to construction of the 25 to 26 feet high approach fill and eight feet surcharge.

The SPT data from the surrounding boreholes show the lean clays to have blowcounts less than 10 and the silty sands to have blowcounts ranging from 20 to 40. Blowcounts in the silty sand layer located about 50 feet below the surface yielded large values (over 100) showing the competency of this layer to serve as a bearing layer for the piles. CPT data shows very low cone resistance (about 15 tsf), broken up by occasional spikes due to silty sand layers, until a depth of 40 feet below the ground surface. In contrast, cone resistance averages approximately 300 tsf in the dense sand layer. Figure 3-21 shows a side-by-side comparison of the undrained shear values and the SPT test results.

3.3.2 Summary of SLCIA Site Geotechnical Investigation

The primary resource for information used in the preceding sections comes from boreholes 03-NB-3, 4 & 5. Borehole 03-NB-5 is located closest to the test pile. The soil profile at this site contains alternating layers of lean clays and silty sands. These layers typically have a thickness of about 5 feet for the first 30 feet, then increase in thickness. The soils below a depth of 40 feet are considerably stiffer and stronger as indicated by the in-situ tests. The piles for this abutment were eventually driven into a relatively dense sand layer to a total depth of 65 feet below the ground surface.

3.3.2.1 Laboratory and In-Situ Testing

The Atterberg limit tests for this site yield average values of 41 for the liquid limit, 23 for the plastic limit and 18 for the plasticity index. Consolidation testing from various samples gives an average value for C_c value of 0.333 and an average C_r value of 0.037. Engineering analyses indicated that consolidation settlement in the silt and clay

layers above 40 feet would be between 8.5 and 9.0 inches due to construction of the 27-foot high approach fill.

Undrained shear strength tests, including unconfined compression and torvane tests, also show a general decrease in strength with depth for the upper 15 feet. Below this dessicated crust, strengths generally increase with depth, especially below 40 feet. Values range from 20 to 3786 psf.

The SPT testing done shows low blowcounts (below 10) for the first 40 feet, then increasing to an average value of 38 for the next 20 feet. After this a thin, weak layer was encountered and then values climbed back up to a higher average of 49 down to a depth of 93 feet. Figure 3-22 shows a side-by-side comparison of the preconsolidation pressure, vertical effective stress, undrained shear strength parameters (includes unconfined compression strength and torvane tests), and SPT N_{60} blowcount values for the SLCIA site.

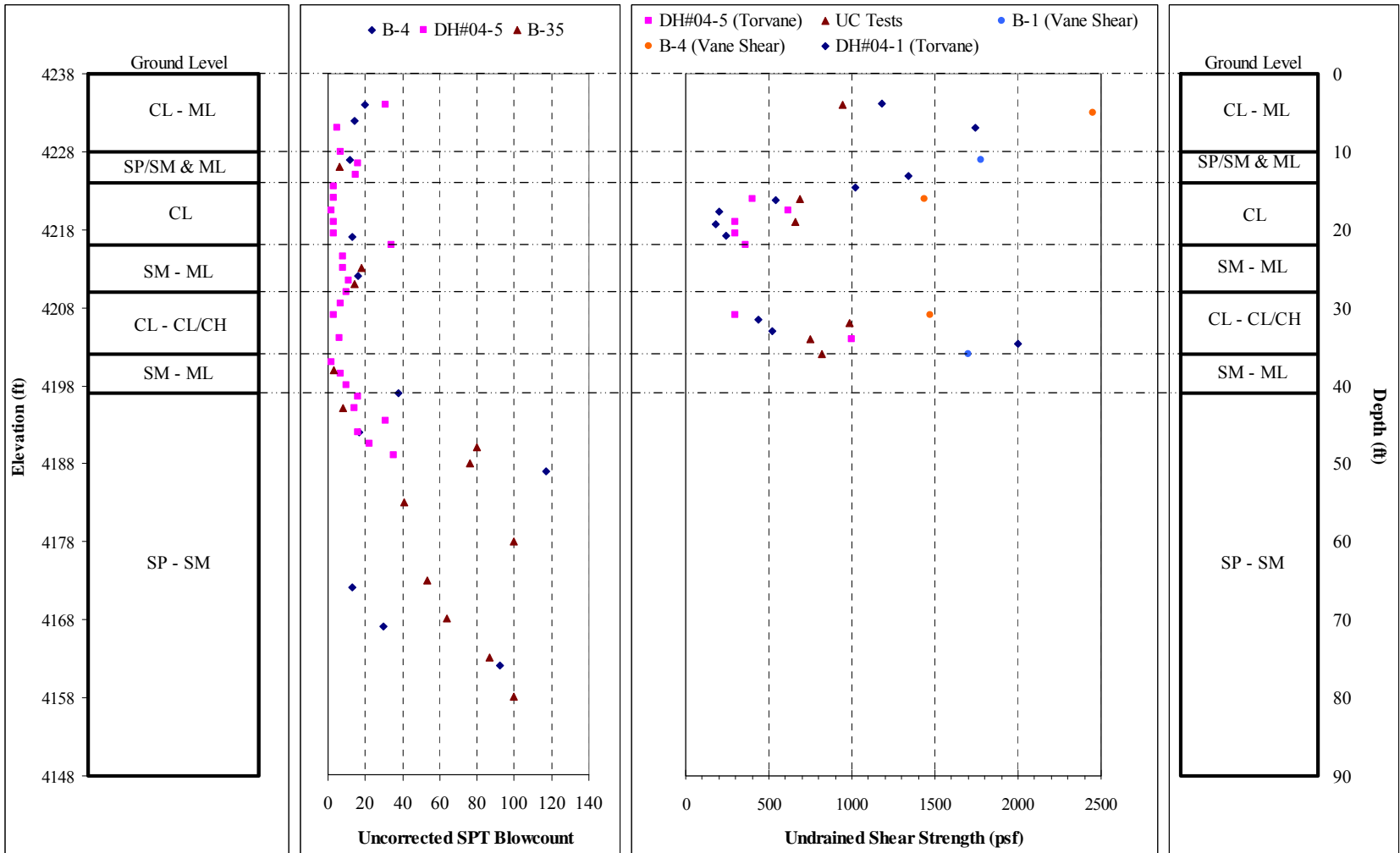


Figure 3-21 Summary of Uncorrected SPT Blowcount and Undrained Shear Strength Values for Redwood Road & SR-201 Site

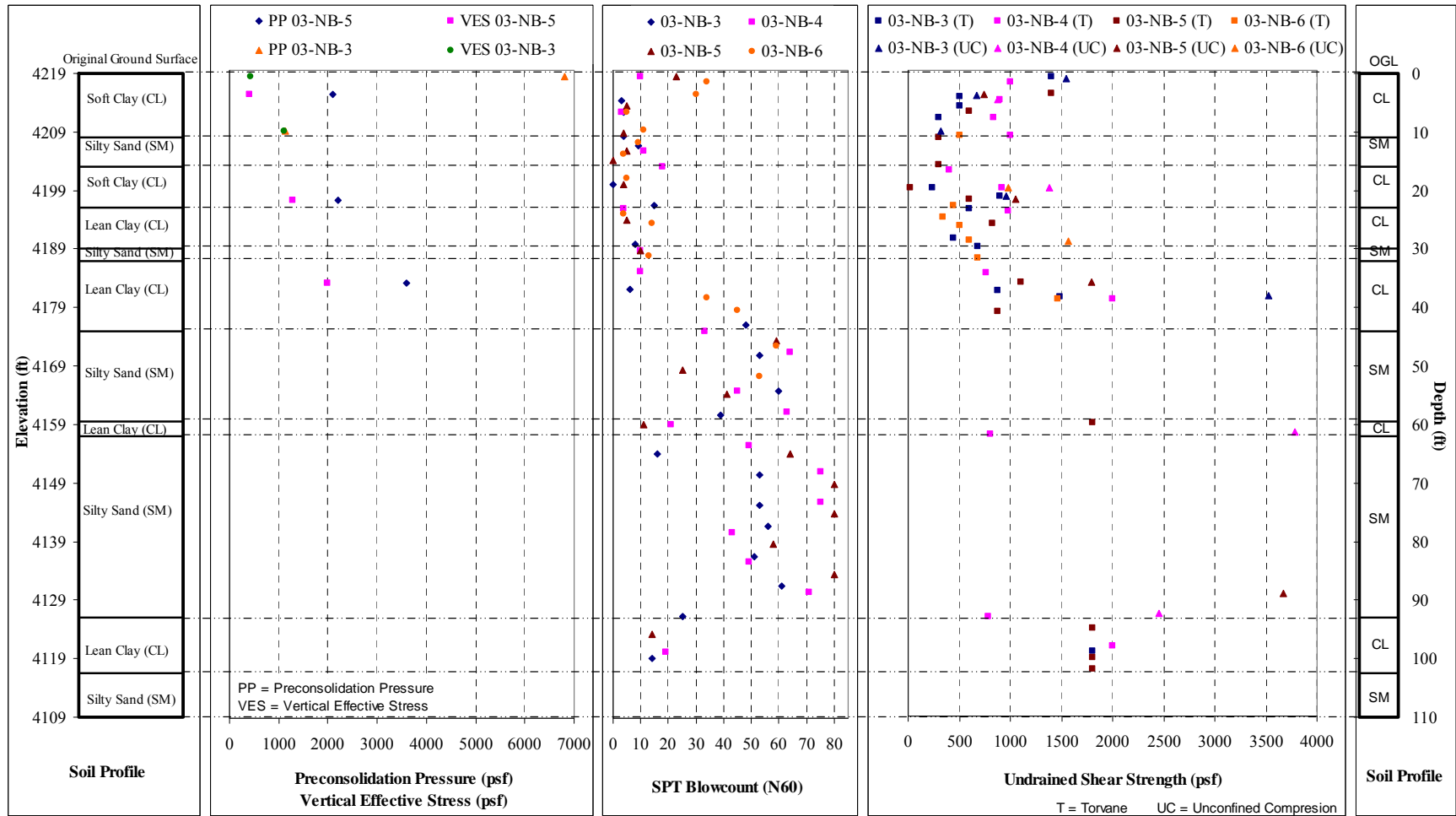


Figure 3-22 Summary of Consolidation Parameters, Undrained Shear Strength Parameters and SPT N₆₀ Blowcount Values for SLCIA Site

4.0 Pile Instrumentation and Method of Analysis

The pile instrumentation and the various methods of analyzing the acquired data will be set forth in this chapter. Three different sites were instrumented to collect the desired data, but instrumentation at the first site experienced near total failure. For this reason, no geotechnical site characterization was given for this site. Lessons learned from the first experience led to improvements in the instrumentation method and generally led to successful instrumentation performance at the two subsequent sites. The first site was located near Springville, Utah on the newly reconstructed overpass for SR-75 over Interstate 15. A different method was employed at this site which proved very unsuccessful. The two sites currently in use and functioning properly are those located in Salt Lake City and the geotechnical characteristics of these sites were discussed in Chapter 3. An explanation of the methods used to instrument all three sites and a discussion of the lessons learned are provided in this chapter.

4.1 Instrumentation Procedure for Test Pile in Springville, UT

The Springville project involved the instrumentation of a pile located in the east abutment of the new SR-75 overpass at I-15. Forty-four piles in two rows were to be driven to support each abutment. Each pile was to be approximately 130 feet in length and was to be installed by welding two lengths of pipe sections together. Two different

methods were discussed for the installation of strain gauges. The first method was to place the gauges on horizontal bars that could be lowered to the desired depth after the pile had been driven and then concrete would be used to keep the gauges in position. The second option was to place the gauges on the outside of the pile and place a piece of angle iron to protect the gauges during driving. The first method was ruled out because a way could not be readily found to place the gauges or to protect them as the concrete was poured in the pile. Therefore, the second option was decided upon. Gauges were installed at 10 different depths with two gauges at each depth placed on opposite sides of the pile from each other. This placement would provide a way to account for potential bending and eccentricity.

4.1.1 Gauge Type and Characteristics used at Springville, UT

Strain gauges were purchased from Geokon Inc., of Lebanon, NH, which specializes in geotechnical instrumentation. The gauges used for this project were Model 4000 vibrating wire strain gauges. This model of gauge was used because the design allowed welding of end blocks onto the steel of the pipe pile to which the gauge could then be attached. These gauges have a range of 3000 microstrain ($\mu\epsilon$), a sensitivity of 1.0 $\mu\epsilon$ and can work in environments from -20°C to 80°C. Figure 4-1 shows a picture of the gauge as obtained from the Geokon Inc. website. This gauge operates by the use of a vibrating wire and a “plucker.” The wire is encased in the bar portion of the gauge and is attached at both ends and either tightens or slackens as the pile is compressed or put in tension, which in turn changes the resonant frequency of the vibrating wire. The “plucker” plucks the wire by use of an electromagnetic coil, and the resonant frequency of the wire is determined. The reading is sent through a signal cable to a readout box

which gives a reading in microstrain. The amount of compression or tension can be found by comparing latter readings to the initial reading.

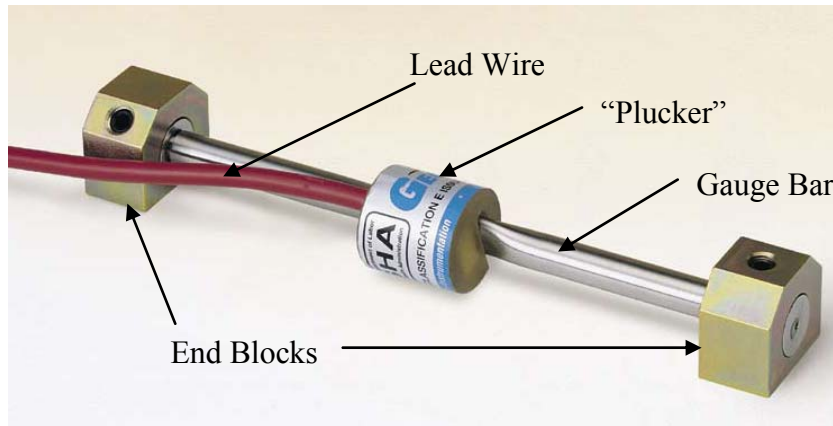


Figure 4-1 Series 4000 Vibrating Wire Strain Gauge (from company website, www.geokon.com)

4.1.2 Gauge Installation at Springville, UT

The gauges were prepared for installation by using a spacer bar and a welding jig as shown in Figure 4-2. The spacer bar is the same length as the gauge bars and the welding jig helps to position the end blocks at the right spacing and orientation.

Two end blocks as seen in Figure 4-1 were placed on the ends of the spacing bar and tightened into place. After this, the two end blocks were welded to the steel pile at predetermined locations as seen in Figure 4-3 (the black arrow on the pile is the location for the middle of the gauge bar which was measured previous to placement of the end blocks).

The strain gauge bar could then be slid through the openings and the gauge “plucker” placed on the bar and secured using a metal hose clamp. The lead wire was then taped to the pile to keep it from being damaged during driving.

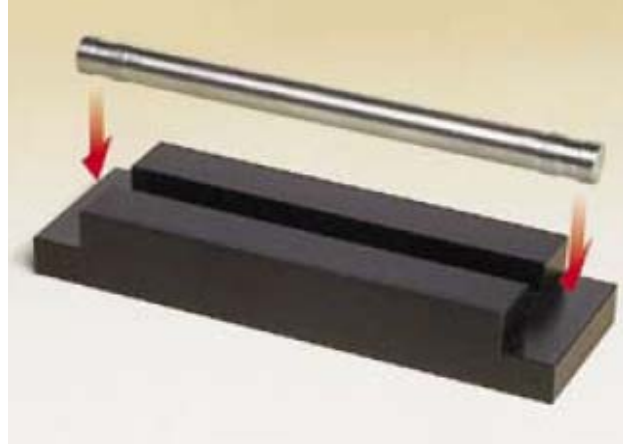


Figure 4-2 Spacing Bar and Welding Jig Provided to Assist in Correct Placement of End Blocks for Welding (from company website, www.geokon.com)



Figure 4-3 End Block after being Welded to the Pile

A completed assembly with wires from previous gauges joining with another gauge is shown in Figure 4-4. Angle iron was placed over the wires and gauges and was then welded into place. This completed the assembly for the bottom section of the pile. The upper section was done in the same way with only one exception. To facilitate

bringing the wires from the top of the bottom section to the top of the second section of pile, a piece of PVC pipe was placed under the angle iron which would enable the wires to be pulled from the bottom half up through the upper section after the bottom section had been driven.

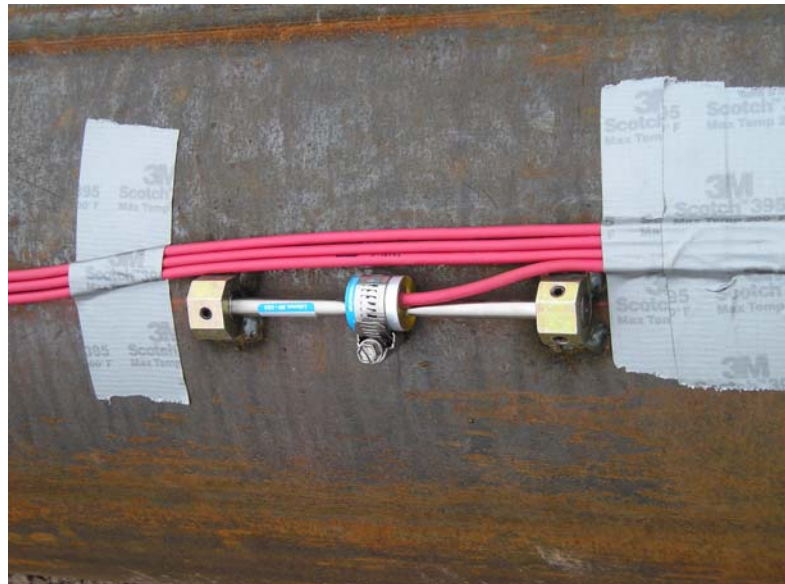


Figure 4-4 Placement of Gauge and Wires along Pile

After the bottom section was driven, the top section was welded on and a section of angle iron was also welded in the gap to cover the gauge wires. To protect the wires while the gap pieces were welded on, a sealant was sprayed over the wires. However, it was discovered after spraying that the sealant was flammable. As much sealant was cleaned off as possible, but during the welding process a fire started under the angle iron. The fire was doused with water as soon as possible, but there was no way to view the possible damage to the wires. The fit between the upper and lower angle irons was relatively good; however, small gaps were still present since it was not possible to weld them together without the potential for damaging the lead wires inside.

While the driving for the top section continued, wires were held away from the machinery as much as possible. As the upper pile section was being driven, soil apparently worked its way into the gaps between the angle iron fittings and began pushing the PVC pipe out of the angle iron. By the time driving was complete the PVC pipe on both sides of the pile had moved upward about 10 to 15 feet. It is not known if the pipe damaged any wires or gauges on its ascent out of the angle iron. The ends of the PVC pipe were carefully cut off and removed. During the driving an unforeseen difficult layer was encountered at about 110 feet below the surface. From the soil borelogs, the layer should not have exhibited the resistance manifested, but while driving through this zone, the penetration resistance was at least 50 blows/foot. During this period of heavy driving, it was observed that the welds attaching the angle iron to the pile were cracking in various locations. As noted in this section, a number of the problems discussed above could have led to problems with the strain gauges. These problems could have been caused by a single factor or be the result of a combination of factors.

The pile driving was completed on 5 April 2005. After the entire installation was completed, the wires were run through pipes to maneuver them out of the way of the construction for the pile cap. After connecting the gauges to the data logging system the next day, only 12 of the 20 gauges were transmitting temperature measurements and only three were transmitting strain measurements. Five days later only ten gauges were reading temperature and three were reading strain. Five more days later only three gauges were giving temperature measurements and no strain readings were given. Performance such as this was insufficient for measuring the development of downdrag forces, thus the wires were disconnected and the installation abandoned.

4.1.3 Lessons Learned from Springville Installation

The failure of the installation at the Springville site is not believed to be a result of any defect in the gauges secured from Geokon Inc. Rather, the method of installation was riddled with mistakes because of inexperience and unforeseeable problems. Although this approach could likely be used successfully in the future, additional precautions must be taken to avoid similar results. Based on the experience at the Springville site, the following recommendations are provided for future installations of a similar nature.

- Verify, to the extent possible, that soil around pile installation will not exhibit excessive resistance, with the exception of the bearing layer.
- Weld all angle iron connections continuously to prevent intrusion from surrounding soil.
- Protect wires from heat while welding by coating in non-flammable sealant or by placing them in a PVC pipe through the entire pile length.
- Leave some slack for wires to avoid pinching and excessive pulling on the gauge “plucker.”

4.2 Instrumentation Procedure for Test Sites in Salt Lake City, UT

Both of the test piles at the Salt Lake City sites were instrumented using the same method which will only be described in this section. After the failure encountered at the site near Springville, a different method was selected to install the gauges. The gauges were lowered into the pile after driving had taken place using a series of pipes with the gauges attached at specific intervals to metal “stars” as described below. This procedure

helped to eliminate potential damage during driving and allowed for more precise positioning of the gauges.

4.2.1 Gauge Type and Characteristics

For these test piles, a model 4200 vibrating wire strain gauge was selected. This model is designed for embedment in concrete. The basic operational characteristics are the same as in the model 4000 gauge. Figure 4-5 show the strain bar and “plucker” used in these assemblies. Vibrating wire strain gauges were selected for use rather than electrical resistance type strain gauges to avoid problems with drift over a period of months while measurements had to be made. Vibrating wire gauges can maintain a constant zero strain value with the zero strain value tends to change with time for electrical resistance gauges.

4.2.2 Installation Method

The primary component of this installation is a piece of ¼ in. thick sheet metal cut in the shape of a “star”. The metal star piece, shown in Figure 4-6, holds the gauges at a specified distance from each other and from the inside edge of the pile. The star can be positioned at the desired depth on an inclinometer pipe which runs down the center of the pile to the bottom of the pile. Each star can accommodate up to four strain gauges; however, for this project only two gauges were used at each depth.

The vibrating wire gauges were attached to threaded bolts which in turn were attached to opposite sides of the star through pre-drilled holes. The bolts were secured using a washer and nut on each side of the star. The strain bars were attached using small, wooden blocks and bailing wire. The wood blocks were placed on both ends of

the gauge bar between the bolt and the gauge bar. The bailing wire was then wrapped around the three and tightened to keep the gauge bar secure. The plucker was then attached to the bar with a hose clamp as shown in Figure 4-7. The lead wire was then run along the edge of the star and up the pipe to the surface.

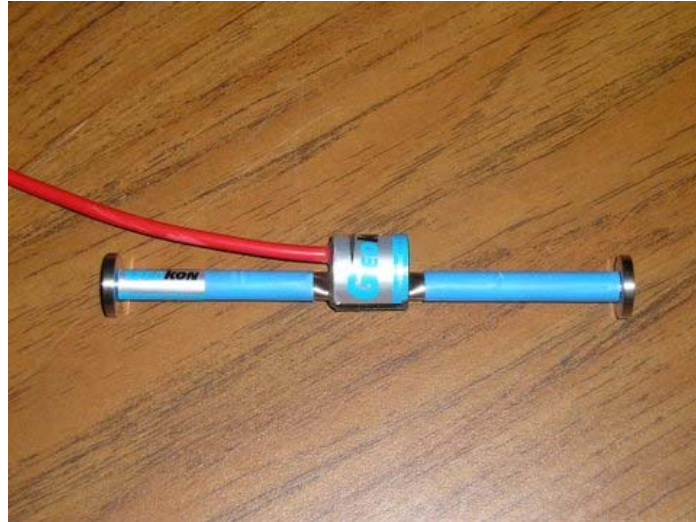


Figure 4-5 Vibrating Wire Strain Gauge Model 4200 used for Installations in Salt Lake City, UT



Figure 4-6 Metal Star used in Gauge Installation and Assembly for Salt Lake City, UT

The star assembly was slid onto the pipe being used. Inclinator pipe was used in these installations and has worked very well because of its durability and flexibility. In order to have the star securely fastened to the pipe, two wooden blocks were cut with an inner diameter just slightly larger than the pipe and were fastened to either side of the star with two bolts. The wood blocks were then fastened to the pipe using hose clamps. Figure 4-7 shows the entire assembly fixed onto its predetermined location of the pipe.

To install the completed pipe segments in the pile two different methods were utilized. Installation at Redwood Road was done without any equipment. Installation was accomplished by attaching sections of pipe together one at a time and manually lowering the assembly down the pile. Steel bars were used to support the assembly as a new section was connected. This method of installation is shown in Figure 4-8.



Figure 4-7 Completed Assembly of Star and Gauges Attached to Inclinator Pipe for Installation

Although this method does not require more than a simple ladder, it is a more time intensive installation and is harder to work with the lead wires. As the sections are

lowered into the pile, the wires were attached to the side of the pipe using duct tape to protect them from damage due to falling concrete. Note that when the sections are lowered that the gauges are below the star. This allows protection for the gauges when the concrete is poured. Ideally, the aggregate in the concrete will hit the metal star and ricochet off; not directly hitting the gauges.



Figure 4-8 Installing Pipe Sections One at a Time at Redwood Road and SR-201 (author photo)

The other way to install the sections is to have a crane, concrete pump truck or forklift available. Using one of these machines, the sections can be put together on the ground and the wires can be taped to the pipe while still on the ground which saves a great deal of time. Up to four sections (40 ft length) can be connected without breaking the pipes as they are lifted up. After the first combined section is lowered down, the next

combined section of pipes can be connected and the wires from the bottom gauges can be taped to the pipe. Figure 4-9 shows an installation done in Sacramento, CA using a forklift. The installation done in Sacramento is not part of this project, but was performed using the same method for three piles at that site.

When concrete is poured, the tremie should be directed as much away from the gauges as possible, but as indicated previously, most aggregate should not hit the gauges directly during free-fall because the gauges are beneath the star. The gauges can be oriented to whichever direction is desired for the data collection process.



Figure 4-9 Installing Multiple Sections using Forklift in Sacramento, CA (author photo)

4.3 Data Logging Equipment Used on Sites

The data acquisition equipment used to collect the data is manufactured by Campbell Scientific Inc., with headquarters in Logan, UT. A CR10X model was being used to collect data at specified periods of time. The CR10X model is capable of collecting 62,000 points of data before it begins to write over the previous information. Communication with the data logger is achieved through a computer program named Loggernet, also created by Campbell Scientific Inc. With Loggernet, the user is able to download data from the data logger and update the program stored in the data logger.

Lead wires are connected to the data logger with the help of three additional components. The first is called a multiplexer. Up to 16 gauges can be connected to the multiplexer, with any additional gauges being connected to the second device. The second device is an AVW1 connector. This part serves to allow expansion in the number of gauges that can be hooked up to a single data logger. The last device is the battery which powers the data logger. The battery can be backed up by a solar panel if long term testing is desired as was the case for these installations. The entire assembly is shown in Figure 4-10. The assembly has been placed in a steel box to keep water out and to provide protection to the equipment. The box can be moved to any place that is out of the way of the construction process so consistent long term monitoring can occur.

For this study, the data logger was programmed to take readings from each gauge every minute and to store a reading every hour on the hour. For the quantity of gauges being used approximately 1300 readings can be taken. This amounts to about 55 days of continual data storage without the need for downloading. Of course, this length of time depends upon the number of gauges installed and being monitored, and decreases it as

more gauges are attached. Data is preserved by downloading the current data before the capacity is exceeded and the previous data is overwritten.



Figure 4-10 Data Logger with other Components and Wires Attached

4.4 Analysis Methods of Collected Data

After being downloaded, the data may be analyzed to find the trends in strain occurring in the pile. For each pile, a strain gauge is located on the east and west side at all depths. Strain readings are obtained from the data logger and can be compared to the initial reading taken shortly after installation.

These readings are corrected for the difference in expansion rate for concrete and steel and also for temperature. Equations are supplied by Geokon Inc. to correct these differences and to calculate the actual load-related strain, which can be used to calculate load and stress for the pile at those depths.

To determine the stress and load in the pile at a gauge location, Equation 4-1 and Equation 4-2 are used respectively. Equations 4-3, 4-4 and 4-5 are provided to supply the terms used in Equations 4-1 and 4-2.

$$\sigma = \varepsilon E_{comp} \quad (4-1)$$

$$P = \varepsilon(AE)_{comp} \quad (4-2)$$

$$E_{comp} = E_{Concrete} + E_{Steel} \quad (4-3)$$

$$(AE)_{comp} = A_{Concrete} E_{Concrete} + A_{Steel} E_{Steel} \quad (4-4)$$

$$E_{Concrete} = 57,000 \sqrt{f'_c} \quad (4-5)$$

In the preceding equations, σ is the stress in the pile (psf or kN/m²), ε is the strain measured from the gauge (dimensionless), E is the Modulus of Elasticity of concrete, steel or the composite (psi or kN/m²), P is the load in the pile (lbs or kN), A is the cross-sectional area for the concrete or steel (in² or m²) and f'_c is the compressive strength of the concrete (must be in units of psi).

Stress and load for each gauge are computed in accordance to Equations 4-1 and 4-2 and are plotted with respect to depth and time. These plots, especially the load plot, are used to determine the neutral plane for the pile-soil system. The neutral plane is located in the vicinity when the load peaks and then drops off. This phenomenon will be seen later in the discussion of the results.

Also calculated from these strain measurements is the unit skin friction (or shear stress) along the length of pile. Based on previous research described in the literature review, the unit side resistance on the pile can be estimated using either the total stress method (α method) or the effective stress method (β method). For the total stress method, the unit shear stress should approach a value approximately equal to the undrained shear strength multiplied by the α value for the soil and then begin to plateau. This plateau-like behavior can be seen by plotting the unit side resistance for each pile segment over time. The unit side resistance has been computed by two different methods, namely, the double segment method and the single segment method. These names are the creation of the author. Each method will be described in more detail in subsequent sections.

4.4.1 The Double Segment Method for Calculating Unit Side Resistance

The double segment method uses the length of pile that spans the distance between three gauges. Each segment is the length between two gauges. Figure 4-11 shows the various terms used in calculating the unit shear stress. The values E_1 , E_2 and E_3 are the elevations of the gauges for the two segments being considered. The values P_1 , P_2 and P_3 are the corresponding load values, calculated previously for the pile at their respective gauge elevation using Equation 4-2.

Equations 4-6 and 4-7 compute the elevations of the midpoints of each section while Equations 4-8 and 4-9 compute the average load for the top and bottom segments respectively.

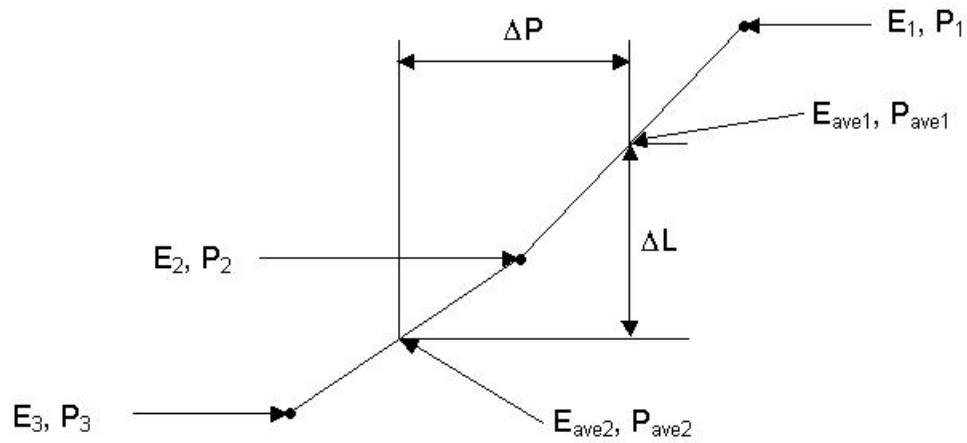


Figure 4-11 Depiction of Double Segment Method for Calculating Unit Skin Friction

$$E_{avg1} = \frac{E_1 + E_2}{2} \quad (4-6)$$

$$E_{avg2} = \frac{E_2 + E_3}{2} \quad (4-7)$$

$$P_{avg1} = \frac{P_1 + P_2}{2} \quad (4-8)$$

$$P_{avg2} = \frac{P_2 + P_3}{2} \quad (4-9)$$

The distance (ΔL) between the two midpoints found in Equations 4-6 and 4-7 is found using Equation 4-10 and the change in load (ΔP) between the midpoints is found in Equation 4-11.

$$\Delta L = E_{avg1} - E_{avg2} \quad (4-10)$$

$$\Delta P = P_{avg1} - P_{avg2} \quad (4-11)$$

After ΔL and ΔP are known, the unit side resistance (τ) between the two midpoints can be calculated using Equation 4-12.

$$\tau = \frac{\Delta P}{\pi D \Delta L} \quad (4-12)$$

where D is the outer diameter of the pile. The double segment method works for all places along the pile except for the two segments above and below the neutral plane. Due to the change in direction of the load curve, the change in load could be positive or negative, resulting in an oscillating plot of shear stress over time.

4.4.2 The Single Segment Method for Calculating Unit Side Resistance

The single segment method is very similar to the double segment method, but as indicated by the name, only uses two gauges and one segment. Figure 4-12 shows a representation of the single segment method and parameters. The following equations are used to calculate the shear stress by this method.

With this approach, ΔL and ΔP are simply based on the values at the segment ends as defined in Equations 4-13 and 4-14 respectively. The unit side resistance is then calculated using Equation 4-15 utilizing the values for ΔL and ΔP found for the single segment.

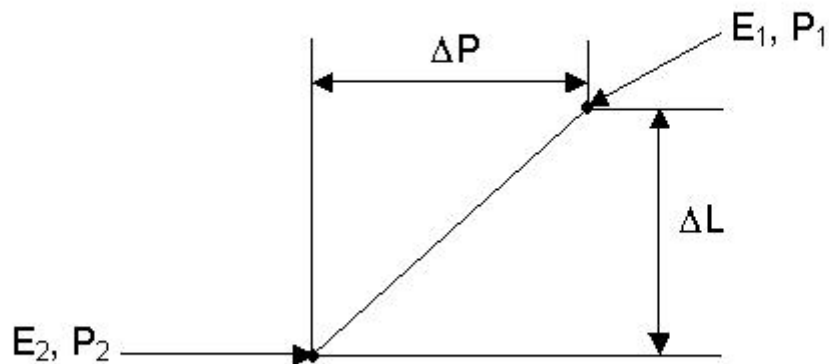


Figure 4-12 Depiction of Single Segment Method for Calculating Unit Skin Friction

$$\Delta L = E_1 - E_2 \quad (4-13)$$

$$\Delta P = P_1 - P_2 \quad (4-14)$$

$$\tau = \frac{\Delta P}{\pi D \Delta L} \quad (4-15)$$

This method does not have the same deficiency as the double segment method does with respect to the neutral plane. Since this method only uses two end points, the change in load and elevation will both be represented accurately. The shear stress values can also be plotted over time to determine their value relative to the undrained cohesion or frictional resistance of the soil. The values for the two methods should yield similar, albeit not equal, results.

4.5 Calculating Pile Settlement

Another parameter that can be calculated from the strain measurements is the settlement (compression) of the pile due to the loads induced by the surrounding soil settling and the structural load on the surface. By calculating pile settlement, the neutral plane can be found. By definition, the location of the neutral plane is the location where the pile and the soil settle at the same rate. If the surrounding soil is being monitored for settlement, especially at various levels within the profile, the settlement of the soil and the settlement of the pile can be placed on the same plot. The location where the two settlements are identical is the location of the neutral plane.

Pile settlement can also be calculated by two different methods, yielding a good definition of the settlement at different locations. The settlement can be calculated at the gauges or at the midpoint between gauges. After calculating by both methods, the two sets of values should lie in the same line. An explanation of each method will now be given. In both methods, the strain, ε_i , is obtained directly from the strain gauge measurements and values calculated from both methods are used to produce a better looking curve.

4.5.1 Method for Calculating Pile Settlement at Gauge Elevations

The best way to demonstrate this method is by the use of Figure 4-13 which shows the various components that enter into the overall method. The values E_i are the elevations of the individual gauges. The values ε_i are the strain values for the gauges at their respective locations. The three lengths identified as L_0 , L_1 and L_5 are used because they are located where the gauges are at either the top (L_5) or bottom (L_0 and L_1) of the pile. The other lengths are determined by subtracting the gauge elevation from the

midpoint of that gauge and the gauge above it or by subtracting the midpoint elevation of two gauges from the elevation of the top gauge. Simply dividing the distance between two midpoints cannot be done unless the gauges are equally spaced, which is not the case for either pile being monitored. The values for Δ_i represent the cumulative settlement (compression) of the pile at that elevation. This settlement begins from the bottom of the pile and accumulates as the surface is approached. The equations to compute the cumulative settlement for each location are shown in the equation to the right of the pile.

4.5.2 Method for Calculating Pile Settlement at Midpoints between Two Gauges

This method is very similar to the previously discussed method, but happens to be simpler. The cause for greater simplicity is that since the lengths involved are distances between two gauges, this distance can be safely divided in two, no matter how the gauges are spaced. In other words, the distance between two gauges does not change, but the distance between midpoints does change. Figure 4-14 shows the setup for calculating settlement using this method. Once again the equations are on the right of the drawing for easy visualization.

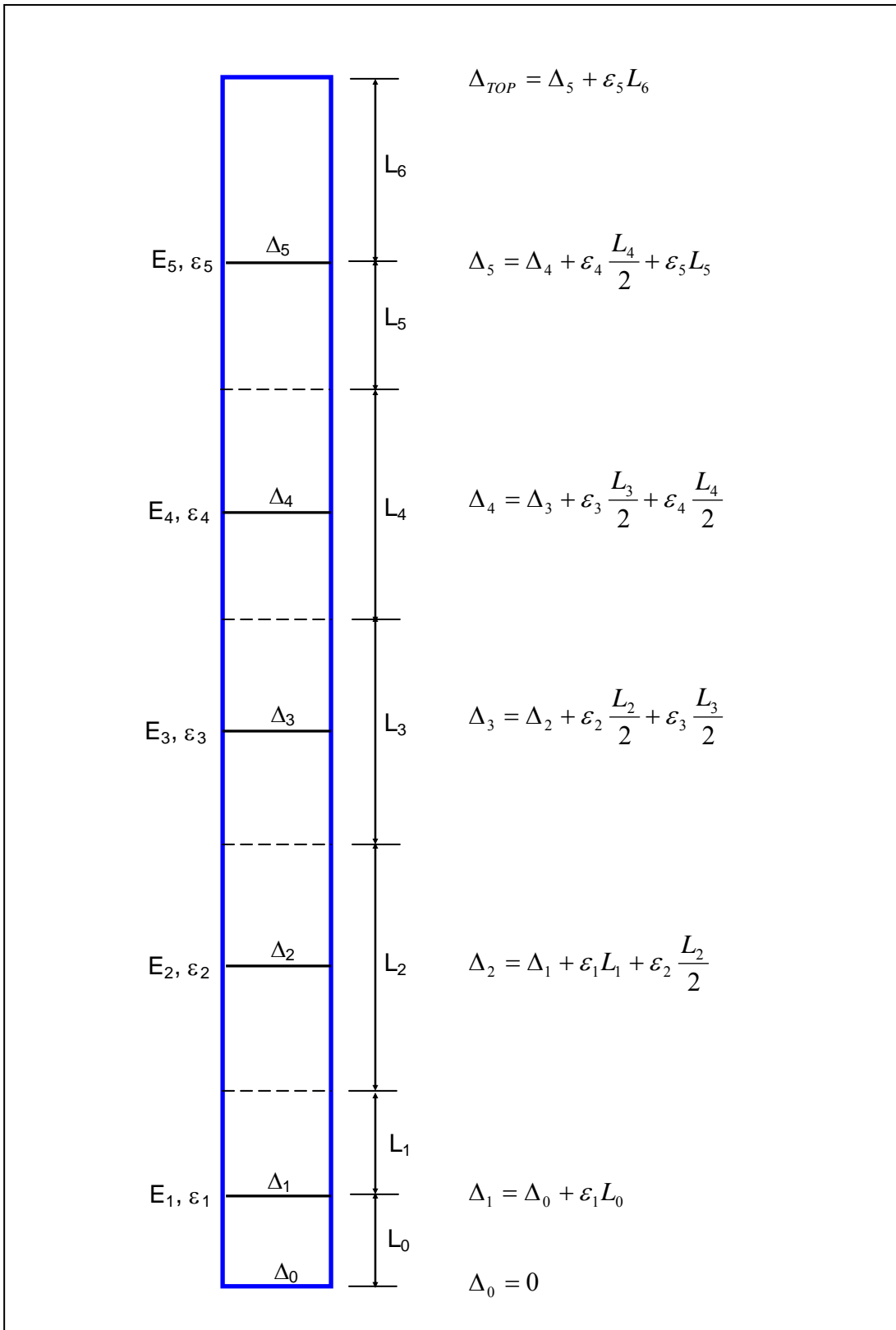


Figure 4-13 Depiction of Calculating Pile Compression at Gauge Elevations

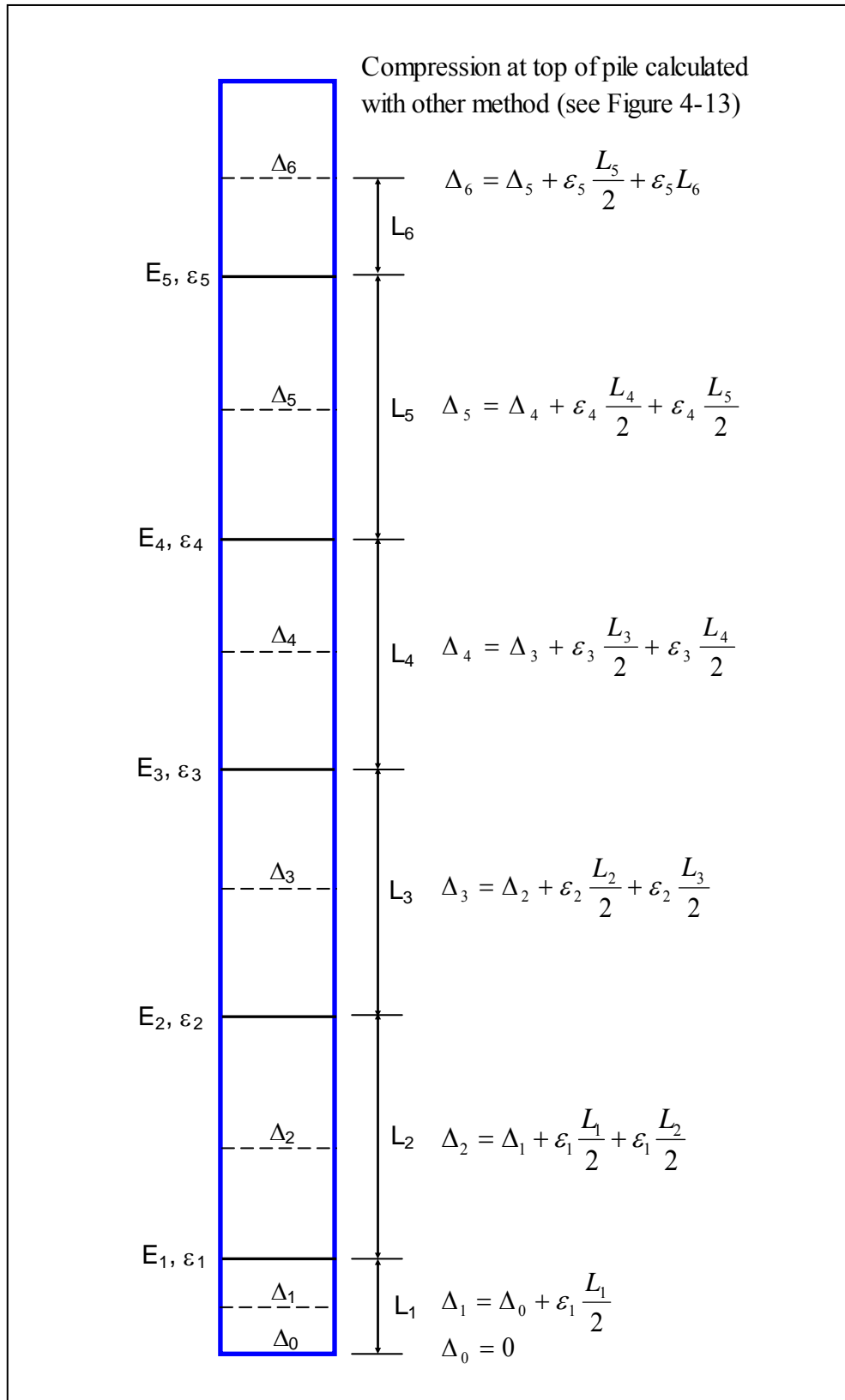


Figure 4-14 Depiction of Calculating Pile Compression at Midpoint of Gauges

5.0 Results from Redwood Road and SR-201 Site

To properly understand the data and conclusions obtained from an analysis of the raw strain gauge data, various details about the Redwood Road and SR 201 site (referred to as the Redwood Road site) need to be given. This information includes: abutment layout (configuration of abutment, pile placement, etc...), construction history, gauge depth placement and orientation, gauge installation details, gauge performance, and the settlement time history. This information will enable a better understanding of the test results as they are presented in load versus depth, shear stress and settlement plots.

5.1 Construction Site Details, Pile Layout and Construction Timeline

5.1.1 Abutment Layout

As previously mentioned in Section 3.1, the test pile is located in the east abutment for the CD-Line bridge. The approach begins approximately 900 feet to the east of the abutment face at approximately original ground elevation and reaches a maximum fill height of approximately 25-26 feet at the pile locations. The approach is bounded on both sides by MSE walls with the MSE wall on the south extending east of the abutment for approximately 323 feet and the MSE wall on the north extending east for about 781 feet.

The foundation system is comprised of seven piles spaced in a slightly irregular fashion ranging from 5' 10 ³/₈" to 7' 1/2" center-to-center. The steel piles are 16-inch OD piles with a wall thickness of 0.5 inches driven closed-ended and the piles were filled with concrete. A pile cap ranging in thickness from 5.0 feet to 6.54 feet was placed on the piles with a bottom El. of 4251. The MSE wall which supports the abutment face is located approximately three feet beyond the western edge of the pile cap. When fill operations were underway, the entire area around the piles and in between the cap and MSE wall was filled. A general schematic drawing of the abutment and approach fill is shown in Figure 5-1.

The pile cap was poured after the final surcharge fill had been placed, but before the surcharge had been removed. This created a cause for concern with regards to settlement below the pile cap. From a project memo numbered 25.6 written on 23 Decemeber 2005 by AMEC, the following two items of information were stated. First, the structural engineer for the project indicated that the piles had been designed for downdrag conditions and "some loss of soil support beneath the pile cap will not adversely affect the structural performance of the bridge." Second, AMEC engineers gave it as their opinion that although some settlement may be fine from a structural standpoint, the void space created by settlement could result in adverse differential settlement and therefore recommended that the voids be filled with cement/sand grout or flowable fill after the surcharge and subsequent settlement was complete.

5.2 Construction Timeline

Five piles were driven at the east abutment prior to the driving of the remaining three piles (one test pile was not used in the final structure). These piles were driven sometime in September or October 2004.

A pile load test (performed in general accordance with ASTM D-1143) was conducted using these test piles on 22 – 23 October 2004. These tests verified the design capacity of the piles for the project. A maximum load of 780 kips was applied with a maximum pile settlement of 0.507 inches and a total permanent deflection of 0.087 inches. A plot of the load-deflection curve for the pile load test data is presented in Figure 5-2. Although readings were taken at 800 kips, the pile load test report from AMEC states, “It is apparent from the shape of the load-deflection curve above 700 kips that the jacking system was unable to fully apply the 800 kip load.”

The installation of strain gauges in the test pile took place on 22 March 2005, with the pile sticking up approximately 1.5 feet above ground. Concrete was poured in the pile the following day. The east abutment sat dormant for approximately three months while work progressed on the west abutment and other areas of the construction site. In June 2005 the author received notification that an additional length of pile would be welded on the existing pile to bring it to the correct elevation for the structure, in preparation for fill placement for the abutment approach. Before the additional pile length was added, the author with the help of other students from Brigham Young University welded a steel box onto the additional pile length to house the data logging equipment to keep it safe from construction activities.

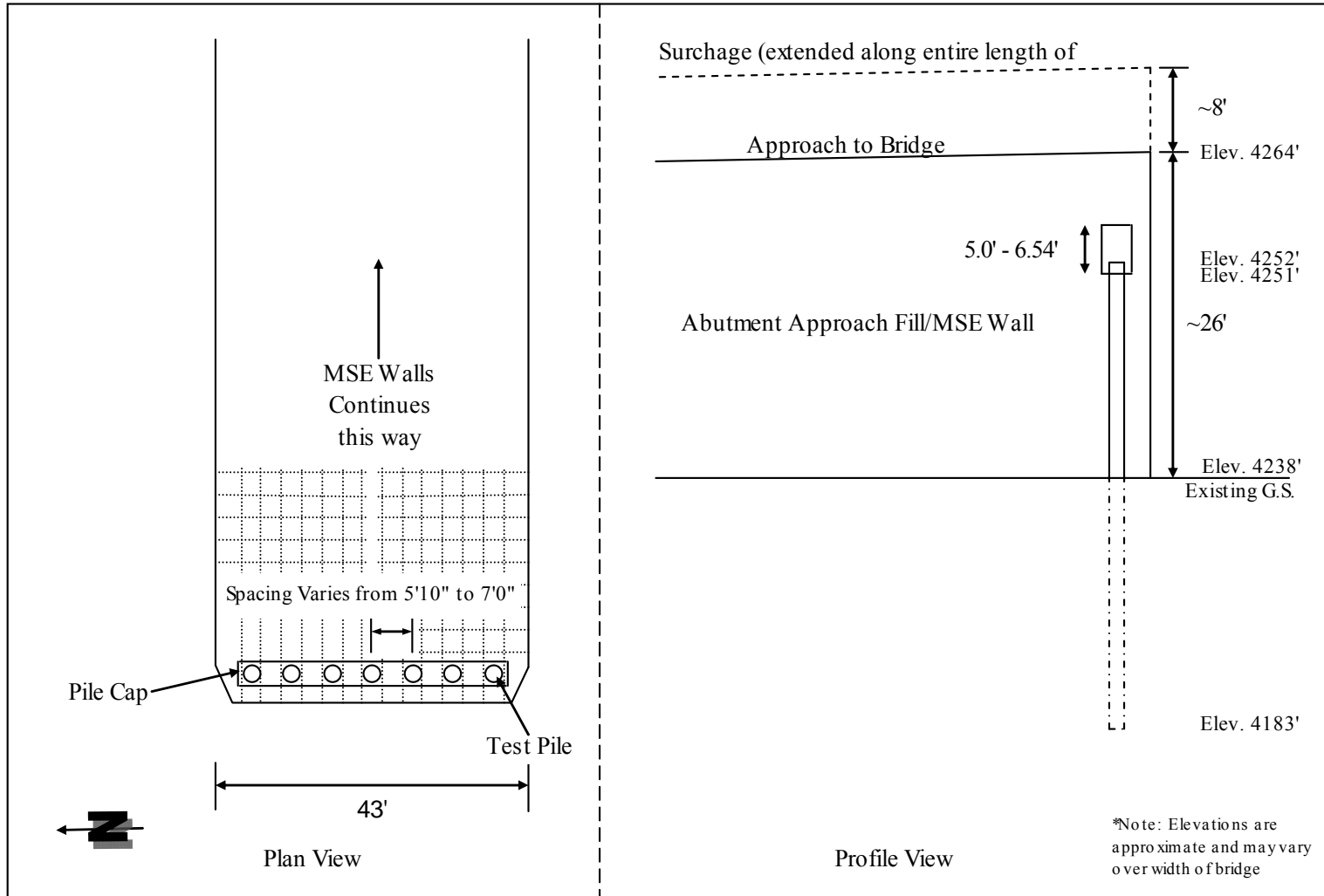


Figure 5-1 Schematic of East Abutment and Approach Fill at Redwood Road and SR-201 Site

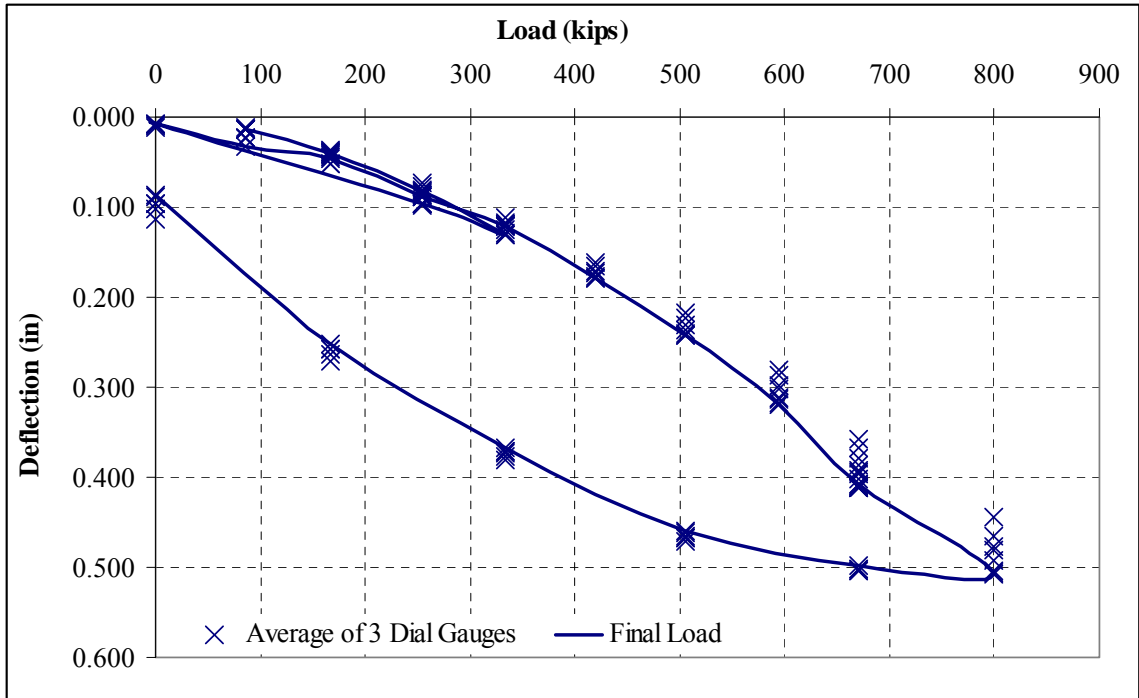


Figure 5-2 Reproduction of Pile Load Test Results for Test Pile at Redwood Road Site

After the additional pile length was added (making a total pile length of 69 feet), the wires were run up the side of the added pipe length (protected by a piece of angle iron) and connected to the data logging equipment. Readings were taken from this location until the pile cap was ready to be poured. Concrete was placed in the added length of the test pile at a later date.

Multiple parts of the structure contribute additional dead load on the pile. The timeline for the various stages of the construction process is summarized in Table 5-1. The load columns include the weight of the concrete and reinforcing steel as calculated from the construction plans and checked against amounts used as supplied by the contractor. The loads reported in Table 5-1 are those felt only by the test pile. Loads for the approach slab were not included as the slab rests on the embankment and not on the piles.

The loads were calculated for the abutment and then multiplied by the tributary area based on the distance to the edge of the abutment and the nearest pile. The tributary area is approximately equivalent to one-eighth of the total load for the abutment. Even though the pile is on the edge, an equivalent area method as used gives a close approximate of the loads felt in the pile. Some piles will “feel” different portions of the structural load in different magnitudes thus attempting to calculate the exact amount for the test pile is not considered necessary for this research, nor is it believed that it would influence the total load by a substantial amount.

Table 5-1 Construction Timeline at Redwood Road and SR-201 Site

Construction Item	Date Placed	Individual Applied Pile Load (kip)	Cumulative Applied Pile Load (kip)
Embankment Fill	Jul '05 - Feb '06	~ 25 ft high	-----
Surcharge Fill	15 Feb 2006	8 ft high	-----
Pile Cap	27 Feb 2006	17.8	17.8
Girders	7 Mar 2006	18.4	36.2
Deck	12 Apr 2006	52.7	88.9
Wingwall C	Between 12 Apr & 15 May 2006	4.6	93.5
Wingwall D		3.4	96.9
Surcharge Fill Removed	15 May 2006	-----	-----
Parapets (on deck)	16 May 2006	13.8	110.7
Diaphragm Wall	17 May 2006	20.4	131.1
Sleeper Slab	31 May 2006	3.4	134.5
Approach Slab	8 Jun 2006	0.0	134.5
Parapets (on abutment)	11 Jun 2006	3.9	138.4

A discussion of the reaction of the pile to these major stages of construction will be given later in this chapter.

5.3 Gauge Information

A summary of the information regarding the location of the gauges on the pile (i.e. the approximate elevation where it rests), their installation, working history and performance will be presented.

5.3.1 Depth Placement

The pile located at the Redwood Road and SR-201 site was instrumented with 16 strain gauges. The gauges were distributed along the length of the pile to define the distribution of load along the pile and identify the location of the neutral plane. Gauges were also placed so as to monitor the unit side resistance within as many soil layers as possible. Therefore, the gauges were usually placed near the interface of two layers, but this was not always possible due to the limited number of gauges. Figure 5-3 shows a drawing with the locations of the strain gauges on the pile in relation to the soil profile from borehole B-35, which was initially used to determine the depths to place the gauges. It should be noted that the profile shown in Figure 5-3 is not identical to that given later in this chapter. The final stratigraphy for this site, as shown in the load versus depth plots, was a product of the three closest borings and not only borehole B-35.

5.3.2 Site Installation and Equipment History

As indicated in Section 5.2 the installation was completed at this site on 22 March 2005 with concrete being poured in the pile the next day. This pile was also instrumented with rapid sensing gauges to be used in a statnamic load test. The statnamic load test was completed on 4 April 2005 with three separate tests at progressively higher force levels.

The pile remained dormant for the next three months during construction activities elsewhere on site.

Initial readings were taken on 15 June and 1 July 2005. No readings were taken between these two dates. The readings taken on 15 June were only to verify that all the gauges were working in proper order. Consistent readings began on 1 July and continue to the present. The data logging system was programmed to take readings every minute and to store a reading every hour on the hour.

Unfortunately, the data logging process wasn't understood well by the author at first and the data was not downloaded for the first time until 8 September 2005. By this time the data logger had reached maximum capacity and had begun to overwrite the first days of data. Due to some of the data being overwritten, the earliest record of continuous data was from 6:00 AM on 14 July 2005.

A brief analysis of the gauge readings shows that no fill activity occurred during the period of time when data was overwritten. Figure 5-4 shows the changes in measurement of the west gauges from the initial reading taken on 15 June 2005 and those taken on 1 July and 14 July 2005. The line with the legend title "1-14 July 2005" is the difference in measurements from 1 July 2005 and 14 July 2005. The maximum change for the west gauges is 13 microstrain ($\mu\epsilon$), which is a not a significant amount.

Figure 5-5 shows a comparison of the east gauges with the same differences in strain measurements being taken. The gauge at the surface shows a change of approximately 27 $\mu\epsilon$, which could at first be seen as a problem, but the relative change between the readings on 1 July and 14 July is only about 1 $\mu\epsilon$. This shows that virtually no change in readings occurred during the period of lost data.

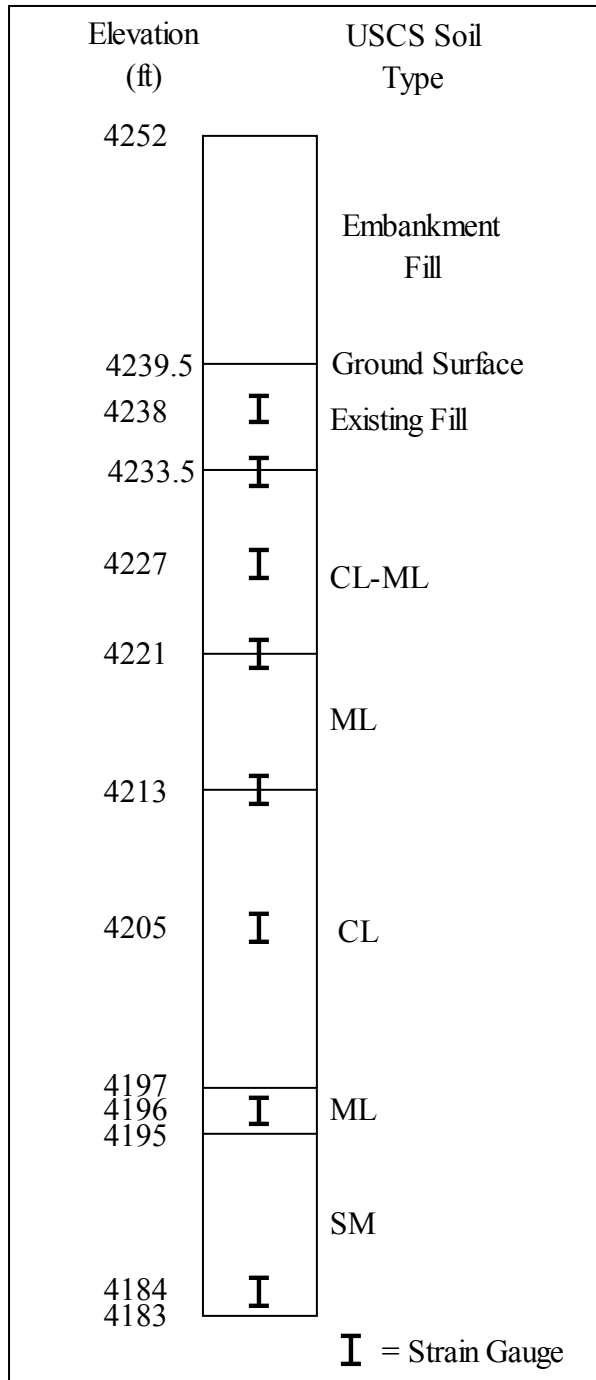


Figure 5-3 Location of Gauges on Test Pile at Redwood Road & SR-201

The last figure on this subject, Figure 5-6, shows a comparison of the change in strain measurements for both the west and east gauges between the readings on 1 July and 14 July 2005. From Figure 5-6 it can be seen that a change of no more than eight (8)

$\mu\epsilon$ was experienced in any of the gauges, indicating initial “unstrained” readings could still be obtained.

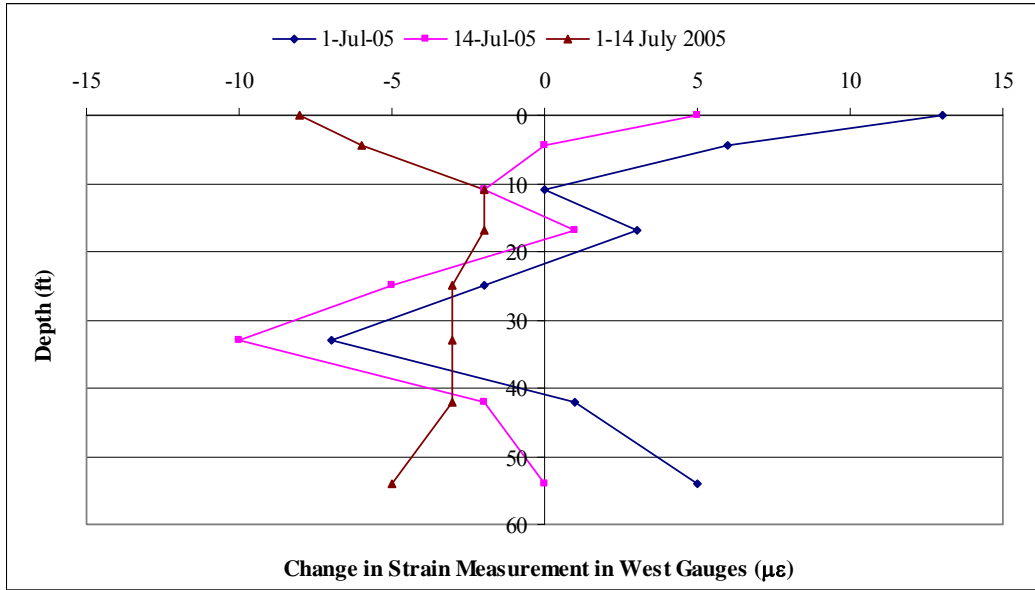


Figure 5-4 Change in Strain Measurements for West Gauges from Initial Reading on 15 June 2005

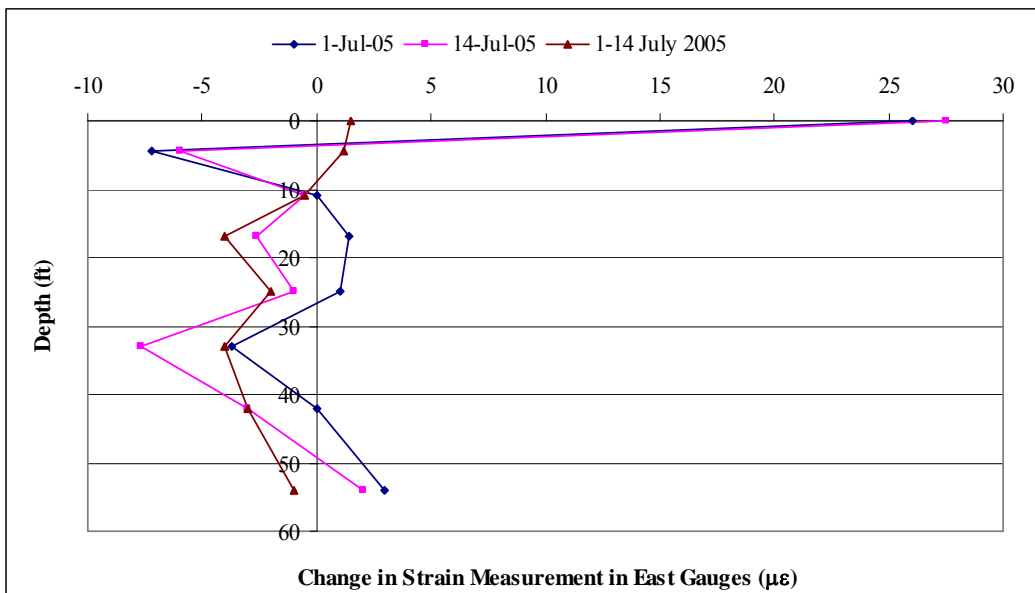


Figure 5-5 Change in Strain Measurements for East Gauges from Initial Reading on 15 June 2005

Continuous readings were obtained from 14 July 2005 through 27 December 2005. On 27 December 2005 almost all gauges experienced a period of malfunctioning. The reason for this malfunctioning is not known. There is a general agreement among the gauges that from 3:00 AM to 3:00 PM (some gauges started as early as 1:00 AM and ended as late as 6:00 PM) some problem was experienced that affected almost all the gauges. Some problems reoccurred the next day, but for very few hours. These readings have been fixed by looking at the readings before and after the problem data and also, if needed and available, the relative change of the gauge opposite on the same level. After the period of malfunctioning the gauges returned to readings close to or identical to the readings prior to the malfunctioning.

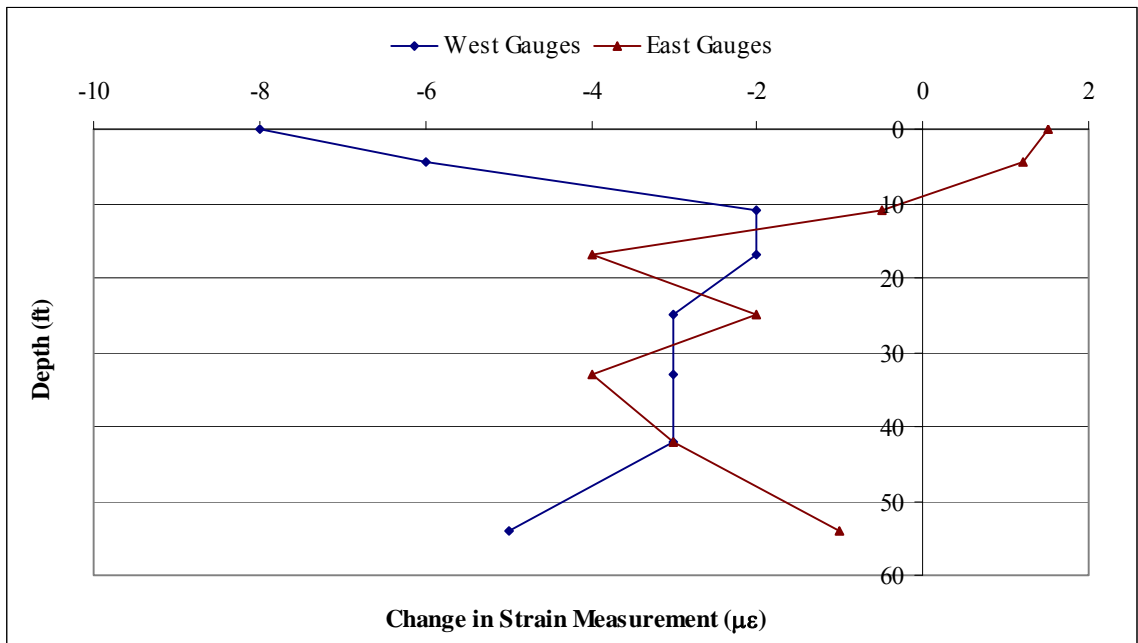


Figure 5-6 Comparison of Change in West and East Gauges between Readings on 1 July and 14 July 2005

Other than the small problem in December, continuous readings were then taken until a shutdown occurred due to water leaking into the box. This shutdown occurred on 15 April 2006. The problem was not diagnosed until the author went to download data on 5 May 2006. The problem was rectified by replacing one of the components and reconnecting all the wires. By this time, the construction process was far enough along to allow for the box to be placed on a shelf on the abutment, located below the bridge deck, where it now sits. The wires were reconnected on 12 May 2006. Luckily, no main components of the structure were placed during the time the system was down and consolidation settlement was essentially complete at this point.

A gap in the readings is present between 3 April 2007 and 3 November 2007. This gap was due to the unavailability of personnel from BYU to download readings after the author's departure from BYU. A similar trouble period was experienced in December 2007 and January 2008 of gauges or the data logger malfunctioning. Beginning on 30 November 2007 until the data was downloaded again on 28 January 2008 the gauges are missing numerous amounts of data, usually blocks of hours in the early morning and sometimes in the evening. There are occasional days in which the readings exist for all hours of the day, and those have been used in the plots to follow in this chapter.

5.3.3 Gauge Performance

When the gauges were connected for the first time in July 2005, all gauges were working properly. This gave confidence in the system of installation, despite the potential damage to gauges due to the falling concrete during installation. All 16 gauges continued to work properly until 16 August 2005. The west side gauge located at El. 4233.5 (4.5 feet down from original ground surface) ceased to give strain measurements

at 11:00 PM. The gauge continues to give temperature measurements. All other gauges have continued to give readings for both temperature and strain.

5.4 Presentation and Discussion of Data and Analyses

The strain readings collected from the individual gauges have been reviewed and reduced to obtain axial stress and axial load; shear stress; and pile settlement as discussed in chapter 4. Analyses have been completed according to the equations defined in chapter 4. Each of these parameters will be discussed in this section.

5.4.1 Axial Stress and Axial Load

Axial stress and axial load are related very closely to each other as one calculation is simply the product of a constant multiplied by the other. For this reason, the axial stress and axial load will be presented and explained together.

5.4.1.1 Derivation of Axial Stress and Axial Load

Axial stress in the pile is a product of the strain and the composite elastic modulus of the pile as defined by Equation 4-1. The individual and composite elastic moduli of the pile are found in Table 5-2. The composite modulus is computed using Equation 4-4.

Table 5-2 Modulus of Elasticity and Cross-Sectional Area for Piles at Redwood Road & SR-201 Site

Material	Elastic Modulus, E (psi)	Cross-Sectional Area, A (in ²)	AE (lbs)
Steel	29,000,000	12.37	358,730,611
Concrete	3,416,673	181.62	620,547,581
Composite	N/A	193.99	979,278,192

The total cross-sectional area of a 16-inch diameter pile is 201.06 in² which is greater than the composite area listed in Table 5-2. The reason for the difference is the

subtraction of the area of the inclinometer pipe (which has a 3-inch outer diameter). The modulus of elasticity for steel is a typical value based on manufacturing specifications. The modulus of elasticity for the concrete is based on the compressive strength of concrete (f'_c), being 3,593 psi. This value is the average of three test cylinders taken during concrete placement on 23 March 2005. The cylinders were broken on 2 April 2005, 10 days following the pour to coincide with a static test. The average compressive strength for the 10-day breaks was 2,695 psi. Typically, the compressive strength at 7 days is approximately 70% of the 28-day compressive strength. Using this correlation and assuming the 10-day strength to be at 75% of the 28-day strength, the value of 3,593 psi is obtained. The minimum acceptable compressive strength for concrete specified in the plans for the piles in this project was 3,000 psi. Strain measurements from the gauges allow stress to be calculated along the length of the pile, but since there is not a gauge at the very top of the pile, the strain is unknown. Therefore, the stress can not be calculated using Equation 4-1. However, because the structural loads acting on the top of the pile are known, the stress can be calculated at the top of the pile as well. This calculation is done by using equation 5-1.

$$\sigma = \frac{PE_{Composite}}{(AE)_{Composite}} \quad (5-1)$$

Values for axial load have been calculated using Equation 4-2. Load is simply the product of the strain multiplied by the composite AE for the pile. The plots for axial stress and axial load look identical in shape and only differ by their respective units.

5.4.1.2 Presentation and Discussion of Results for Stress and Load Analyses

To better understand the discussion to follow, a look at the load versus depth curves for the gauges on each side will be helpful. Figure 5-7 shows the load versus depth curves for the west (left plot) and east (right plot) gauges. Negative load values indicate the gauge is measuring compression. In some cases, there is significant difficulty in assessing if only one gauge is correct or if an average should be used. The following discussion will highlight the opinions of the author as to the use of the gauges and ultimately a load plot will be created using a combination of individual gauges and averages for each elevation. Following the plot in Figure 5-7, the various inconsistencies will be discussed.

5.4.1.2.1 Gauge Inconsistencies

The first problem lies with the gauge at El. 4238, or the original ground surface. The gauges show widely varying results, with the east gauge in much greater compression than the west. Initially, this result suggests that the load on the pile is eccentrically applied.

In Section 5.3.3 it was explained that the west side gauge at El. 4233.5 ceased to function about a month after readings began. This created a problem immediately. When comparing the average increase for gauges at other elevations, the east gauge at El. 4233.5 tends to increase at approximately the same rate as the average of the gauges in the nearby vicinity until loading began and then the readings showed erratic increases much larger than the average. This behavior seems to indicate a problem with the gauge. This discrepancy increases the problem at this elevation since the west side gauge failed.

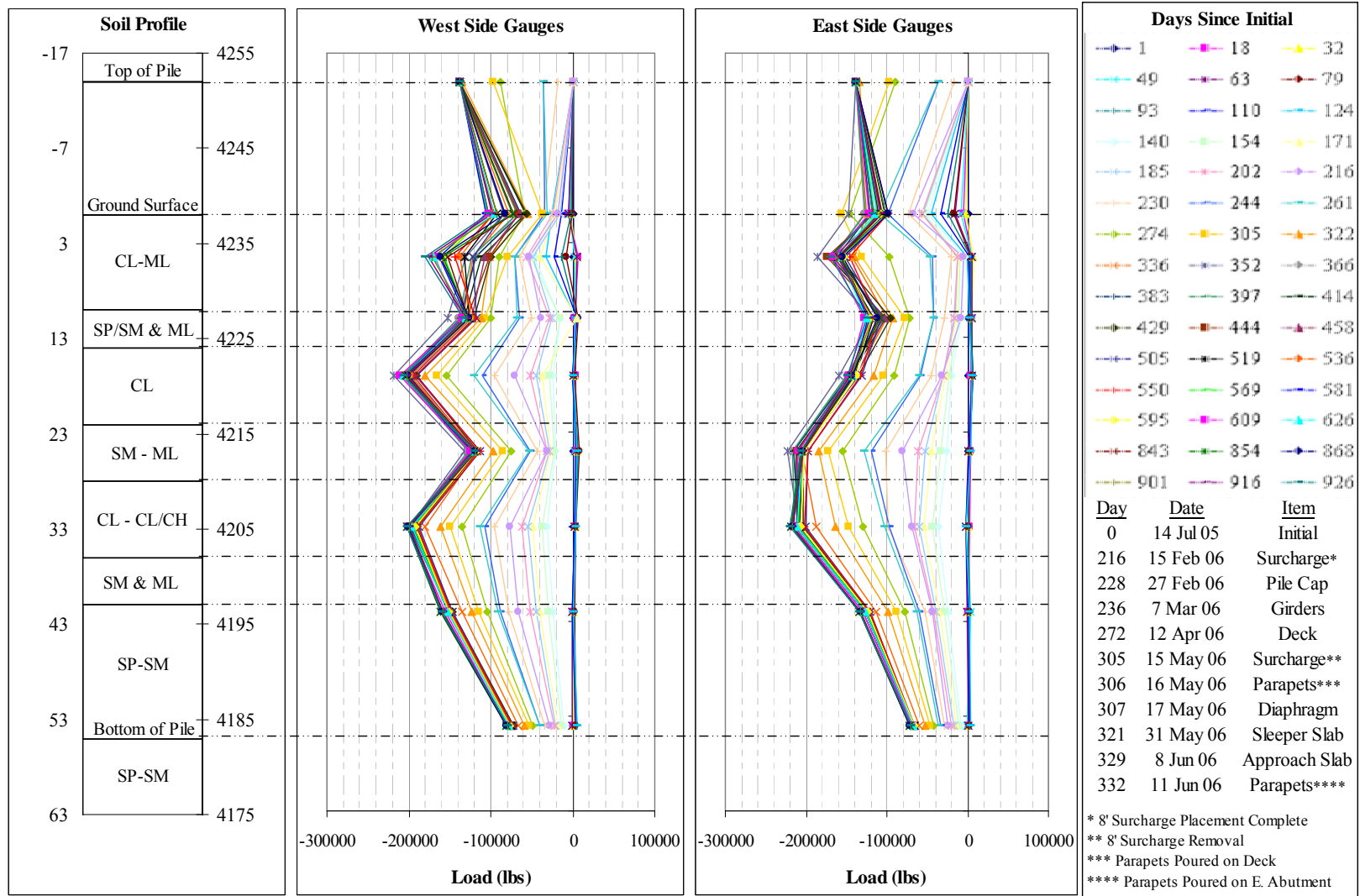


Figure 5-7 Comparison of West and East Gauges for Redwood Road and SR-201 Site

The gauges at El. 4227 show a similar kind of result to that of the gauges at El. 4238. This time the west gauge is larger in compression than the east gauge. For readings taken up through 1 April 2006 the compression measured by the west gauge is less than the gauge above it, which should not be the case as negative skin friction should be present above the neutral plane. The east gauge has shown this same result from the beginning.

Measurements of skin friction should not decrease before the neutral place is encountered. Use of the west gauge seems more reasonable than the east gauge or an average. However, even using the west gauge, does not seem to give a consistent curve. Like the gauges at the elevation just above this, it is difficult to decide on an appropriate action. This conclusion is based primarily on what the correct direction of the skin friction should be.

The gauges at El. 4221 show the west gauge significantly greater in compression than the east gauge. It appears that the use of the gauge average or the west gauge by itself should be used. Choosing between the two available options is not easy since the average of the gauges is more consistent when shear stress is considered, but the use of the west gauge aids to verify conclusions regarding the location of the neutral plane in reference to applied loads.

At El. 4213, it is very apparent that the west gauge is having problems. The gauge is still increasing in compression, but the magnitudes of the gauges above and below indicate that the west gauge is not correct. The east gauge appears to give valid results and therefore seems to be the best candidate for use.

The gauges at El. 4205 are more consistent. Both gauges give magnitudes with a difference no greater than 18,600 lbs. Although the difference seems large, when compared to the measured loads the difference on average amounts to about 10% of the total load. This is encouraging considering the results for the gauges at higher elevations.

The gauges at El. 4196 also show encouraging results, although they are not as consistent as the previous two gauges. Differences in magnitude increase up to 29,200 lbs, or about 27% of the total load. This difference is much larger than for gauges at El. 4205.

The gauges at the bottom, El. 4184, have a maximum of 10,500 lbs difference, which is about 6% of the total load. This is best set of gauges in terms of maximum difference of load, giving slightly better results than the gauges at El. 4205 and much better than the remainder.

Although it is unfortunate that so many inconsistencies appear to exist in the gauges, it is understood that working with equipment in the field, especially when it cannot be reached to either repair or exchange, can be difficult. The results of the gauges are still usable and an explanation follows as to what is recommended for each level.

5.4.1.2.2 Recommendations for Gauge Usage

In the previous section, the various consistencies or lack thereof were discussed for each gauge elevation. This section describes the basis for decisions regarding which gauges to use for the final analysis.

For the gauge at the original ground surface, the decision falls between using just the west gauge or using the average of the gauges. In the end, using the average of the

gauges seems to fit better. Using the west gauge alone seems to produce an unreasonable break in the remainder of the plot.

The gauges at El. 4233.5 present the most difficulty. Since the gauge on the west side failed it would seem that using the east side would be the best option, but as discussed previously the east gauge appears to increase at an unreasonable rate. Using the east gauge will not work. However since the west gauge failed, there is no real data value that can be used. The final decision here is to use an interpolated value for the west gauge. This calculated value is obtained by using the gauge above and the two gauges below on the west side and assume that the closer the gauge is to El. 4233.5 the more likely the gauge at El. 4233.5 will change by the same amount. Equation 5-2 shows the weighting used to calculate the value that will be used at this elevation.

$$\Delta\varepsilon_{4233.5} = \frac{8}{12.5} \Delta\varepsilon_{4238} + \frac{6}{12.5} \Delta\varepsilon_{4227} + \frac{1}{12.5} \Delta\varepsilon_{4221} \quad (5-2)$$

The $\Delta\varepsilon$ terms refer to the change in strain from the previous hourly reading to the current. The subscript number is the elevation. The numerator in the ratio being multiplied by the change in strain is the difference of the maximum distance used in this comparison (i.e. subject El. of 4233.5 and farthest El. of 4221 therefore a difference of 12.5 feet) and the distance between El. 4233.5 and the other gauges elevation. The denominator is the maximum distance. For example, since the gauge at El. 4238 is 4.5 feet away from the gauge at El. 4233.5, the numerator is found by taking $12.5 - 4.5 = 8.0$. The ratio thus becomes $8/12.5$. The ratio for the gauge at El. 4221 needs a slight adjustment since you can't divide into zero.

The two primary reasons for this decision are based on the appearance of curves generated from past research, especially the work by Bozozuk (1981) and the direction of the skin friction that should be present at this location. It should be clearly understood that this is a calculated (interpolated) value, but the results seem reasonable with the lack of credible data.

El. 4227 also presents a problem. Using the east gauge by itself results in positive side friction above the neutral plane or creates two neutral planes, which should not be possible. Using the west gauge creates a sharp break going down to the next gauge level. The possibility of using an average of the gauges at this elevation and the gauges above and below seems reasonable in this case. Equation 5-3 shows the formula used to create this value.

$$P_{4227} = \frac{(P_{4233.5W} + P_{4233.5E} + P_{4227W} + P_{4227E} + P_{4221W} + P_{4221E})}{6} \quad (5-3)$$

The elevation and gauge location is given in the subscripts with “W” meaning west and “E” meaning east. The end result is a reasonable value that seems to agree more closely with previous research.

The gauges at El. 4221 present an interesting challenge. The west gauge and average of gauges are better suited for different aspects of the accompanying research, while the east gauge by itself is not an option. The west gauge is better for theories in respect to applied loads and the location of the neutral plane. The average value is better suited for the results of the shear stress analysis. Deciding which to use overall is difficult, but in the end, the author feels more comfortable in using the west gauge. The rationale behind this is that as load is applied to the pile, the neutral plane works its way to

the surface. This pattern is visible if the west gauge is used, but if the average is used, this entire theory is unsupportable.

The decision for gauges at El. 4213 is fairly easy. The west gauge is obviously having problems and should not be used. The average value is pulled down by the west gauge too much to be used. The only option left is to use the east gauge which appears perfectly reasonable both in terms of shear stress and location of the neutral plane.

For the bottom three gauge locations, there are two options. The first is to use the averages or the larger of the two gauges. Using either option does not seem to alter the shear stress results unreasonably and both options appear very reasonable. The option chosen is to use the average of the two gauges. Table 5-3 contains a summary of the gauges or combinations used at each level. The results are then shown in Figure 5-8.

Table 5-3 Combination of Gauges used to Create Consistent Load Plot

Gauge Elevation (ft)	Gauge(s) Used
4238	Average of East and West gauges
4233.5	Interpolated (Weighted average of gauges at El. 4238, 4227 and 4221)
4227	Interpolated (Average of both gauges at El. 4233.5, 4227 and 4221)
4221	West gauge only
4213	East gauge only
4205	Average of East and West gauges
4196	Average of East and West gauges
4184	Average of East and West gauges

After the axial stress and load in the pile have been calculated at each of the gauge elevations using the combinations described previously, they can be plotted by depth for various times as shown in Figure 5-8.

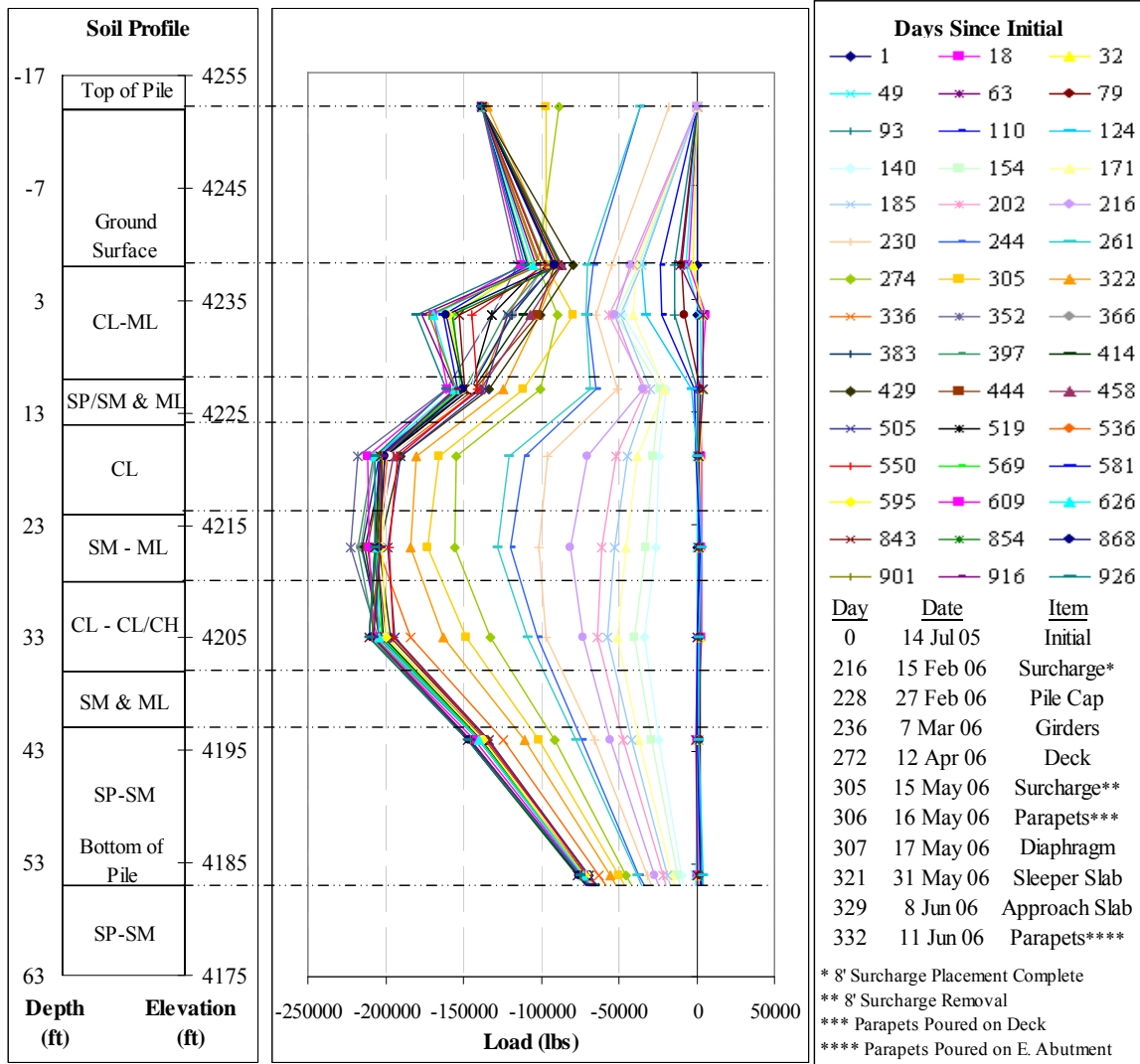


Figure 5-8 Plot of Axial Load vs. Depth and Time using Best Combination of Gauges for Redwood Road and SR-201

In Figure 5-8, the key indicates the number of days after the first strain measurements was completed. Day “0” is considered to be 14 July 2005 since only incomplete measurements exist before then. Although readings are recorded hourly, plotting a curve for every day would create too much clutter on the plot. For this reason, a curve is typically plotted for the 1st and 15th of every month (with some exceptions). This still provides a great deal of clutter, as seen in Figure 5-8. The values plotted in Figure 5-8 are calculated by taking the average of all 24 hourly readings for each gauge

and then taking the average of the east and west gauges. Values also correspond to the combination of gauges, interpolation or a single gauge as summarized in Table 5-3. Following the adjustments to the gauge readings, the location of the neutral plane is more easily identified in Figure 5-8. A simplified version of Figure 5-8 is shown in Figure 5-9 that reduces the clutter and shows the load in the pile at key times throughout the duration of the monitoring.

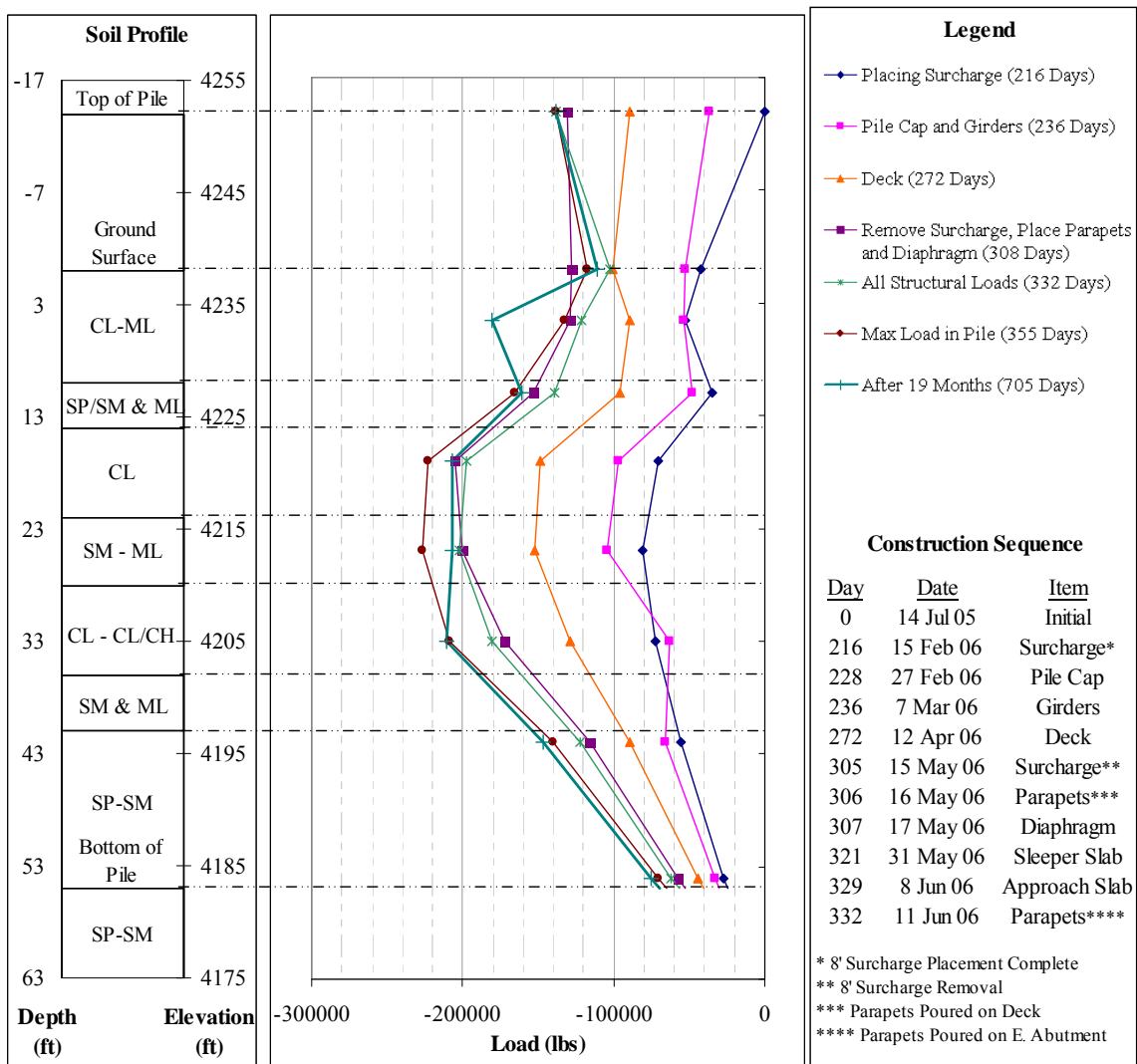


Figure 5-9 Simplified Plot of Axial Load vs. Depth and Time for Redwood Road Site

The load versus depth profile shown in Figure 5-8 is generally consistent with the expected behavior shown in Figure 5-10 developed by Briaud and Tucker (1997). Downdrag load developed after settlement as shown in Figure 5-10(2). When structural loads were applied while settlement was continuing, the profile shown in Figure 5-10(3) developed as dragloads near the top of the pile decreased (or at least did not increase) and yet the total load in the pile did increase slightly. At first, when structural loads were applied after consolidation settlement was completed, the measured load profile remained similar to that shown in Figure 5-10(3). Overall, the current profile for the test pile appears to be approaching the profile shown in Figure 5-10(4), with dragload slightly increasing, but with the exception of the upper gauges continuing to show behavior similar to Figure 5-10(3), which to some extent may be caused by their interpolated values. It appears that continued settlement in the upper layers has been insufficient to cause the complete profile to advance to the profile shown in Figure 5-10(4).

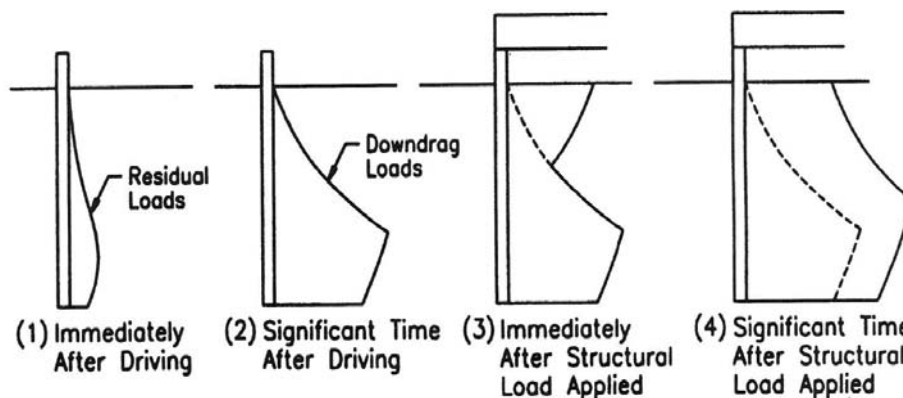


Figure 5-10 Expected Development of Downdrag Load for Piles at a Bridge Abutment (Briaud and Tucker, 2007)

5.4.1.3 The Neutral Plane and History of Dragloads

The neutral plane has been shown in previous research (Leung et al., 2004; Fellenius, 1989) to shift in response to the loads from both the structure and surrounding soil. The general trend that has been observed is that the neutral plane will tend to begin near the bottom of the compressible layers after an embankment or surcharge loading is placed. As structural loads are placed, previous research has shown that the dragloads are reduced and if sufficient loads are imposed, the neutral plane can migrate upward towards the surface.

A close look at the day-to-day behavior of the loads in the pile at the various gauge levels allows for a look into factors that affect the location of the neutral plane as well as the immediate effect of structural loading on the magnitude and location of the neutral plane.

For the first 167 days of recording (near the first part of December 2005), the loads in the pile and the different gauge locations did not assume a clear pattern. After this time the neutral plane appeared to settle down to El. 4205, near the bottom of the majority of the more compressible layers of soil. Some vacillating took place until day 192 (22 January 2006) when the neutral plane appeared steady at El. 4205. On day 206 (5 February 2006) the neutral plane shifted up to El. 4213. The reason for the shift is not known. It is possible that the dragloads accumulated up to that point were beginning to drag the pile down sufficiently, perhaps coupled with most of the primary consolidation settlement in the lower lean to fat clay layer (between El. 4210 and El. 4202) being completed.

The neutral plane remained at El. 4213 for some time. The load in the gauges at El. 4221 (next level up) appeared to increase at an overall faster rate during the placement of various structural loads until the load in the pile at El. 4221 exceeded the load at El. 4213 for two days. This occurrence happened on days 308 and 309 (18 and 19 May 2006). Following this very temporary shift of the neutral plane, the neutral plane returned to El. 4213 and remained there for nearly ten months.

The reason for the brief change in location of the neutral plane is believed to be caused by at least two factors. First, the added increase in structural loading. Second, the removal of the surcharge load after primary consolidation settlement was complete. Settlement readings taken by AMEC showed that approximately 11.0 inches of total settlement had occurred at the end of March 2006 near the test pile location, signaling the end of primary consolidation. The settlement readings taken by AMEC are shown in Figure 5-11.

It is interesting to note that despite the relatively large loads applied by the girders and the bridge deck, the location of the neutral plane did not change. The most likely reason for this is that these structural components were placed while significant settlement was being caused by the 8-foot surcharge. Since the definition of the neutral plane is the location along the pile where the pile is settling at the same rate as the surrounding soil, with the soil settling at the rate shown in Figure 5-11 (about 2 inches in 45 days), it is very improbable that the pile could settle that fast. When the majority of primary consolidation was complete and structural load continued to be added, the change could occur. It must be noted that the difference in total load in the pile between

El. 4221 and El. 4213 during these two days was no more than 4,800 lbs (about 2.3% of the total load).

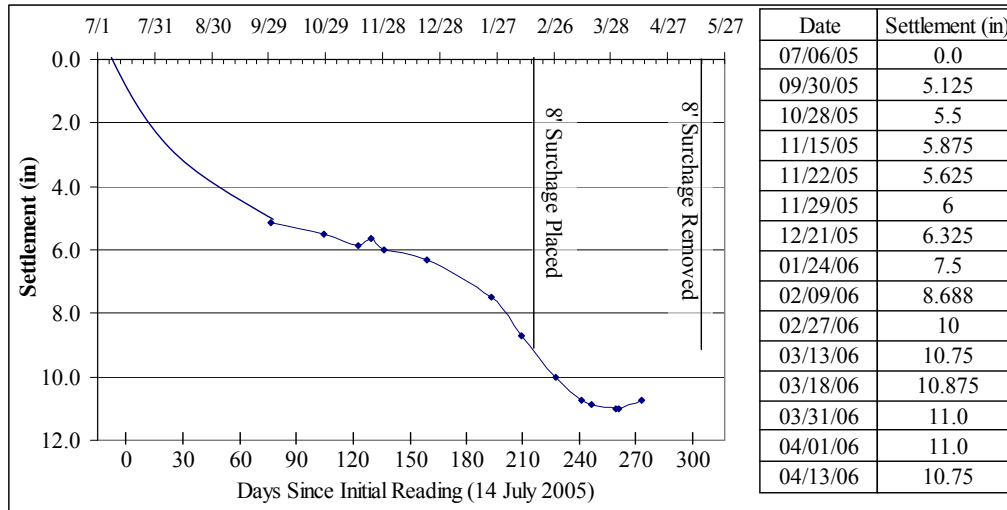


Figure 5-11 Settlement Time History Near East Abutment for Redwood Road and SR-201 Site

The neutral plane stayed at El. 4213 until day 596 (8 March 2007) when it shifted up to El. 4221 and remained there with few exceptions until day 621 (2 April 2007) which was the last time readings were downloaded before a large break in downloading. Once again, the difference in load between the elevations was very small (no more than 1,150 lbs). The reason for the shift at this time is unknown. All structural loads had been in place since June 2006 and the occurrence of secondary consolidation would be more likely to lower the neutral plane.

Sometime between the download on 2 April 2007 and the next available reading around the first of November 2007, the neutral plane had shifted to El. 4205. If secondary consolidation is occurring, which is likely, this shift may be caused by that settlement. The neutral plane remained at El. 4205 to the end of the readings last downloaded on day 707 (28 January 2008).

Looking at the history of the dragload in the pile sheds some light on the interaction between structural load, settlement and their combined influence on the magnitude of the dragload in the pile. Table 5-4 shows a summary of the more important times when the magnitude of the dragload in the pile is of particular interest.

Table 5-4 History of Dragload for Pile at Redwood Road Site

Date/Description	Days Since Initial	Total Load (kips)	Structural Load (kips)	Dragload (kips)	Elevation of Neutral Plane (ft)
2-14-06/Maximum Dragload before surcharge	215	79.83	0	79.83	4213
2-26-06/After surcharge-Just before Pile Cap	227	89.16	0	89.16	4213
2-27-06/After Pile Cap	228	94.18	17.78	76.40	4213
3-6-06/Just before Girders	235	100.11	17.78	82.33	4213
3-7-06/After Girders	236	104.37	36.21	68.16	4213
4-11-06/Just before Deck	271	134.20	36.21	97.99	4213
4-12-06/After Deck	272	152.16	88.90	63.26	4213
5-15-06/Surcharge Removed (Settlement Completed)	305	172.79	96.91	75.88	4213
5-18-06/After surcharge removed, After Deck Parapets and Diaphragm Wall	308	205.97	131.10	74.87	4221
6-11-06/All Structural Loads in Place	332	201.76	134.48	67.28	4213
7-4-06/Maximum Recorded Load in Pile	355	226.68	134.48	92.20	4213
1-26-08/Last Reading (19 Months after all Loads)	705	210.80	134.48	76.32	4205

As it can be seen in Table 5-4, the maximum dragload in the pile before any structural loads were placed was about 89.2 kips. After placing the pile cap, the dragload was reduced by about 13 kips, nearly all, but not quite the full amount of the load of the pile cap. With each successive addition of structural loading, the dragload was decreased, but by only a fraction of the load added. The best example of this is the

addition of the deck. The deck added about 52.7 kips to the pile, but the dragload was only reduced by 34.7 kips. As indicated before, the relatively large amount of settlement still occurring during this time appears to override at least a portion of the structural loads as they are added. It is apparent that dragloads are reduced by the addition of structural loads, although it also seems apparent that if structural elements are placed during primary consolidation then they do not affect the dragload by the maximum amount possible.

Other items of note from Table 5-4 is the maximum load in the pile of 226.7 kips, which occurred on day 355 (4 July 2006). The corresponding dragload at this time was 92.2 kips, nearly the maximum dragload recorded. Although not in the table, it should be noted that the maximum dragload ever experienced in the pile was 100.4 kips on day 264 (4 April 2006). At the end of the currently downloaded readings, the dragload is slightly less than the dragload just before the surcharge was placed.

The maximum load corresponds to an axial stress in the pile at the neutral plane of about 7500 psi. The ultimate compressive strength in the pile (calculated as the summation of the yield strength of the steel times the area of steel and the compressive strength of the concrete times 0.85 and the area of the concrete) is approximately 789.4 kips, approximately 3.5 times larger than the maximum load recorded in the pile.

Since the monitoring of this pile is taking place on a real construction project subject to deadlines and timetables not in the power of the author to alter, the process of construction introduces a number of questions as to the real cause of the changes seen in the gauge measurements. Placing of a surcharge fill directly before erecting structural components creates a difficult situation to diagnose. In further research, if it is possible,

construction should be done in separate and distinct steps to minimize overlapping of reactions.

5.4.1.4 Immediate Effect of Structural Loading

It was the initial intent to look into the hour-by-hour readings recorded after various structural components were added. After completing a thorough analysis of an eight-day time period beginning one day before the load was placed and continuing to six days after, it was observed that the recorded readings showed no definitive conclusions. The typical display of readings for the day the load was placed for the various periods analyzed appeared as shown in Figure 5-12. This particular plot is for the time period when the pile cap was poured. The readings, especially at El. 4205 alternate back and forth and show no consistent pattern; therefore, to limit any further confusion, the results of these analyses will not be presented.

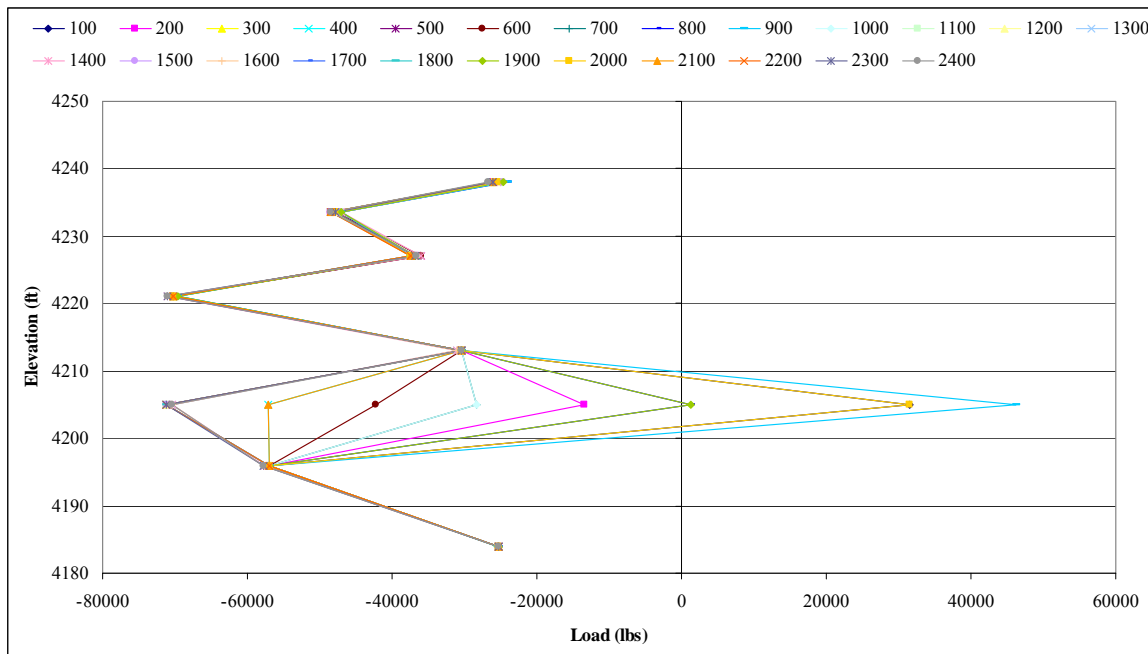


Figure 5-12 Plot of Hourly Readings for West Gauge on 28 February 2006

5.4.2 Shear Stress

Calculating shear stress along the pile is a way to quantify the skin friction acting on the pile at various elevations. This becomes useful as the α and/or β coefficients can be back-calculated for either a total or effective stress analysis, respectively.

5.4.2.1 Derivation of Shear Stress Calculations

The shear stress for the different segments has been calculated by both the “double segment” and “single segment” methods as discussed in Sections 4.4.1 and 4.4.2. A complete review of the equations will not be given here. However, in summary, the single segment method calculates a shear stress with a representative elevation in the middle of the two gauges. For the double segment method, the representative elevation is the average of the middle elevations of the two segments (three gauges) involved. A short comparison of the two methods will be useful to show the similarities and differences between the methods.

The following three plots, Figure 5-13, Figure 5-14 and Figure 5-15, show the shear stresses calculated by the single segment method for two consecutive segments compared to the shear stress calculated by the double segment method for the same length of pile. Two of the plots Figure 5-13 and Figure 5-14, are taken from segments completely above the current location of the neutral plane and Figure 5-15 is taken for the bottom two pile segments. The legend entries for the shear stress are described with “SS” if they are calculated using the single segment method and “DS” for the double segment method. The numbers are the span of elevations for the segment. The vertical lines on the plots provide a time reference to various placements of the bridge structure and embankment of the construction process (see Table 5-1 for exact dates).

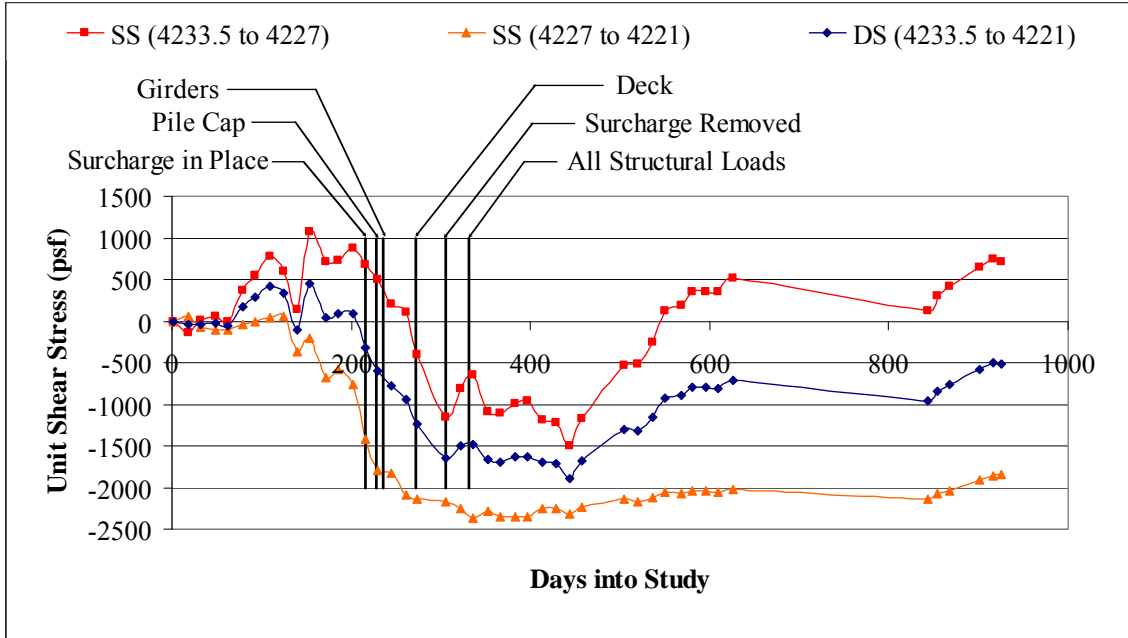


Figure 5-13 Comparison of Single Segment and Double Segment Methods for Calculating Shear Stress between El. 4233.5 and El. 4221

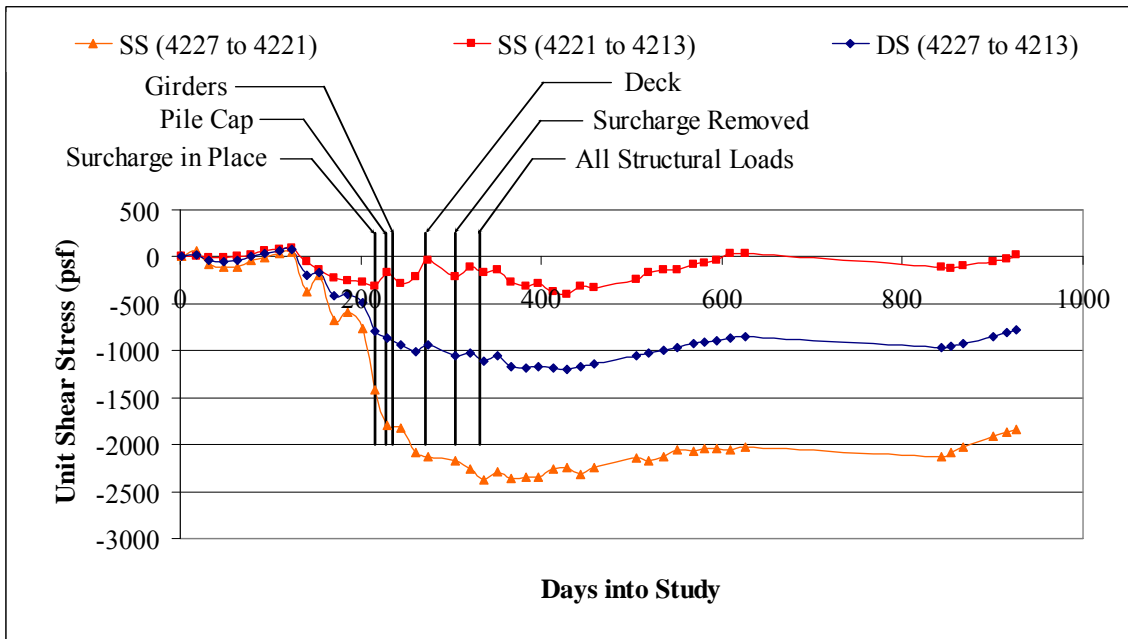


Figure 5-14 Comparison of Single Segment and Double Segment Methods for Calculating Shear Stress between El. 4227 and El. 4213

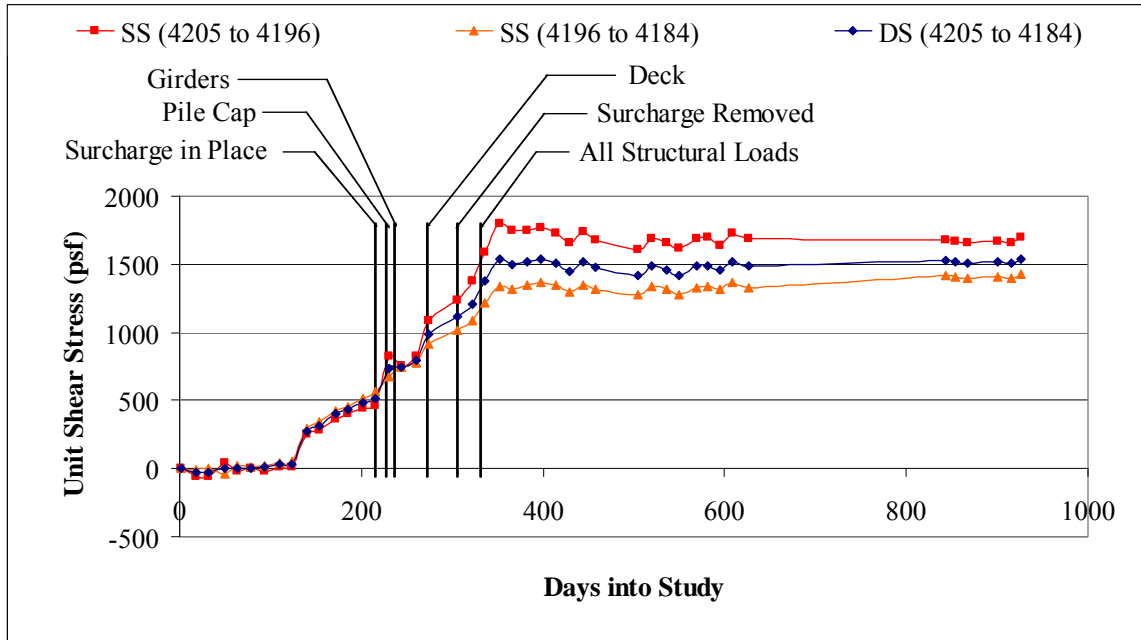


Figure 5-15 Comparison of Single Segment and Double Segment Methods for Calculating Shear Stress between El. 4205 and El. 4184

It can easily be seen that the double segment method gives almost an exact average of the two single segment readings. This would be a predictable conclusion since, in reality the double segment method is taking an average of the shear stress at the midpoint elevations of the two segments, which is the same as the shear stress calculated for the two segments with the single segment method.

Because the results for the double segment and single segment methods give very comparable results and also since the double segment method cannot be used accurately when being calculated with the two segments creating the neutral axis, the results from the single segment method will be presented in the discussion for each segment to follow.

5.4.2.2 Shear Stress Data and Analyses

The results of the shear stress analyses will now be given for each section of the pile between two gauges. As each segment is discussed it is important to remember the following:

- Shear stress for segments above the neutral plane should be negative due to downdrag at least prior to structural loading.
- Shear stress for segments below the neutral plane should be positive.
- Alternations between positive and negative shear stress generally indicate a change in neutral plane elevation.
- Data used for gauge El. 4233.5 and El. 4227 are based on interpolated values (not actual data) since failure or malfunctioning occurred in one or both gauges at those elevations.

Day “0” on the following plots is 14 July 2005. On each plot from the beginning to approximately day 154, there is either little development of shear stress or repeatedly alternating patterns of positive to negative values that are likely the result of initial embankment fill placement and construction activities. After day 154, more recognizable patterns are visible.

5.4.2.2.1 Shear Stress between El. 4252 and El. 4238 (Within Approach Fill)

Figure 5-16 shows the plot of shear stress versus time. This section is located in the embankment fill placed above ground surface. The shear stress for this section of pile shows negative skin friction reaching a maximum magnitude of approximately 730 psf on 15 February 2006. Then due to structural loading, the shear stress becomes positive and peaked at just below 1,500 psf on 15 September 2006. The addition of each structural

load discussed previously caused the shear stress for this segment to increase. Notice the jumps in shear stress after the various loadings represented by the vertical lines.

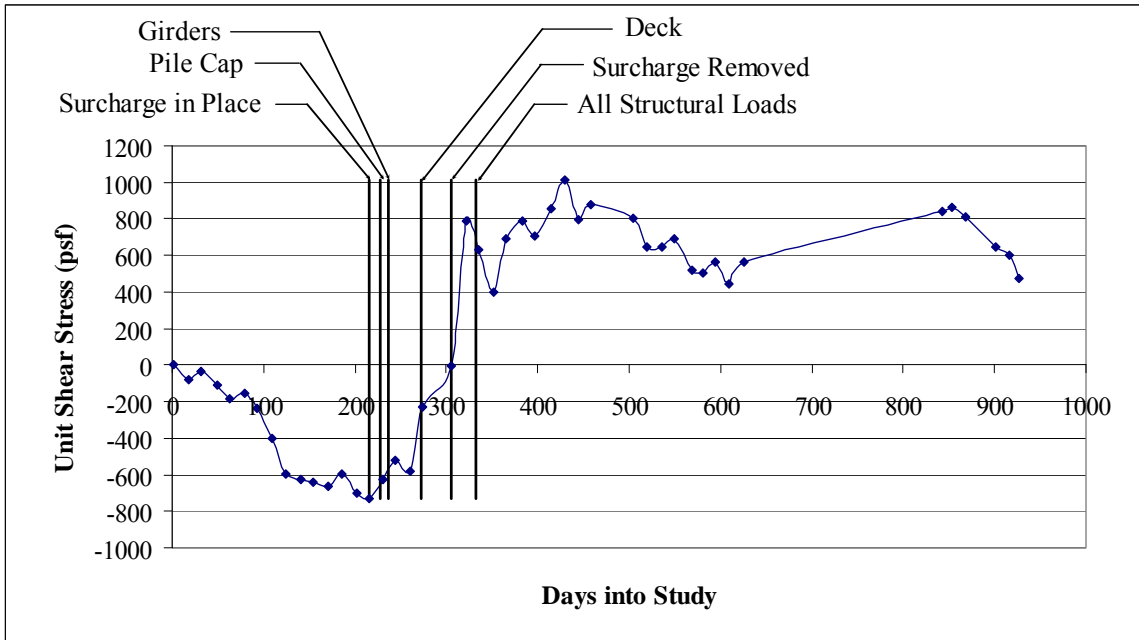


Figure 5-16 Shear Stress on Pile at Redwood Road & SR-201 from El. 4252 to El. 4238 (Within Approach Fill)

5.4.2.2.2 Shear Stress between El. 4238 and El. 4233.5

Figure 5-17 shows the plot of shear stress versus time. This section is located in thin layers of silty sand (SM), lean clay (CL) and sandy silt (ML). The shear stress in the pile for this section shows no real trend. Stress values tend to stay positive until about the first of December 2005 and then go negative. The load associated with the placement of the deck caused a shift back to positive shear stress, however, sometime after the diaphragm wall was placed, the stress dropped back down and became negative.

The first shift from positive to negative seems reasonable as that is the same time frame during which the embankment was placed. The shift back to positive shear stress

also seems reasonable as the structural loading of the deck should have been sufficient to induce pile settlement and engage positive skin friction. The last shift back to negative friction happened between 15 May and 1 June 2006, and would seem to indicate that sufficient settlement induced negative skin friction again.

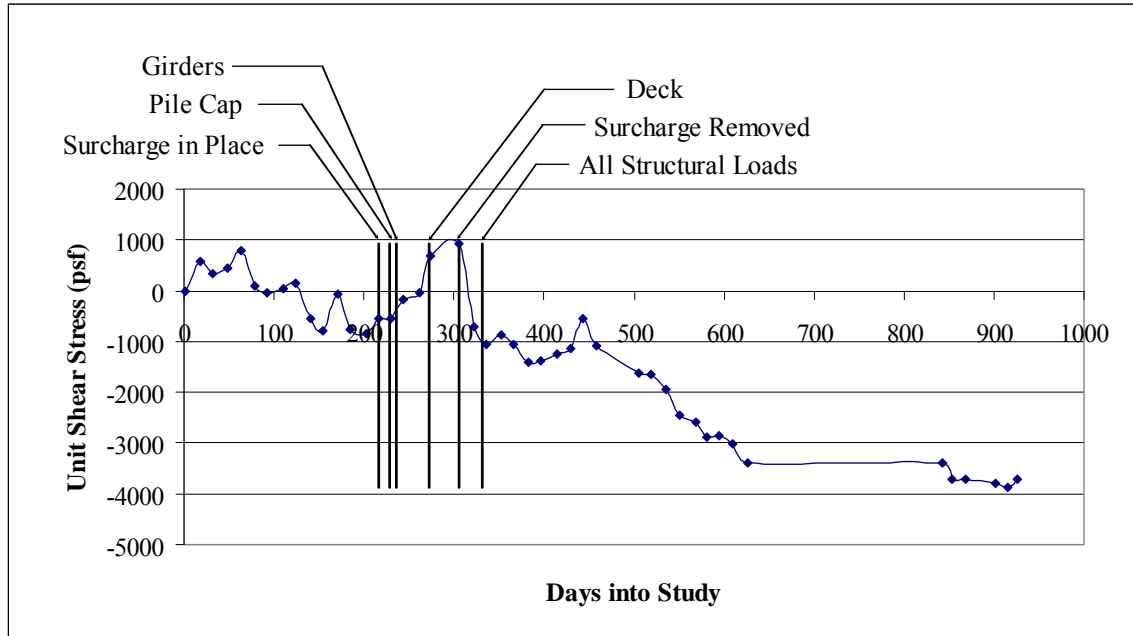


Figure 5-17 Shear Stress on Pile from El. 4238 to El. 4233.5

However, this time period includes the removal of the surcharge and the placement of the deck parapets and diaphragm wall which would be most likely to continue positive skin friction. On the other hand, negative skin friction should exist above the neutral plane so the switch back to negative skin friction should be logical. During long-term readings the stress has remained relatively constant. It should be noted that the magnitude of shear stresses shown for this section appears significantly greater than may be expected from the shear strengths of the soils as encountered during field and laboratory testing summarized in Chapter 3. This may be, in part, due to the fact that

strain gauge values at El. 4233.5 are interpolated, which may cause irregularities in movement and magnitude that is not consistent with what is actually occurring.

5.4.2.2.3 Shear Stress between El. 4233.5 and El. 4227

Figure 5-18 shows the plot of shear stress versus time. This section is primarily in lean clay (CL) with occasional layers of sandy silt (ML) and silty sand (SM). The gauge at El. 4227 appears to be in more sandy material while the gauge at El. 4233.5 is primarily in lean clay material. This section initially experiences positive skin friction. The positive shear stress peaked during the time of the embankment material being placed and after this time began the transition to negative skin friction. The transition from positive to negative skin friction took place between 1 and 15 March 2006. This location continued to gain in negative skin friction, reaching a maximum of approximately 1,200 psf. After reaching this maximum, the diaphragm and approach slab were placed and the surcharge was removed which reduced the negative shear stress to a somewhat lower value for a short period time period, but then the negative shear stress recovered to about the same value as prior to the loading. The negative skin friction ultimately increased to a maximum magnitude of about 1,500 psf. There is not an apparent reason for the transition back to positive skin friction which occurred sometime after day 536 (1 January 2006). Even with long-term monitoring of the pile, the behavior remains questionable. According to theory and the performance of other gauges, this section should remain in negative skin friction. One possible reason is that this section is still dependent upon the interpolated values used for the gauge at El. 4233.5.

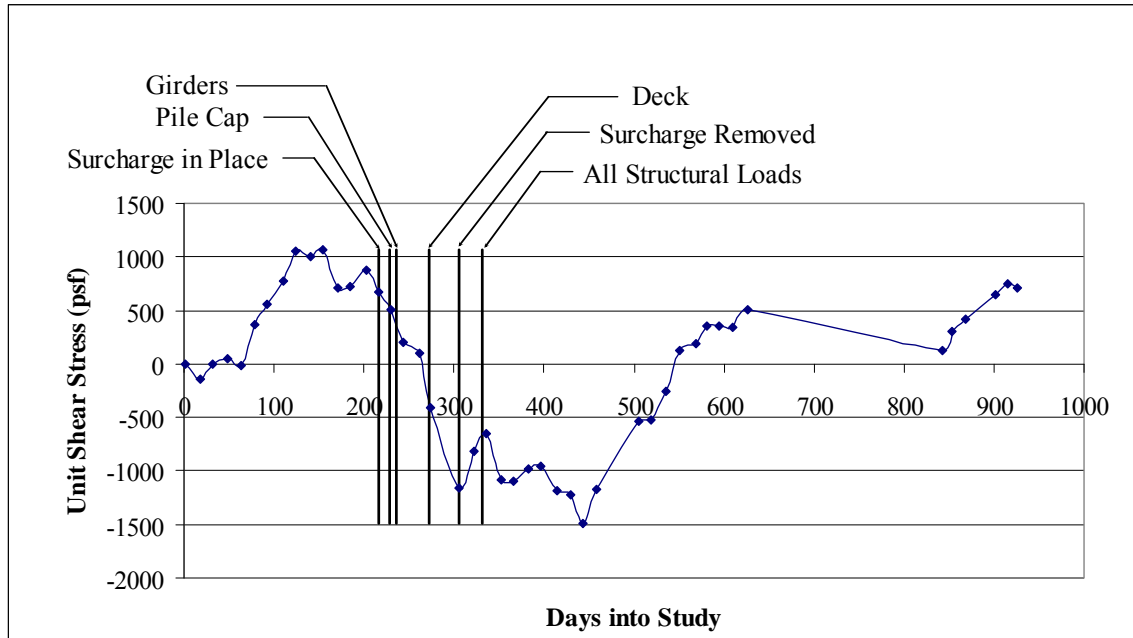


Figure 5-18 Shear Stress on Pile from El. 4233.5 to El. 4227

5.4.2.2.4 Shear Stress for Section between El. 4227 and El. 4221

Figure 5-19 shows the plot of shear stress versus time. The top gauge for this section is in sandy soils (SM, ML) and the bottom gauge is likely in silty clay (CL) material. In between the gauges is about half and half sandy and clayey soils. This section stayed close to zero until the first part of December. Starting at that time until the middle of April 2006 there was a fairly steady increase in negative stress. Since mid-April the shear stress has leveled off at a value of approximately 2,000 psf even though it has been slowly decreasing in magnitude. This magnitude is somewhat higher than expected based on soil strength properties discussed in Chapter 3. These results are promising as they indicate the behavior expected.

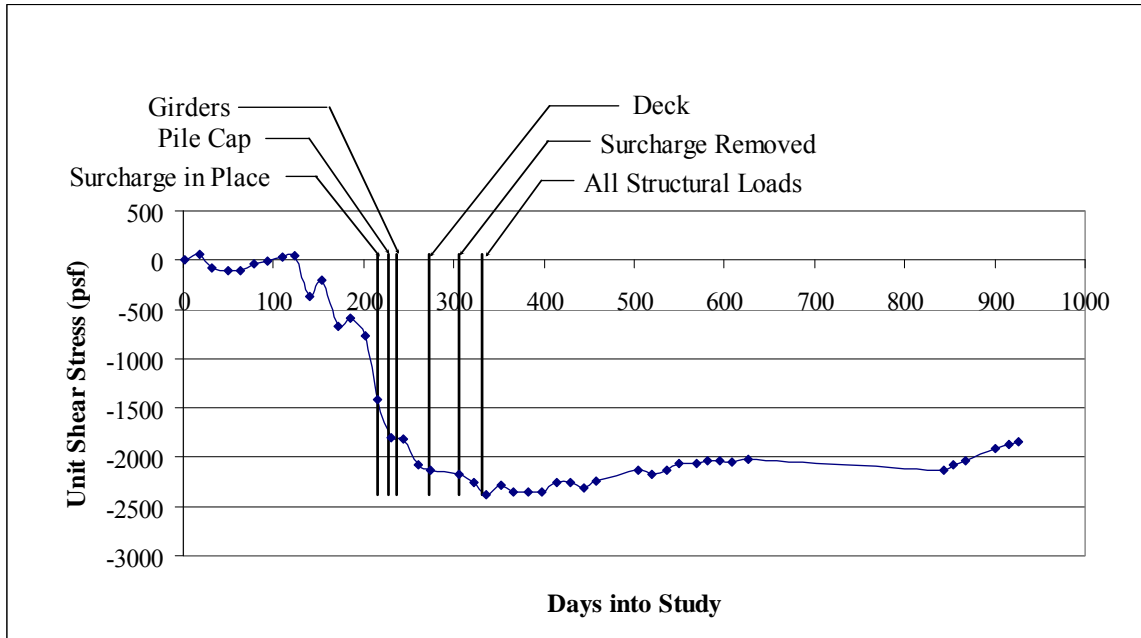


Figure 5-19 Shear Stress on Pile from El. 4227 to El. 4221

5.4.2.2.5 Shear Stress for Section between El. 4221 and El. 4213

Figure 5-20 shows the plot of shear stress versus time. The top gauge of this section is likely in silty clay (CL) material and the bottom gauge is likely near a border of silty sand and silty clay (SM, CL). Multiple alternating layers of sandy, silty and clayey soils exist between the gauges. Positive friction is seen from the start until the first part of December 2005 when the shear stress became negative as was the case with many of the gauges. When the shift in the neutral plane occurred at that time, the shear stress turned negative and became progressively more negative until the surcharge was placed. It appears the construction of the pile cap caused a trend toward positive stress. This was later overcome by additional settlement and it appears the shear stress oscillates toward positive stress and back again. These upward oscillations appear to be caused by structural loadings, however, they are overcome each time by the settlement and oscillate

back down. Readings shown in the vicinity of day 350 to day 450 seem to indicate that the neutral plane is having a tendency to sink lower in depth. The change in direction of the shear stress as values approach 0 indicate that the neutral plane is tending to rise from El. 4213 to El. 4221. This is seen in the load values as the slope between these two gauge locations becomes increasingly steeper. As seen in the cross over between days 595 and 609 (actual date of cross over is 8 March 2007, day 596), the neutral plane shifted up to El. 4221.

Long-term monitoring has shown that the neutral plane is able to shift to any of three elevations relatively easily as the load in the pile is very close in magnitude between El 4221 and El. 4205. Sometime during the lapse of readings from 3 April 2007 to 3 November 2007 the neutral plane switched to a lower elevation. The cross-over between the last two readings is unaccounted for as the neutral plane has remained at El. 4205.

5.4.2.2.6 Shear Stress for Section between El. 4213 and El. 4205

Figure 5-21 shows the plot of shear stress versus time. The gauge at El. 4213 is likely near the border of silty sand and silty clay layers (SM, CL) while the bottom gauge is within a relatively thick layer (7 to 10 feet) of lean to fat clay (CL/CH). The layers housing the two gauges also make up the soil between the gauges.

The results on this section are fairly consistent with the expected behavior of the skin friction forces. The shear stress remains on the negative side until mid-February. This is consistent with its location above the neutral plane. The neutral plane was located at El. 4205 until the first portion of February and then it shifted to El. 4213. While the neutral plane was located lower, the section was on the upper side of the neutral plane

and should thereby register negative friction. After the neutral plane shifted to El. 4213 the section was below the neutral plane, thereby changing to positive skin friction.

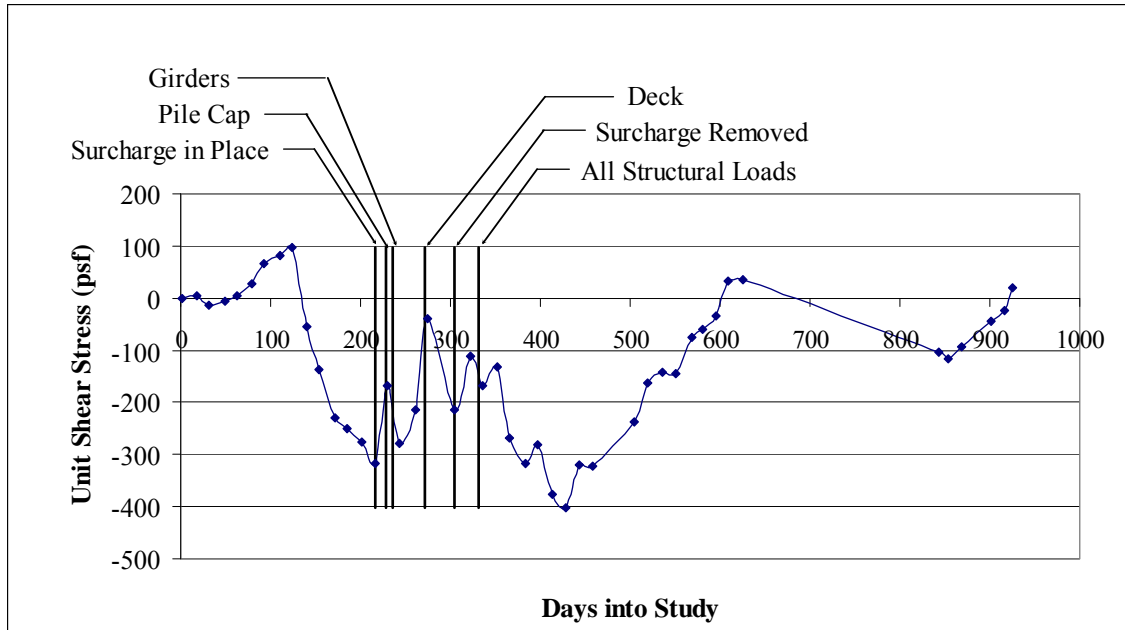


Figure 5-20 Shear Stress on Pile from El. 4221 to El. 4213

The skin friction took a dip towards negative friction after the surcharge fill was placed, but the addition of structural loads caused the neutral plane to remain at the top of the section and the positive skin friction increased to a peak value of approximately 750 psf. After this the shear stress leveled and then began to regress towards negative skin friction. This would seem to indicate that the loads from the structure have been overcome by continuing settlement in the soil and the neutral plane is starting to shift back down. This is consistent also with previous findings from other full-scale tests. Fellenius (1989) notes that since piles are infinitely more rigid than soil, all piles will undergo downdrag forces ultimately in the long-term. This statement is significant when considering the final state of the pile. After structural loading the soil will still be

settling, even if in miniscule amounts, and this settling will once again reinstate downdrag loads forcing the neutral plane to shift down. Previous to the final data download the neutral plane was very close to shifting from El. 4213 to El. 4205. After the last data download, the neutral plane has made the shift to a lower elevation.

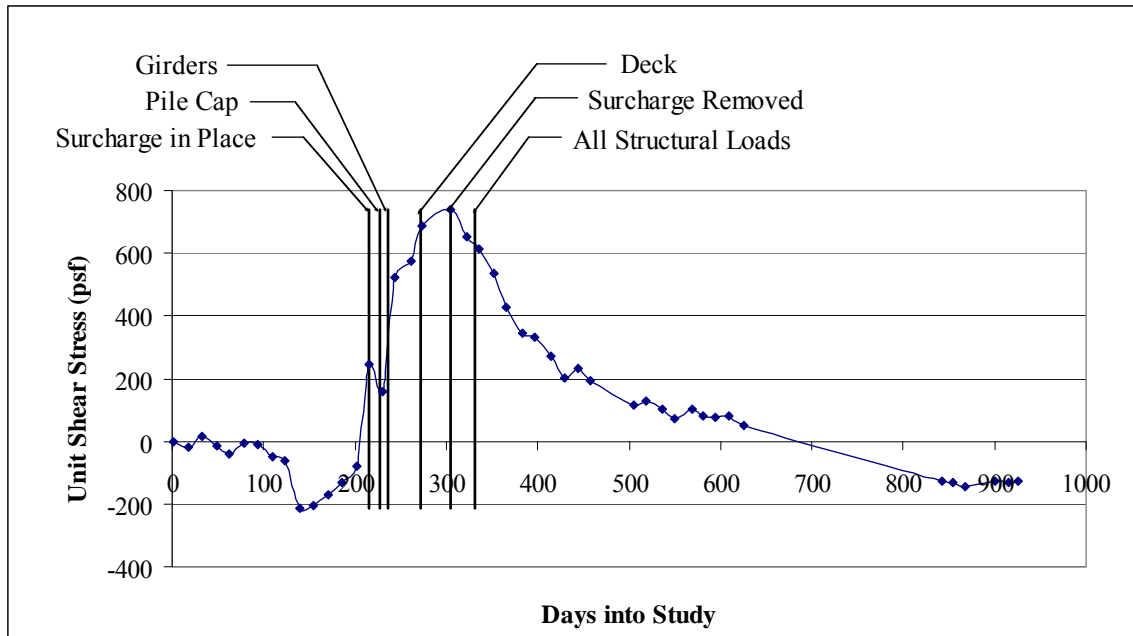


Figure 5-21 Shear Stress on Pile from El. 4213 to El. 4205

5.4.2.2.7 Shear Stress between El. 4205 and El. 4184 (Two Sections)

Figure 5-22 and Figure 5-23 show the plots of shear stress versus time for the two sections from El. 4205 to El. 4196 and El. 4196 to El. 4184, respectively. The gauge at El. 4205 is in lean to fat clay (CL/CH), the gauge at El. 4196 is within thin (6 inches to 1-foot thick) layers of sandy silt and silty sand (ML, SM) and the gauge at El. 4184 is a thick (about 20 feet) layer of silty sand (SP/SM). Soil between the gauges is similar to

the soil found at the gauges and ranges in thickness from thin (1-foot) to relatively thick (5 feet or more) layers.

The shear stresses for the remaining two sections are very similar. Positive skin friction has been typical, as expected, for both of these sections. The shear stresses in each section began close to zero and remained at that value until the first of December. After this, each section continued to increase consistently until the first of July 2006. The shear stress seems to be leveling off as of the last readings taken on 13 July 2006. The section from El. 4205 to El. 4196 has reached a maximum shear stress of approximately 1,800 psf. The shear stress for the last section has peaked out at about 1,400 psf. Over time the unit shear stress tends to decrease, although this is a very gradual decrease interspersed with slight undulations in the readings.

5.4.2.3 Summary of Shear Stress Values for Sections of Piles

Overall, the plots for shear stress show encouraging results for most of the pile. Erratic patterns do exist between El. 4238 and El. 4227 which is likely the result of using interpolated values caused by gauge malfunctioning. The key to understanding the various shifts in direction between positive and negative shear stress is to remember the various effects from embankment, the surcharge fill and structural loadings on the location of the neutral plane.

Values for shear stress tend to begin high near the surface and then become quite low in the vicinity of the neutral plane. Shear stress increases again near the bottom of the pile.

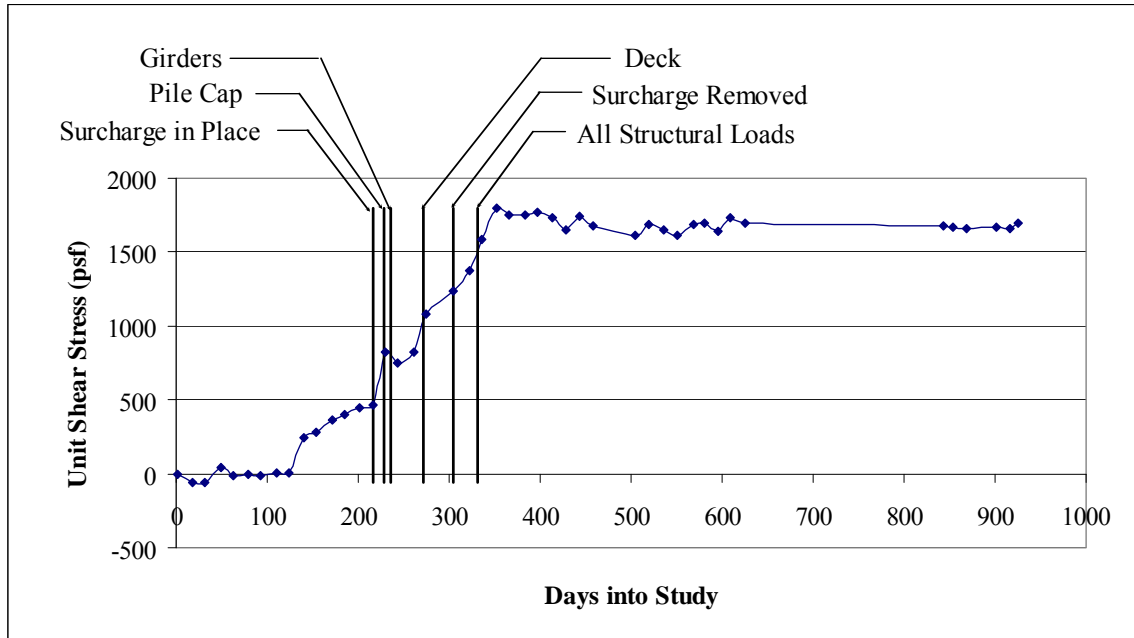


Figure 5-22 Shear Stress on Pile from El. 4205 to El. 4196

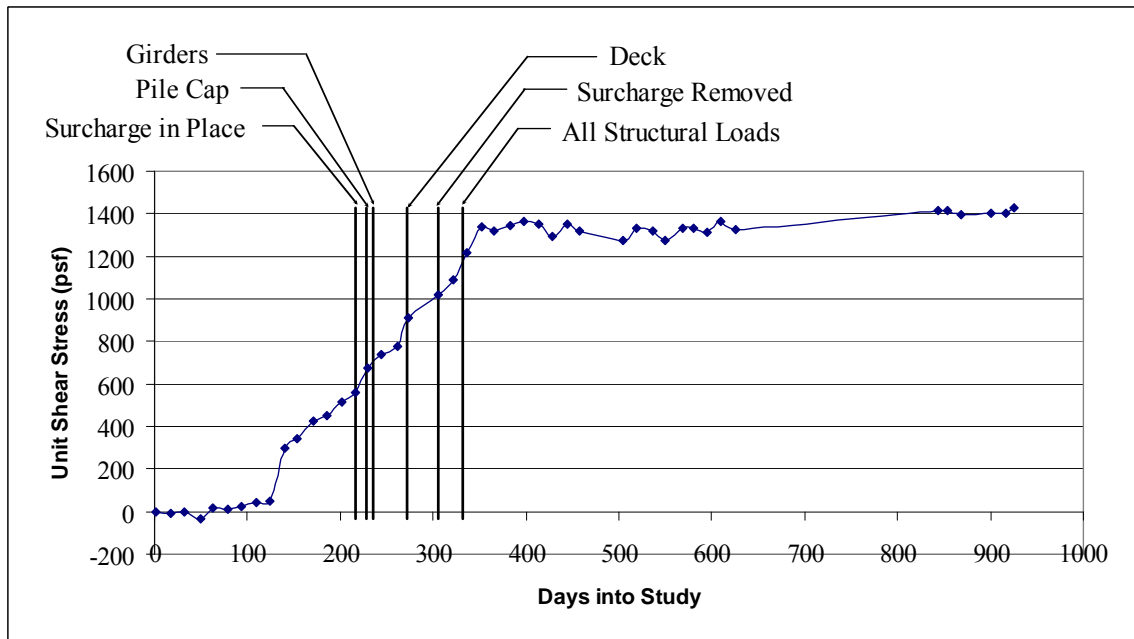


Figure 5-23 Shear Stress on Pile from El. 4196 to El. 4184

5.4.3 Comparison of Estimated to Measured Results

Engineers are faced with the responsibility of estimating the magnitude of loads that will be applied to the pile foundation. To accomplish this, a proper understanding of the interaction between the pile and soil must be understood and adequate characterization of the soil profile must be known. The accurate estimation of the location of neutral plane, which then leads to the estimation of the dragload magnitude, is essential for a design that will not be overly conservative or overly aggressive. The following sections will discuss the methodology for estimating the location of the neutral plane and the calculation of the loads in the pile, as well as a comparison to the measured results from strain gauge readings.

5.4.3.1 Estimating the Location of the Neutral Plane

In the design process, since actual loads are not known, the location of the neutral plane must be determined. Two methods have been used in conjunction with this thesis to estimate the location. The first method is described in the “Unified Design” method by Fellenius (1989) and will be followed by the method described by Briaud and Tucker (1997). Both of these methods require the estimation of the side resistances for each layer of the soil profile.

5.4.3.2 Estimation of Side Resistance

The side resistance in layers of cohesive soil can be estimated in two ways, the alpha (total stress) and/or beta (effective stress) method. The side resistance for clays in this thesis has been calculated based on the alpha method, where the side friction (f_s) is calculated using the equation

$$f_s = \alpha s_u \quad (5-4)$$

where s_u is the undrained shear strength and α was assumed to be 1.0. The values of the average undrained shear strength and side resistance for cohesive layers are provided in Table 5-5.

In the initial geotechnical investigation of the site there were no unconfined compression (UC) tests or unconsolidated undrained (UU) tests done to determine the compressive strength and undrained shear strength of the clay layers. RBG completed torvane tests on samples obtained in the field and vane shear tests were completed in the lab by AMEC. These tests can provide an estimate of the undrained shear strength, but the data from these tests are likely not as accurate or as useful as the UC or UU tests. However, it should be remembered, as indicated in Chapter 3, that supplemental drilling was undertaken to obtain samples for unconfined compressive testing and seven (7) tests were performed.

The side resistance for layers of cohesionless soil is calculated using the beta method according to the equation

$$f_s = k \sigma'_v \tan \delta \quad (5-5)$$

where k is the earth pressure coefficient (range of values taken from the Navy Manual (NAVFAC, 1982) as 1.0 to 1.5 for a driven single displacement pile); σ'_v is the vertical effective stress; and δ is the soil-pile friction angle. The range of values for δ/ϕ was taken as 0.7 – 0.9 based on recommendations from Kulhawy et al., (1983) for a sand/rough steel interface. The factors k and $\tan\delta$ are often joined together into one value, β . Values

for the unit weight and friction angle in each layer were estimated using correlations from in situ data, such as the SPT values and are shown in Table 5-5. The β values shown are assume a value of 1.25 for k and a value of 0.8 for δ/ϕ . As indicated previously, α was assumed to be 1. The vertical effective stress shown is without any embankment fill. In addition, the side resistance of the fill material has been estimated to be 800 psf based on the results from the gauges due to lack of information about the fill material.

Table 5-5 Summary of Soil Parameters Used to Estimate Side Resistance

Elevation Extents of Soil Layer		USCS Class	γ_m	σ'_{vo}	ϕ	β	S_u	f_s
			pcf	psf	deg		psf	psf
4252	4238	Random Fill	125	----	----	----	----	800
4238	4228	CL	125	625	----	----	1190	1190
4228	4224	SP/SM & ML	118	1360	30	0.56	----	760
4224	4216	CL	122	1710	----	----	285	285
4216	4210	SM-ML	118	2116	32	0.61	----	1290
4210	4202	CL-CL/CH	112	2480	----	----	440	440
4202	4197	SP-SM	120	2820	32	0.61	----	1720
4197	4183	SP-SM	125	3405	38	0.72	----	2460

The unit side resistances (f_s) shown in Table 5-5 can be used to calculate the dragloads or positive skin resistance for each layer, ΔF_s , using the equation

$$\Delta F_s = \pi D(\Delta L)f_s \quad (5-6)$$

where ΔL is the thickness of the soil layer for which the load is to be calculated and D is the diameter of the pile.

Both the Fellenius (1989) and the Briaud and Tucker (1997) methods require, in addition to the side resistance along the pile, the calculation of the settlement of the pile and surrounding soil. The settlement of the pile consists of the elastic compression of the

pile due to the loads in the pile and the settlement of the pile into the bearing layer. In order to apply these methods, the subject of pile and soil settlement will now be discussed.

5.4.3.3 Derivation of Pile Compression and Pile Settlement

Settlement of the pile is a combination of the elastic compression of the pile and settlement of the pile at the pile tip. The equations for the compression of the pile at gauge elevations and at midpoint elevations between gauges were presented in Sections 4.5.1 and 4.5.2 as shown in Figure 4-13 and Figure 4-14 and will not be repeated at this time.

In addition to and as a check on the pile compression calculations from the strain gauges, elastic compression of the pile ($s_{\text{compression}}$) was computed using the equation

$$s_{\text{compression}} = \frac{QL}{A_p E_p} \quad (5-7)$$

where Q is the average load in the pile; L is the length of the pile; A_p is the cross-sectional area of the pile; and E_p is the modulus of elasticity of the pile. In cases where the pile is composed of multiple materials, i.e. steel and concrete, a composite AE should be used.

Using an input parameter of 160,550 lbs for the average pile load, a pile length of 69 feet (828 inches), and a composite AE of 9.79×10^8 psi, a compression value of 0.14 inches is calculated. This matches very well with the calculated compression of the pile from readings of the strain gauges.

Settlement of the pile into the bearing stratum is somewhat more difficult to determine with exactness. No surveying could be done to assess the pile head elevation

before and after the loading sequences began because construction of the pile cap would not allow for measurement of the top of the pile. Therefore, four approaches proposed by various investigators have been used to estimate the settlement at the tip of the pile. [Equations 5-8 (Das, 1999), 5-9 (FHWA, 2006), 5-10 (FHWA, 2006) and 5-11 (Briaud and Tucker, 1997)]. The first approach computes the pile tip settlement (s) using elastic theory according to the equation

$$s = \frac{q_{wp} B}{E_s} (1 - \mu_s^2) I_{wp} \quad (5-8)$$

where q_{wp} is the point load per unit area at the pile toe (total load divided by the area of the pile at the toe); B is the diameter of the pile; E_s is the modulus of elasticity of the soil below the pile point; μ_s is the Poisson's ratio of the soil at the pile point; and I_{wp} is an influence factor of 0.85. Consistent units are required in applying this equation.

Input parameters used in Equation 5-8 were 353 psi for q_{wp} (using 70,930 pounds for the approximate maximum load at the base of the pile), pile diameter of 16 inches, modulus of Elasticity of 7,500 psi (from range of 5,000 to 10,000), and a Poisson's ratio of 0.375 (from range of 0.3 to 0.45). Using these values, a settlement of 0.55 inches was calculated.

The second approach computes the pile tip settlement using a correlation with the SPT penetration resistance given by the equation

$$s = \frac{4p_f \sqrt{BI_f}}{N'} \quad (5-9)$$

where p_f is the foundation pressure in ksf (load divided by area); B is the width of the pile group in feet, N' is the average corrected SPT N' value within a depth B below the pile tip; and I_f is an influence factor for group embedment equal to $1-[D/8B]$ limited to a value greater than 0.5, with D being the pile embedment depth in feet. This equation is meant for use with pile groups.

Input parameters for Equation 5-9 were 1290.165 kips for a total group load (weight of superstructure on pile cap); pile group are of 43 feet (width, B) by 3.5 feet (depth, not thickness); depth of embedment of 69 feet; and an influence factor equal to 0.8. The average corrected blowcount value is more difficult to ascertain since in the boring that went deeper than the pile tip, two of the SPT attempts yielded values of 80 blows for 5". Below this very dense layer, a silty clay layer was found with a blowcount of 13, and the last two blowcounts of 30 and 92 coming from silty sand layers. Although the average of the last three values is 45, the two attempts stopping at 80 indicate that blowcounts for these layers could very likely be near 200. If this is the case, then the average blowcount goes up to approximately 110, which seems more reasonable. Using a corrected blowcount of 110, Equation 5-5 calculates a settlement of approximately 1.63 inches.

The third approach correlates settlement with cone tip resistance using the equation

$$s = \frac{p_f B I_f}{2q_c} \quad (5-10)$$

where the terms, p_f , B and I_f were defined previously in Equation 5-8, and q_c is the average static cone tip resistance within a depth B below the pile tip, in units of ksf.

For Equation 5-10, the only new value, relative to the previous equations, is the value for q_c . After analyzing the CPT sounding displayed in Figure 3-10, an average value for the cone tip resistance from 55 to 90 feet seems to be between 250 and 300 tsf. Using the lower bound of 250 tsf which is equal to 500 ksf, Equation 5-9 gives a settlement value of 0.29 inches.

The last approach given by Briaud and Tucker (1997) calculates the pile settlement with an equation nearly identical to Equation 5-8 and given as the equation

$$s = \frac{\pi}{4} (1 - \nu^2) \frac{Q_p D}{AE_s} \quad (5-11)$$

where Q_p is the bearing resistance (equal to the load on the pile at the toe), D is the outside pile diameter, A is the cross sectional area at the base of the pile, and E_s is the modulus of elasticity below the pile point. The only difference between this equation and Equation 5-8 is the influence factor in Equation 5-8, I_{wp} is replaced with the quantity $\pi/4$ (0.785).

All the values used in Equation 5-11 were described in the solution of Equation 5-8. The result when using Equation 5-11 is 0.54 inches, which is nearly identical to that obtained with Equation 5-8. It may also be helpful to give the range of values for different input values of Poisson's ratio (0.3 to 0.45) and the modulus of elasticity (5,000 psi to 10,000 psi). The range of settlement is from 0.35 to 0.81 inches.

Equations 5-8, 5-10 and 5-11 are relatively close to each other in comparison to the settlement predicted by Equation 5-9, although the estimation of parameters for each equation is obviously a determining factor in the results. The large difference is suspect in and of itself, but in addition to this, results from a pile load test (discussed in Section 5.2) completed on one of the adjacent piles indicates that for a maximum load of about 780 kips a total settlement of just over 0.5 inches was observed for a 55-foot pile. Since the combination of the structural loads and dragloads existing on the test pile are much less than 780 kips, it seems unreasonable to expect 1.6 inches of settlement, not even including pile compression. With this in mind, the values calculated from Equation 5-8 and Equation 5-11 even appear too high. For these reasons, the settlement predicted using Equation 5-8 based on the CPT sounding appears to be the most reasonable approach for predicting the pile tip settlement at this site. Therefore, using a pile compression of 0.14 inches and a pile settlement of 0.29 inches, a total pile head settlement of 0.43 inches appears to be reasonable.

5.4.3.4 Presentation of Measured Pile Compression vs. Depth Curves

Using the calculation methods set forth in Sections 4.5.1 and 4.5.2 to calculate the compression of the pile due to the various loads, whether from the bridge structure or the dragloads, the pile has undergone an elastic compression of about 0.129 inches as of 26 January 2008. The pile had been compressed by approximately 0.128 inches by 1 July 2006 (352 days) and later rebounded to a compression of only 0.111 inches on 15 September 2006 (429 days). The rebound in the pile would indicate a decrease in total load on the pile, which was the case for the time period from the beginning of July to the middle of September 2006. Since the structural loads have not changed, dragloads were

decreasing at that time. This assumption is verified by the load versus depth over time curve as presented in Figure 5-8. The compression of the pile over time is shown in Figure 5-24. Each curve represents the elastic compression of the pile on the day indicated in the legend. From the beginning of the monitoring up to 1 December 2005 (140 days), no distinct settlement had been measured. For this reason and to reduce clutter on the plot, the curves for the readings prior to 140 days are not plotted and plotted curves are generally spaced one month apart.

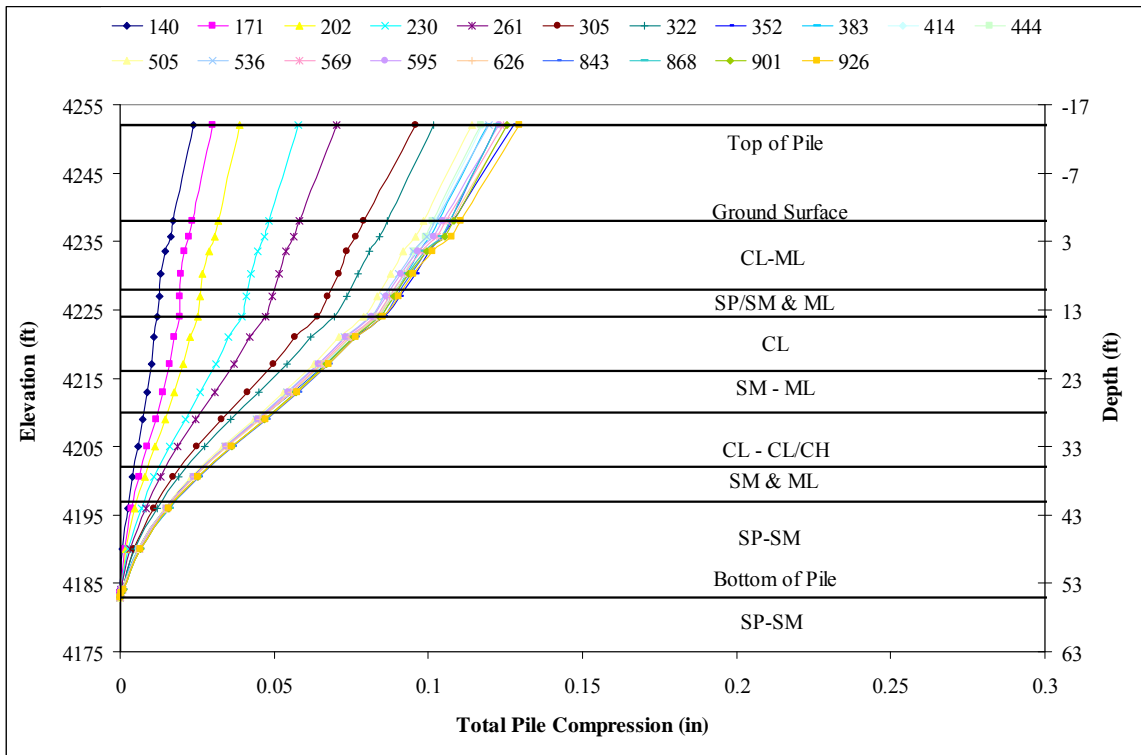


Figure 5-24 Pile Compression over Time for Redwood Road and SR-201 Site

5.4.3.5 Presentation of Soil Settlement vs. Depth Curves

During the placement of fill for the abutment at the test pile, settlement was monitored using open standpipe manometers. The settlement history was presented in

Figure 5-1, with a maximum of 11.0 inches of settlement observed. Using available data from testing done by AMEC and empirical relationships, the values for consolidation analyses were estimated. The total observed settlement of 11.0 inches was used to calibrate the compression and recompression indexes. The estimated values for the cohesive layers are shown in Table 5-6 and the expected contribution calculated for each layer to the total settlement is summarized in Table 5-7.

Table 5-6 Estimated Properties for Settlement Analysis of Cohesive Layers for Redwood Road Site

Elevations of Layer Limits		Vertical Effective Stress, σ'_v	Preconsolidation Pressure, σ'_p	Change in Effective Stress, $\Delta\sigma'_v$	Compression Index, C_c	Recompression Index, C_r
feet	feet	psf	psf	psf		
4238	4228	550	4000	4000	0.22	0.022
4224	4216	1152.5	4000	3900	0.18	0.015
4210	4202	2350	1500	2500	0.29	0.020

Table 5-7 Summary of Contributing Settlement for Soil Profile at Redwood Road and SR-201

Elevations of Layer Limits		Layer Thickness	Type of Soil	Contributing Settlement	Cumulative Settlement
Top El.	Bottom El.				
Feet	feet	feet	-----	inches	inches
4238	4228	10	CL – ML	1.7	0 (11.0)
4228	4224	4	SP/SM	0.1	1.7 (9.3)
4224	4216	8	CL	1.3	1.8 (9.2)
4216	4210	6	SM – ML	0.3	3.1 (7.9)
4210	4202	8	CL/CH	7.5	3.4 (7.6)
4202	4197	5	SM – ML	0.1	10.9 (0.1)
4197	4183	14	SP – SM	0.0	11.0 (0.0)

Note in Table 5-7 that the first number in the last column is the cumulative settlement increasing with depth while the number in parenthesis is the cumulative

settlement from the bottom to the top. It was assumed that no settlement is occurring in the dense sands and gravels below the pile tip.

5.4.3.6 Estimating the Location of the Neutral Plane and Magnitude of Loads using Fellenius (1989) and Briaud and Tucker (1997) and Comparison to Actual Results

Now that the elastic compression of the pile, the settlement of the pile into the bearing layer and the settlement of the soil are known, both methods may be utilized to estimate the location of the neutral plane and distribution of load present in the pile can be computed.

The Fellenius (1989) method involves starting with the structural load (dead load only) anticipated to be carried by the pile and then making an envelope of dragload using the side resistances shown in Table 5-5 and Equation 5-6. The dragloads calculated are added to the structural load and should obviously increase with depth. The ultimate base resistance was calculated using the equation

$$Q_p = A_p q_p \quad (5-12)$$

where Q_p is the ultimate base resistance, A_p is the area of the pile at the toe, q_p is the bearing pressure on the base of the pile and equals the product of $\gamma D N_q$, γD is the vertical effective stress at the base, and N_q is a bearing capacity factor.

The area of the pile point is 1.40 ft² and the vertical effective stress at the pile point is approximately 3,840 psf. Using a value of 36° for the friction angle of the soil at the base of the pile, a value of 90 for N_q was approximated from the Berezantsev et al. (1961) correlation of N_q vs. ϕ . Based on recommendations by the American Petroleum

Institute (API, 1987), the value of q_p is limited to a maximum of 200 kips/ft² for piles bearing in dense sand. Using Equation 5-12, and with the limitation on q_p occurring for this case, the ultimate base resistance for the pile was estimated to be 279 kips.

The positive skin friction is similarly calculated, starting at the bottom of the pile and an envelope of the positive skin resistance added to the ultimate base resistance is drawn. The location where these two envelopes intersect is the location of the neutral plane. Using the ultimate base resistance rather than the ultimate base force divided by a safety factor provides a conservative (deeper) estimate of the neutral plane. This intersection of the two curves should also correspond to the intersection of the total pile settlement and the surrounding soil settlement. For a graphical illustration of the above description, refer to Figure 2-16. Using the data provided in Table 5-5 the load vs. depth curve shown in Figure 5-25 was developed. Based on this curve, the neutral plane was estimated to be located at approximately El. 4193 with a maximum load in the pile of 382 kips. This corresponds to a dragload of about 244 kips.

The Briaud and Tucker (1997) method was described in detail in Section 2.4 and involves more of an iterative methodology. Briefly, this method involves calculating the dragload, positive skin resistance, end bearing, elastic compression of the pile and pile settlement into bearing stratum at each elevation along the pile, assuming that the neutral plane was at that elevation. This creates a pile movement envelope that is compared to the settlement profile of the surrounding soil. Where these two profiles intersect is considered to be the neutral plane and the corresponding loads associated with this elevation of the neutral plane are the estimated loads in the pile. Using the same set of side resistance data shown in Table 5-5, the Briaud and Tucker (1997) method predicts

the load vs. depth curve shown in Figure 5-25. Based on this curve, the neutral plane is estimated to be at approximately El. 4198.5 with a maximum load in the pile of 330 kips. This corresponds to a dragload of about 191.6 kips.

A comparison of the curves in Figure 5-25 indicates that the Fellenius method gives a much more conservative estimate of the load in the pile. This is caused in large part by using the total base resistance the pile is capable of rather than only a portion of it. The location of the neutral plane is the key factor in the maximum dragload. Since the Fellenius method typically estimates the neutral plane to be at a lower elevation, the method will naturally produce a larger maximum load. A comparison of the two estimated load vs. depth curves with the curves measured from the strain gauges is also shown in Figure 5-25.

From the plot in Figure 5-25 and also from previous discussion in this chapter, the neutral plane was at El. 4205 as of the last downloaded readings. This indicates that the elevation for the neutral plane for both estimation methods is lower than the measured, thus providing the main reason for the difference in magnitude of the loads. The maximum recorded load in the pile was about 227 kips with a maximum dragload of 98 kips. Relative to these measured values, both estimations are conservative, with the Fellenius (1989) overestimating the maximum force by 68% and the Briaud and Tucker (1997) method overestimating by 45%.

In addition to the information about the load in the pile to determine the neutral plane, the location can also be checked by comparing the pile settlement and soil settlement. This comparison is shown in Figure 5-26. However, since the settlement of

the soil is significantly larger than that of the pile, a close up version of the profiles is shown in Figure 5-27.

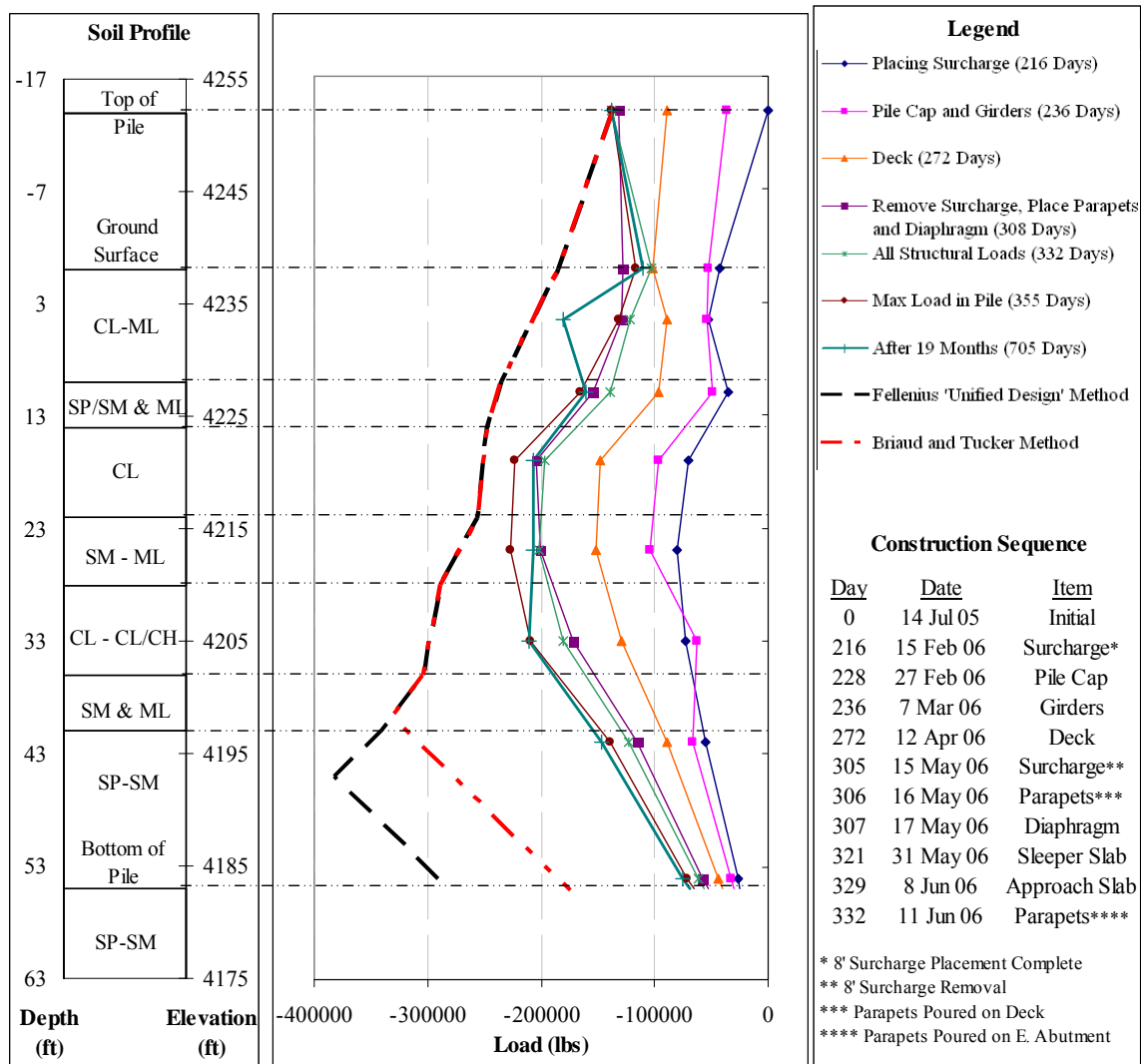


Figure 5-25 Plot of Select Load vs. Depth Curves for Redwood Road and SR-201 Site Showing Comparison of Estimated Load in Pile from Methods by Fellenius (1989) and Briaud and Tucker (1997)

From the pile and soil settlement curves, it can be seen that the point of intersection is at approximately El. 4202. This location for the neutral plane agrees relatively well with that from the most recently downloaded readings. However, it

should also be noted that the neutral plane was at El. 4213 for the majority of the time since monitoring began. If it would have been possible to measure the settlement within the profile over time to know the settlement occurring at different depths, it is possible that a better match during the embankment and bridge construction would be possible. However, since this information is not available, no additional assumptions can be made. Nevertheless, the long-term comparison of elevation is very encouraging.

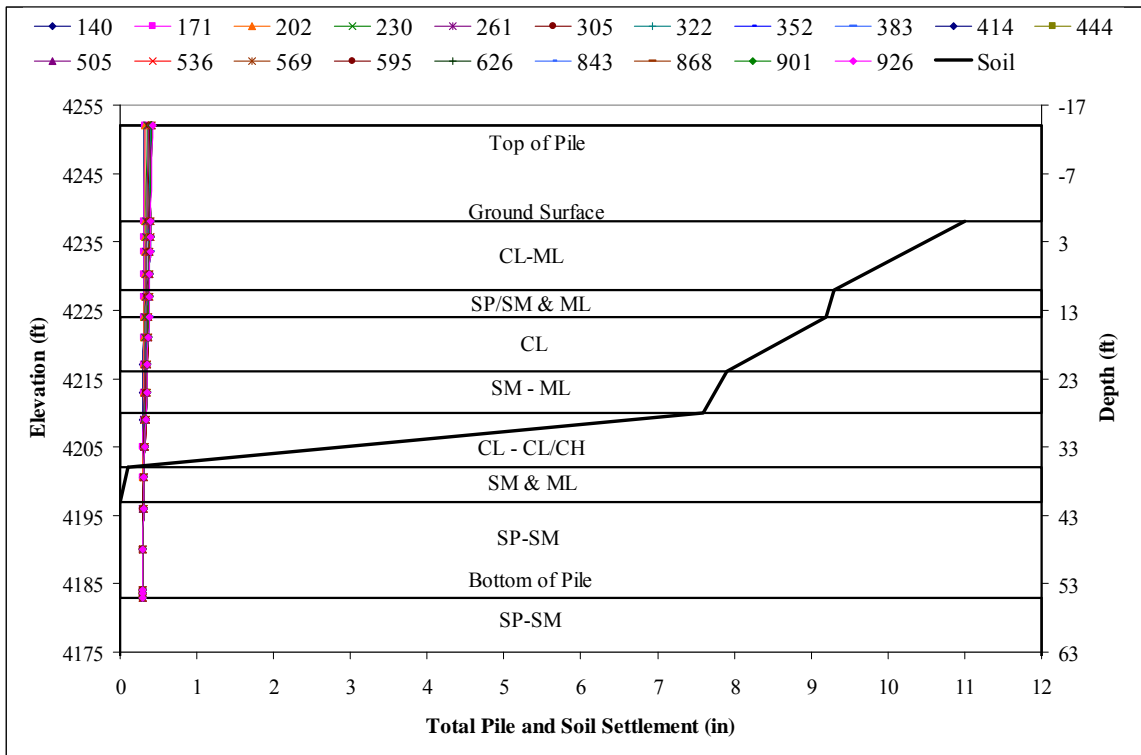


Figure 5-26 Settlement of Pile and Soil for Redwood Road and SR-201

5.4.3.7 Comparison of Undrained Shear Strength and Side Friction

Now that the two methods of design have been used to estimate the location of the neutral plane and the magnitude of load in the pile using the information from the laboratory and field testing, it is appropriate to show a comparison of how the computed

side friction values compare with the measured friction. The maximum measured side friction is plotted as a function of depth in Figure 5-28 along with the upper and lower bounds of the undrained shear strength as measured from the laboratory and/or in-the-field tests in each clay layer. If the α value is assumed to be 1.0, then the undrained shear strength would be equal to the side friction in the clay layer. Upper and lower bound curves were not calculated for cohesionless soil layers and therefore do not have bounds as do the cohesive layers. The squares on the plot correspond to the unconfined compression test results performed on samples from a boring drilled by RBG after construction. Overall, there is a good general agreement in most cohesive layers, although the presence of sand layers makes an interpretation difficult in some cases.

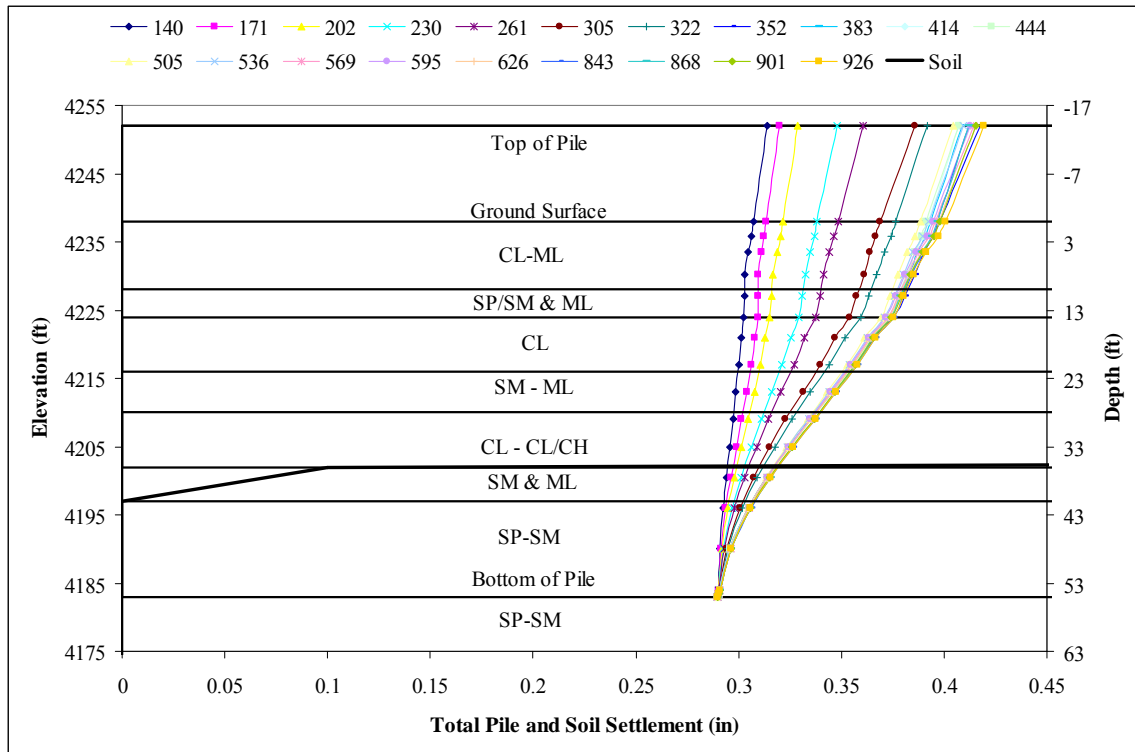


Figure 5-27 Close up of Pile and Soil Settlement for Redwood Road and SR-201

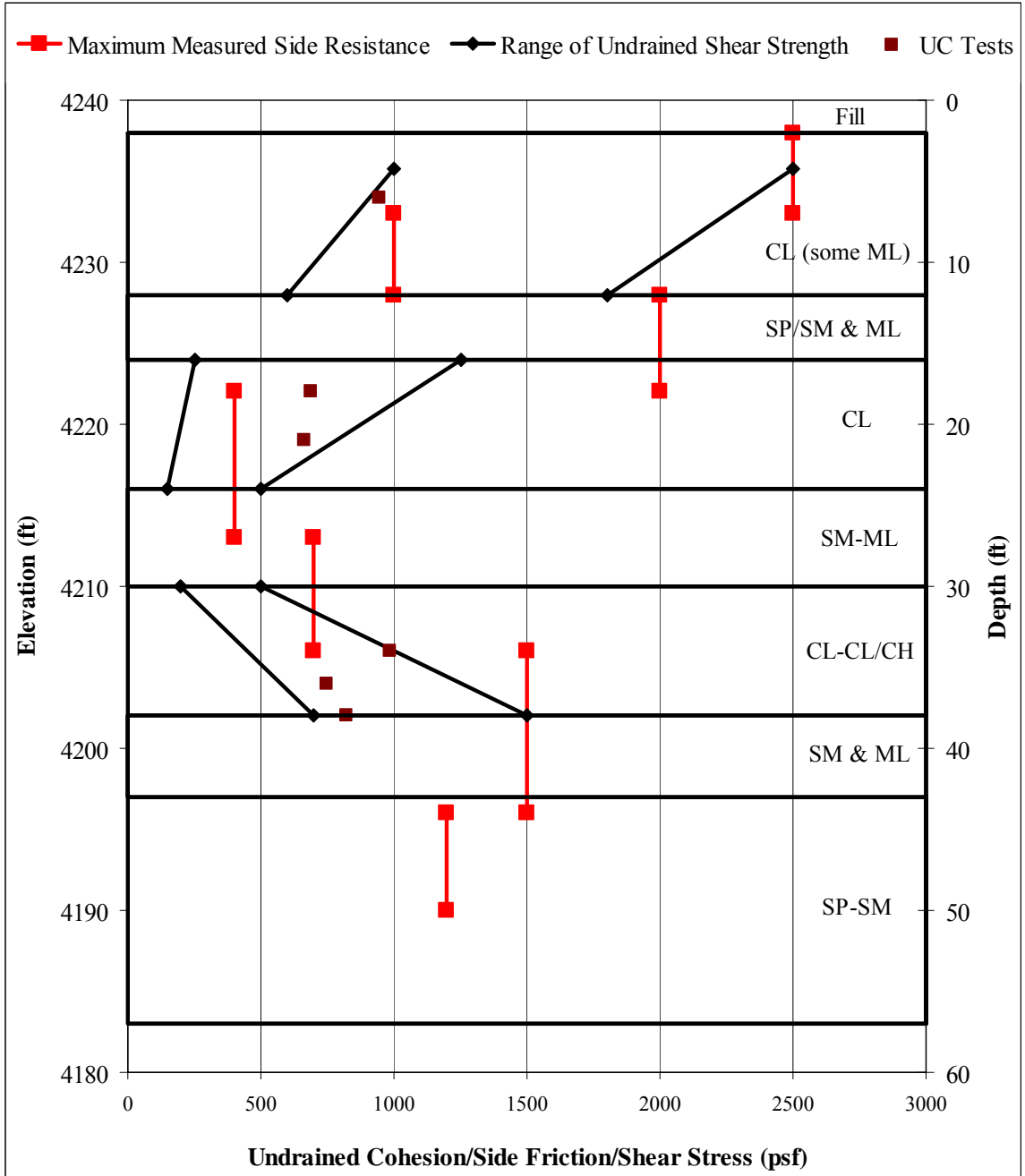


Figure 5-28 Comparison Plot of Measured Undrained Cohesion or Calculated Side Friction and Maximum Measured Shear Stress vs. Depth for Redwood Road and SR 201 Site

In addition to the plot shown in Figure 5-28, the actual values for the alpha and beta coefficients have been back-calculated from the measured side resistance for comparison with the values used to predict the side resistance. These α values were

calculated by dividing the measured side resistance by the undrained shear strength for cohesive layers and the β values were calculated by dividing the measured side resistance by the initial vertical effective stress for cohesionless layers. Table 5-8 gives a summary of the back-calculated α and β values. For alpha values, a range is given since there is a range of undrained shear strength. For the cohesionless layer from El. 4216 to El. 4210 a range is given since the gauge is directly in the middle of the layer and is used with the gauge above and below to calculate a side resistance for that layer. It appears that the estimated and back-calculated values are in general agreement although there are some discrepancies. For example, the back-calculated β values from El. 4228 to El. 4224 are much higher than predicted. In addition, the upper range of the back-calculated α values is considerably higher than the estimate of 1.0. These higher values are likely associated with low undrained shear strength values which result from sample disturbance.

Table 5-8 Summary of Back-Calculated Alpha and Beta Values for Soil Profile at Redwood Road and SR 201

Measured and Estimated alpha (α) Values				
Elevation Range of Soil Layers		USCS Class	Back-calculated α	Estimated α
4238	4228	CL	0.40 – 4.2	1.0
4224	4216	CL	0.32 – 2.7	1.0
4210	4202	CL-CL/CH	0.47 – 7.5	1.0
Measured and Estimated beta (β) Values				
Elevation Range of Soil Layers		USCS Class	Back-calculated β	Estimated β
4228	4224	SP/SM & ML	1.5	0.56
4216	4210	SM-ML	0.19 – 0.33	0.61
4202	4197	SP-SM	0.53	0.61
4197	4183	SP-SM	0.35	0.72

6.0 Results from Salt Lake City International Airport Site

To properly understand the data and conclusions obtained from an analysis of the raw strain gauge data, various details about the Salt Lake City International Airport site (referred to as the SLCIA site) need to be given. This information includes the following information: abutment layout (configuration of abutment, pile placement, etc...), construction history, gauge depth placement and orientation, gauge installation details, gauge performance, and the settlement time history. This information will enable a better understanding of the data as they are presented in load versus depth, shear stress and settlement plots.

6.1 Abutment Layout

The overpass structure constructed at this site was supported by piles at the east and west abutments along with a center pier. The test pile is located in the west abutment, where six 14-inch outside diameter steel pipe piles were driven in a single line. An overview plan of the project site is shown in Figure 6-1, taken from the geotechnical investigation report prepared by RB&G Engineering (RBG, 2004). Based on the plans, it appears the overpass superstructure spans a distance, along the centerline of the overpass, of 132 feet from the west abutment to the center pier.

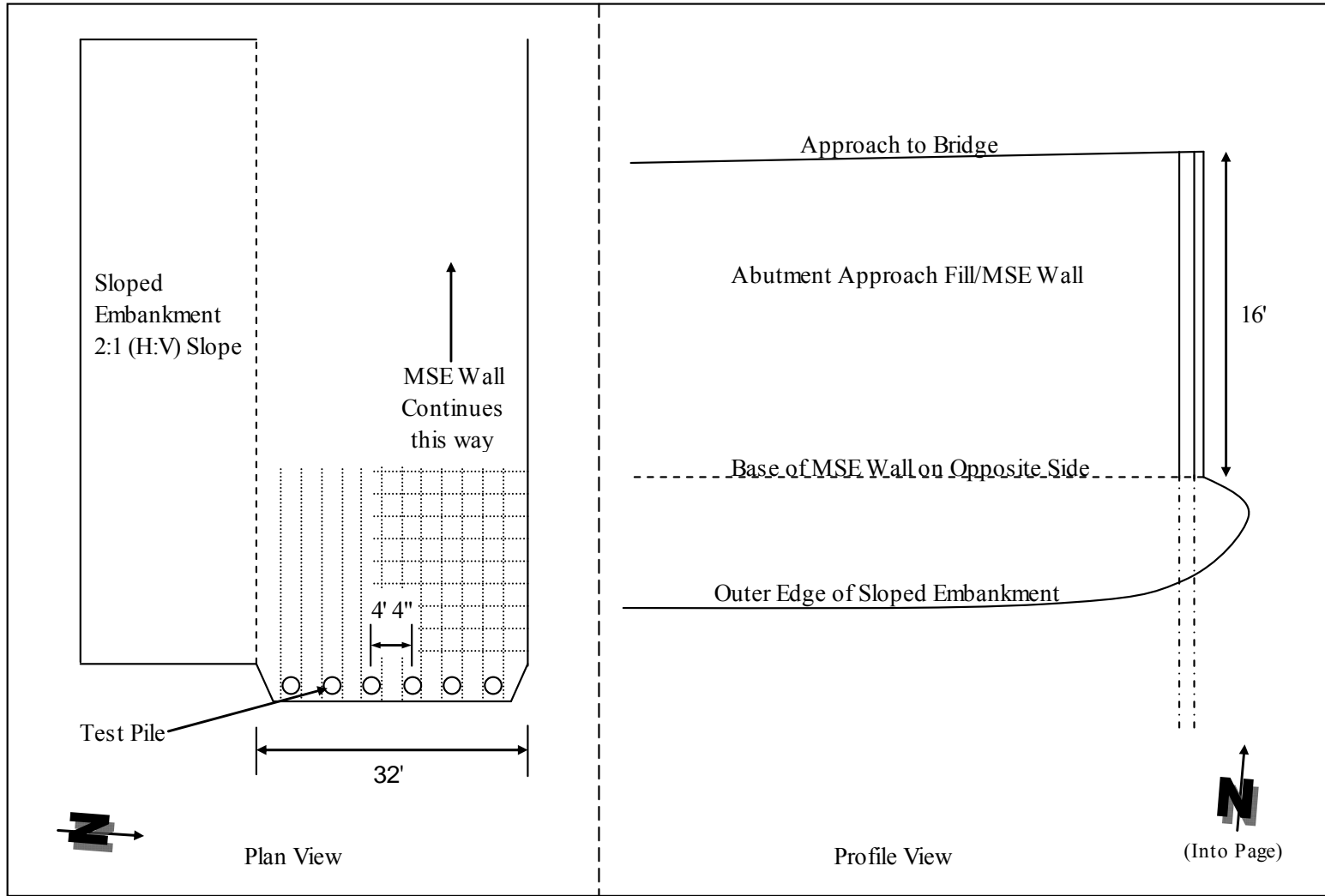


Figure 6-1 Plan and Profile View of West Abutment at SLCIA Site

The approximate layout of the west abutment will be a combination of MSE walls on the abutment face and the north side and an embankment slope on the south side. The abutment layout is shown in Figure 6-1. The embankment was initially designed to be approximately 27 feet high at the abutment, but was later scaled back to be about 16 feet high. The MSE embankment begins approximately 300 feet west of the test pile. The bridge abutment support rests on the six piles previously mentioned, of which the test pile is the 2nd from the south. The piles are regularly spaced 4'-4" apart, with a 3'-7" space between the two end piles and the MSE wall. A space of approximately two feet exists between the edge of the pile and the east edge of the abutment (MSE) wall face.

6.2 Construction Timeline

The piles for the west abutment were driven on 19 August 2005 with each pile in the abutment being driven 65 feet below the ground surface placing the pile tips at approximately El. 4152.5. About 20 feet of pile remained above ground surface at the time of driving. Before the strain gauges were installed in the pile, the pile was cut down approximately 4.5 feet, giving a pile top elevation of approximately 4233 feet. Gauges for the site were assembled at Brigham Young University and transported to Salt Lake City for installation on 20 September 2005. The strain gauge setup was assembled and installed as described in Section 4.2.2.

Fill operations began shortly after the strain gauge installation. Settlement plates were placed on the west and east ends of the west approach embankment. According to data provided by RB&G Engineering, the settlement plates were placed on 19 October 2005 and fill was placed to a height of 13 feet by 5 November 2005 at the east plate (location nearest piles). Fill reached a maximum height of 17 feet during the settlement

monitoring period, attaining this height on 3 February 2006. The abutment fill remained constant while expected consolidation settlements occurred. By 5 June 2006 settlement had reached a maximum at about 9.66 inches according to readings taken by RB&G.

Preparations for the remainder of the construction began in September and continued through December 2006 when the parapets were poured. The ramp was open to traffic by late January or early February 2007. Table 6-1 shows the dates that various components of the abutment and bridge were placed, as well as applicable loads applied to the test pile by the structural components. The loads shown in Table 6-1 are those felt by the test pile. The same procedure was used to calculate these tributary loads as was used for the Redwood Road site (note the same exclusion of any load for the approach slab as done for Redwood Road). The tributary area for this pile is approximately 15% of the total for the abutment.

Table 6-1 Construction Timeline for SLCIA West Abutment

Construction Item	Date Placed	Individual Applied Pile Load (kip)	Cumulative Applied Pile Load (kip)
Embankment Fill	Oct '05 - Feb '06	~ 16 ft high	-----
Pile Cap	1 Sept 2006	8.19	8.19
Wingwalls	1 Sept 2006	5.63	13.82
Diaphragm Wall	1 Sept 2006	9.74	23.56
Girders	25 Sept 2006	22.17	45.73
Deck	13 Nov 2006	61.57	107.3
Approach Slab	22 Nov 2006	0	107.3
Parapets	14 Dec 2006	22.98	130.28

6.3 Gauge Information

In this section, a summary of the information regarding the location of the gauges on the pile (i.e. the approximate elevation of each gauge), their installation, working history and performance will be presented.

6.3.1 Depth Placement

The pile located in the west abutment of the NBAR Flyover Bridge at the SLCIA site was instrumented with 18 strain gauges. Gauge placement was based on the profile found in Boring 03-NB-5, which is shown in Figure 3-15. The methodology for determining the depths at which gauges would be placed was the same as that used at Redwood Road, namely to place a gauge in as many different soil types as possible and at the interface of two layers. Figure 6-2 shows the placement of the gauges in relation to the soil profile. The profile shown in Figure 6-2 is taken from the idealized soil profile (with smaller layers often within the generally identified layers) used for the settlement and stability analyses performed by RB&G.

6.3.2 Site Instrumentation and Equipment History

Strain gauges at the SLCIA site were installed on 20 September 2005, as discussed in Section 6.2. Concrete was placed in the pipe pile the same day, immediately following the placement of the gauges within the pile. Strain gauges were connected to the programmed data logging system and initial readings were taken on 26 September 2005. Readings were to be taken every minute and stored every hour on the hour.

Continuous readings were taken from 26 September 2005 until 24 January 2008. Throughout this time, there are four (4) periods in which readings are missing or

erroneous. The first time period spans from 7 September 2006 to 15 September 2006. When the author went to the site to download data on the 7 September 2006, the data logger would not connect to the computer to download the readings. The data logger was exchanged with a spare data logger by 15 September 2006 and the malfunctioning data logger was sent to the company for repair. The data stored prior to 7 September 2006 was recovered, provided to the author and the logger was repaired.

The next period of missing/errant data spans from 14 December 2006 to 26 January 2007. During this time period the data logger operated erratically. A large number of readings (totaling to 192 hours between all the gauges) were missing and an additional 14 hours show erroneous readings. The reason for this malfunction is not known. It is possible that severe weather could have been the culprit, since most of the missing readings tended to be in the late night or early morning hours when it would have been coldest, but this theory is not verifiable. While comparing the outside conditions during the previous winter when little or no malfunctioning occurred, the temperatures were not significantly different, thus making it difficult to understand why this malfunctioning occurred. It is also possible that small amounts of water may have frozen on the data logger and caused momentary shorting until they thawed, before they refroze. Whatever the reason or reasons, the data logger seems to have returned to accurate and consistent readings from that time on.

The third period of missing data is from 29 January 2007 to 20 February 2007. The gap in readings during this time period was caused by a delay in downloading the data. The readings taken after 20 February 2007 do not indicate any significant variation

from readings prior to the gap, and thus do not compromise the overall results of the monitoring process.

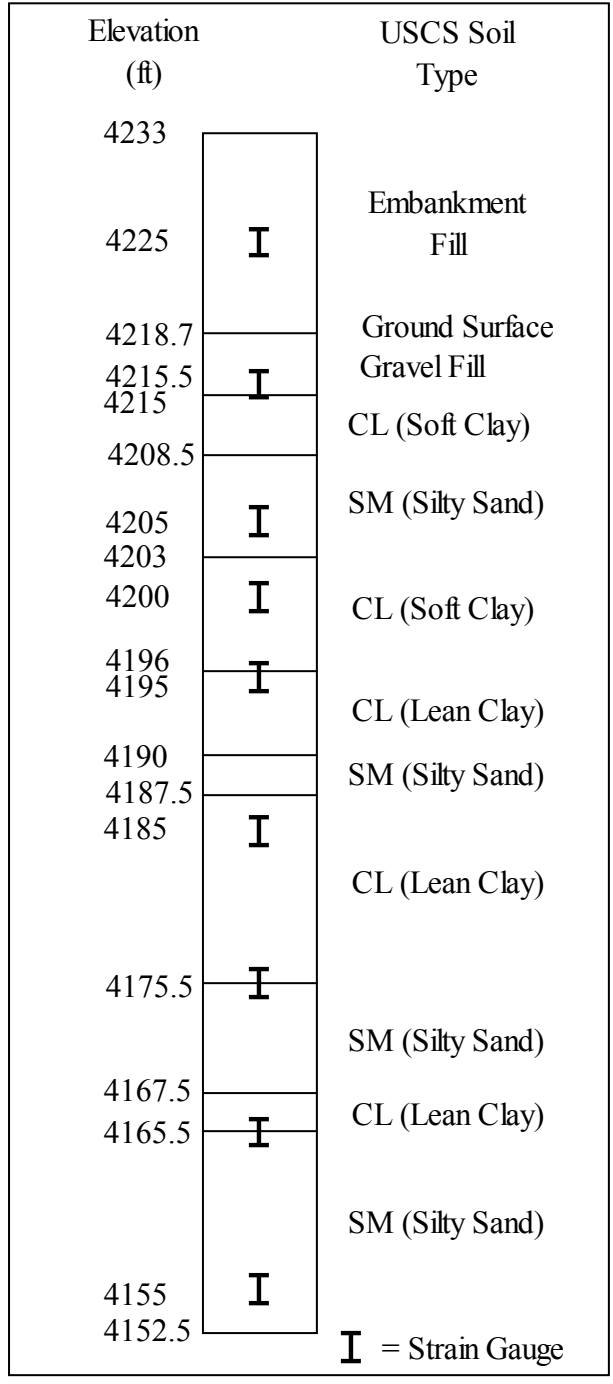


Figure 6-2 Location of Gauges on Test Pile at SLCIA Site Relative to the Soil Layering

A fourth time period, similar to the previously mentioned periods, occurred from 1 December 2007 to 31 December 2007 and again from 6 January 2008 to 12 January 2008. A total of 11 days during the December time frame contained missing information for more than one hour of the day. Later, the gauges appeared to stabilize and gave readings which appear to be consistent.

6.3.3 Gauge Performance

From the time the gauges were initially hooked up to the data logger, all gauges have worked with no major difficulties or problems, besides those enumerated in the previous section, with two exceptions. The gauge on the east side of the pile at a depth of 32.5 feet (El. 4185) recorded erratic values for strain and no values for temperature from the beginning of monitoring. A few days later, on 30 September 2005, the gauge ceased to give any strain measurements. However, after the replacement of the data logger on 15 September 2006, the gauge began to record both temperature and strain measurements that seem credible and consistent. The data from that time is not being used in the results of the data, primarily due to the fact that no firm initial value can be used since the gauge gave erratic measurements from the start.

The other exception is one gauge within the embankment fill at El. 4225. Beginning 11 June 2007 (622 days) the west gauge missed temperature readings, typically for a block of hours. The typical block of hours was from 3 AM to 9 AM, but at times would extend from 8 PM to 11 AM. By 21 August 2007 (693 days) the temperature readings were having fewer problems, with less frequent missing occurrences. From 4 September 2007 to 5 October 2007 the temperature readings were accurate. Then, again from 6 October 2007 to the present, occasional temperature

readings are missing, but not in a large quantity. The missing readings were calculated using the relative change in the east gauge, which has worked without fail.

6.4 Presentation and Discussion of Data and Analyses

The strain readings collected from the individual gauges have been reviewed and reduced to obtain axial stress and axial load; unit shear stress; and pile settlement/compression as discussed in Chapter 4. Analyses have been completed according to the equations stated in Chapter 4. Each of the previously stated items will be discussed in the following sections. The same methodology for analysis, reporting and discussion is used in this chapter as was used in Chapter 5 in the discussion of the Redwood Road and SR 201 site.

6.4.1 Axial Stress and Axial Load

Axial stress and axial load are related very closely to each other as one calculation is simply the product of a constant multiplied by the other. For this reason, the axial stress and axial load will be presented and explained together.

6.4.1.1 Derivation of Axial Stress and Axial Load

Axial stress in the pile is a product of the strain and the composite elastic modulus of the pile. The individual elastic moduli and cross sectional areas, in addition to the composite EA of the pile are found in Table 6-2. The area of the inclinometer pipe has been subtracted from the area of the concrete.

The modulus of elasticity for steel is a typical value based on manufacturing specifications. The modulus of elasticity for the concrete is based on the value for f_c' being 4,420 psi. This value is taken from 28-day compressive strength tests performed

on cylinders taken from the concrete poured on the day the gauges were installed. The tests were performed by RB&G Engineering on 18 October 2005. Two separate cylinders both yielded a failure stress of 4,420 psi. The minimum acceptable compressive strength for concrete specified in the plans for the piles in this project was 4,000 psi. Strain measurements at the very top of the pile are calculated in the same manner as they were for the Redwood Road and SR 201 site by using Equation 5-1. Using the composite AE value for the pile and concrete, the values for axial load have been calculated using Equation 4-2.

Table 6-2 Values for Modulus of Elasticity for Test Pile at the SLCIA Site

Material	Elastic Modulus, E (psi)	Cross Sectional Area (in ²)	AE (lbs)
Steel	29,000,000	10.80	313,177,518
Concrete	3,789,536	136.07	515,642,986
Composite	N/A	146.87	828,820,504

6.4.1.2 Presentation and Discussion of Results for Load vs. Depth Curve

Plots of the load versus depth curves at various times for the east and west side gauges are presented in Figure 6-3. The same difficulty is presented in the results for the gauges on the test pile at the SLCIA site as was manifest at the Redwood Road and SR 201 site. A step-by-step discussion of the gauge results at each location will be provided as part of the effort to configure a load plot that is consistent for the pile. This discussion focuses on the plots provided in Figure 6-3.

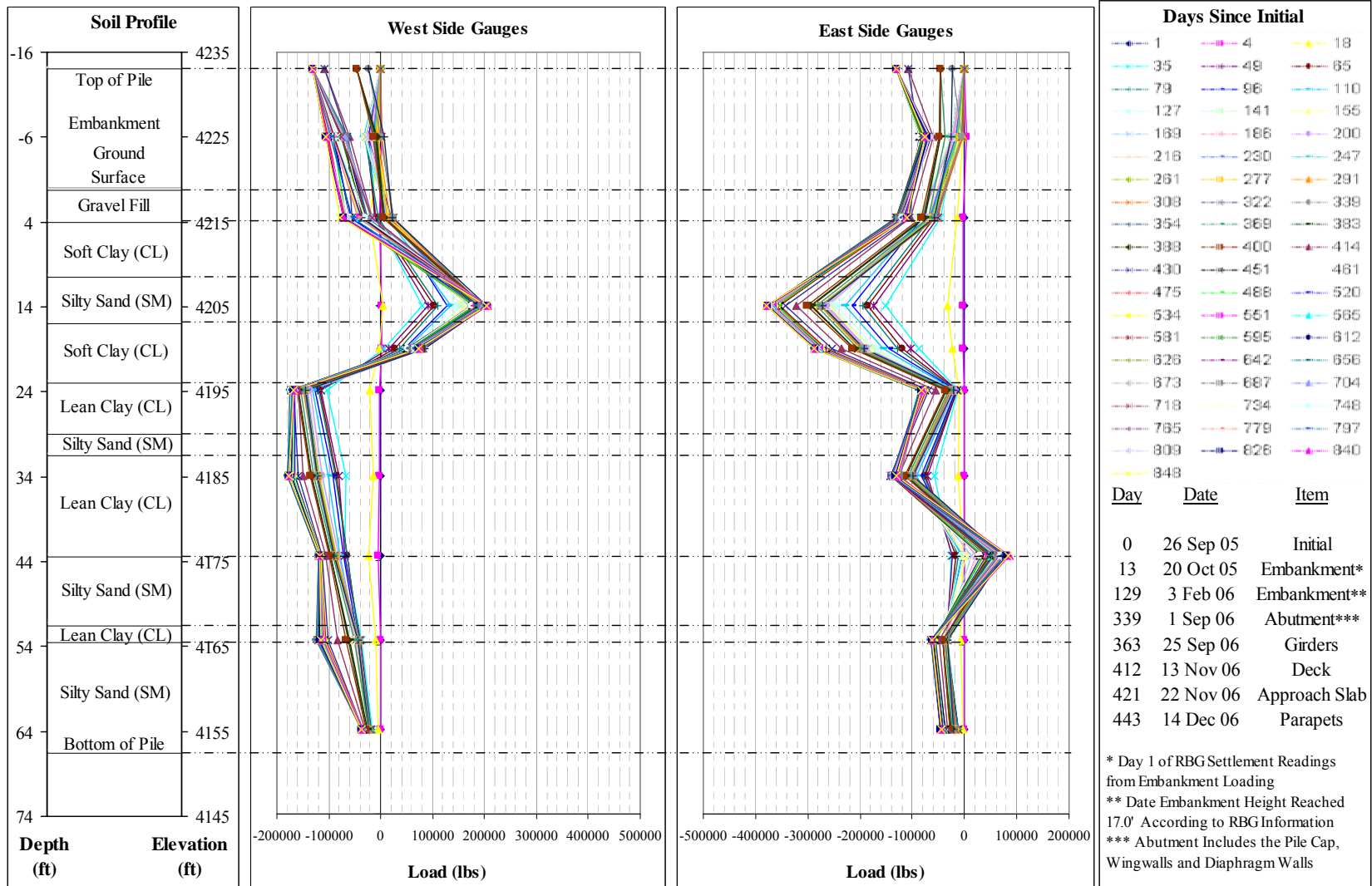


Figure 6-3 Comparison of West and East Gauges for SLCIA Site

6.4.1.2.1 Gauge Inconsistencies

Overall, the decision making process for these gauges was much easier than for the Redwood Road site. For the first gauges at El. 4225, placed in the embankment fill, both gauges seem to be working consistently enough that using the average of the two gauges seems to correct all but one errant value near the beginning of the recording process.

At El. 4215.5 (2 feet below original ground surface, OGS) the gauge for the west side tends to split half and half with positive (tension) and negative (compression) loading. However, the east gauge shows the pile completely in compression. When an average of the two gauges is used, the larger magnitude of the east gauge is sufficient to keep the pile in compression loading, thus making this option appear to be the most feasible. However, it is quite possible that bending in the pile may be occurring.

The two gauges at El. 4205 show dramatically different results. The west side gauge indicates significant tension, while the magnitude of the east gauge is generally 1.5 to 2 times that of the west side load, but in compression. This would seem to indicate a large bending that may exist in the pile. The direction of the bending does seem to be rational as the majority of the embankment is behind the piles, with only two (2) feet of soil in front of, and between the piles and MSE wall. This difference in quantities of soil may be causing the top of the pile to bend slightly towards the abutment wall face, thus putting the east side in compression and the west side in tension. This would also be possible since the gauges are approximately 12.5 feet below OGS, and hence are high enough up to possibly exhibit a bend. As far as deciding between what to use for this elevation, the decision was made to use an average value. This is done for two reasons.

First, using the high tension value from the west gauge would be completely inconsistent with all trends the data should be showing. Second, the use of only the east gauge, with its large value would not be consistent with the trend of values for the remaining gauges. For these reasons, an average of the two gauges appears to be the best option.

A similar, yet not as dramatic pattern is seen in the gauges at El. 4200 (17.5 feet below OGS). Since it is likely the case that a bend may exist, with the maximum bending at El. 4205, it is expected that at greater depths the curvature should right itself and possibly show a small tendency towards the other direction, creating a slight wave pattern. The use of an average value at this elevation also appears to be the most correct and consistent with results for other gauges.

Gauges at El. 4195 (22.5 feet below OGS) do show a possible tendency for a change in curvature in the pile following the large bend exhibited at El. 4200. At this elevation both gauges are in compression, however the east gauge in this instance is less in compression. The magnitude of the difference between gauges is much smaller than that for the two preceding depths, but shows an expected trend, based on the two sets of gauges directly above this elevation. Since the gauges show fairly consistent results, an average of the two appears to be appropriate.

At El. 4185 (32.5 feet below OGS) rests the one gauge that did not properly work since the beginning of the recording. The east gauge, as stated in Section 6.3.3, gave erratic values from the time it was hooked up and only after being hooked up to a different data logger almost a year later has given measurements that appear to be plausible. Since data for this east gauge has been interpolated based on the performance

of the gauges in the near vicinity, and also since the data for the west gauge seems to exhibit credible behavior, using just the west gauge appears to be the best option.

Readings at El. 4175.5 (42 feet below OGS) show an anomaly that is not easily explainable. Since very little to no bending should be occurring at this depth, and also noting the consistent behavior of the gauges above and below, especially on the west side, the behavior of the east side gauge seems highly unlikely and may be the result of a damaged or otherwise malfunctioning gauge. The use of an average value is tainted by the sufficiently high magnitudes of the east gauges and it therefore follows that the use of the west gauge by itself may be the best.

Readings for El. 4165.5 and El. 4155 (52 and 62.5 feet below OGS, respectively) seem to show consistent behavior for both gauges. An average of the two gauges at both elevations seems appropriate.

6.4.1.2.2 Recommendations for Gauge Usage

The opinion of the author has been stated as to the use of one or both gauges for each elevation in the preceding section. In making the decisions as to what gauge or combination of gauges should be used, similar reasoning and justification as used in the discussion of the Redwood Road site has been used. An effort was made to create a plot showing consistent results of the data available, and to allow for useful comparisons in other facets of the analyses. Table 6-3 shows a summary of the author's decisions regarding the use of gauges to create a "best fit" plot of data for the load versus depth profile. Figure 6-4 shows the "best fit" load versus depth plot of the gauges chosen for this pile. The overall appearance of the curves looks as it should and appears to be much more consistent than that seen at the Redwood Road site. In large part, this is likely due

to less malfunctioning of the gauges than what occurred at Redwood Road. A simplified version of the load versus depth curves over time is presented in Figure 6-5. This plot highlights key points in time over the duration of monitoring.

Table 6-3 Combination of Gauges used to Create Consistent Load Plot

Gauge Elevation (ft)	Gauge(s) Used
4225	Average of East and West gauges
4215.5	Average of East and West gauges
4205	Average of East and West gauges
4200	Average of East and West gauges
4195	Average of East and West gauges
4185	West gauge only
4175.5	West gauge only
4165.5	Average of East and West gauges
4155	Average of East and West gauges

6.4.1.3 The Neutral Plane and History of Dragloads

The position of the neutral plane for this pile is much more constant than what was seen for the Redwood Road site. The neutral plane was not clearly identifiable at any particular elevation until day 18 (15 October 2005) when it settled at El. 4175.5. The neutral plane remained at this location until day 37 (3 November 2005) when it moved up to El. 4185.

A look at the settlement time history as monitored by personnel from RBG will be helpful in understanding the position of the neutral plane with respect to at least the settlement during primary consolidation. The settlement device was placed near the test pile location and was monitored during the embankment construction to an embankment fill height of 17 feet (the redesigned embankment height). Figure 6-6 contains the settlement versus fill relationship for the 17-foot high embankment.

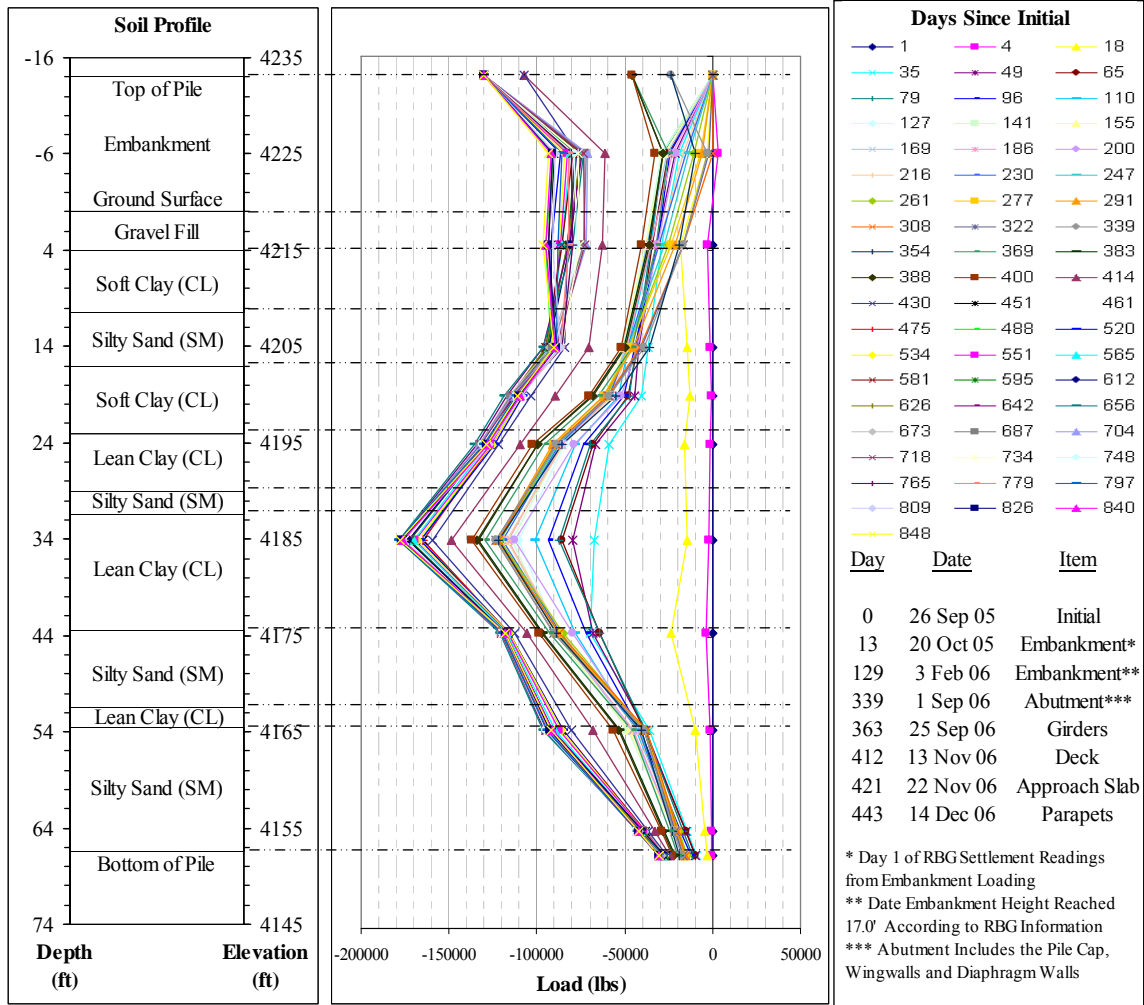


Figure 6-4 Plot of Axial Load vs. Depth and Time using Best Combination of Gauges for SLCIA Site

It can be seen that most of the settlement was complete by the beginning of March 2006. A quick survey of the loads in the pile indicate that dragloads developed and increased quickly during the first three to four weeks and then more gradually after that to about the first of March 2006. After this time, dragloads continued to increase, but at a slower rate, until structural loads were introduced

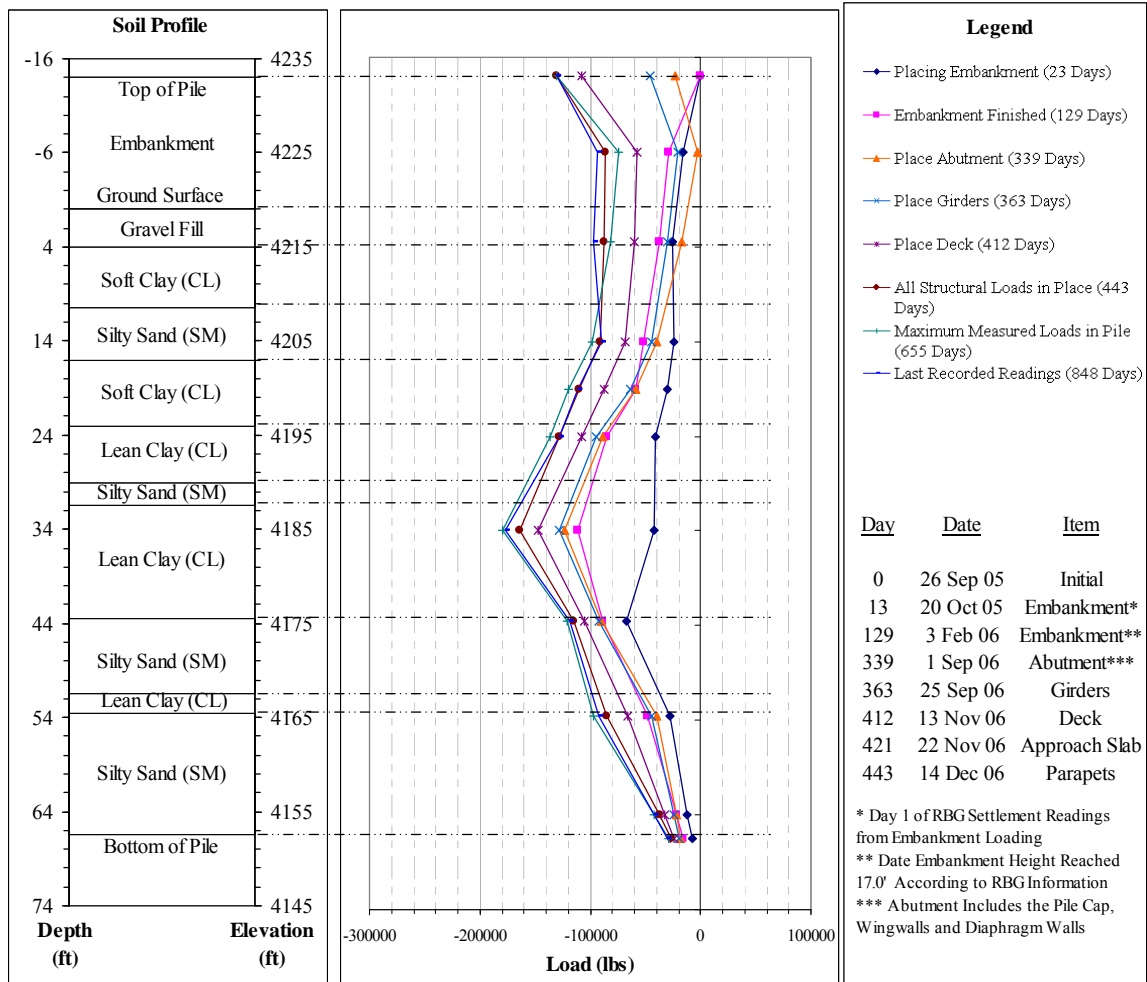


Figure 6-5 Simplified Plot of Axial Load vs. Depth and Time for SLCIA Site

The neutral plane has remained at El. 4185 up to the last time data was downloaded on 24 January 2008. Despite any and all structural loads that were placed for the bridge, the neutral plane has not appeared to have any tendencies to change to a different elevation, although the dragloads in the pile have been effectively reduced by their addition.

Looking at the history of the dragload in the pile, as was done for the Redwood Road site, sheds light on the interaction of embankment and structural loading with

dragloads. Table 6-4 gives a summary of the dragloads for some of the more important times.

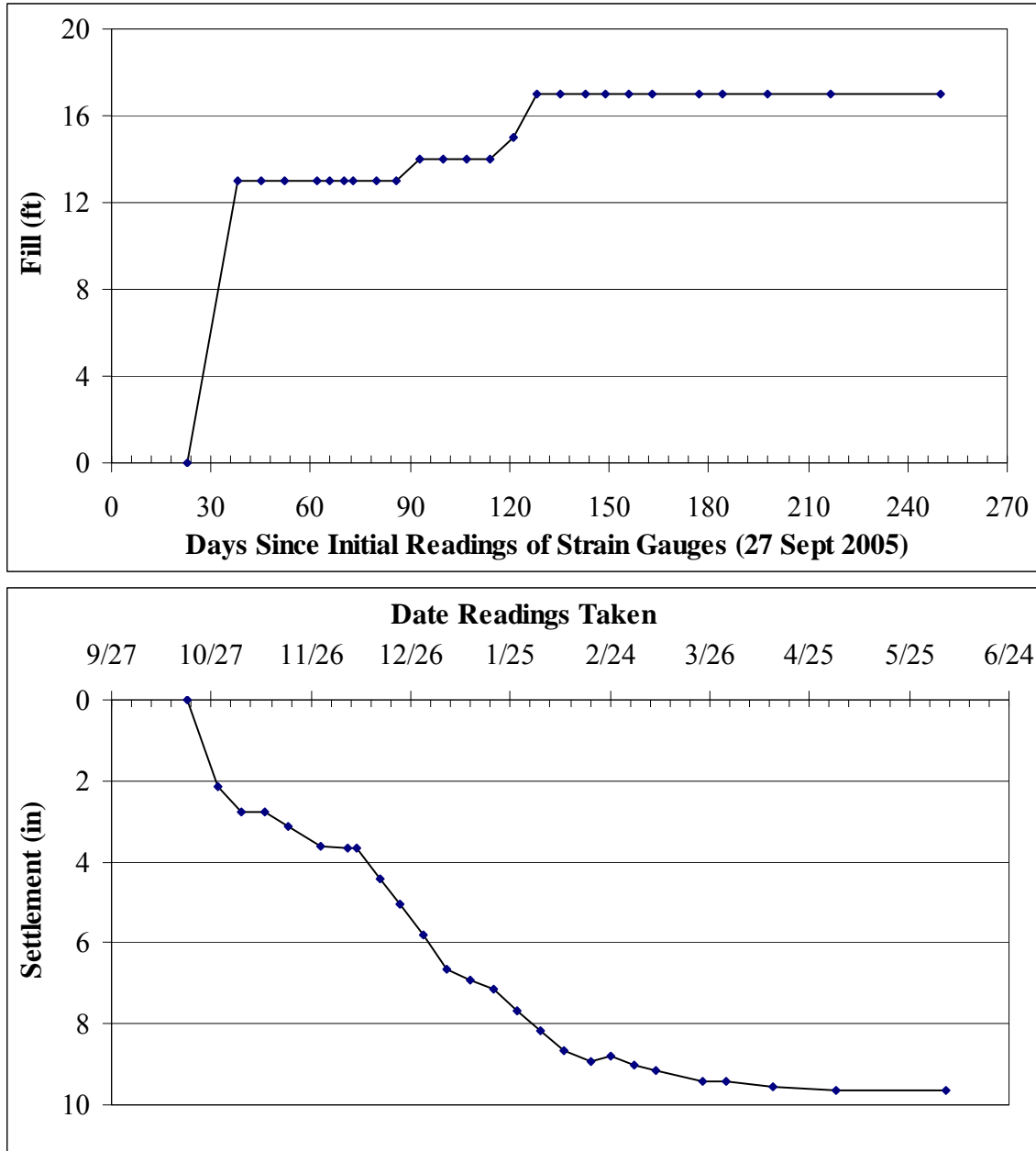


Figure 6-6 Settlement vs. Fill Height for SLCIA Site (data provided by RB&G Engineering)

Table 6-4 History of Dragload for Pile at SLCIA Site

Date/Description	Days Since Initial	Total Load (kips)	Structural Load (kips)	Dragload (kips)	Elevation of Neutral Plane (ft)
6-5-06/End of Settlement (last RBG reading)	251	125.14	0	125.14	4,185
8-27-06/Maximum Dragload before Structural Loads	334	127.26	0	127.26	4,185
9-1-06/After Abutment	339	127.12	23.55	103.57	4,185
9-24-06/Just before Girders	363	130.31	23.55	106.76	4,185
9-25-06/After Girders	364	132.23	45.72	86.51	4,185
11-12-06/Just before Deck	411	151.63	45.72	105.91	4,185
11-13-06/After Deck	412	151.75	107.30	44.45	4,185
12-14-06/All Structural Loads in Place	443	169.16	130.28	38.88	4,185
7-14-07/Maximum Load Recorded in Pile	655	184.78	130.28	54.50	4,185
1-23-08/Last Reading (13 Months after all Loads)	848	183.05	130.28	52.77	4,185

As can be seen in Table 6-4, consolidation settlement was essentially completed at 251 days and the maximum dragload in the pile of 127.3 kips occurred at this point before any structural loads were placed. After placing the abutment/pile cap, the dragload was reduced by the full amount of the load of the abutment/pile cap. With each successive addition of structural loading, the dragload was decreased, generally by a value very close to the load applied by the structural component. A good example of this is the addition of the deck. The deck added about 61.6 kips to the pile, and the dragload was reduced by about 61.5 kips. Therefore, even though 130 kips were applied to the top of the pile by structural loads, the maximum (total) load in the pile due to downdrag and structural load combined only increased by about 42 kips.

A close review of the data in Table 6-4 indicates that the 42 kip increase was due to a redevelopment of dragload with time after the structural loads were placed. This

could be a result of secondary settlement in combination with the placement of the approach slab in late November which may have induced some additional consolidation settlement. During the last 13 months of the record after the last structural loads were applied, the dragload has increased by 14 to 16 kips. This increase could also be attributed to soil settlement produced by secondary consolidation.

The reduction in the dragload produced by the application of structural loads at the SLCIA sites stands in contrast to observations at the Redwood Road site where the dragload remained relatively constant even after structural loads were applied. The difference appears to be attributable to the fact that primary consolidation was essentially completed before the structural loads were applied to the piles at the SLCIA site. In contrast, consolidation settlement was continuing while structural loads were applied at the Redwood Road site. Based on this information, it can be seen that when relatively large amounts of settlement are still occurring, the dragload will not decrease as substantially as it would were the settlement complete.

Another item of note from Table 6-4 is the maximum load in the pile of 184.8 kips, which occurred on day 655 (14 July 2007) after all the structural loads had been applied. The corresponding dragload at this time was 54.5 kips, which is less than half of the maximum dragload recorded prior to structural loading. At the end of the currently downloaded readings, the dragload is less than half the dragload just before the surcharge was placed and is not increasing at a significant rate.

6.4.1.4 Immediate Effect of Structural Loading

The analysis of the structural loading sequence for the SLCIA site was done in the same manner as it was done for the Redwood Road site. Full details of the purpose of

this analysis are found in Section 5.4.1.4. An analysis of the various loadings (in the following order: abutment – comprised of pile cap, diaphragm and wingwalls; girder placement; concrete deck pour; approach slab; and parapets) shows the same inconsistencies and problems as observed during the analysis of the Redwood Road site. Since, unfortunately, no conclusions can be reached by the analysis of the data, no further discussion will be given on this topic. In further research, it is possible that taking readings in smaller time increments, such as 5 or 10 minutes, may catch changes more clearly. However, it is also possible these smaller time increments may show reactions of the pile to brief construction related operations and obscure the effects of the structural loading itself.

6.4.2 Shear Stress

Calculating shear stress along the pile is a way to quantify the skin friction acting on the pile at various elevations. This becomes useful as the α and/or β coefficients can be back-calculated for either a total or effective stress analysis, respectively.

6.4.2.1 Derivation of Shear Stress Calculations

As described in Section 5.4.2.1, the shear stress for the different segments has been calculated by both the “double segment” and “single segment” methods as discussed in Sections 4.4.1 and 4.4.2. No review of the equations will be repeated here. Just as in the calculation of the shear stress for the Redwood Road site, the double segment shear stress calculation provides an average value of the two single segment calculations (see Figure 6-7). Since using the double segment method runs into difficulties near the neutral plane, the single segment method was also used for this pile.

6.4.2.2 Presentation of Shear Stress Data and Analyses

In this section, the measured shear stress will be plotted as a function of time for each section of the pile between two gauges. As each segment is discussed it is important to remember the following:

- Shear stress for segments above the neutral plane should be negative due to downdrag at least prior to structural loading.
- Shear stress for segments below the neutral plane should be positive.
- Alternations between positive and negative shear stress generally indicate a change in neutral plane elevation.
- Data used for gauges at El. 4185 and El. 4175.5 are based on the west gauge only since values for the east gauge were either inconsistent or nonexistent.
- Day “0” on the following plots is 27 September 2005.

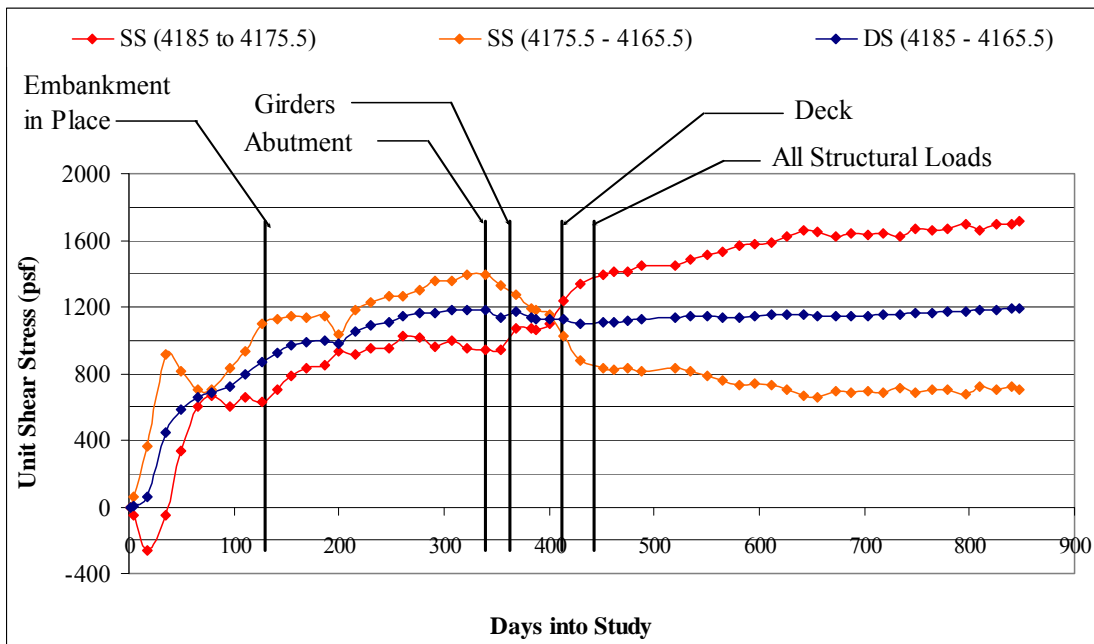


Figure 6-7 Comparison of Single Segment and Double Segment Methods for Calculating Shear Stress between El. 4185 and El. 4165.5

6.4.2.2.1 Shear Stress between El. 4233 and El. 4225

This section runs from the top of the pile to approximately the middle of the embankment fill. The fill material, according to the subsurface investigation report prepared by RBG indicated a granular material within the MSE wall with a friction angle of 35° and a unit weight of 135 pcf. The shear stress time history plot for this section is shown in Figure 6-8.

The trends in the plot are consistent with what is taking place. From the beginning of the readings to the time just prior to the structural loading, negative shear stress develops as the soil settles relative to the pile due to the stress induced by the embankment. After structural loads are applied, the shear stress changes from negative to positive because the loads cause the pile to settle relative to the surrounding soil and resist the applied load. Compression of the pile is greatest near the point where the load is applied. From gauge measurements, the maximum shear strength appears to be near 2000 psf.

6.4.2.2.2 Shear Stress between El. 4225 and El. 4215.5

The soil around this section consists of granular fill composed of silty sandy gravel (GP-GM). The gauges cover a zone about 7.5 feet above the original ground surface to a depth of 3 feet below the original ground surface. Firstly, it should be noted that the shear stress has always remained negative, as would be expected because it is above the neutral plane. The increase in negative shear stress at the start was likely caused by placement of the embankment fill. A close comparison of the settlement over time for this site indicates a correlation between the times of slower (less magnitude) settlement and the decrease in negative shear stress. This change is logical and expected.

After settlement once again picked up, a similar increase in negative shear stress is observed.

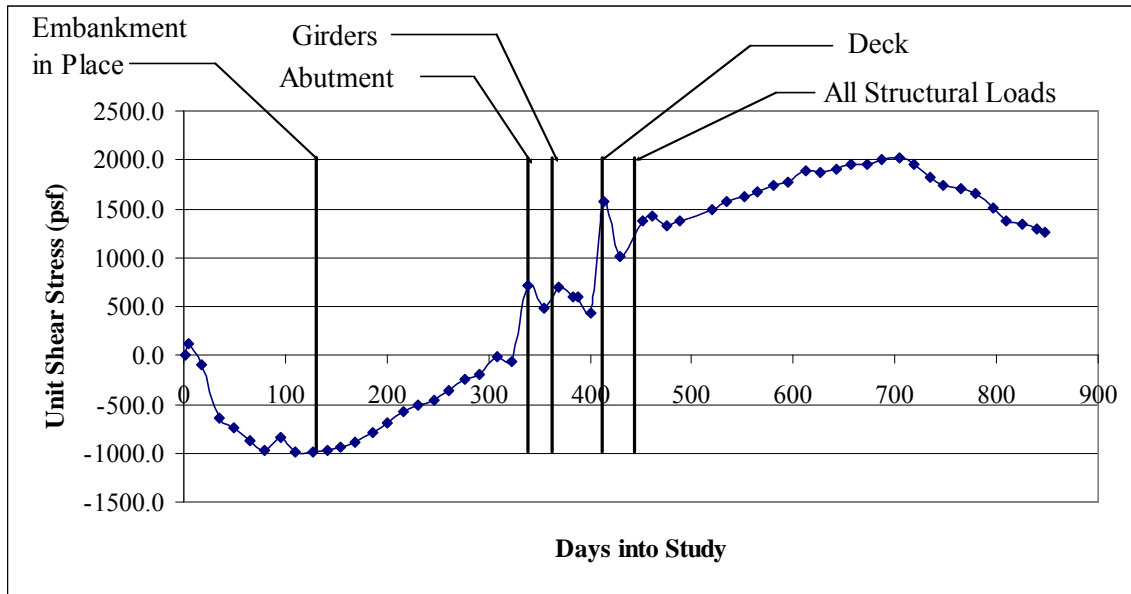


Figure 6-8 Plot of Shear Stress between El. 4233 and El. 4225

As structural loads were placed, beginning with the abutment the shear stress rapidly changed from -500 psf to around -100 psf. This pattern is in accordance with previous research and the general theory of negative skin friction. As additional load is added to the piles, thus causing the piles themselves to compress and/or settle, negative skin friction should be decreased or eliminated if the applied load is great enough. An undulating pattern is very evident in the plot of the shear stress for this section as shown in Figure 6-9, and is considered to be caused by the proximity to the structural loading. This section is second only to the section above it in terms of being affected by transitory (short-term) loads that may or may not be felt by other sections located deeper in the pile. Overall, there has been a general leveling in the amount of shear stress, although it does still fluctuate. The transition back and forth between negative and positive shear stress

near the end of the time history, may be due to continued creep in the pile, then followed by continued secondary consolidation.

6.4.2.2.3 Shear Stress between El. 4215.5 and El. 4205

The shear stress time history for this section, as shown in Figure 6-10, is similar in many ways to the section just above it, except without the excessive undulation in the later portion of the plot history. The soil adjacent to the pile within this section consists of a 6-foot layer of lean clay (CL-ML) and a 4.5-foot layer of silty sand (SM).

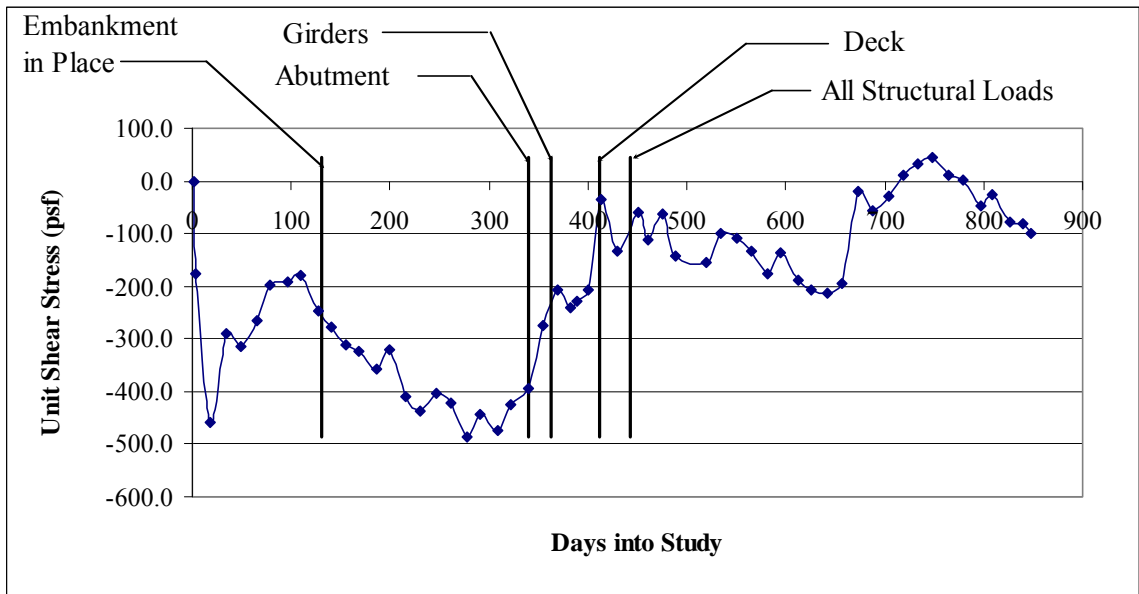


Figure 6-9 Plot of Shear Stress between El. 4225 and El. 4215.5

One thing to point out is that the three change-overs from positive to negative shear stress do not indicate, in this instance, a change in location of the neutral plane since the settlement of the soil is still greater than that of the pile. The neutral plane, with the exception of the first 18 days, has always been at least 32.5 feet below the original ground surface. Since this section is still near the original ground surface (within the top

13 feet), susceptibility to short-term loads is a possible factor influencing the behavior seen in this section. Once again it can be seen that the structural loading caused the negative shear stress, which reached a maximum of 650 psf to become positive for a time. However, subsequent settlement has apparently led to a resumption of negative skin friction of about 500 psf. The reason for the final shift back to positive skin friction is not known, especially since the sections above and below this depth show more positive and expected trends. Although the neutral plane has not shifted up to this elevation, it is clear that the combination of structural loads and surrounding soil settlement has caused continual change in this section.

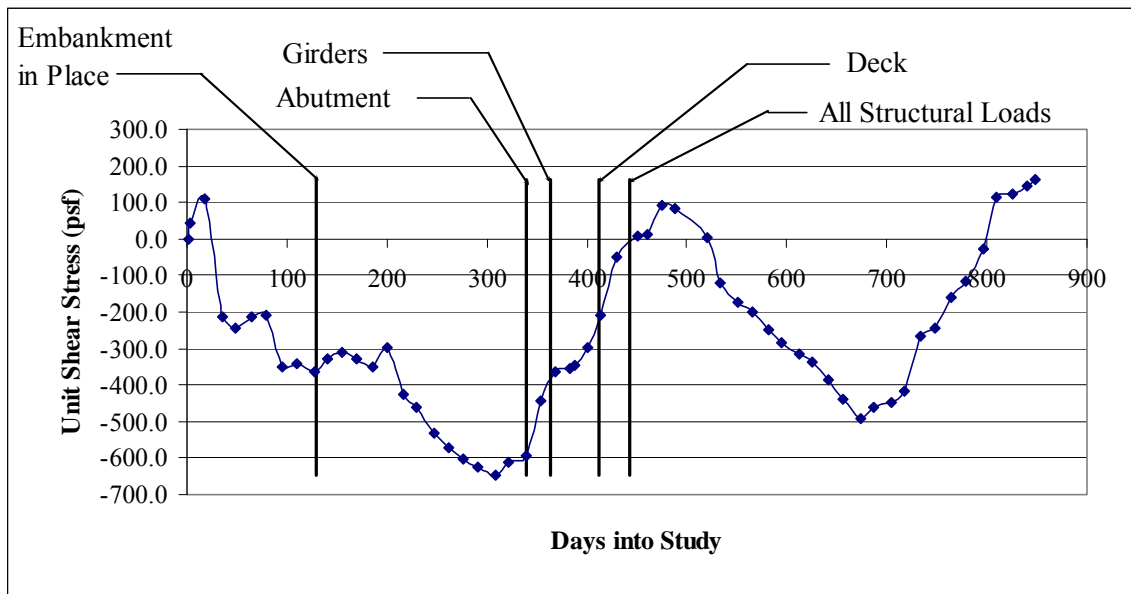


Figure 6-10 Plot of Shear Stress between El. 4215.5 and El. 4205

6.4.2.2.4 Shear Stress between El. 4205 and El. 4200

Shear stress in this section generally follows the pattern expected. This section has the upper gauge located in silty sand (SM) layers, as mentioned previously with the

bottom gauge located near a thin (one foot) clay (CL) layer sandwiched between two silty sand (SM) layers. In between the gauges are two- to three-foot thick layers of lean clay (CL-1) and silty sand (SM) soils. As shown in the time history in Figure 6-11, the shear stress in this section is positive until shortly after the 15-day reading. As described in Section 6.4.1.3 in the discussion of the location of the neutral plane, the neutral plane did not settle on a single location until day 18 (15 October 2005) which explains the slight positive side friction at the very beginning. When settlement began and continued, negative skin friction was mobilized. This behavior is clearly shown in Figure 6-11. During consolidation and before the abutment was poured, the negative shear stress increased with some consistency. After the abutment was poured, negative skin friction was arrested, although it did not decrease significantly. The slight reduction in negative shear stress may have been caused by slow creep in the pile, but was evidently not sufficient to overcome the remaining secondary consolidation occurring in the soil, thus an increase in negative shear stress is still seen.

6.4.2.2.5 Shear Stress between El. 4200 and El. 4195

The shear stress behavior in this section, shown in Figure 6-12 follows the same general pattern as the sections above it. The upper gauge lies in the sandwiched clay (CL) layer spoken of in the preceding section and the lower gauge rests near the border of a sandy silt/clay (CL/ML) layer and a lean clay (CL) layer. A lean clay (CL-2) layer lies in between these layers.

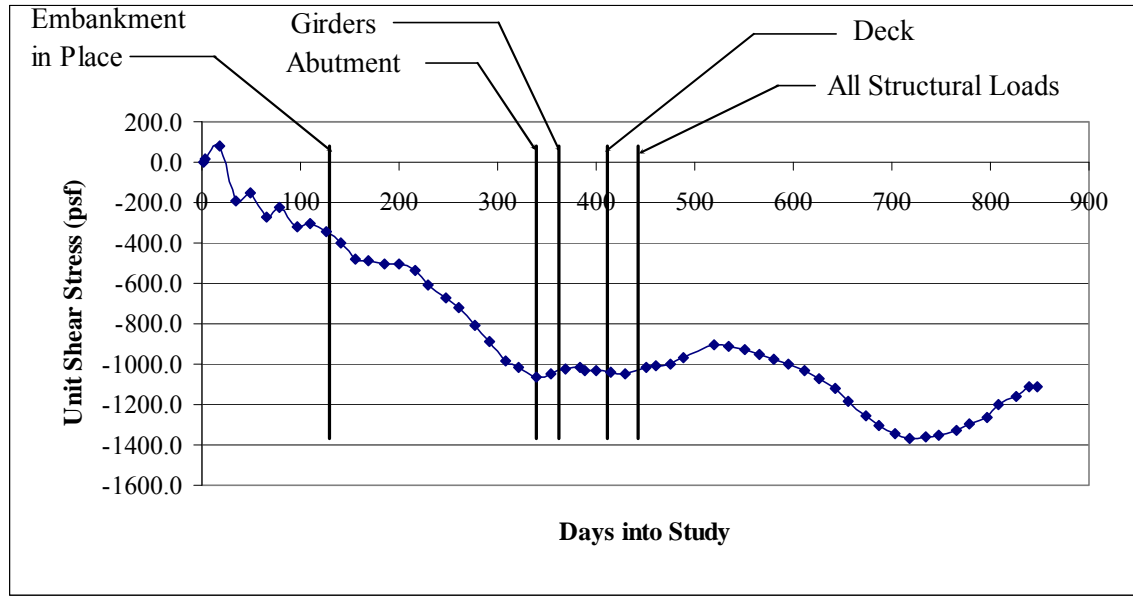


Figure 6-11 Plot of Shear Stress between El. 4205 and El. 4200

The only marked difference between this section and the others that have been discussed is the large shift in shear stress immediately after the deck was poured. It seems that settlement had done most of its work at inducing negative skin friction by about 150 days into the process, with a small amount of increase as time went on. After the abutment and girders were constructed the negative skin friction was arrested for a time, and then a large (700 psf) jump is seen. The other notable part of this occurrence is that consistent behavior has been recorded following this occurrence. It is possible that there has been relatively little soil settlement at or below this location, thus not able to induce a significant increase in negative shear stress. However, the fact that the final stress level is consistent with that for the sections above and below suggests that the earlier strain gauge readings may have overestimated the actual shear stress.

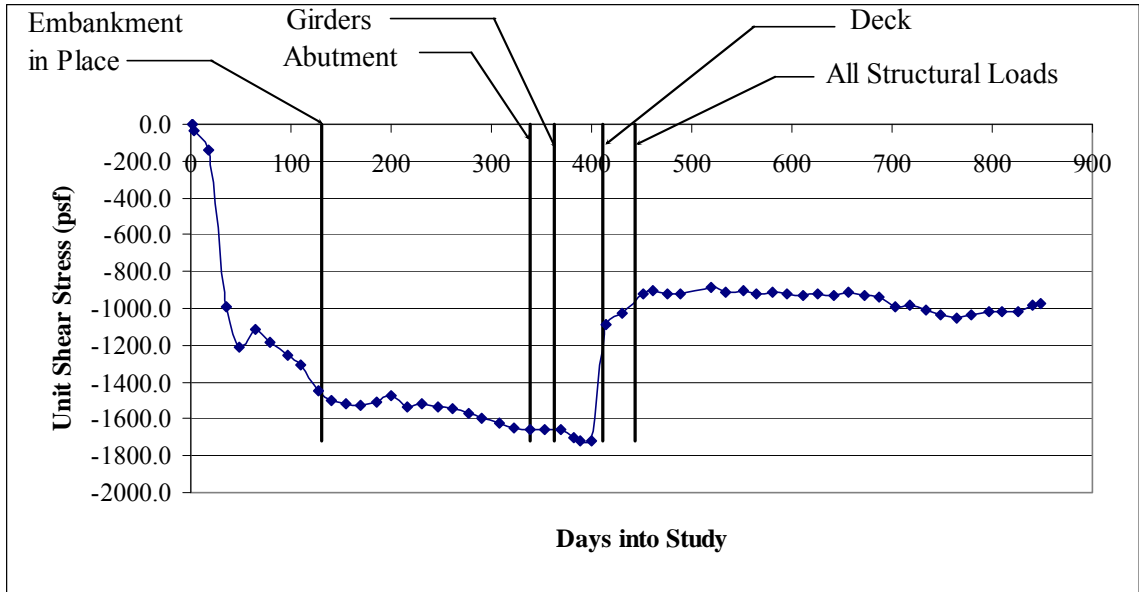


Figure 6-12 Plot of Shear Stress between El. 4200 and El. 4195

6.4.2.2.6 Shear Stress between El. 4195 and El. 4185

The section between El. 4195 and El. 4185 shows generally consistent behavior relative to the other gauges but with a problematic ending. The soil within this section consists of 5 feet of lean clay (CL) with sand lenses, 2.5 feet of silty sand (SM), and nearly 3 feet of silty, sandy lean clay (CL/ML).

Initially, the shear stress in this section, as shown in Figure 6-13, becomes progressively more negative as settlement occurs; however, the behavior after day 400 appears to be in conflict with the logical pattern that would be expected. The first problem is the slight increase in negative skin friction after the deck was poured instead of a decrease as recorded by the other sections. In addition, rather than staying constant after the completion of settlement and the application of structural loads, the shear stress becomes progressively more negative. There does not seem to be an explanation for this

behavior, except that the increase could potentially be caused by drift in the strain gauges over time.

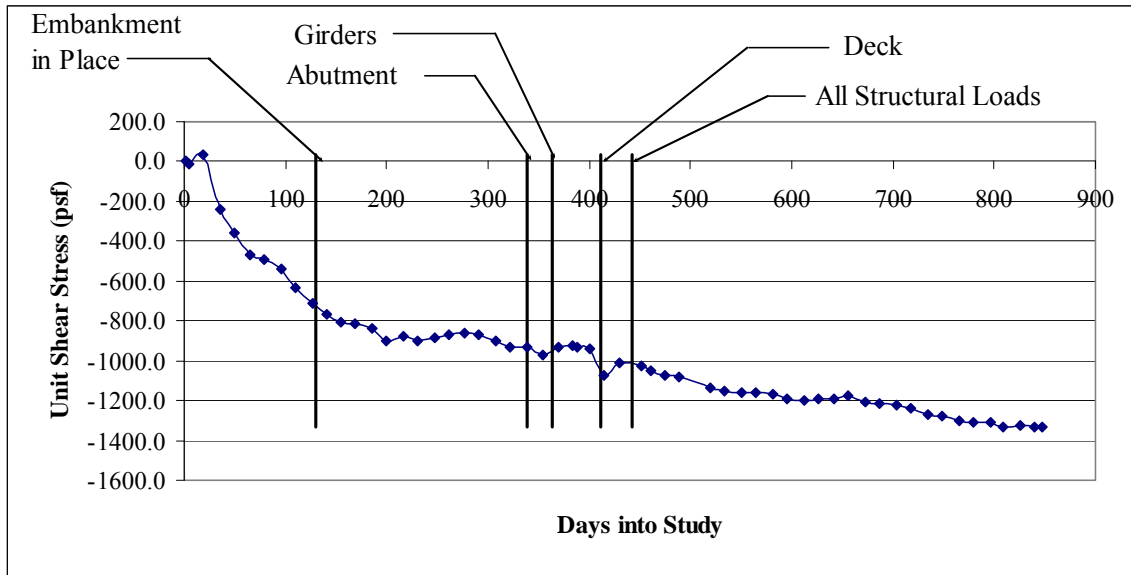


Figure 6-13 Plot of Shear Stress between El. 4195 and El. 4185

6.4.2.2.7 Shear Stress between El. 4185 and El. 4175.5

The soil within this section consists almost entirely of lean clay (CL). As mentioned in Section 6.4.1.3 and Section 6.4.2.2.4, the neutral plane resided alternately between El. 4225 and El. 4215.5 for the first 17 days of recording after which it rested near El. 4175.5 for an additional 19 days and then made its final move to near El. 4185 where it has remained. Confirmation of the above information is manifest in Figure 6-14, as the change from negative to positive skin friction occurs after 38 days of recording. Over time, positive skin friction has built up, with noticeable increases occurring after the girders and deck were placed/poured. Although the shear stress continues to increase

slightly with time, it appears that an equilibrium state has been reached. The small increases in stress here could potentially be due to gauge drift.

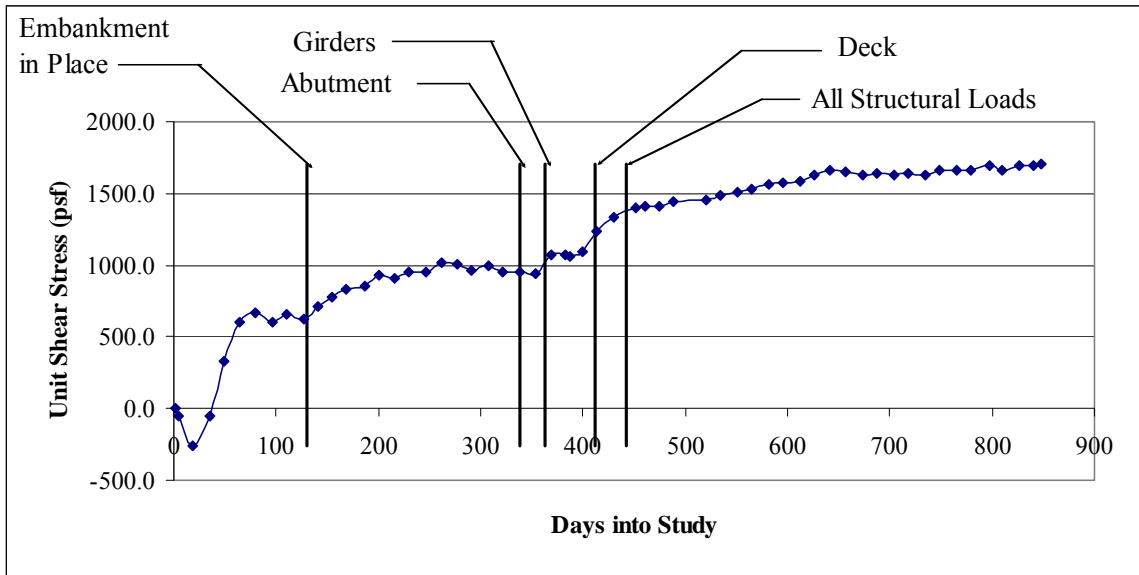


Figure 6-14 Plot of Shear Stress between El. 4185 and El. 4175.5

6.4.2.2.8 Shear Stress between El. 4175.5 and El. 4165.5

The upper gauge for this section rests near the border of the silty lean clay (CL) and poorly graded sand with silt (SP-SM) mentioned in the previous section and the lower gauge rests near the border of a layer of silty clay with sand (CL) and a silty fine sand (SM) layer. A three foot thick layer of silty sand (SM) was encountered between the layers already mentioned.

The behavior of this section has a similar abnormality as did the section from El. 4195 to El. 4185 as discussed in Section 6.4.2.2.6. The increase in positive shear stress near the beginning of the history shown in Figure 6-15 is expected as this section is near the toe of the pile. However, the 200 psf decrease between days 35 and 65 does not seem

to correlate with any other known construction activities. It is possible the reduction and subsequent increase in the positive shear stress could be associated with the pile settlement due to the development of end-bearing resistance. The problematic part about this history is the decrease in positive shear stress after structural loads are applied to the piles. At this depth, positive skin friction would normally be expected to increase as structural loads are applied. The reduction in shear stress could be associated with strain-softening in the denser sands in this interval. Readings over the last number of months seems to indicate that an equilibrium has been reached, but the cause for it to be at a value nearly 700 psf less than the maximum shear stress. This could be the residual stress for the soil in this section.

6.4.2.2.9 Shear Stress between El. 4165.5 and El. 4155

Shear stress in this section appears to typify the expected reaction to applied loadings, both fill surcharge and structural loads. This section's upper gauge rests near the border of a two foot thick silty clay with fine sand (CL) layer and a five foot thick layer of silty fine sand (SM) as mentioned previously and the lower gauge is located within a four foot thick layer of silty fine sand (SM). A 2.5-foot lean clay (CL) layer is found among the predominantly silty sand soils.

The shear stress climbed in the positive direction as the embankment fill was placed and leveled off as it reached its peak. As the embankment induced settlement decreased in speed and magnitude, the shear stress even decreased somewhat. However, after structural loads were placed, especially the girders, the shear stress increased by more than double the value it was at the time just prior to the abutment construction.

After the structural loads were all placed, the shear stress has leveled off again and has remained relatively constant for the past 100 days.

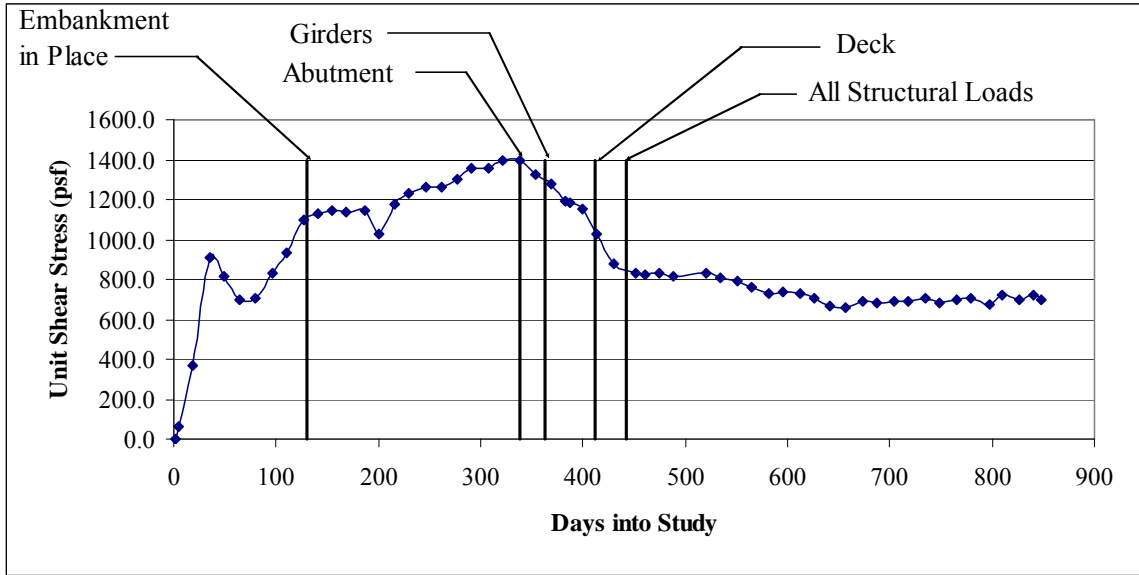


Figure 6-15 Plot of Shear Stress between El. 4175.5 and El. 4165.5

6.4.2.2.10 Summary of Shear Stress Values for Sections of Pile

Overall, the results of the shear stress analysis for this pile agree reasonably well with the expected behavior, with a few obvious exceptions as noted in the previous sections. The expected behavior largely comes from the position of the neutral plane over the course of time. The sections that appear to have more obvious abnormalities are those sections from El. 4215.5 to El. 4205, El. 4195 to El. 4185 and El. 4175.5 to El. 4165.5. These sections tend to follow the expected behavior until at least day 100 and often until day 400 before going astray. Despite the irregularities shown in these sections, the overall results are encouraging and tend to support the reliability of the information obtained from the strain gauges.

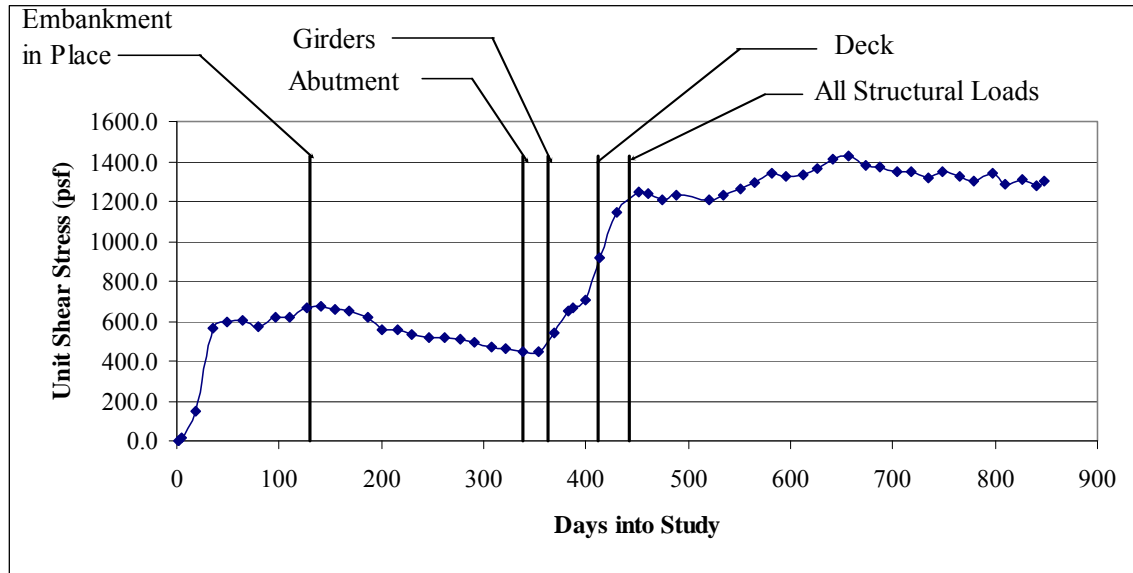


Figure 6-16 Plot of Shear Stress between El. 4165.5 and El. 4155

6.4.3 Comparison of Estimated to Actual Results

The same manner of presentation and discussion of the two methods used for the Redwood Road site will be used here. Explanations given for the Redwood Road site will not be repeated and the reader is referred to Section 5.4.3 to review any explanations required.

6.4.3.1 Estimating the Location of the Neutral Plane

Once again, the “Unified Design” method by Fellenius and the method developed by Briaud and Tucker will be used to estimate the location of the neutral plane with the information provided by the laboratory and field data.

6.4.3.2 Estimation of Side Resistance

Table 6-5 shows the summary of the soil parameters used to compute the unit side resistance for each layer along with the side resistance estimated for each soil layer.

Once again, the α value has been assumed to be 1.0 for all clay layers. Based on the unit side resistance shown in Table 6-5, the dragloads or positive skin resistance were calculated by using Equation 5-6.

Table 6-5 Summary of Alpha and Beta Values and Estimated Side Resistance for SLCIA Site

Elevation Extents of Soil Layer		USCS Class	γ_m	σ'_{vo}	ϕ	β	S_u	f_s
			pcf	psf	deg		psf	psf
4233	4219	-----	135	----	----	----	----	1500
4219	4215	GP	125	230	33	0.61	----	140
4215	4208.5	CL	115	665	----	----	380	380
4208.5	4203	SM	115	980	28.5	0.53	----	520
4203	4196	CL	105	1275	----	----	325	325
4196	4190	CL	105	1550	----	----	410	410
4190	4187.5	SM	125	1755	30	0.56	----	980
4187.5	4175.5	CL	115	2150	----	----	630	630
4175.5	4167.5	SM	130	2738	34	0.64	----	1745
4167.5	4165.5	CL	115	3060	----	----	760	760
4165.5	4150	SM	130	3635	34	0.64	----	2315

6.4.3.3 Derivation of Pile Compression and Pile Settlement

As set forth in Section 5.4.3.3, settlement of the pile is a combination of the elastic compression of the pile and settlement of the pile at the pile tip. The equations for the compression of the pile at gauge elevations and at midpoint elevations between gauges were presented in Sections 4.5.1 and 4.5.2 as shown in Figure 4-13 and Figure 4-14. An equation to calculate the expected elastic compression of the pile, $S_{\text{compression}}$, was given as Equation 5-7. Equation 5-8 through Equation 5-11 were also used to calculate the settlement of the pile into the bearing stratum. Equation 5-10 cannot be used for this site since no CPT testing was performed. A summary of the pile compression and settlement values is given in Table 6-6.

Table 6-6 Summary of Calculated Pile Compression or Settlement Values

Type of Settlement	Equation Used	Calculated Compression or Settlement
Elastic Pile Compression	Equation 5-7	0.13 inches
Pile Tip Settlement	Equation 5-8	0.38 inches (range of 0.27 to 0.61 inches)
Pile Tip Settlement	Equation 5-9	1.98 inches
Pile Tip Settlement	Equation 5-11	0.35 inches (range of 0.25 to 0.56 inches)

The following values were used in the calculation of the above settlements: For Equation 5-7; Q_p is 110,500 lbs, L is 82 feet (984 inches), AE is 8.2882×10^8 ; for Equation 5-8; q_{up} is 280 psi (using 43,100 lbs for load at base), B is 14 inches, E_i is 7,500 psi, μ is 0.375 and I_{up} is 0.85; for Equation 5-9; pf is 988.3 kips, B is 28.83 feet, pile cap width is 3 feet, D is 82 feet and N' is 80; for Equation 5-11 all required terms are same as Equation 5-8.

Settlements calculated by Equations 5-8 and 5-11 are close to each other (as they should be) and once again the settlement predicted by Equation 5-9 does not appear credible. No load tests were performed at this site, therefore, it is not possible to compare against measured load-settlement data. A pile compression of 0.13 inches and a pile settlement of 0.35 inches will be assumed to approximate the total movement of the pile giving a total pile head movement of 0.48 inches.

6.4.3.4 Presentation of Measured Pile Compression Results

Curves showing the computed elastic distortion of the pile throughout time are shown in Figure 6-17. These curves were calculated by the methods set forth in Sections 4.5.1 and 4.5.2 and are based on the compression of the pile due to loads produced by dragload and structural load. These curves do not include settlement of the pile due to compression of the soil underneath the pile cap. As of 23 January 2008 the maximum

compression of the pile was approximately 0.133 inches. The elastic distortion settlement curves have remained relatively consistent with time for the past year. The pile compression calculated by Equation 5-7 compares very well with the pile compression of 0.133 inches indicated by strain gauge measurements.

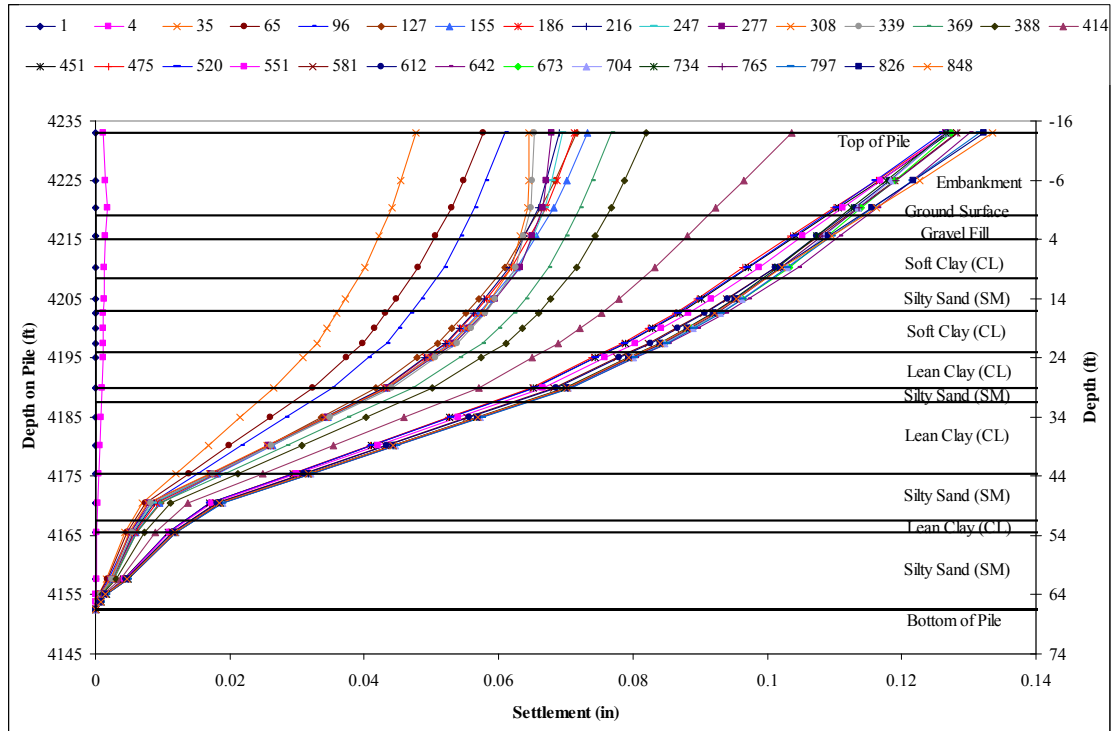


Figure 6-17 Pile Compression over Time for SLCIA Site

6.4.3.5 Presentation of Soil Settlement

During placement of the fill for the abutment near the test pile, settlement was monitored from a settlement plate and occasional surveys. The settlement history was shown in Figure 6-6, with a maximum of 9.66 inches of settlement being recorded. It should be noted that construction activities did interfere with some of the settlement monitoring equipment on a few occasions. Any problems caused by these interferences

were resolved. Settlement analyses performed by RBG based on an embankment/MSE wall 27 feet high predicted 18 inches of settlement at the back of the MSE wall and nine inches at the face of the wall. It should be remembered, however, that the final height of the wall was changed to reach about 16 feet high. Using the computed settlements from the subsurface investigation report submitted by RBG, contributory settlement from each layer was estimated proportionally to obtain a value equal to the measured settlement. These settlement values can be found in Table 6-7. The values in the last column show cumulative settlement from the top-down and from the bottom-up in parentheses.

Table 6-7 Summary of Contributing Settlement for Soil Profile at SLCIA Site

Elevations of Layer Limits		Layer Thickness	Type of Soil	Contributing Settlement	Cumulative Settlement
Top El.	Bottom El.				
feet	feet	feet	-----	inches	inches
4219 (Ground Surface)		-----	-----	0.0	0 (9.66)
4219	4215	3.7	GP-GM	0.05	0.05 (9.61)
4215	4208.5	6.5	CL	2.6	2.65 (7.01)
4208.5	4203	5.5	SM	0.08	2.73 (6.93)
4203	4196	7	CL	5.4	8.13 (1.53)
4196	4190	6	CL	1.2	9.33 (0.33)
4190	4187.5	2.5	SM	0.03	9.36 (0.3)
4187.5	4175.5	12	CL	0.3	9.66 (0)
4175.5	4167.5	8	SM	0.0	9.66 (0)
4167.5	4165.5	2	CL	0.0	9.66 (0)
4165.5	4150	15.5+	SM	0.0	9.66 (0.0)

6.4.3.6 Estimating the Location of the Neutral Plane and Magnitude of Loads using Fellenius (1989) and Briaud and Tucker (1997) and Comparison to Actual Results

The load vs. depth curves computed by both the Fellenius (1989) and the Briaud and Tucker (1997) methods are shown in Figure 6-18. The ultimate end bearing resistance was estimated to be 214 kips using Equation 5-12 with a pile area of 1.07 ft², a

vertical effective stress of about 3990 psf and a value for N_q of 65. This value for q_p was limited to 200 kips/ft² for this pile also. Using the Fellenius (1989) method with the side resistance values in Table 6-5 and Equation 5-6, the location of the neutral plane was estimated to be near El. 4168 with a maximum load of 332 kips. This corresponds to a dragload of about 202 kips.

The Briaud and Tucker (1997) approach estimated the neutral plane to be near El. 4189.5 with a maximum load of 248 kips. This maximum load corresponds to a dragload of about 118 kips.

A comparison of the load vs. depth curves predicted by the two methods relative to the measured load in the pile is shown in Figure 6-18. Both methods overestimated the load in the pile relative to the measured value of 185 kips; however, the Briaud and Tucker approach only overestimates the measured value by 34% while the Fellenius approach overestimates the total load by 79%. In this case, the overestimate appears to be due to (1) the reduction in dragload due to the structural loads after settlement was complete, and (2) the overestimate of the depth to the neutral plane.

From the plot in Figure 6-18 and also the discussion earlier in this chapter, the measured neutral plane has always been at El. 4185. For this site, the Fellenius method once again estimated the neutral plane to be below the real location. In contrast, the Briaud and Tucker approach estimated it to be above the real neutral plane. As indicated previously, the Fellenius approach assumes that the end-bearing resistance is fully mobilized in computing the neutral plane location which leads to a deeper, more conservative value than the Briaud and Tucker approach. The elevation estimated by the

Briaud and Tucker approach is within five feet of the measured value, thus showing a relatively good approximation to the actual neutral plane for this pile.

To do a final check on the location of the neutral plane at this site, a look at the calculated pile settlement (compression and settlement) and the soil settlement can be taken. The full plot of both the pile and soil settlement is shown in Figure 6-19 while the close up version is shown in Figure 6-20.

From the plot of the settlement curves, it can be seen that the neutral plane is located at about El. 4190. This is within five feet of the location indicated by the load in the gauges, but is almost the same as the location estimated by the Briaud and Tucker approach.

6.4.3.7 Comparison of Undrained Shear Strength and Side Friction

Similarly to what was shown for the Redwood Road site, a plot with the ranges of undrained shear strength is plotted along with the measured unit side resistance in the pile as calculated from the gauge readings. The bounds for this plot are vertical since the undrained shear strength at this site did not vary as much with depth within the same layer. This comparison is shown in Figure 6-21. The measured side resistance in layers from the ground surface down to about El. 4208 and from El. 4187 to the bottom of the pile agrees well with the laboratory test results. However, from El. 4208 to El. 4187 the measured side resistance is consistently higher than the upper bound of the shear strengths found in laboratory testing. It is not immediately apparent why these known why these layers exhibit much higher strengths than it would appear they should based on laboratory testing; however, it should be noted that these layers involve soft clays where reduced strength due to sampling disturbance could be a potential problem.

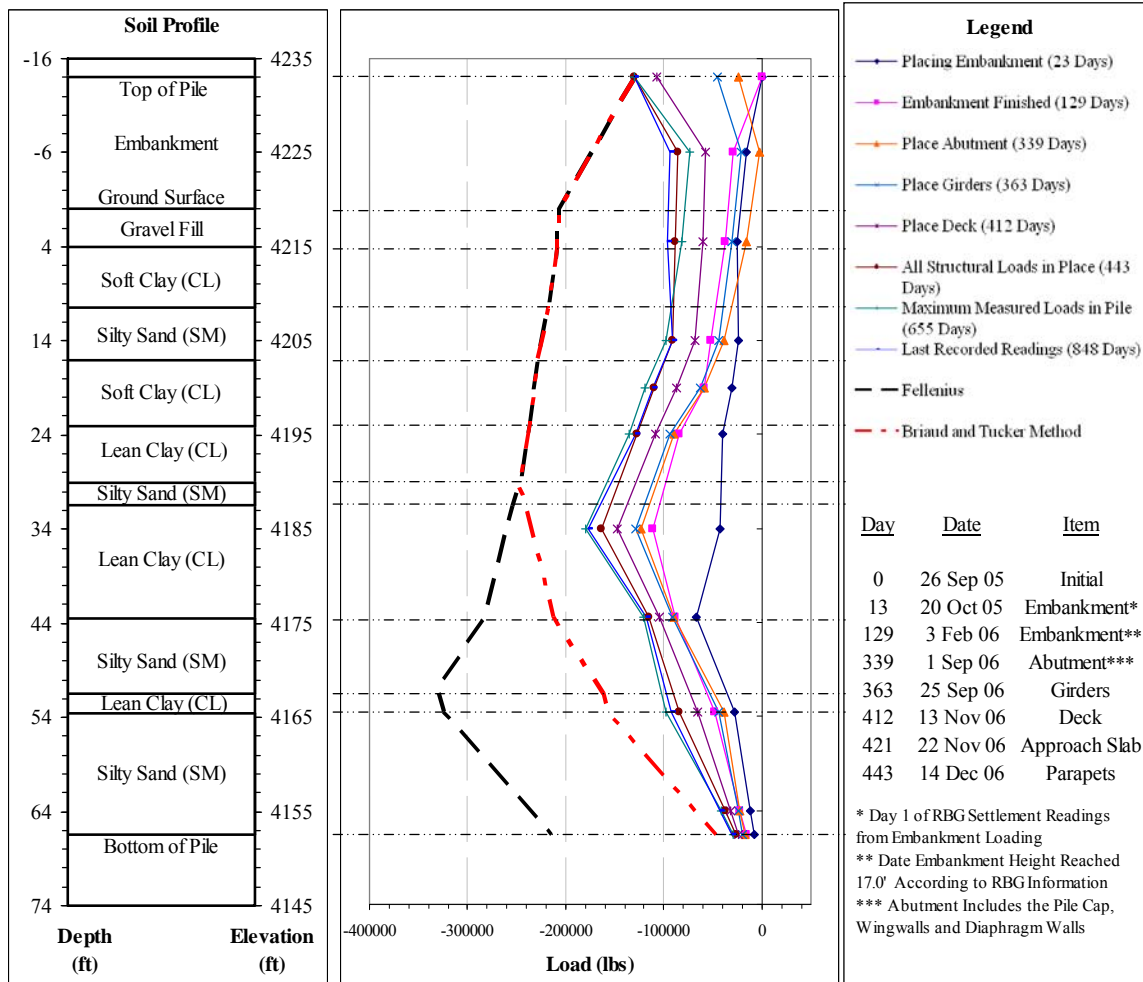


Figure 6-18 Plot of Load versus Depth for the SLCIA Site Showing Comparison of Estimated Load in the Pile from the "Unified Design" Approach by Fellenius (1989) and Braund and Tucker (1997) Method

Finally, the alpha and beta values have been back-calculated for the cohesive and cohesionless soil layers, respectively, and are shown in Table 6-8 relative to the predicted values. Where a range of values is given for beta, it indicates that a strain gauge was located near the middle of the layer, thus the shear stress within portions of the layer were calculated in two different segments. It is clear to see in Table 6-8 that the range of alpha values for the majority of the cohesive layers using alpha values does not include the assumed value of 1.0 used to estimate the side resistance. This is further verification of

the pattern recognized in the plot in Figure 6-21. The back-calculated beta values are generally reasonably close to the values assumed in computing the unit side resistances with the exception of the top layer where the back-calculated value is considerably higher.

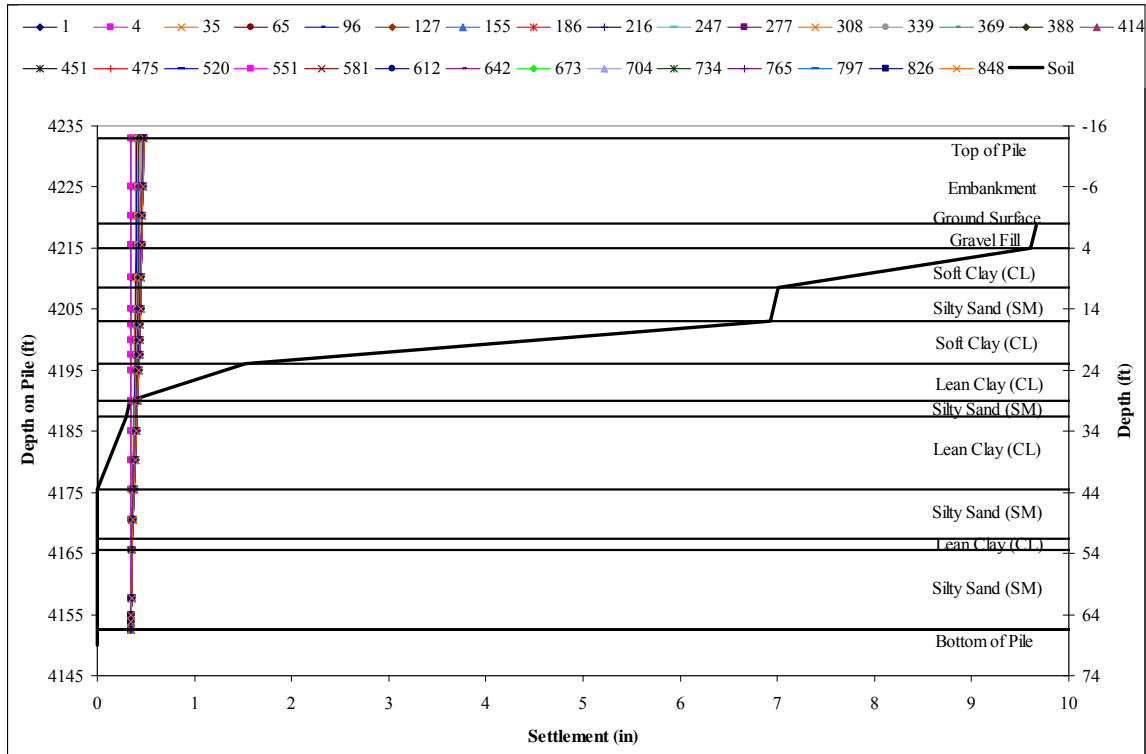


Figure 6-19 Settlement of Soil and Pile for SLCIA Site

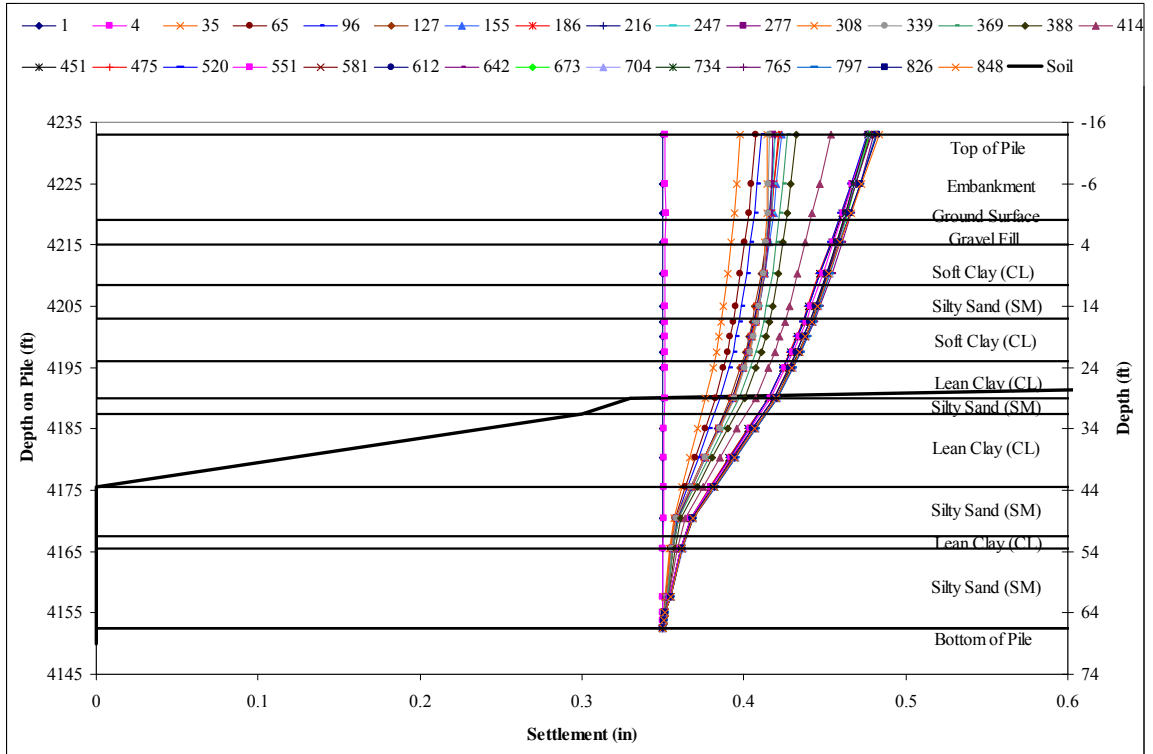


Figure 6-20 Close-up of Soil and Pile Settlement for SLCIA Site

Table 6-8 Summary of Alpha and Beta Values for Soils Profile at SLCIA Site

Measured and Estimated alpha (α) Values				
Elevation Ranges of Soil Layer		USCS Class	Back-calculated α	Estimated α
4215	4208.5	CL	0.65 – 2.2	1.0
4203	4196	CL	1.1 – 7.2	1.0
4196	4190	CL	1.4 – 4.4	1.0
4187.5	4175.5	CL	0.89 – 2.4	1.0
4167.5	4165.5	CL	0.78 – 1.7	1.0
Measured and Estimated beta (β) Values				
Elevation Ranges of Soil Layer		USCS Class	Back-calculated β	Estimated β
4219	4215	GP	2.1	0.61
4208.5	4203	SM	0.66 – 1.4	0.53
4190	4187.5	SM	0.76	0.56
4175.5	4167.5	SM	0.51	0.64
4165.5	4150	SM	0.39	0.64

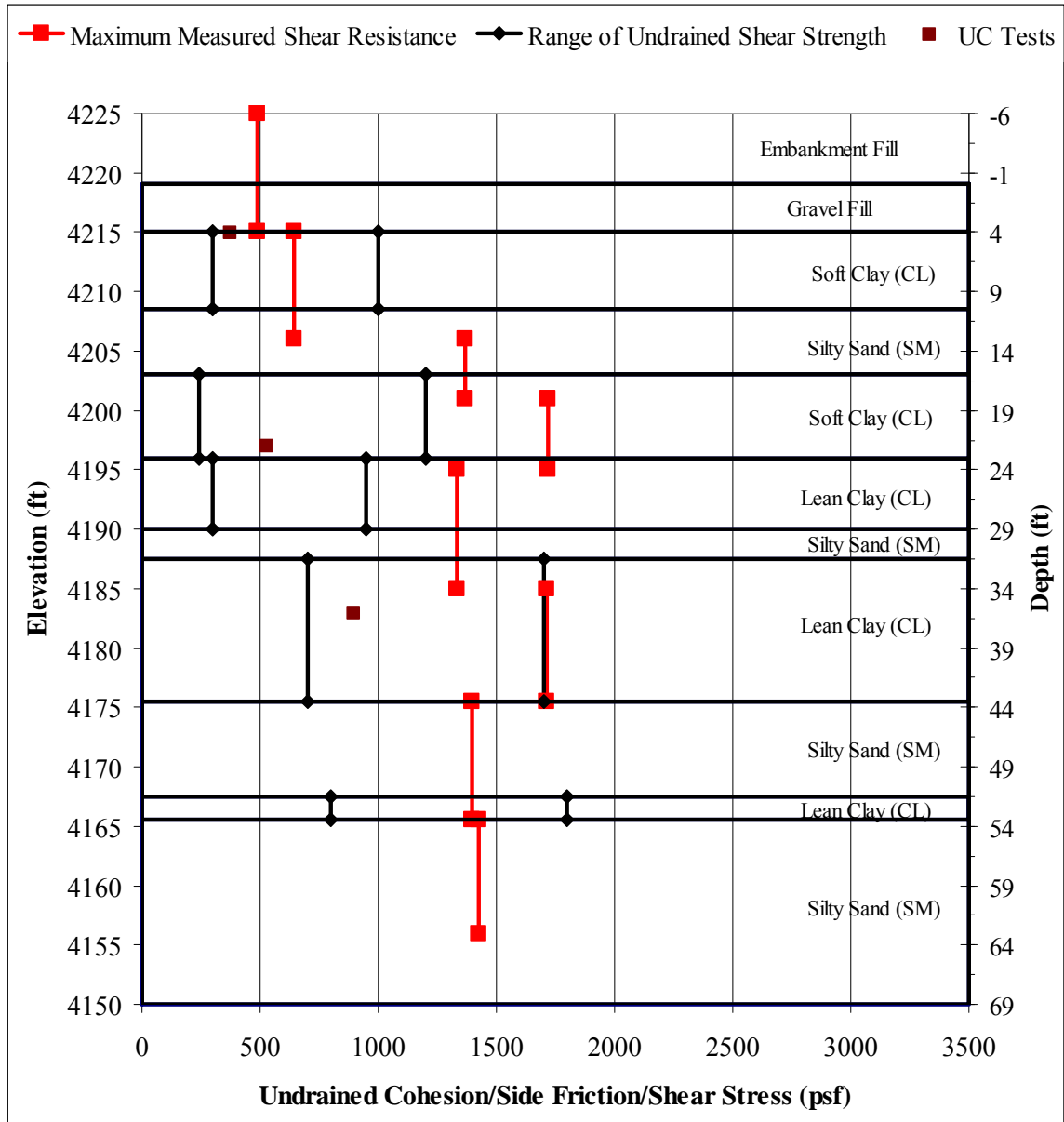


Figure 6-21 Comparison Plot of Measured Undrained Cohesion or Calculated Side Friction and Maximum Measured Shear Stress vs. Depth for SLCIA Site

7.0 Summary, Conclusions and Recommendations

7.1 Summary

To investigate the behavior of piles supporting bridge abutments which are subjected to downdrag produced by approach fills, two test piles were monitored over nearly a three year period. The test piles were instrumented with strain gauges immediately after driving and were used to compute the force in the pile as a function of depth. Strain gauge monitoring was performed while the approach fills were constructed and ground surface settlements exceeded nine inches at each site. Monitoring continued as the overpass structures were constructed and applied dead load to the abutment piles. Finally, monitoring was continued for about 12 to 19 months after the construction of the overpasses to evaluate the effect of soil settlement due to secondary consolidation.

Analysis of the readings from the strain gauges used for this thesis has shown that most gauges provided reasonable and consistent data, but they were not immune to problems. Unfortunately, most of the gauges that seem to have problems are located in the upper 30 feet of the pile. This makes accurate explanations of what is occurring near the surface somewhat more difficult. Nevertheless, the available gauges and understanding provided by previous research made it possible to construct load versus depth profiles.

7.2 Conclusions and Recommendations

Based on the monitoring of soil settlement and the load in the test piles, the following conclusions have been developed:

1. The ultimate pile capacity should not be reduced by the dragload. Field measurements show that as load is applied to the pile head, the negative skin friction decreases from the top down and becomes positive skin friction. At the ultimate state, positive skin friction would be developed along the entire length of the pile. This observation is consistent with recommendations made by Fellenius (1989).
2. When structural dead loads were applied to a test pile prior to the completion of primary consolidation settlement, the maximum load at the neutral plane generally increased by a substantial portion of the increase in structural load nearly immediately or shortly after placement. Continued soil settlement apparently allowed additional dragload to develop, despite the axial compression produced by the dead load.
3. When structural dead loads were applied to the test pile after the completion of primary consolidation settlement, the maximum load at the neutral plane increased by much less than the increase in structural load, and in some cases did not immediately increase but did so over time. This often resulted in a decrease in the dragload force. Soil settlement was apparently insufficient to induce additional dragload equal to that produced by the dead load.
4. Because the consolidation settlement was completed prior to the application of all or some of the dead load for both piles, both the Fellenius (1989) and the Briuad

and Tucker (1997) methods significantly overestimated the dragload and therefore, the maximum load in the pile at the neutral plane relative to the measured load profiles at both test sites. The Fellenius method overestimated the maximum load by 68% to 79% while the Briaud and Tucker method overestimated the maximum load by 34% to 45%. However, these approaches are designed to produce a conservative estimate of the dragload and the maximum pile load, so the error is not necessarily undesirable.

5. The measured neutral plane was better estimated by the Briaud and Tucker (1997) method than by the Fellenius (1989) approach. Because the Fellenius method makes the conservative assumption that the end bearing resistance is fully mobilized, it always predicts a deeper neutral plane than the Briaud and Tucker approach which iterates to better estimate the end bearing pressure.
6. Fifteen months after the bridge construction, soil settlement due to secondary consolidation had only produced relatively minor increases in dragload in the two test piles.
7. The maximum measured shear stress (either positive or negative) was reasonably estimated using the total stress approach (α method) in cohesive soil and the effective stress approach (β method) in the cohesionless soil. However, in some cases involving soft clay the back-calculated α value was significantly higher than 1.0.
8. The maximum loads in the piles produced by dragload were both substantially less than the axial capacity of the piles in both cases and pile head settlement was estimated to be less than 0.43 to 0.48 inches for the Redwood Road and SLCIA

sites, respectively, despite the dragload. Therefore, the dragload posed no significant threat to the integrity of the piles supporting the bridge abutments.

9. For future downdrag measurements, soil settlement should be measured at various depths along the length of the test pile if at all possible.

References

- Acar, Y. B., Avent, R. R. and Taha, M. R. (1994) Down Drag on Friction Piles: A Case History, *ASCE GSP 40*, "Vertical and Horizontal Deformations of Foundations and Embankment", pp. 986-999.
- American Petroleum Institute (1987), "API Recommended Practice for Planning, Designing and Constructing Fixed Offshore Platforms," Report RP-2A.
- Auvinet, G. and Hanell, J. J. (1982), Negative Skin Friction on Piles in Mexico City Clay, *Proceedings of the Tenth International Conference on Soil Mechanics and Foundation Engineering (ICSMFE)*, Stockholm, 2, pp. 599-604.
- Berezantzev, Khristoforov, and Golubkov (1961), "Load Bearing Capacity and Deformation of Piled Foundations, *Proceedings of the Fifth International Conference on Soil Mechanics and Foundation Engineering*, Vol. 2, p. 11.
- Bjerrum, L., Johannessen, I. J., and Edie, O. (1969), Reduction of Negative Skin Friction on Steel Piles to Rock, *Proc. 7th ICSMFE*, Mexico City, 2, pp. 27-33.
- Bozozuk, M. (1970), Field Observations of Negative Skin Friction Loads on Long Piles in Marine Clay, *Proceedings of the Conference on Design and Installation of Pile Foundations and Cellular Structures*, Bethlehem, pp. 273-280.
- Bozozuk, M. (1972). "Downdrag Measurements on a 160 ft. Floating Pipe Test Pile in Marine Clay." *Canadian Geotechnical Journal*, 9(2), pp. 127-136
- Bozozuk, M. (1981), Bearing Capacity of Pile Preloaded by Downdrag, *Proc. 10th ICSMFE*, Stockholm, 2, pp. 631-636.

- Briaud, Jean-Louis and Tucker, Larry (1997), Design and Construction Guidelines for Downdrag on Uncoated and Bitumen-Coated Piles, TRB Report 393.
- Burland, J. B. (1973), Shaft friction of piles in clay, *Ground Engineering*, 6(3), 30-42.
- Buisson, M., Ahu, J., and Habib, P. (1960), Le Frottement Negatif, *Annales de l'Institut Francis du Batiment et des Travaux Publics, Sols et Foundations*, No. 31, 29-46.
- Bush, R. K. and Briaud, J. (1994), Measured Downdrag on Seven Coated and Uncoated Piles in New Orleans, *ASCE GSP 40, "Vertical and Horizontal Deformations of Foundations and Embankment"*, pp. 1011-1027.
- Chellis, R. D. (1951), *Pile Foundations*, 1st Edition, McGraw-Hill Book Company, New York, New York.
- Clemente, F. M., Jr. (1982), Downdrag on Bitumen Coated Piles in a Warm Climate , *Proc. 10th ICSMFE*, Stockholm, 2, pp. 673-676.
- Das, Braja M. (1999), *Principles of Foundation Engineering*, 4th Edition, PWS Publishing at Brooks/Cole Publishing Company, Pacific Grove, California
- Elmasry, M. A. (1963). The Negative Skin Friction of Bearing Piles. Thesis presented to the Swiss Federal Institute of Technology, Zurich.
- Endo, M., Minov, A., Kawasaki, T. and Shibata, T. (1969), Negative Skin Friction Acting on Steel Pipe Pile in Clay, *Proc. 7th ICSMFE*, Mexico City, 2, pp. 85-92.
- Fellenius, B. H. (1972), Downdrag on Piles due to Negative Skin Friction, *Canadian Geotechnical Journal*, 9(4), pp. 323-337.
- Fellenius, B. H. (1989), Unified Design of Piles and Pile Groups, Transportation Research Board, Washington, TRB Record 1169, pp. 75-82.
- Fellenius, B. H. (1998), "Recent Advances in the Design of Piles for Axial Loads, Dragloads, Downdrag, and Settlement." Proceedings of a Seminar by American Society of Civil Engineers, ASCE, and Port of New York and New Jersey, April 1998, 19 p.

Fukuya, T., Todoroki, T., and Kasuga, M. (1982), "Reduction of Negative Skin Friction with Steel Tube NF Pile." *Proceedings of the 7th Southesast Asian Geotechnical Conference.*, Hong Kong, Vol. 1, 333-347.

Geokon, Incorporated, images downloaded from www.geokon.com in June 2006.

Gue, S. S., Liew S. S., and Tan, Y. C. (1999), Instrumentation Results on Negative Downdrag Force of Abutment Piles Underneath the Reinforced Earth Wall Embankment, 5th International. Symposium on Field Measurements in Geomechanics., Singapore.

Indraratna, B., Balasubramaniam, A. S., Phamvan, P., and Wong, Y. K. (1992). "Development of Negative Skin Friction on Driven Piles in Soft Bangkok Clay." *Canadian Geotechnical Journal*, 29(3), 393 – 404.

Johannessen, I. J. and Bjerrum, L. (1965), Measurement of the Compression of a Steel Pile to Rock due to Settlement of the Surrounding Clay, *Proc. 6th ICSMFE*, Montreal, 2, pp. 261-264.

Koerner, R. M. and Mukhopadhyay, C. (1972), Behavior of Negative Skin Friction on Model Piles in Medium-Plasticity Silt, *Highway Research Record No. 405*, 34-44.

Kulhawy, F. H., Trautmann, C. H., Beech, J. F., O'Rourke, T. D., McGuire, W., Wood, W. A., and Capano, C. (1983). "Transmission Line Structure Foundations for Uplift-Compression Loading." *Report. No. EL-2870*, Electric Power Research Institute, Palo Alto, CA.

Leifer, S. A. (1994), The Effect of Live Load on Downdrag Forces, *ASCE GSP 40*, "Vertical and Horizontal Deformations of Foundations and Embankment", pp. 949-961.

Leung, C. F., Liao, K. B., Chow, Y. K., Shen, R. F., and Kog, Y. C. (2004), Behavior of Pile Subject to Negative Skin Friction and Axial Load, *Soils and Foundations*, Vol. 44, No. 6, Dec. 2004, pp. 17-26.

Little, J. A. (1994), Downdrag of Piles: Review and Recent Experimentation, *ASCE GSP 40*, "Vertical and Horizontal Deformations of Foundations and Embankment", pp. 1805-1826.

- Locher, H. G. (1965), Combined Cast-In-Place and Precast Piles for the Reduction of Negative Friction Caused by Embankment Fill, *Proc. 6th ICSMFE*, Montreal, 2, pp. 290-294
- Mapquest (2008), image downloaded from www.mapquest.com on 19 July 2008.
- Matyas, E. L. and Santamarina, J. C. (1994), Negative Skin Friction and the Neutral Plane, *Canadian Geotechnical Journal*, 31, pp. 591-597.
- Mohan, D., Bhandari, R. K., Sharma, D. and Soneja, M. R. (1981), Negative Drag on and Instrumented Pile – A Field Study, *Proc. 10th ICSMFE*, Stockholm, 2, pp. 797-790.
- Meyerhof, G. G. (1976), Bearing Capacity and settlement of piled foundations, *Proceedings of the American Society of Civil Engineers*, GT3, pp. 197 – 228
- NAVFAC (1982). “Foundations and Earth Structures.” *Design Manual 7.2*, U.S. Department of the Navy, Alexandria, VA.
- Poulos, H. G., and Davis, E. H. (1980). *Pile Foundation Analysis and Design*, Wiley, New York.
- Poulos, H. G., and Mattes, N. S. (1969). “The Analysis of Downdrag in End-Bearing Piles.” *Proc. 7th ICSMFE*, Mexico, 2, pp. 203-208.
- RB&G Engineering, Inc. (2004), “North Bar Flyover Bridge & Approach Fills, Salt Lake City International Airport, Salt Lake City, Utah”, Geotechnical Investigation Report Submitted to HNTB Architects Engineers Planners.
- Terzahi, K. and Peck, R. B. (1948), *Soil Mechanics in Engineering Practice*, 1st Edition, John Wiley and Sons, New York, New York.
- Tomlinson, M. J. (1957), The Adhesion of Piles Driven in Clay Soils, *Proc. 4th ICSMFE*, London, 2, pp. 66-71.
- Tomlinson, M. J. (1986), *Foundation Design and Construction*, 5th Edition, Pitman Books Ltd., London, England.

United States Geological Survey, USGS, (2003), images downloaded from
www.terraser-USA.com on 12 June 2006.

Walker, L. K. and Darvall, P. L. P. (1973), Dragdown on Coated and Uncoated Piles,
Proc. 7th ICSMFE, Moscow, 2.1, pp. 257-262.

Wong, K. S. and Teh, C. I (1995), Negative Skin Friction on Piles in Layered Soil
Deposits, *Journal of Geotechnical Engineering*, Vol. 121, No. 6, June 1995, pp.
457-465.

Zeevaert, L. (1959). Reduction of Point Bearing Capacity of Piles because of the
Negative Friction. *First Pan-American Conference on Soil Mechanics and
Foundation Engineering*, Mexico, Vol. 3, pp. 1145-1152.

Zeevaert, L. (1973), *Foundation Engineering for Difficult Subsoil Conditions*, Van
Nostrand Reinhold, New York, New York.

Appendix

PROJECT UDOT, SR201, Redwood Road
STA 256+20, LT 150.

LOG OF TEST BORING NO. B-1

JOB NO. 4-817-004821 DATE 06-09-04

Depth in Feet	Continuous Penetration Resistance	Graphical Log	Sample Type	Blows/foot 140 lb. 30" free-fall drop hammer	Dry Density lbs. per cubic foot	Moisture Content Percent of Dry Weight	Unified Soil Classifi- cation	REMARKS	VISUAL CLASSIFICATION
0							GM FILL	dry	SILTY FINE TO COARSE SANDY FINE AND COARSE GRAVEL; no topsoil; brown; FILL
			D 17 5-6-11				CL	slightly moist stiff	SILTY CLAY with trace fine sand; brown to light brown
5			D 12 3-5-7					moist	grades with occasional silty fine sand seams; brown to gray-brown
10			D 9 3-4-5		91	31.6		medium stiff	grades with numerous silty fine sand and fine sandy silt seams; brown-gray
15			D 15 2-3-12				SM	saturated "loose"	SILTY FINE SAND; gray
20			D 10 2-3-7				SP	saturated loose	FINE TO COARSE SAND with trace silt; gray
							ML	saturated loose	FINE SANDY SILT; gray
25							CL/ ML/ SM	saturated medium dense/ stiff	ALTERNATING LAYERS UP TO 3" THICK OF SILTY CLAY, FINE SANDY SILT, AND SILTY FINE TO MEDIUM SAND; gray

DEPTH	HOUR	DATE
8.3	16:00	07-13-04

- SAMPLE TYPE
- A - Auger cuttings
 - S - 2" O.D. 1.38" I.D. tube sample.
 - U - 3" O.D. 2.42" I.D. tube sample.
 - T - 3" O.D. thin-walled Shelby tube.
 - D - 3 1/4" O.D. 2.42" I.D. tube sample.
 - C - California Split Spoon Sample

FIGURE 3A



Figure A-1 Borelog of Boring B-1 Performed by AMEC for Redwood Road Site

PROJECT UDOT, SR201, Redwood Road
 STA 256+20, LT 150.

Page 2 of 4
LOG OF TEST BORING NO. B-1

JOB NO. 4-817-004821 DATE 06-09-04

Depth in Feet	Continuous Penetration Resistance	Graphical Log	Sample Type	Sample Type Blows/ft 140 lb. 30" free-fall drop hammer	Dry Density lbs. per cubic foot	Moisture Content percent of dry weight	Unified Soil Classifi- cation	RIG TYPE <u>Marl M10</u>	
								REMARKS	VISUAL CLASSIFICATION
25			D	33 11-12-21					
30			D	12 2-4-8					
35							CL/ CH	saturated medium stiff	SILTY CLAY with trace fine sand and occasional silty fine sand seams; gray and dark gray
35			D	10 4-4-6	86	33.5			
40							ML/ SM	saturated loose	ALTERNATING LAYERS UP TO 2" THICK OF FINE SANDY SILT AND SILTY FINE TO MEDIUM SAND; gray-brown
45			D	23 8-9-14					grades with numerous silty and fine sandy clay layers to 1/2" thick
50									

GROUNDWATER		
DEPTH	HOUR	DATE
8.3	16:00	07-13-04

- SAMPLE TYPE
- A - Auger cuttings
 - S - 2" O.D. 1.38" I.D. tube sample.
 - U - 3" O.D. 2.42" I.D. tube sample.
 - T - 3" O.D. thin-walled Shelby tube.
 - D - 3 1/4" O.D. 2.42" I.D. tube sample.
 - C - California Split Spoon Sample

FIGURE 3A
 (con't)


Figure A-1 Borelog of Boring B-1 Performed by AMEC for Redwood Road Site (continued)

PROJECT UDOT, SR201, Redwood Road
STA 256+20, LT 150.

LOG OF TEST BORING NO. B-1

JOB NO. 4-817-004821 DATE 06-09-04

Depth In Feet	Continuous Penetration Resistance	Graphical Log	Sample	Sample Type	Blows/ft. 140 lb. free-fall drop hammer	Dry Density lbs. per cubic foot	Moisture Content Percent of Dry Weight	Unified Soil Classifi- cation	REMARKS	VISUAL CLASSIFICATION
50			D 64		10-20-38				medium dense	grades without clay layers
55			D 39		5-13-26			SM/ SP	saturated medium dense	FINE TO COARSE SAND with some silt with some occasional silty fine sand layers to 1/2"; gray
60			D 51		10-17-34					grades without fine sandy silt layers
65			D 99		18-30-19				very dense	
70			D 126		29-46-88					grades to fine sand with some silt with numerous silty fine sand layers and occasional fine sandy silt and clayey silt seams; gray
75										

GROUNDWATER		
DEPTH	HOUR	DATE
8.3	16:00	07-13-04

- SAMPLE TYPE
- A - Auger cuttings
 - S - 2" O.D. 1.38" I.D. tube sample.
 - U - 3" O.D. 2.42" I.D. tube sample.
 - T - 3" O.D. thin-walled Shelby tube.
 - D - 3 1/4" O.D. 2.42" I.D. tube sample.
 - C - California Split Spoon Sample


FIGURE 3A
 (con't)


Figure A-1 Borelog of Boring B-1 Performed by AMEC for Redwood Road Site (continued)

LOG OF TEST BORING NO. B-1

JOB NO. 4-817-004821 DATE 06-09-04

Depth in Feet	Continuous Penetration Resistance	Graphical Log	Sample Type	Blows/foot 140 lb. 30" free-fall drop hammer	Dry Density lbs. per cubic foot	Moisture Content Percent of Dry Weight	Unified Soil Classifi- cation	REMARKS	VISUAL CLASSIFICATION
75			D 113 10-33-80						grades to fine to coarse sand with some silt; gray
80									Stopped drilling at 75.0'. Stopped sampling at 76.5'. Installed 1-1/4" diameter slotted PVC pipe to 15.0'.
85									
90									
95									
100									The discussion in the text under the section titled, SUBSURFACE CONDITIONS, is necessary to a proper understanding of the nature of the subsurface materials.

GROUNDWATER		
DEPTH	HOUR	DATE
8.3	16:00	07-13-04

- SAMPLE TYPE
- A - Auger cuttings
 - S - 2" O.D. 1.38" I.D. tube sample.
 - U - 3" O.D. 2.42" I.D. tube sample.
 - T - 3" O.D. thin-walled Shelby tube.
 - D - 3 1/4" O.D. 2.42" I.D. tube sample.
 - C - California Split Spoon Sample



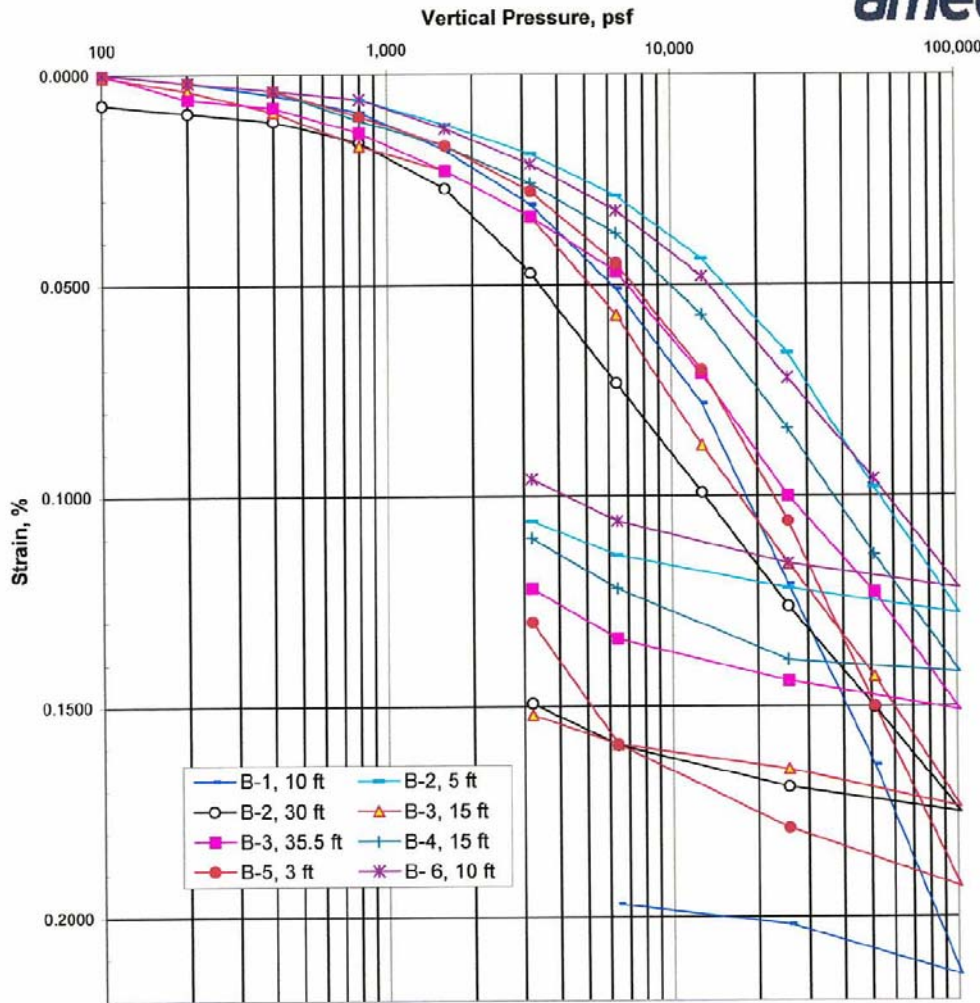
Figure A-1 Borelog of Boring B-1 Performed by AMEC for Redwood Road Site (continued)

DRILL HOLE LOG		PROJECT: SR-201 / REDWOOD ROAD		PROJECT NO.: 200301.068										
BORING NO. 04-1		CLIENT: UTAH DEPT. OF TRANSPORTATION		DATE: 1/14/04										
Sheet 1 of 2		LOCATION: SEE SITE PLAN: N 9198, E 43073		ELEVATION: 4236.8'										
		DRILLER: D. SAMPSON, N. BAILEY, K. FALKENTHAL		LOGGED BY: R.J., V.N.B.										
		EQUIP./DRILL METHOD: CME-55 / N.W. CASING		WEL. GROUND SURFACE										
		DEPTH TO WATER - INITIAL: 5.8' AFTER 24 HOURS: 5.7'												
Elev. (Feet)	Depth (Feet)	Lithology	Type	Blows Per 6"	USCS (AASHTO)	Material Description	Moisture Content, %	Liquid Limit, %	Plasticity Index, %	Gravel, %	Sand, %	Silt, %	Clay, %	Last 1/2" / Last 0.005mm
4235						SANDY CLAY TO CLAYEY SAND								
	5			13.3	CL	dk. brown, moist								
				0.59	CL	lt. brown, moist, stiff								
						LEAN CLAY								
				12.5	CL	lt. brown, very moist, stiff, w/pinholes								
				0.87	ML (A-4(4))	lt. gray, very moist, rusty-orange spots throughout sample	18.0			NP	0	46	54	
						SANDY SILT								
	10			2.3,6	ML (A-4(4))	lt. brown, med. fine to coarse	23.4			NP	0	42	58	
				1.3,3	SM	lt. brown, wet								
				0.61	CL	lt. brown, wet, stiff								
						SANDY LEAN CLAY								
				1.2,2	CL	lt. brown, wet, stiff, some rusty streaks								
				0.67	CL	lt. brown, wet, stiff								
						LEAN CLAY W/CLAYEY SAND LENSES								
				0.2,2	CL	lt. brown, wet								
				0.61	CL	lt. brown, wet								
						LEAN CLAY W/CLAYEY SAND LAYERS								
				1.1,1	CL	gray, wet, very soft								
				0.10	CL	gray, wet, very soft								
						LEAN TO FAT CLAY W/CLAYEY SAND LENSES								
				1.1,1	CL/CH	gray, wet, very soft								
				0.09	CL/CH	gray, wet, very soft								
						LEAN TO FAT CLAY W/CLAYEY SAND LENSES								
				1.1,1	SM	gray, wet, dense								
				0.12	SM	gray, wet, dense								
						SILTY SAND								
				7.0,4	SM	gray, wet								
						VERY FINE SANDY CLAYEY SILT W/THIN CLAY LENSES								
				1.3,4	CL-ML (A-4(B))	gray to black, wet, very soft	30.5	25		5	0	11	91	
						LEAN TO FAT CLAY								
				1.3,10	CL/CH SM (A-2-4)	gray, wet	20.4			NP	0	76	24	
				0.15	SM (A-2-4)	gray, wet								
						SILTY SAND								
				3.2,3	SM (A-2-4)	gray, wet	26.4			NP	0	73	27	
						SILTY SAND								
				3.8,10	SM (A-2-4)	gray, wet	22.1			NP	0	67	33	
						SILTY SAND								
				3.5,4	SM (A-4(2))	gray, wet, w/1 clay layer 0.25" thick	25.7			NP	0	56	44	12
						ALTERNATING LAYERS OF LEAN & FAT CLAY 1" TO 2" THICK								
				2.3,1	CL/CH	gray to dk. gray, wet, soft								
				0.22	CL/CH	gray to dk. gray, wet, soft								
						1.5" SILTY SAND								
				0.8", 2/4", 3	CL	gray-brown, wet, soft to stiff								
				2.26,0.64	CL	gray-brown, wet, very stiff								
						LEAN CLAY W/SILTY SAND LENSES								
				3.4,5	CL	gray to dk. gray, wet, soft to stiff, slight organic odor								
				1.00"	CL	gray to dk. gray, wet, soft to stiff, slight organic odor								
						SANDY CLAY								
				2.2,4	CL	gray to dk. gray, wet, soft to stiff, slight organic odor								
				0.10	CL	gray to dk. gray, wet, firm								
						SANDY CLAY								
				0.3,3	CL	gray to dk. gray, wet, firm								
				0.76	CL	gray-brown, wet, firm								
				0.82	CL	gray-brown, wet, firm								
						SANDY CLAY								
				2.3,8	CL (A-4(B))	gray-brown, wet, firm	27.9	32		9	0	6	94	
				0.58	SM (A-2-4)	wet	20.7			NP	0	64	36	
						SILTY SAND								
				6.8,9	SM/ML	gray-brown, wet								
						ALTERNATING LAYERS OF SILTY SAND & SANDY SILT 0.5" TO 1" THICK								
				2.8,20	SM/ML	gray-brown, wet								
						SILTY SAND W/SILT LAYERS TO 0.5" THICK								
				4.10,18	SM	gray-brown, wet								
						flowing sand at 43.5'								
				3.8,21	SM	gray-brown, wet								
						SILTY SAND W/SILT LAYERS TO 0.5" THICK								
				10.15,12	SM	gray-brown, wet								
						SILT W/SAND								
				4.4,5	ML (A-4(B))	gray-brown, wet	25.3			NP	0	20	80	
				0.25	ML (A-4(B))	gray-brown, wet								
						2" SANDY CLAY								
				4.6,9	ML (A-4(4))	gray-brown, wet	27.7			NP	0	49	51	
				0.58	ML (A-4(4))	gray-brown, wet								
						SANDY SILT								
				5.19,24	CL-ML	SANDY SILTY CLAY								
				0.75	CL-ML	SANDY SILTY CLAY								
						SILTY SAND								
				14.24,31	SM	gray-brown, wet								
						SILTY SAND								

Figure A-2 Borelog of Boring B-04-1 Performed by RB&G for Redwood Road Site

DRILL HOLE LOG		PROJECT: SR-201 / REDWOOD ROAD			PROJECT NO.: 200301.068																
		CLIENT: UTAH DEPT. OF TRANSPORTATION			DATE: 1/13/04																
		LOCATION: SEE SITE PLAN: N 9032, E 43052			ELEVATION: 4237.8'																
BORING NO. 04-2		DRILLER: D. SAMPSON, N. BAILEY, K. FALKENTHAL			LOGGED BY: M.H., V.N.B.																
Sheet 1 of 2		EQUIP./DRILL METHOD: CME-55 / N.W. CASING			DEPTH TO WATER - INITIAL: 8.9' AFTER 24 HOURS: 8.3'																
Elev. (Feet)	Depth (Feet)	Lithology	SAMPLE		USCS (AASHTO)	Material Description	Liquid Limit (%)	Plasticity Index (%)	Atterberg Limits	Gradation	Liquid Limit (%)	Plasticity Index (%)									
			Blows Per Foot	USCS (AASHTO)																	
4235	5		26	12	6,6,6	CL-ML	lt. brown, moist														
4230	10		10	17	2,2,3	CL	lt. brown, moist to wet														
	15		14	18	3,3,5	CL-ML	lt. brown, wet														
	20		7	18	2,2,2	CL	lt. brown, wet														
	25		7	18	1,2,2	CL	lt. brown														
	30		5	18	1,1,2	CL	lt. brown														
	35		5	18	1,2,1	ML (A-4(B))	lt. brown				26.4	27	4	0	19	81					
	40		8	11	3,2,3	CL-ML SM	lt. brown, brown, wet														
	45		39	12	8,12,15	SP-SM	dk. gray, wet, fine to coarse														
	50		10	9	3,4,3	CL-ML?	dk. gray, wet, fine to coarse sand looks fluffy like cuttings														
	55		51	16	8,20,17	SM	dk. gray														
	60		11	3	7,4,4	SP-SM (A-2-4)	dk. gray, wet				20.4		NP	11	75	14					
	65		12	5	7,6,3	CL (A-4(B))	dk. gray				30.0	30	B	0	11	89	10				
	70		12	17	4,6,3	SP-SM CL/CH	dk. gray														
	75		18	13	0,5,9	ML (A-4(4))	gray, wet, fine to med.				21.7		NP	0	44	56					
	80		10	7	3,5,3	SM (A-2-4)	gray, wet, some coarse				20.9		NP	0	77	23					
	85		5	11	0,04	UH SM (A-2-4)	black, wet				21.2		NP	0	61	39					
	90		1	18	0/12,1	CL	lt. to dk. gray, wet, stratified														
	95		6	18	0,2,3	CL	lt. to dk. gray														
	100		8	18	0,3,4	CL/CH	black, wet														
	105		8	18	0,3,5	CL	gray, wet														
	110		6	18	0,08	CL	gray, wet														
	115		6	18	2,2,3	CL	gray, wet														
	120		8	18	0,3,4	CL	4" soft, lt. to dk. gray														
	125		11	15	2,3,7	CL	dk. gray, wet														
	130		24	17	6,10,12	SM	gray-brown, wet														
	135		37	16	5,13,22	SM	gray-brown, wet														
	140		21	10	4,7,15	SP-SM (A-3)	gray-brown, wet, fine to med., some white coarse sand				25.4		NP	0	95	5					
	145		17	12	7,7,9	CL-ML	gray-brown, wet														
	150		10	16	0,8,3	CL-ML	gray-brown, wet														
	155		17	14	2,6,11	ML/SM ML (A-4(B))	gray-brown, wet				25.7		NP	0	23	77					
	160		22	13	6,7,15	ML (A-4(5))	gray-brown, wet				25.1		NP	1	38	61					
	165		38	15	7,13,25	SM/ML	gray-brown, wet														
	170		41	12	8,18,24	SM	gray-brown, wet														

Figure A-3 Borelog of Boring B-04-2 Performed by RB&G for Redwood Road Site




	B-1, 10 ft		B-2, 5 ft		B-2, 30 ft		B-3, 15 ft	
	Initial	Final	Initial	Final	Initial	Final	Initial	Final
Dry Density, pcf	91.1	111.3	89.0	110.5	72.5	103.5	70.2	104.4
Water Content, %	25.9%	22.8%	24.5%	25.3%	41.5%	27.2%	45.2%	29.7%
Total Density, pcf	114.7	136.7	110.8	138.5	102.6	131.7	101.9	135.4
USCS Class	CL		CL		CL		CL	

	B-3, 35.5 ft		B-4, 15 ft		B-5, 3 ft		B-6, 10 ft	
	Initial	Final	Initial	Final	Initial	Final	Initial	Final
Dry Density, pcf	86.1	114.5	86.7	113.0	91.6	107.7	88.7	111.7
Water Content, %	33.2%	23.7%	31.6%	24.7%	27.1%	22.1%	29.1%	24.0%
Total Density, pcf	114.7	141.6	114.1	140.9	116.4	131.5	114.5	138.5
USCS Class	CL		CL		CL/CH		CL	

Figure 8
Consolidation Test Results

Figure A-4 Consolidation Test Results for Samples from AMEC for Redwood Road Site

DRILL HOLE LOG		PROJECT: S.L.C.I.A. - N BAR FLYOVER BRIDGE & APPROACH FILLS		PROJECT NO.: 9820-27										
BORING NO. 03-NB-3		CLIENT: H.N.T.B.		DATE: 12/9/03 TO 12/11/03										
Sheet: 1 of 2		LOCATION: SEE SITE PLAN: N 1766, W -1821		ELEVATION: 4221.4'										
		DRILLER: D. SAMPSON, K. WARD		LOGGED BY: M.H., R.J.										
		EQUIP./DRILL METHOD: CME-55 / N.W. CASING												
		DEPTH TO WATER - INITIAL: ~6.0'		AFTER 24 HOURS: 7.2'										
Elev. (Feet)	Depth (Feet)	Lithology	Type	Rec. (in.)	SAMPLE Blows Per 6" & Torvane (tsf)	USCS	Material Description	Dry Density pcf	Moisture Content, %	Liquid Limit, %	Plasticity Index, %	Alter.	Gradation	Other Tests
4220					13 8,11,13	GM/GP-GM	4" ASPHALT PAVEMENT red-brown, moist SANDY GRAVEL W/SILT							
	5				14 Pushed 0.70	CL-2	lt. brown to green-brown, slightly moist, firm LEAN CLAY	105.6	18.6	45	23			CT UC
4215					18 Pushed 0.25	CL-2	lt. brownish-green, very wet, soft to firm	91.8	32.0	49	27			UC
	10				18 0/9", 1/3", 1 0.25	CL	lt. green, wet, w/rusty silty sand lenses							
4210					24 0/3", 1/9", 1, 2 0.15	CL	pinkish-brown, soft LEAN CLAY W/SILTY SAND LENSES LESS THAN 0.03" THICK							
	15				18 Pushed 0/3", 1/9", 2 0.18	CL-2 SM CL SM	brown-green pinkish-brown brown-green SILTY SAND LEAN CLAY SILTY SAND	73.2	51.2	40	18			CT UC
4205					13 0/4", 3/2", 4	SC/SM	dk. gray, loose, wet CLAYEY TO SILTY FINE TO MED. SAND slight to low plasticity							
	20				6 Pushed 0/18" 0.12	SM CH	very dk. gray black & gray FAT CLAY slight organic odor							
4200					18 Pushed 0.45	CL	black, very wet, soft LEAN CLAY	84.0	43.3	47	22			UC
	25				24 3,4,4,8 0.30	CL/ML	gray, wet, firm SILTY LEAN CLAY/CLAYEY SILT							
4195					15 Pushed 0.22	ML SC/SM	gray gray, wet, loose, 1.5" clay layer LEAN CLAY/SILTY FINE SAND							
4190					18 2,2,4 0.34	SC/SM		27.5					0 39 61	
	35				18 2,2,3 0.44	CL/ML	gray, wet, firm SILTY LEAN CLAY W/SAND LENSES LESS THAN 0.25" THICK & 1" TO 4" APART							
4185					17 Pushed 0.74	CL-2	SAND gray, moist, firm to stiff LEAN CLAY	101.3	26.1	43	19			UC
4180					6 10,19,19	SM	gray SILTY FINE TO MED. SAND trace coarse sand							
4175														
	50													



**RB&G
ENGINEERING
INC.**
Provo, Utah


LEGEND

2,3,2 ← Blow Count per 6"
0.45 ← Torvane (tsf)
Disturbed Sample
Undisturbed Sample
Groundwater Elevation

UC - Unconfined Compression Test
CT - Consolidation Test
SG - Specific Gravity Test

Figure A-5 Borelog of Boring 03-NB-3 Performed by RB&G for SLCIA Site

DRILL HOLE LOG		PROJECT: S.L.C.I.A. - N BAR FLYOVER BRIDGE & APPROACH FILLS				PROJECT NO.: 9820-27								
BORING NO. 03-NB-3		CLIENT: H.N.T.B.				DATE: 12/9/03 TO 12/11/03								
Sheet: 2 of 2		LOCATION: SEE SITE PLAN: N 1766, W -1821				ELEVATION: 4221.4'								
		DRILLER: D. SAMPSON, K. WARD				LOGGED BY: M.H., R.J.								
		EQUIP./DRILL METHOD: CME-55 / N.W. CASING												
		DEPTH TO WATER - INITIAL: ~6.0'				AFTER 24 HOURS: 7.2'								
Elev. (Feet)	Depth (Feet)	Lithology	Type	SAMPLE		USCS	Material Description	Dry Density, pcf	Moisture Content, %	Atter.		Gradation		Other Tests
				Blows Per 6" & Torvane (tsf)						Liquid Limit, %	Plasticity Index, %	Gravel, %	Sand, %	
4170				16	8,18,24	SM	gray, wet, dense SILTY SAND mica flakes, some thin clay lenses							
	55			13	Pushed	SM	LEAN CLAY W/CLAYEY SAND LENSES							
4165				16	9,20,28	SC/SM,SM	gray SILTY SAND							
	60			8	10,17,14	SM	gray-brown, wet, dense, trace organics CLAYEY/SILTY FINE SAND							
4160				8	10,17,14	SM	gray-brown, dense SILTY FINE TO MED. SAND							
	65			14	Pushed	CL SM	CLAY							
4155				18	3,5,8	SM	gray-brown, wet, med. dense SILTY FINE SAND	25.6		0	78	22		
	70			14	3,16,26	SM	brown-gray, dense VERY SILTY FINE SAND & SILTY FINE TO MED. SAND							
4145				13	15,18,24	SP-SM,SM	dk. gray & white, dense, bone fragment							
	80			18	4,12,33	SP-SM,SM	dk. gray & white, dense INTERBEDDED SAND W/SILT & SILTY SAND trace fine gravel, layers 1" to 3" thick							
4140				13	11,18,23	SP-SM,SM	dk. gray & white, dense	22.0		0	88	12		
4135				9	11,23,26	SP-SM	dk. gray & white, dense FINE TO COARSE SAND W/SILT							
4130				18	4,8,12	CL	gray-brown, moist, stiff to very stiff LEAN CLAY w/a few rootlets, med. plasticity, layers							
4125				18	Pushed	CL SM SM CL	brown VERY SILTY VERY FINE SAND LEAN CLAY							
4120				-	5,4,6 0.90+									



RB&G ENGINEERING INC.
Provo, Utah


LEGEND

- 2,3,2 ← Blow Count per 6"
- 0.45 ← Torvane (tsf)
- Disturbed Sample
- Undisturbed Sample
- Groundwater Elevation

UC - Unconfined Compression Test
CT - Consolidation Test
SG - Specific Gravity Test

Figure A-5 Borelog of Boring 03-NB-3 Performed by RB&G for SLCIA Site (continued)

DRILL HOLE LOG		PROJECT: S.L.C.I.A. - N BAR FLYOVER BRIDGE & APPROACH FILLS		PROJECT NO.: 9820-27										
BORING NO. 03-NB-4		CLIENT: H.N.T.B.		DATE: 12/31/03										
Sheet: 1 of 3		LOCATION: SEE SITE PLAN: N 1690, W -1912		ELEVATION: 4220.7'										
		DRILLER: D. SAMPSON, N. BAILEY		LOGGED BY: R.J., V.N.B.										
		EQUIP./DRILL METHOD: CME-55 / N.W. CASING												
		DEPTH TO WATER - INITIAL: $\frac{1}{2}$ N.M.		AFTER 24 HOURS: $\frac{1}{2}$ NOT MEASURED										
Elev. (Feet)	Depth (Feet)	Lithology	Type Rec. (in.)	Blows Per 6" & Torvane (tsf)	USCS	Material Description	Dry Density, pcf	Mixture Content, %	Liquid Limit, %	Plasticity Index, %	Gravel, %	Sand, %	Silt/Clay, %	Other Tests
4220				8,10,12	ML/GM	3" ASPHALT PAVEMENT red-brown, moist, med. dense GRAVELLY SILT TO SILTY GRAVEL W/SAND (fill)								
				4,4,4 0.50	CL	gray-green, moist, stiff SANDY LEAN CLAY								
4215	5			Pushed 0.45	CL-2	lt. gray, wet, firm LEAN CLAY W/ROOTS & SAND LENSES	93.0	33.9	44	21				UC
4210	10			1/12", 1 0.42	CL	lt. gray, wet, soft to firm, some root layers LEAN CLAY W/SILTY SAND LENSES & LAYERS 0.5" TO 2" THICK								
				Pushed 0.50	SM	gray-green, wet, loose SILTY SAND								
4205	15			4,4,5 0.20	CL	gray, wet lt. gray-brown LEAN CLAY								
				2,8,6 0.20	CL/CH	gray dk. gray, wet, firm SILTY SAND TO SANDY SILT LEAN TO FAT CLAY								
4200	20			Pushed 0.46	CH	gray, wet, firm FAT CLAY	63.1	69.7	69	39				UC
4195	25			0.60 1,1,2 0.49	CL	gray-green, moist, firm LEAN CLAY W/SILTY SAND LENSES								
4190	30			Pushed 2,4,4 0.40	SM SM CL	gray, wet gray, wet, loose gray, wet, firm SILTY SAND LEAN CLAY W/SILTY SAND LAYERS		23.9			0	71	29	
4185	35			2,3,5 0.38	CL	gray-brown, moist, firm ALTERNATING LAYERS OF SILTY SAND & LEAN CLAY 1" TO 2" THICK								
4180	40			Pushed 1.00+	SM CL	gray gray, wet, stiff SILTY SAND LEAN CLAY								
4175	45			11,16,10	ML	gray, wet, very stiff SANDY SILT		27.4	NP		2	46	52	
	50			11,23,28	SM	gray, wet, very dense SILTY SAND								



RB&G ENGINEERING INC.
Provo, Utah

LEGEND

- 2,3,2 ← Blow Count per 6"
- 0.45 ← Torvane (tsf)
- Disturbed Sample
- Undisturbed Sample
- Groundwater Elevation

UC = Unconfined Compression Test
CT = Consolidation Test
SG = Specific Gravity Test

Figure A-6 Borelog of Boring 03-NB-4 Performed by RB&G for SLCIA Site

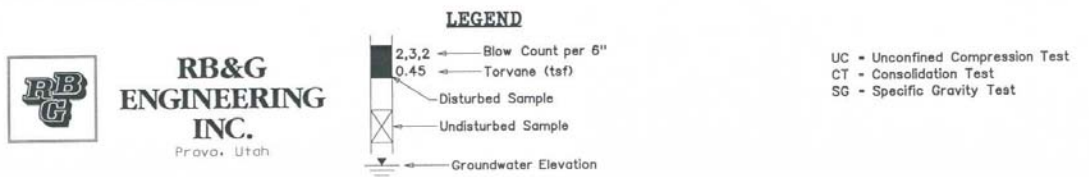
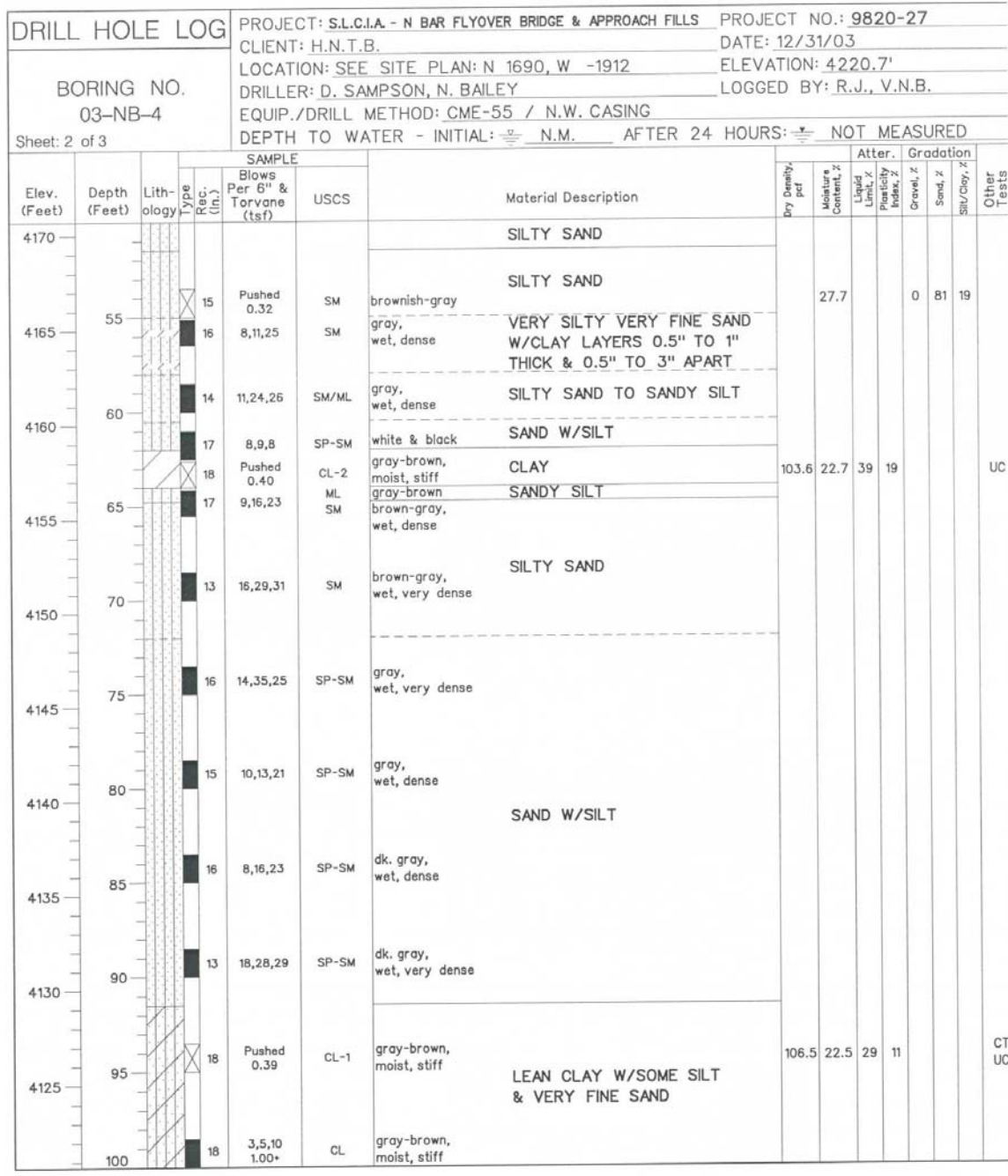



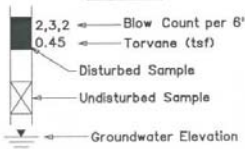
Figure A-6 Borelog of Boring 03-NB-4 Performed by RB&G for SLCIA Site (continued)

DRILL HOLE LOG		PROJECT: S.L.C.I.A. - N BAR FLYOVER BRIDGE & APPROACH FILLS				PROJECT NO.: 9820-27							
BORING NO. 03-NB-4		CLIENT: H.N.T.B.				DATE: 12/31/03							
Sheet: 3 of 3		LOCATION: SEE SITE PLAN: N 1690, W -1912				ELEVATION: 4220.7'							
		DRILLER: D. SAMPSON, N. BAILEY				LOGGED BY: R.J., V.N.B.							
		EQUIP./DRILL METHOD: CME-55 / N.W. CASING											
		DEPTH TO WATER - INITIAL: $\frac{10}{16}$ N.M. AFTER 24 HOURS: $\frac{10}{16}$ NOT MEASURED											
Elev. (Feet)	Depth (Feet)	Lithology	SAMPLE			Material Description	Dry Density, pcf	Moisture Content, %	Atter.		Gradation		Other Tests
			Type	Rec. (in.)	Blows Per 6" & Torvane (tsf)				Liquid Limit, %	Plasticity Index, %	Gravel, %	Sand, %	
4120													
	105					LEAN CLAY W/SOME SILT & VERY FINE SAND							
	110												
	115												
	120												
	125												
	130												
	135												
	140												
	145												
	150												



**RB&G
ENGINEERING
INC.**
Provo, Utah

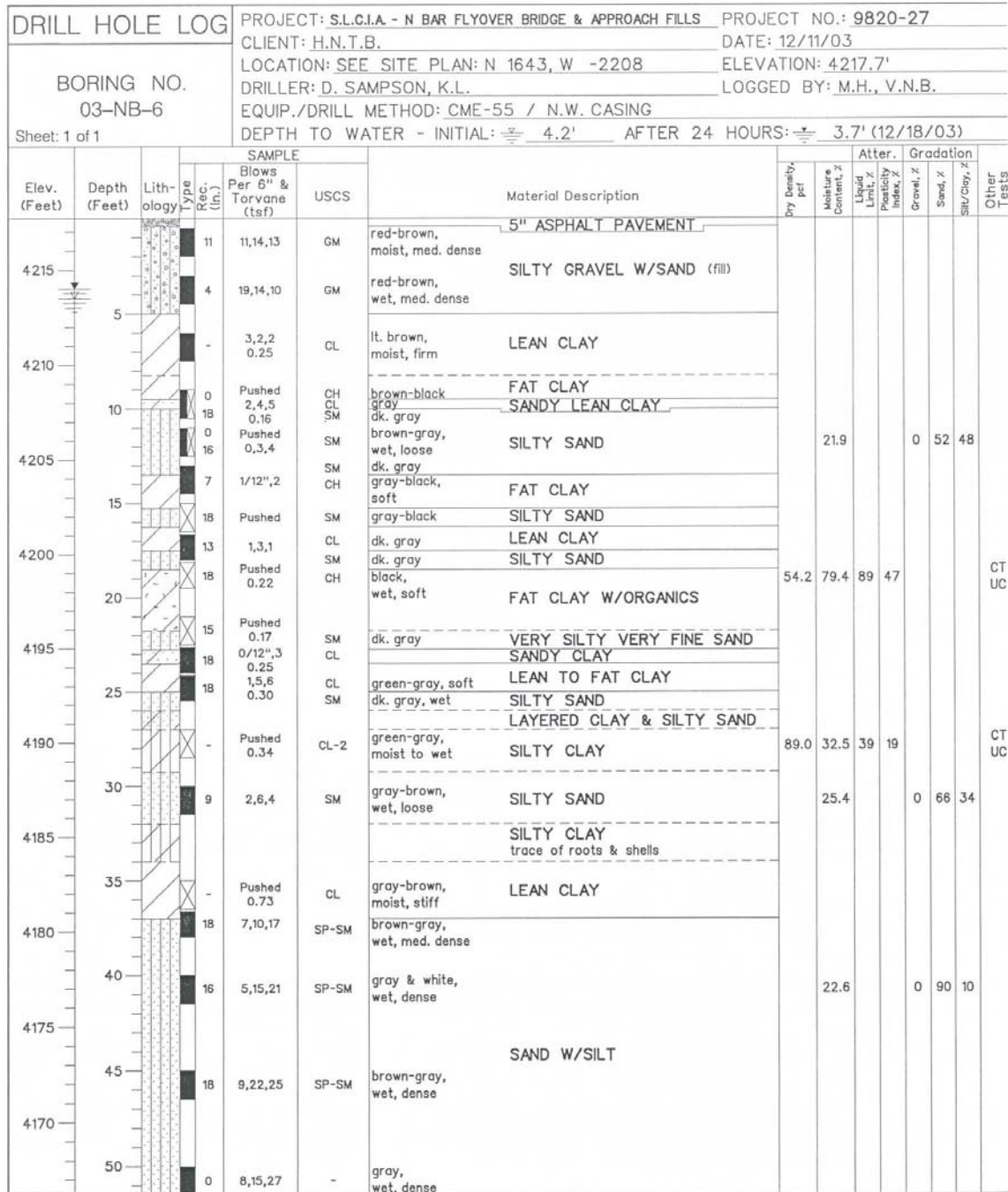
LEGEND




2,3,2 ← Blow Count per 6"
0.45 ← Torvane (tsf)
Disturbed Sample
Undisturbed Sample
Groundwater Elevation

UC - Unconfined Compression Test
CT - Consolidation Test
SG - Specific Gravity Test

Figure A-6 Borelog of Boring 03-NB-4 Performed by RB&G for SLCIA Site (continued)





**RB&G
ENGINEERING
INC.**
Provo, Utah

LEGEND

- 2, 3, 2 ← Blow Count per 6"
- 0.45 ← Torvane (tsf)
- Disturbed Sample
- Undisturbed Sample
- Groundwater Elevation

UC = Unconfined Compression Test
CT = Consolidation Test
SG = Specific Gravity Test

Figure A-7 Borelog of Boring 03-NB-6 Performed by RB&G for SLCIA Site

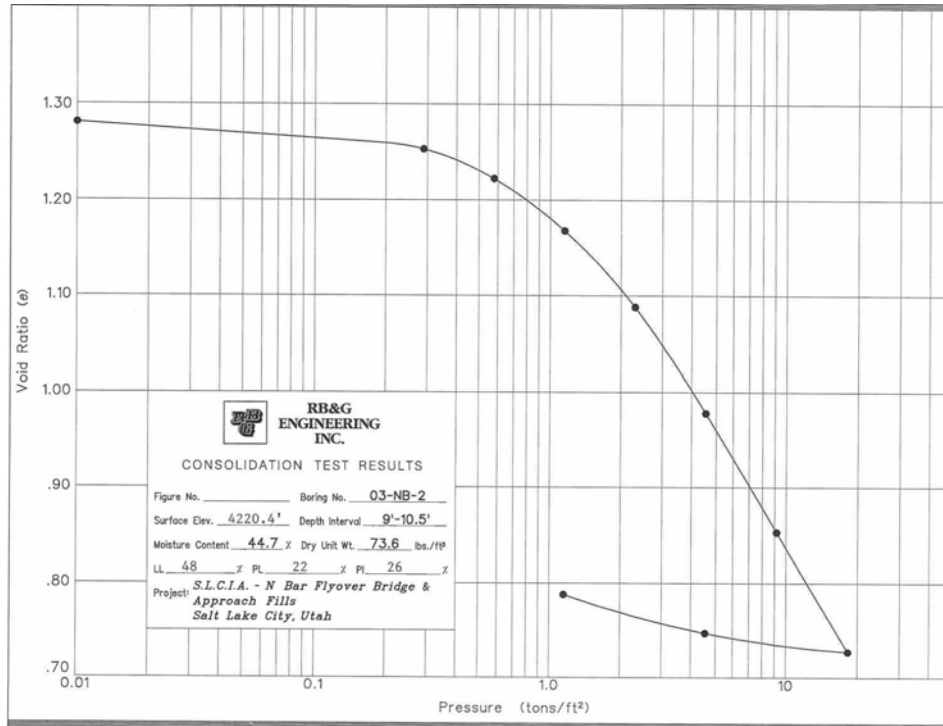


Figure A-8 Void Ratio vs. Pressure Curve for Consolidation Test from Boring 03-NB-2, 9' - 10.5'

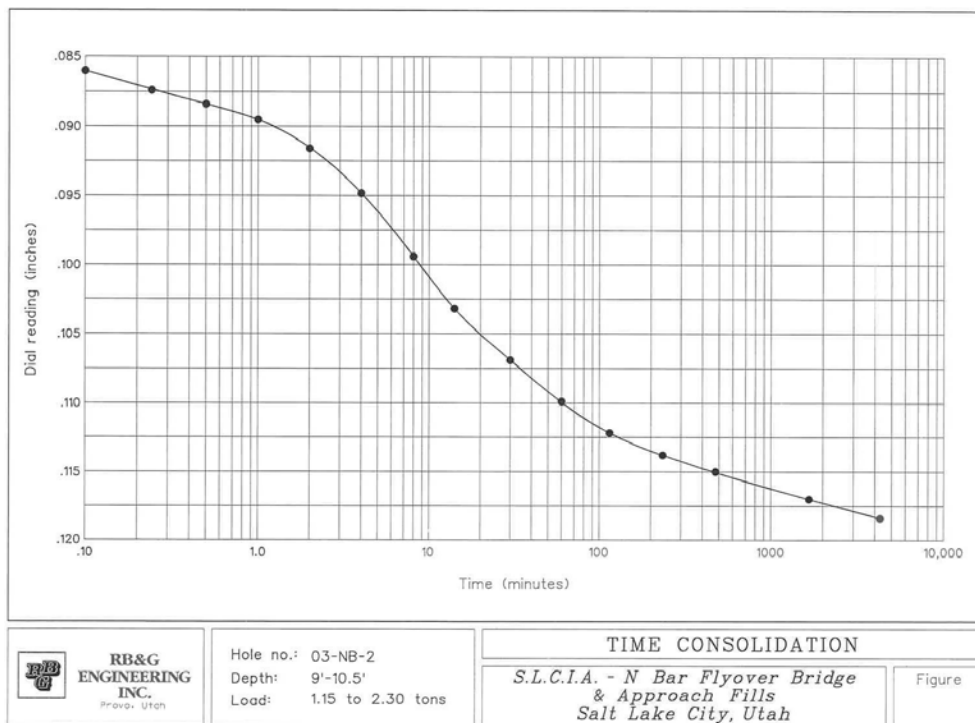


Figure A-9 Log of Time Series Curve for Sample from Boring 03-NB-3, 9' - 10.5', 1.15 to 2.3 Tons

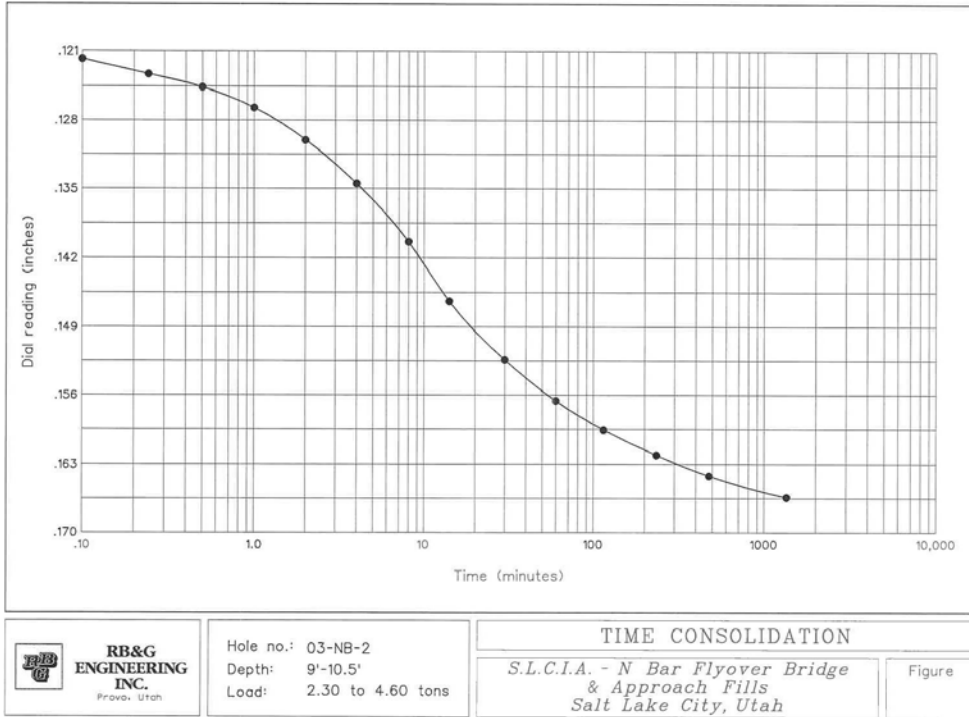


Figure A-10 Log of Time Series Curve for Sample from Boring 03-NB-3, 9' - 10.5', 2.3 to 4.6 Tons

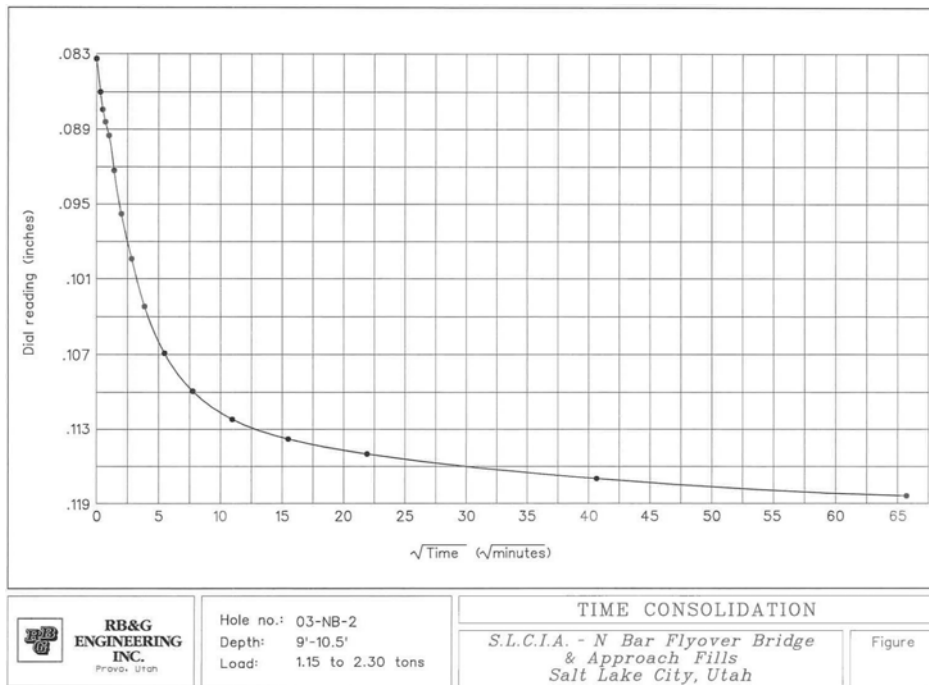


Figure A-11 Square Root of Time Series Curve for Sample from Boring 03-NB-3, 9' - 10.5', 1.15 to 2.3 Tons

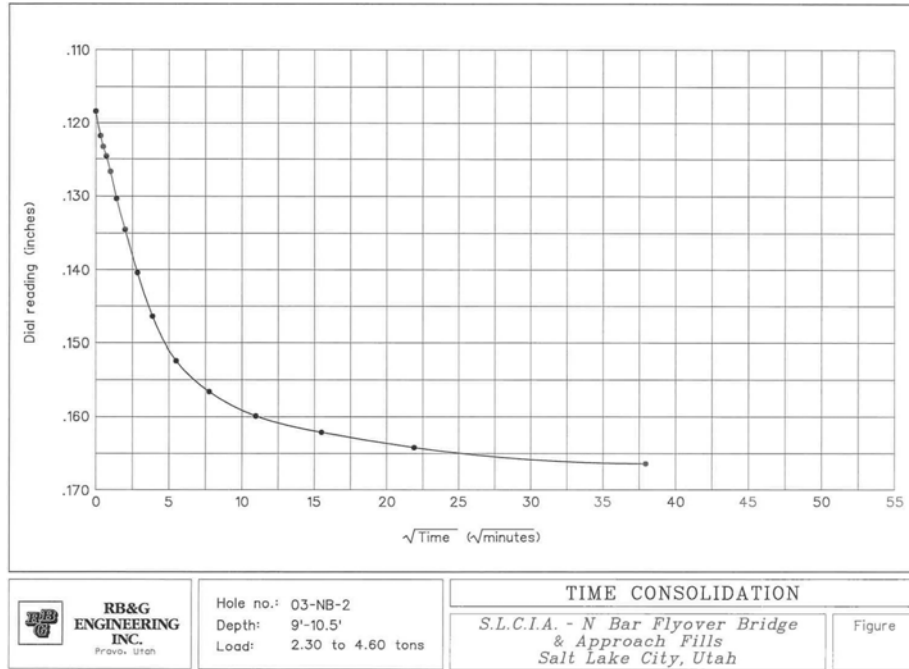


Figure A-12 Square Root of Time Series Curve for Sample from Boring 03-NB-3, 9' - 10.5', 2.3 to 4.6 Tons

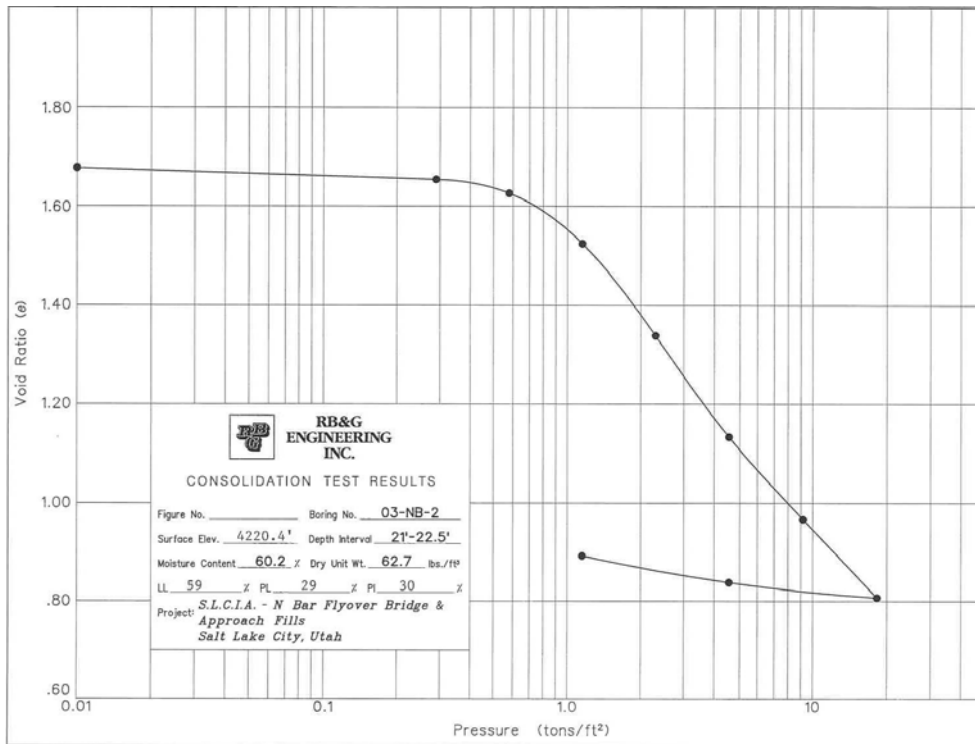


Figure A-13 Void Ratio vs. Pressure Curve for Consolidation Test from Boring 03-NB-2, 21' - 22.5'

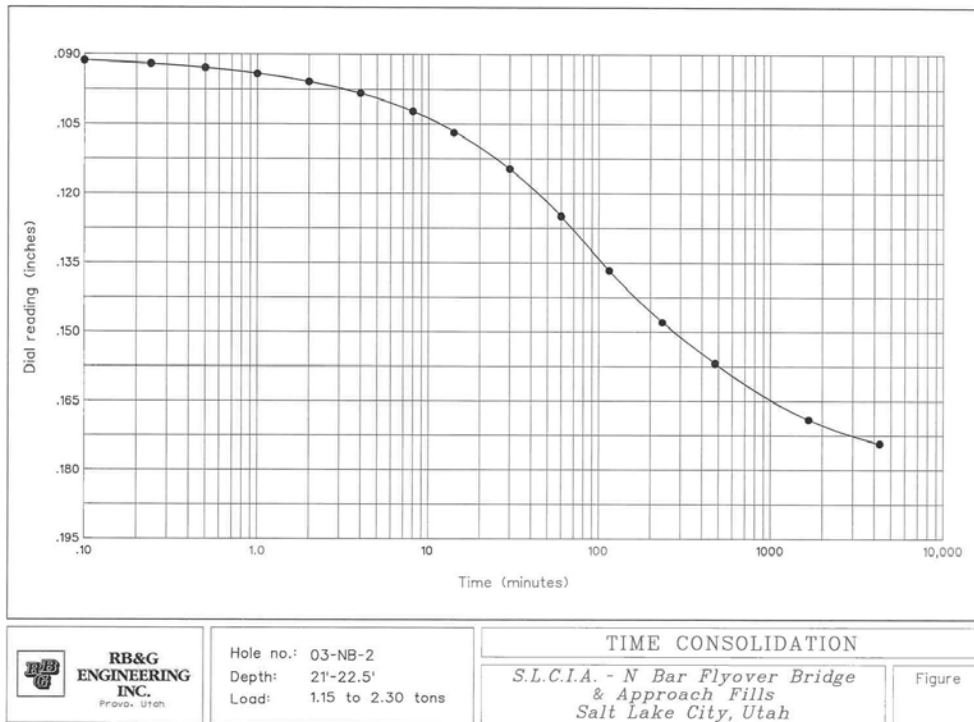


Figure A-14 Log of Time Series Curve for Sample from Boring 03-NB-3, 21' - 22.5', 1.15 to 2.3 Tons

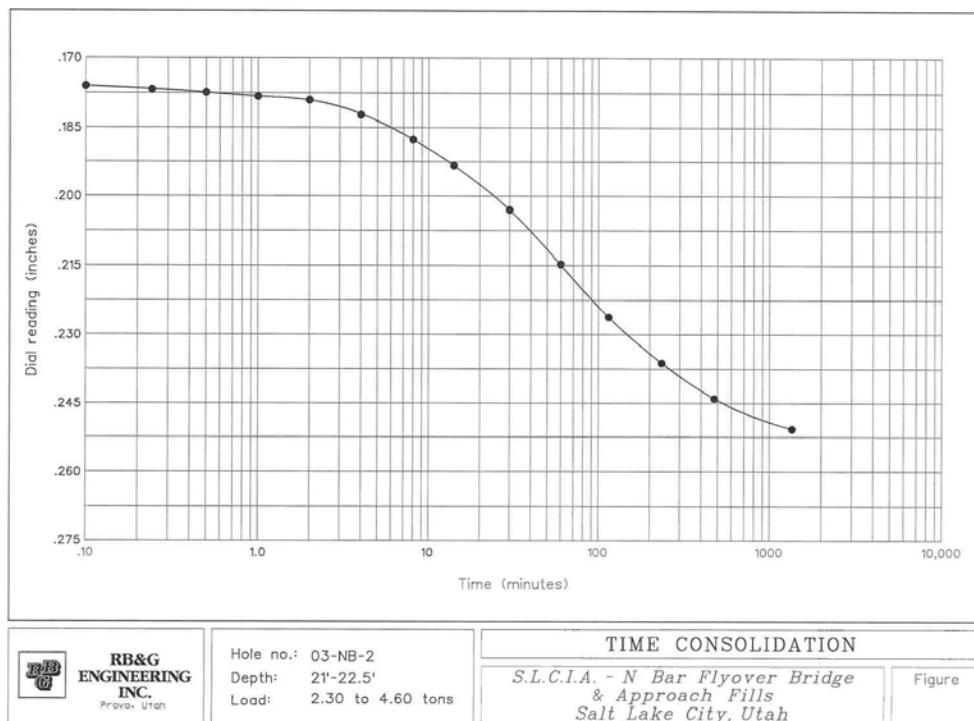


Figure A-15 Log of Time Series Curve for Sample from Boring 03-NB-3, 21' - 22.5', 2.3 to 4.6 Tons

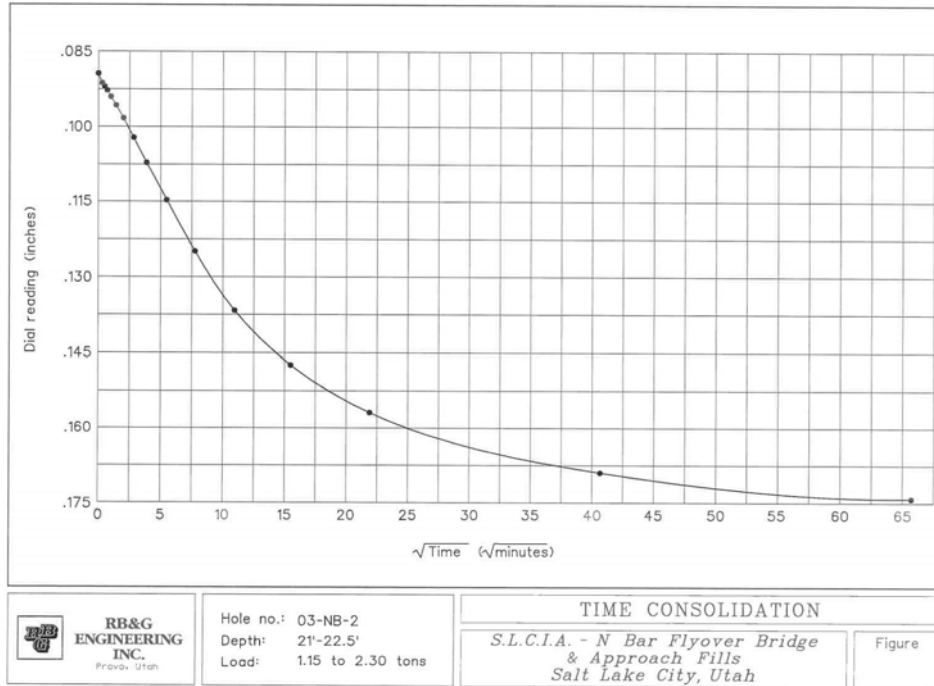


Figure A-16 Square Root of Time Series Curve for Sample from Boring 03-NB-3, 21' - 22.5', 1.15 to 2.3 Tons

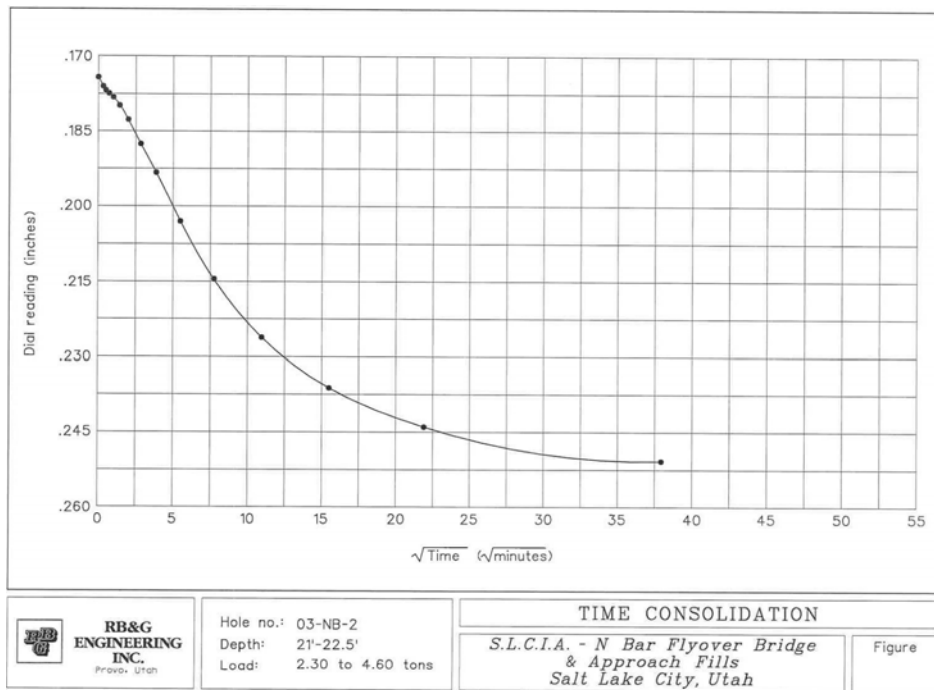


Figure A-17 Square Root of Time Series Curve for Sample from Boring 03-NB-3, 21' - 22.5', 2.3 to 4.6 Tons

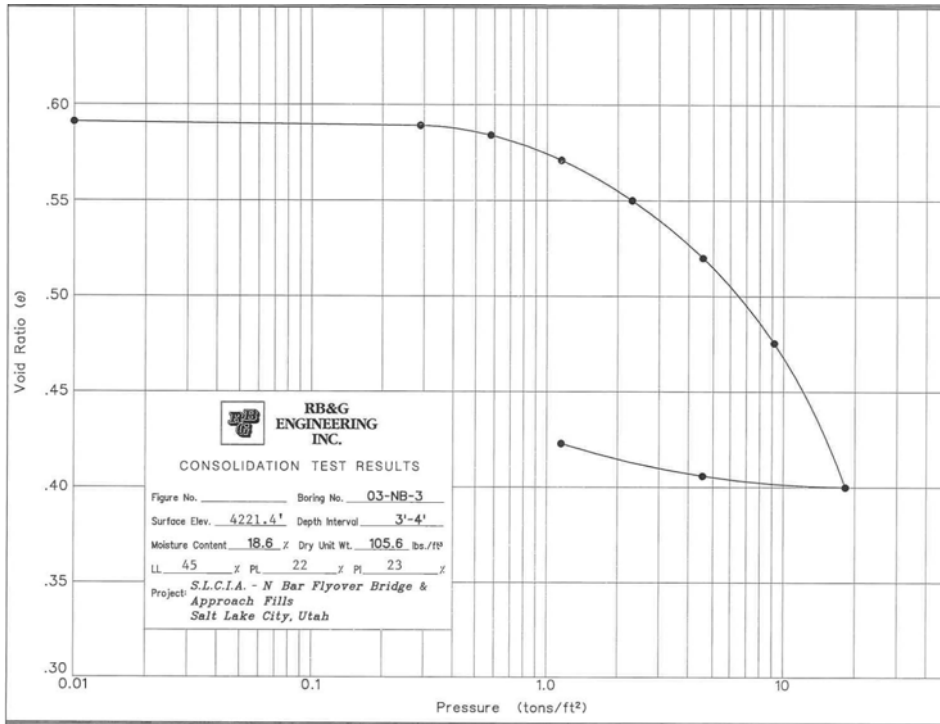


Figure A-18 Void Ratio vs. Pressure Curve for Consolidation Test from Boring 03-NB-3, 3' - 4'

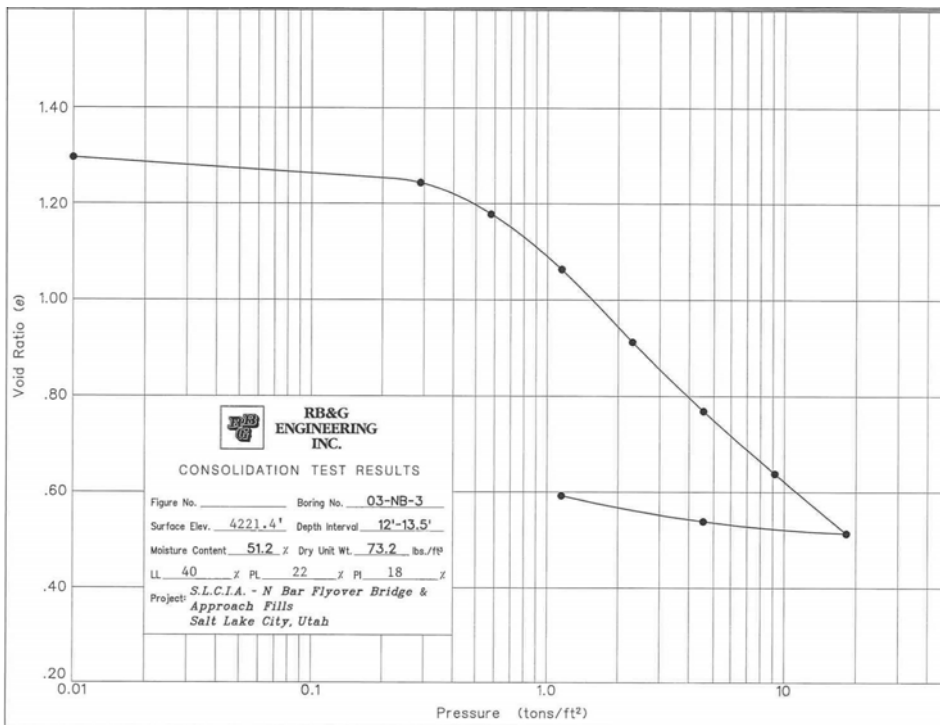


Figure A-19 Void Ratio vs. Pressure Curve for Consolidation Test from Boring 03-NB-3, 12' - 13.5'

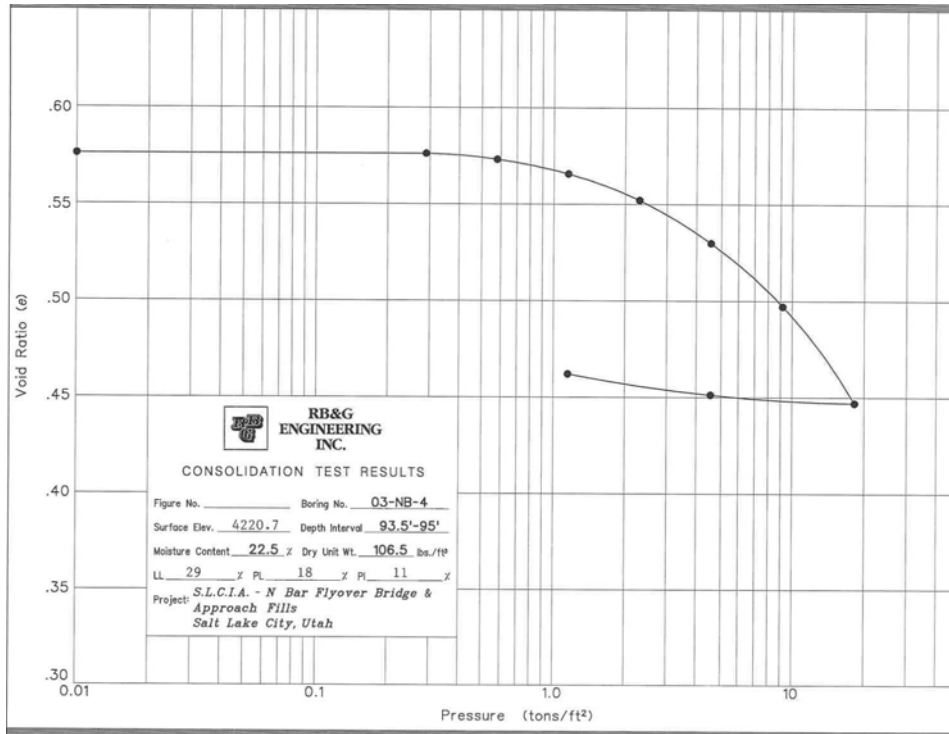


Figure A-20 Void Ratio vs. Pressure Curve for Consolidation Test from Boring 03-NB-4, 93.5' - 95'

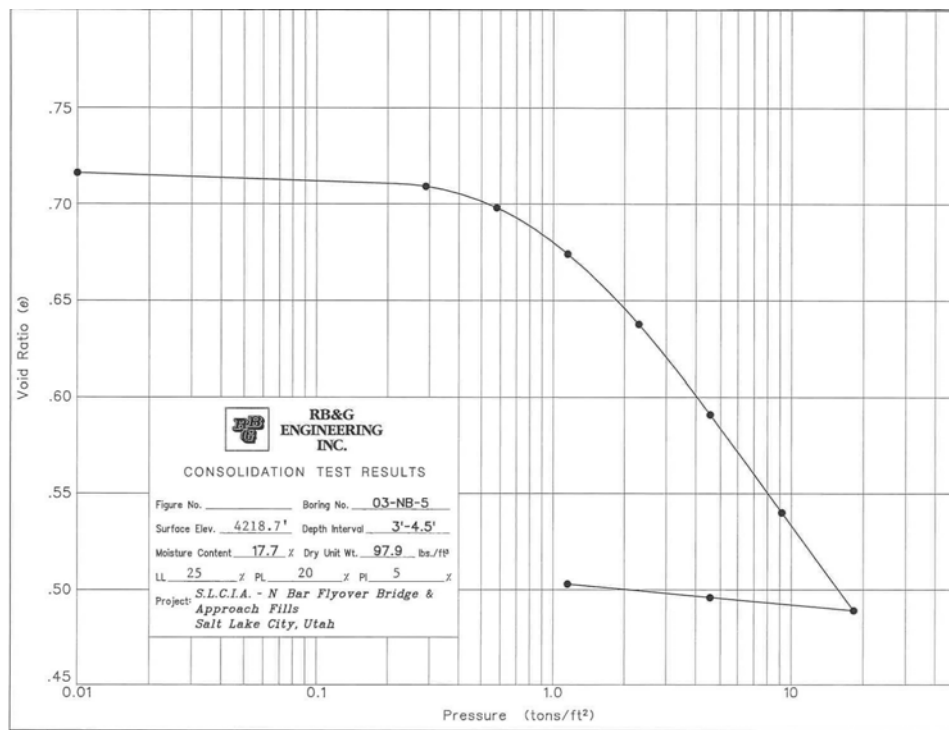


Figure A-21 Void Ratio vs. Pressure Curve for Consolidation Test from Boring 03-NB-5, 3' - 4.5'

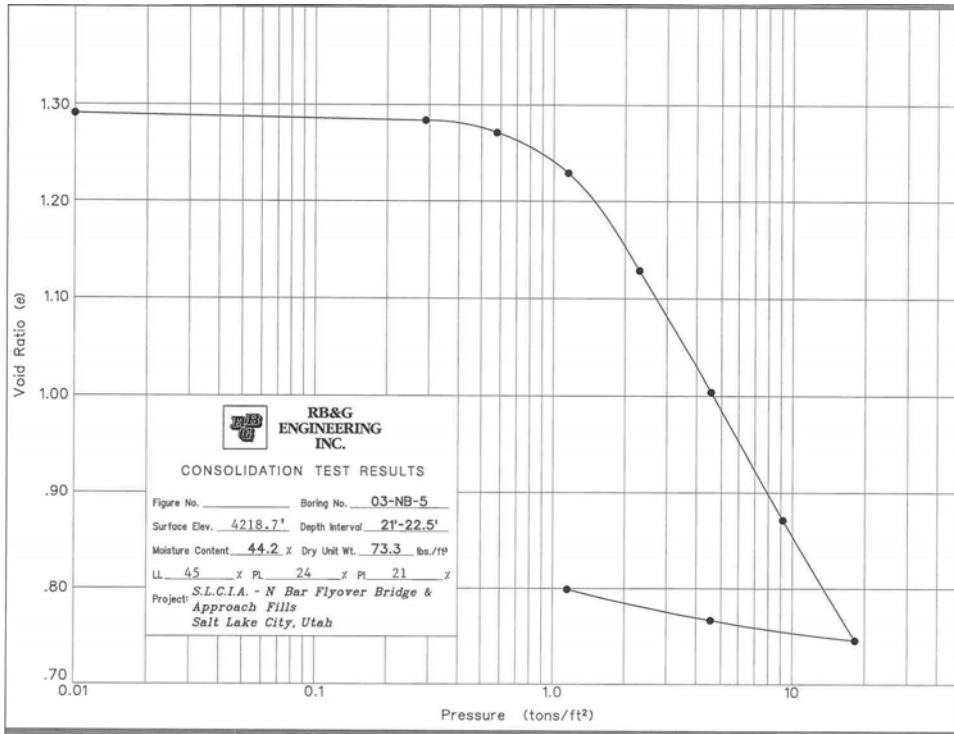


Figure A-22 Void Ratio vs. Pressure Curve for Consolidation Test from Boring 03-NB-5, 21' - 22.5'

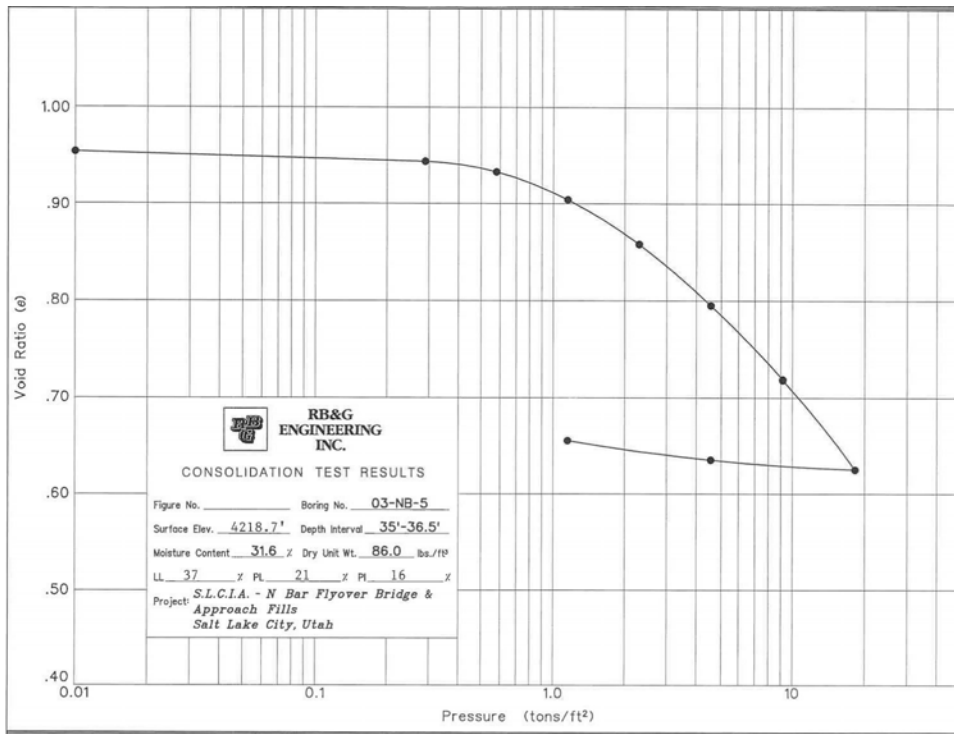


Figure A-23 Void Ratio vs. Pressure Curve for Consolidation Test from Boring 03-NB-3, 35' - 36.5'

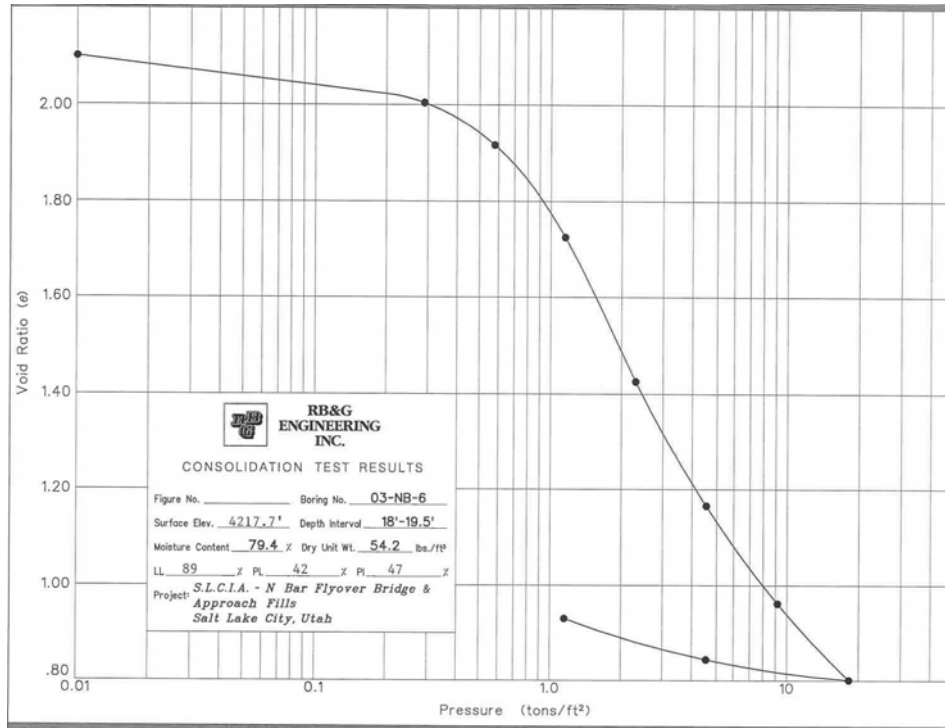


Figure A-24 Void Ratio vs. Pressure Curve for Consolidation Test from Boring 03-NB-6, 18' - 19.5'

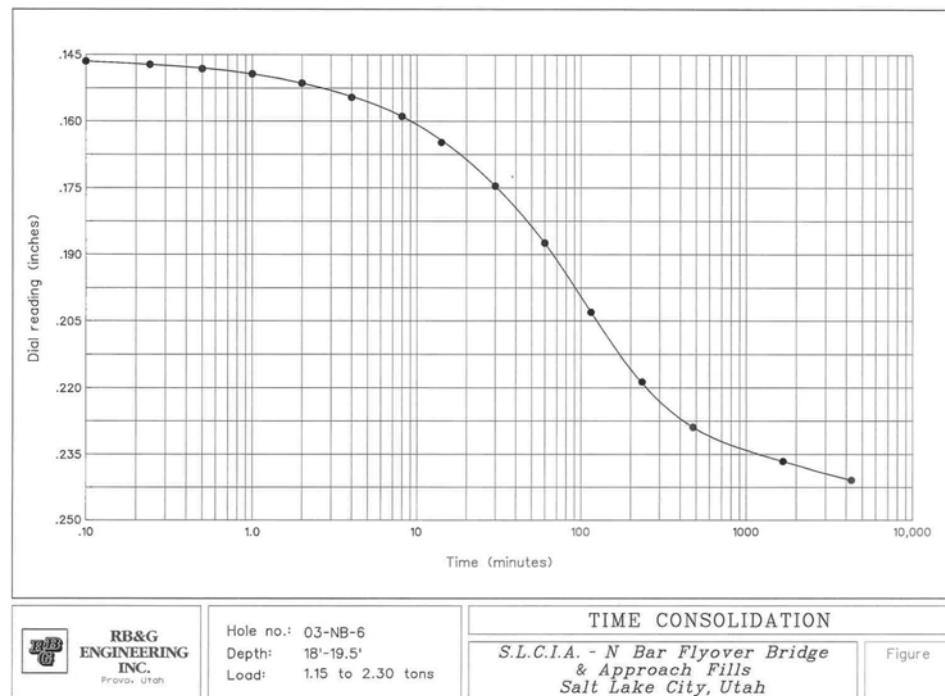


Figure A-25 Log of Time Series Curve for Sample from Boring 03-NB-6, 18' - 19.5', 1.15 to 2.3 Tons

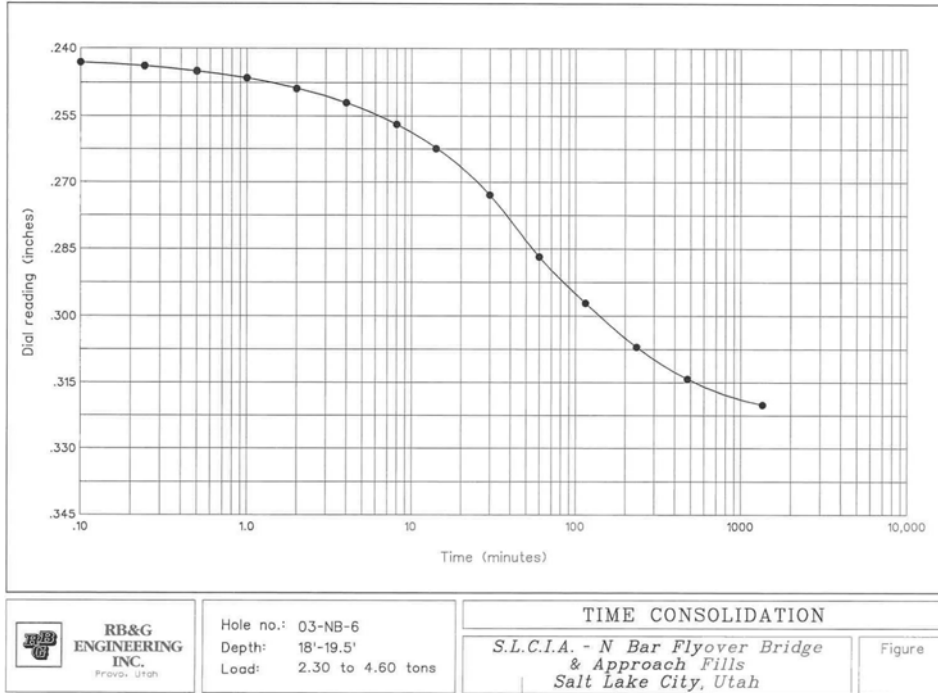


Figure A-26 Log of Time Series Curve for Sample from Boring 03-NB-6, 18' - 19.5', 2.3 to 4.6 Tons

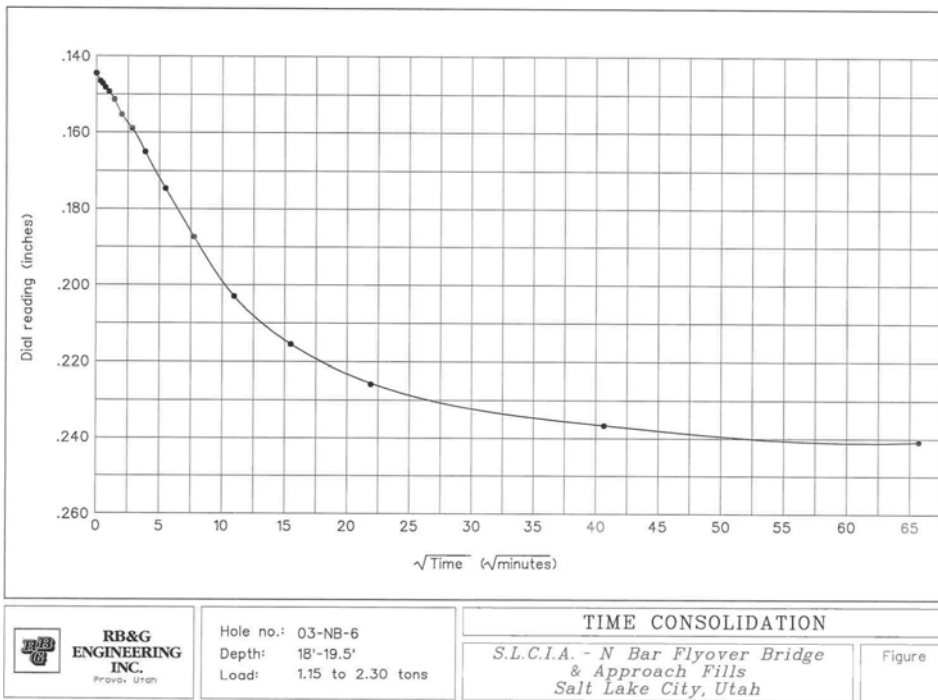


Figure A-27 Square Root of Time Series Curve for Sample from Boring 03-NB-6, 18' - 19.5', 1.15 to 2.3 Tons

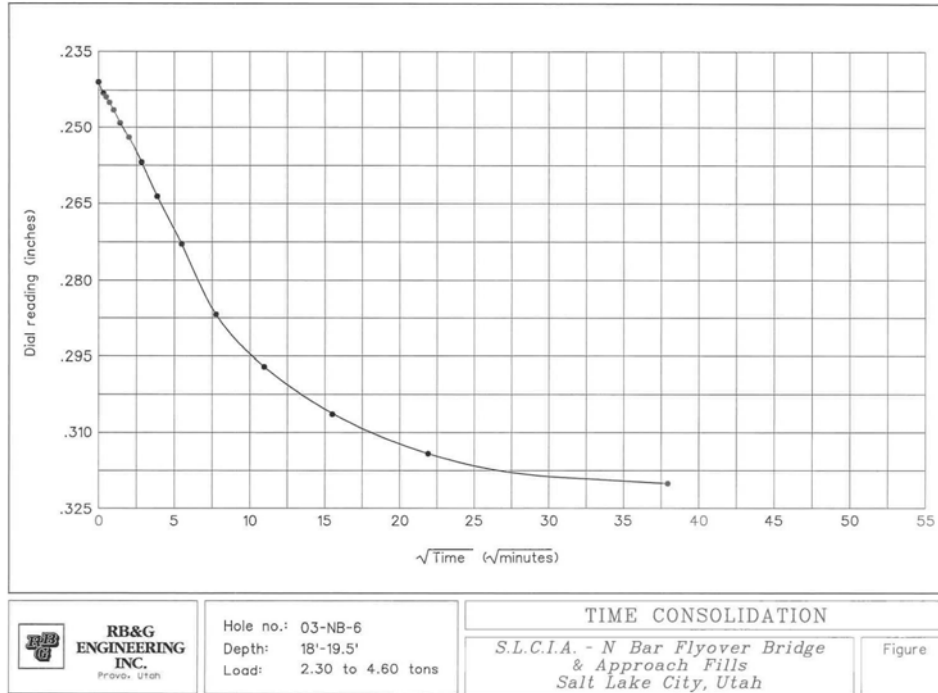


Figure A-28 Square Root of Time Series Curve for Sample from Boring 03-NB-6, 18' - 19.5', 2.3 to 4.6 Tons

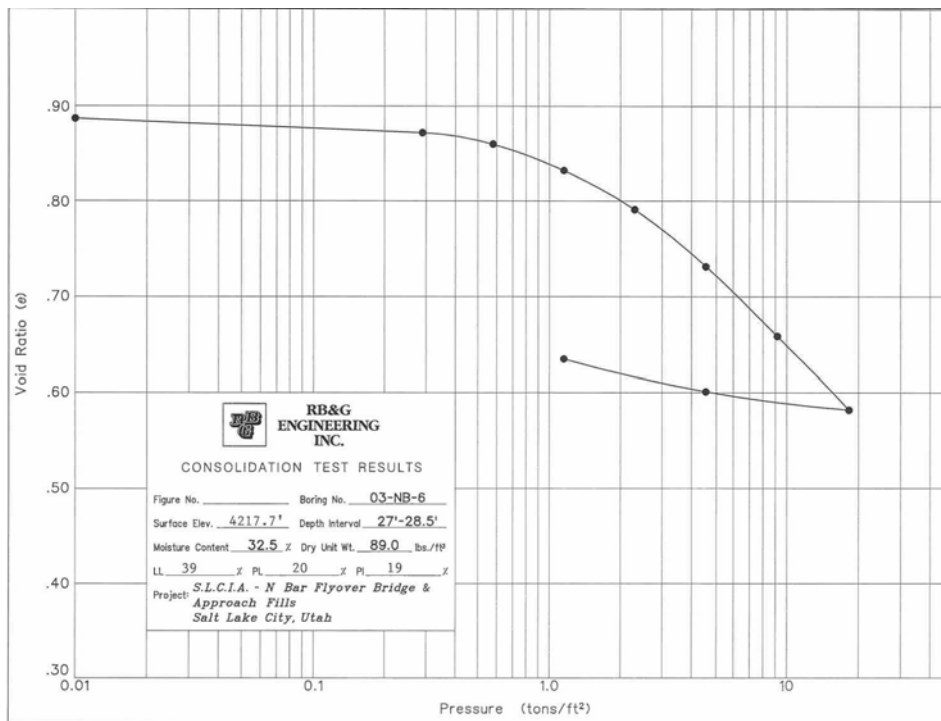


Figure A-29 Void Ratio vs. Pressure Curve for Consolidation Test from Boring 03-NB-6, 27' - 28.5'

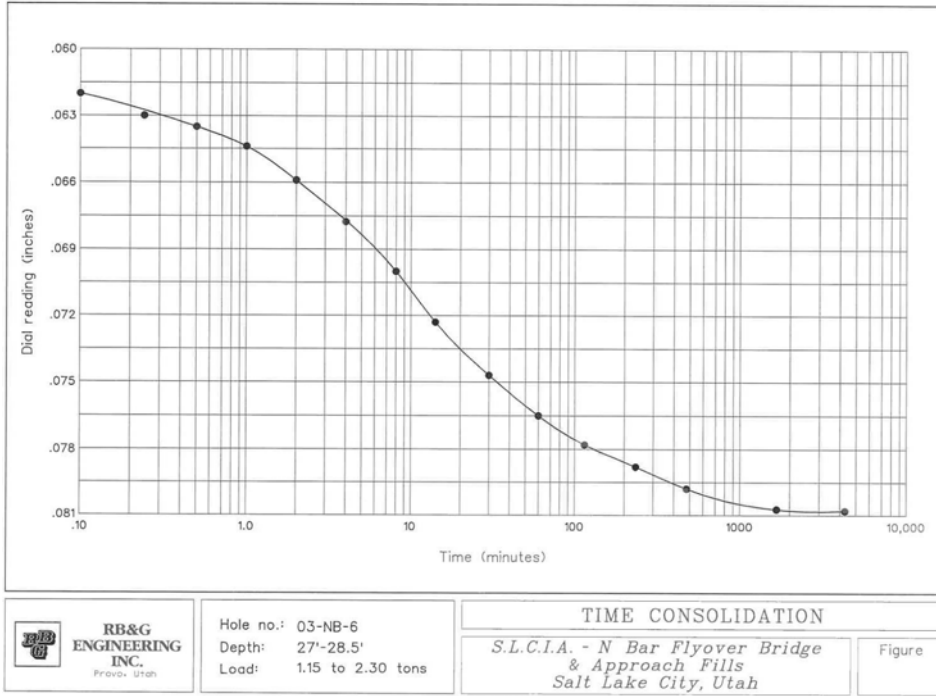


Figure A-30 Log of Time Series Curve for Sample from Boring 03-NB-6, 27' - 28.5', 1.15 to 2.3 Tons

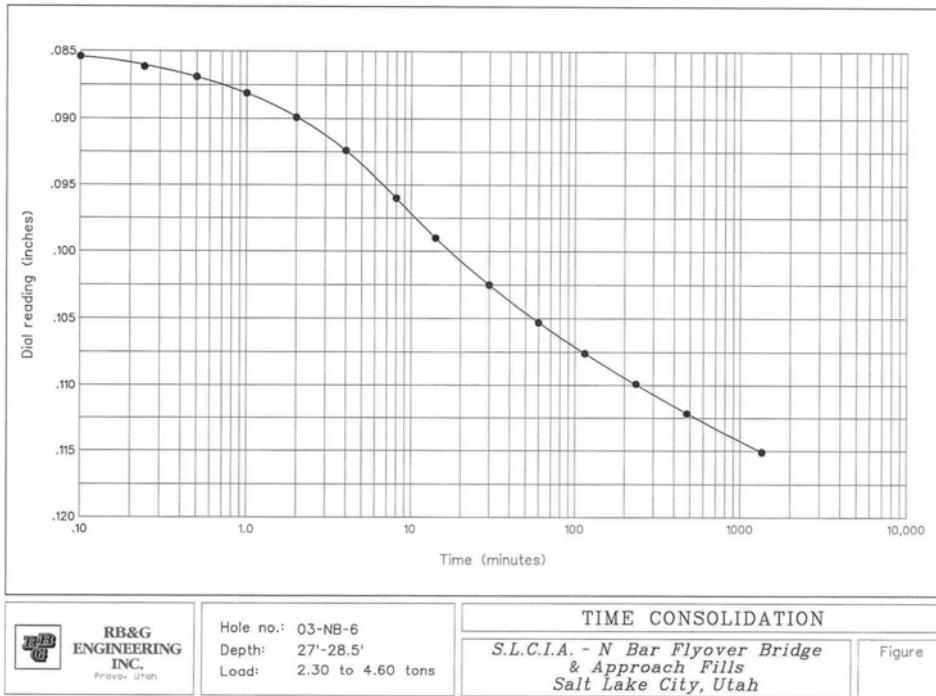


Figure A-31 Log of Time Series Curve for Sample from Boring 03-NB-6, 27' - 28.5', 2.3 to 4.6 Tons

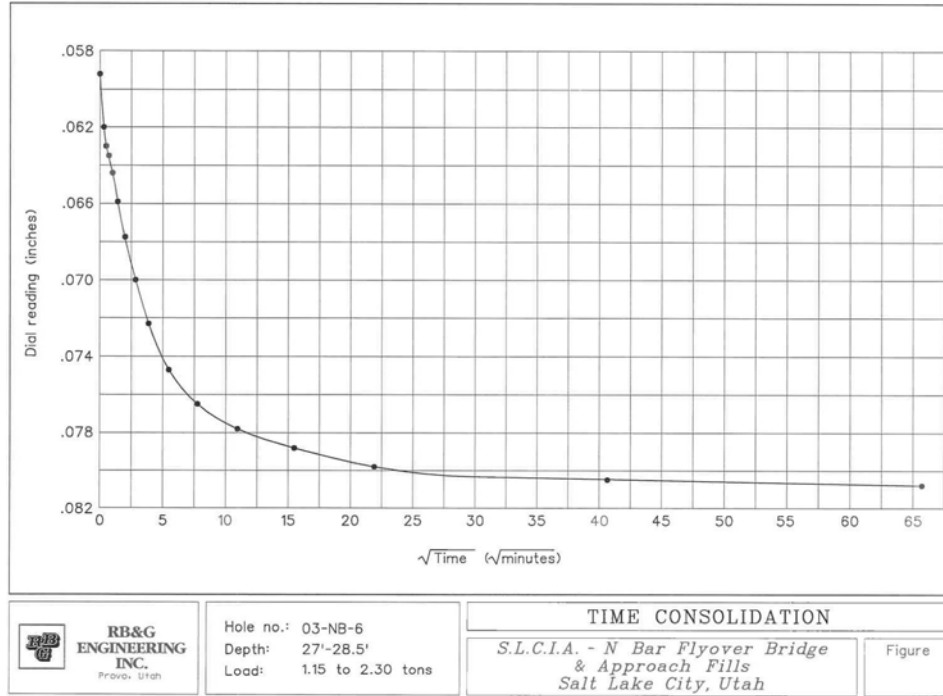


Figure A-32 Square Root of Time Series Curve for Sample from Boring 03-NB-6, 27' - 28.5', 1.15 to 2.3 Tons

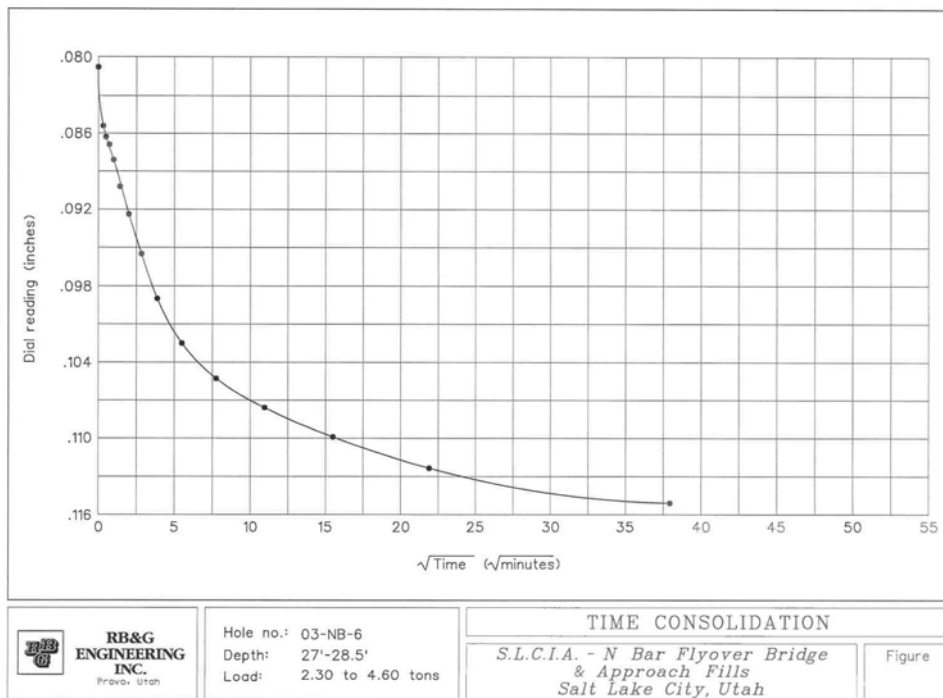


Figure A-33 Square Root of Time Series Curve for Sample from Boring 03-NB-6, 27' - 28.5', 2.3 to 4.6 Tons

